Title	Theoretical Approach for the Developmental Basis of the Robustness and Stochasticity in Floral Organ Numbers
Author(s)	北沢, 美帆
Citation	大阪大学, 2015, 博士論文
Version Type	VoR
URL	https://doi.org/10.18910/52294
rights	
Note	

Theoretical Approach for the Developmental Basis of the Robustness and Stochasticity in Floral Organ Numbers

（花器官数の頑健性とばらつきを生み出す発生基盤の理論的探究）

Kitazawa, Miho S.

Laboratory of Theoretical Biology, Department of Biological Sciences,
Graduate School of Science, Osaka University

大阪大学大学院理学研究科 生物科学専攻 理論生物学研究室
北沢美帆

Contents

Abstract

How do multicellular organisms determine the number of body parts precisely during their development? The number, such as the finger number of human, the body-segment number in insects, and the floral organ number in plants, might have been constrained during their evolution by the ecological adaptation or the requirement of the developmental process. The determining process of the number of body part is a fundamental question in morphogenesis of organisms asking the relationship between evolution and development.

I focused on the floral organ number in flowering plants (angiosperms), because of their fascinating features for studying the number-determination process. First, flower is a reproductive organ that regulates speciation by the reproductive isolation in evolutionary process. Second, the floral organ number is constrained to numbers specific to the phylogenetic clades. The floral organ number in eudicots, the most diverged clade in angiosperms, is four or five, whereas it is three in monocots and magnoliids, the rest clades. Thus the change of floral organ number may have led to the branching of eudicots, or the change of developmental process associated with the branching may have changed the floral organ number. Either way, the floral organ number should have clue to elucidate how the developmental process affect the evolution, or is affected by the evolution. Third, the floral organ number shows both robustness and stochasticity. Besides the specific modal number of floral organ is conserved within the clade, it varies even within an individual in some species. Therefore we can access this question from two sides, namely, the robustness and stochasticity, by employing floral organ number as a target.

I employed the mathematical modelling approach to examine the robustness of floral organ number, focusing on the arrangement of floral organs. I consulted models of phyllotaxis, the arrangement of leaves around a stem, because of the similarity of developmental process between phyllotaxis and the floral organ arrangement. Integrating the phyllotaxis models and the floral development observed in eudicots, I proposed a mathematical model, and found that the four and five are robust to parameter change compared to other numbers. This result suggests that the dominance of four and five in eudicots comes from the properties of floral development.

With respect to the stochasticity, I performed field observations for variations of floral organ numbers in wild populations. I calculated the statistical quantities for the data collected by myself and prior researchers, and found that there are four types of variations (symmetric, positively skewed, negatively skewed, and multi-modal variations), and there are three types in the relationship between the average number (mean) and degree of variation (standard deviation) among the populations. The latter implies that there are at least two sources of the stochasticity in floral organ numbers in the developmental process. I applied four models based on plausible developmental process to the variations and evaluated the best-fit model by statistical model selection. I found that the model selected as the best is different depending on organ-type and genera, and that a model I newly proposed based on the fate-determination process of floral organ primordia is selected in the highest frequency for the organ number variations.

Publication List

1. **Kitazawa, Miho S. and Fujimoto, Koichi.** (2014) A Developmental basis for stochasticity in floral organ numbers. *Frontiers in Plant Evolution and Development*, 5:545.

2. **Kitazawa, Miho S. and Fujimoto, Koichi.** A dynamical phyllotaxis model to determine floral organ number. *accepted to PLOS Computational Biology.*

I am preparing a submission of the contents in Sec. 3 as follows:

Kitazawa, Miho S. and Fujimoto, Koichi. The developmental robustness of lateral organ numbers and the species diversity — an integrated approach of statistical analysis and mathematical modelling.

1 General Remarks

The number of organs of multicellular organisms, such as the finger number of human, the body-segment number in insects, and the floral organ number in plants, is a key to study evolution of organisms. The floral organ number might have been constrained by the adaptation in the evolution, or by the requirement of the developmental process. In this thesis, I focus on the number of the floral organ, since it associates with the evolution of angiosperms.

Flower and the evolution of flowering plants. Angiosperms, or so-called flowering plants, are largely divided into three clades: The early divergent basal dicotyledons (basal dicots), monocotyledons (monocots), and the largest group eudicotyledons (eudicots). Eudicots is subdivided into core eudicots, a monophyletic group with rather uniform morphology, and basal eudicots represented by Ranunculales, which is a paraphyly branched early in the eudicot evolution and has varied morphology.
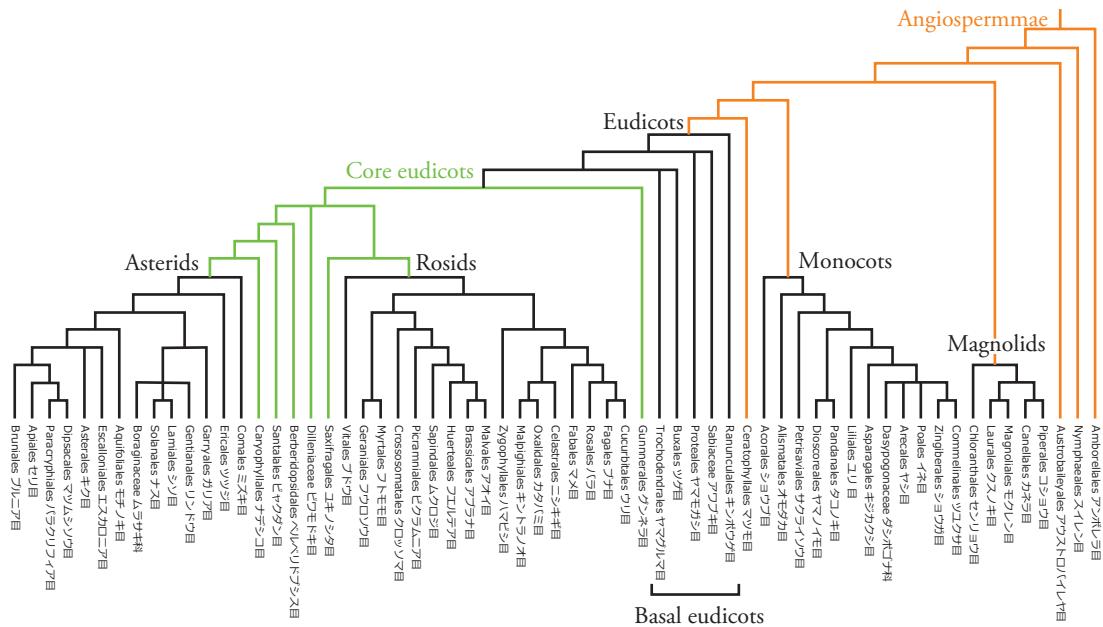
Figure 1.1: **The phylogenetic tree of angiosperms [15].**

As their informal name "flowering plants" indicates, angiosperms have flowers, which are reproductive structure that regulates speciation by the reproductive isolation in evolutionary process. Several types of floral organs have evolved to satisfy the reproductive function (Fig. 1.2A,B; see also Appendix A.6). The female organ that embraces seeds is the carpel, which is denoted by a single character G. The gynoecium composed by carpel(s) usually occupies the central part of the flower. stamens (A), which are the male organs to produce pollen, compose the androecium surrounding the gynoecium. Gynoecium and androecium are surrounded by the perianth, which have been evolved to attract pollinators such as insects and birds (animal-pollinating flowers), or to enable efficient access to wind (wind-pollinating/anemophilous flowers), specifically in Angiospermae.

The flowers of the three clades of angiosperms, namely, basal dicots, monocots, and eudicots, have distinct features. One of these features is the merosity, which represents the basic number of floral organs using the Greek word *méros* (Fig. 1.2C). In eudicots, the floral organs are usually in the set of five (pentamerous). The tetramerous and dimerous flowers are also found commonly in various eudicot taxa. Other numbers, such as three (trimerous), six (hexamerous), and seven (heptamerous), are rare in core eudicots. On the other hand, monocots and magnoliids, which occupies majority of basal dicots, develop trimerous flowers. Thus the change of floral organ number may have led to the branching between the clades, or a change of developmental process associated with the branching
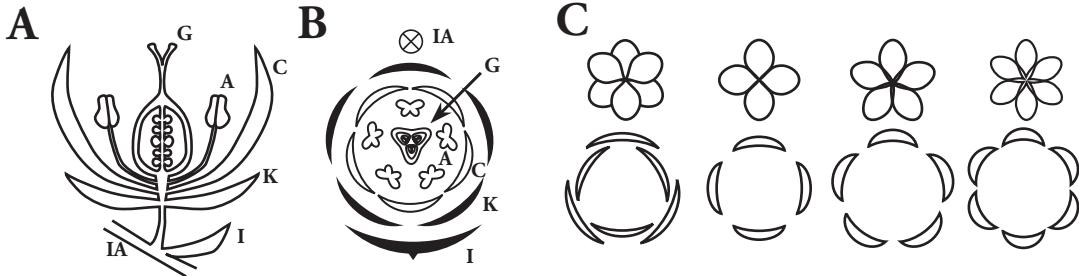
Figure 1.2: **Schematic representation of merosity of flower. A, B.** Longitudinal (A) and latitudinal (B) section of eudicot flower. **C.** Radial symmetric flowers. The number of symmetric axes (merosity) is three (trimerous), four (tetramerous), five (pentamerous), and six (hexamerous), respectively from left to right. For example, a corolla with a whorl composed of five petals is pentamerous, or the merosity is five. The most frequently observed merosity is five or three, but four or two are not uncommon. The angiosperms with whorled flowers are divided into two main groups by the merosity: magnoliids and monocots with trimerous or dimerous, and eudicots with pentamerous or tetramerous flowers. The studies for the morphological and evolutionary relationship between different merosities can shed light to the understanding of angiosperm evolution.

may have changed the floral organ number.

The robustness of floral organ numbers: The peculiarity of five. At latest in Renaissance period, it is known that the most common floral organ number is five. Familiar flowers, such as, pinks (Caryophyllales), cherry blossoms (Rosales), *Geranium* (Geraniales), *Azalea* (Ericales), and *Campanula*, all have the pentamerous (five-lobed) flower. After the birth of Linnean taxonomy, the floral organ numbers are related to plant taxa. For example, Eicher wrote in 19th century, "The number within a whorl can vary from 2 to about 30, if we ignore the possibility of increase by splitting. The most common number is 5-, 4-, and 3-merous: The pentamerous and tetramerous are known to be very common to dicotyledons, whereas trimerous is common to monocotyledons" [83, p.9]. Therefore the dominance of three, four, and five, — especially five — is the consensus of scientists.

It is not intuitively understandable, however, that the various flowers with various size (e.g. the floral meristem size ranges from 50 to 3500μm [285, p. 47]) all have set-of-five floral organs. Turing [311] stipulated the question for this dominance, showing that the pattern formations in the nature, such as those in vegetative whorls, rarely show preference for specific number but depends mainly on the size ratio between the component and whole system.

The answer for the question has been sought for long time. Some philosophers and scientists, such as Kepler and those in Pythagoras school, have believed the mystical meaning of number. They have looked for the meanings in the intention of god or the creator, and tried to find hidden meanings of the these numbers. Others, and the majority after the Renaissance, have related floral organ numbers to a series of numbers called Fibonacci sequence. In a sight of contemporary science after Darwin, the evolutionary selection is more plausible as a scientific meaning of the dominance of specific merosity. After Haeckel, the relationship between phylogeny and ontogeny, and the impact of the development on the evolution, have gradually attracted attentions. But the reason why the numbers do not show the same frequency is still largely a mystery.

In this thesis, I stand on the developmental point of view, and constructed a mathematical model, from which I found that the dominance of five and four is originated from the developmental process.

Number determination process during floral development. Flower is a shoot comprising very short stem and several lateral organs, which are in specific form such as sepal, petal, stamen, and carpel. As in other shoot homologous to flower, i.e., vegetative and inflorescence shoots, the position of floral organ is determined by the spatial distribution of plant hormone auxin (Appendix B.2). Although the central players of pattern formation

are similar to vegetative and inflorescence shoots, there two important processes in floral development that are not emphasised in the other shoots: The transition from helical initiation to whorled-type arrangement, and the specification of floral organ identity.

Many eudicot species show helical initiation of floral organ primordia and semi-whorled arrangement in blooming flower. Sepal primordia in pentamerous flowers in various clades from basal to core eudicots, such as Ranunculaceae [229], Caryophyllaceae [174], and Solanaceae [130], show the one-by-one initiation in helical order (Fig. 1.3). It results in pseudo-whorls with quincuncial aestivation, or even in radial symmetric whorls. It is not simple development, because if there is no post-meristematic modification, it should result in spiral arrangement (Fig. 1.3, the first row). Hereafter I refer this whorled-type arrangement initiating from helical initiation as semi-whorled arrangement.

The semi-whorled arrangement stabilises floral organ number. How does the semi-whorl arrangement affect the floral organ number? To relate them, fate-specification process of floral organ primordia must be referred.

The genetic model of the fate specification of floral organ primordia is known as ABCE model [60, 300]. The essential concept of this model is, floral organ identity is specified by the combination of several classes of floral organ identity genes, named A, B, C, and E class genes, which act in distinct regions within a floral meristem [60]. The change of expression patterns of these genes causes homeosis that transforms petal to sepal, sepal to leaf, and so on. Thus this model shows the molecular substance of Goethe's foliar theory, which insists that the floral organs are the transformed leaves [110].

These ABCE genes express in a concentric manner. A genes express in the outer part of floral bud, whereas the C genes express at the centre. B genes express in doughnut shape manner, in the intermediate position of the floral bud. In consequence, the floral bud is divided into four concentric regions with expression of AE, ABE, BCE, CE from outside to inside, corresponding to four floral organs in eudicots, namely, sepal, petal, stamen, and carpel, respectively. Therefore, the primordia number within the expression domain of ABCE class genes directly correspond to the floral organ number.

Standing upon these knowledge, let me compare the stability of floral organ number between spiral and semi-whorled arrangement. If the floral organ arrangement is in the spiral position as in the first row of Fig. 1.3, the slight shift of expression domain, which can be caused by the stochastic change of the floral bud size, heterogeneous cell division pattern, or some more else, leads to the change of floral organ number. It is not plausible to high stability of floral organ number in many eudicots, which show abnormal number in frequency of less than 0.1 %. On the other hand, if the floral organs are in semi-whorled arrangement and the expression boundary of ABCE is located between two successive semi-whorls, the number will not change by a little change of expression domain. In this concept, the primordia number within a semi-whorl corresponds to the floral organ number with high robustness. Therefore, semi-concentric arrangement of floral organ primordia stabilises the floral organ number, and the determination of primordia number within a semi-whorl should be the critical process underlying robustness of floral organ number.

The establishment of whorled-type arrangement from helical initiation is striking process for both the robustness and stochasticity of floral organ numbers. I have showed the importance of the semi-whorled arrangement. Then, how do flowers achieve the semi-whorled arrangement and what parameters determine the primordia number within the semi-whorl? Is there any special number, which shows high stability and robustness to something? Is the stable number common to all species, or different among species? And does the discord of semi-whorl position and expression boundary of ABCE genes really cause the variation in floral organ numbers? To answer these questions, I performed a series of studies using theoretical approach.

First, I constructed a mathematical model of floral development and demonstrated the repulsion between organ primordia spontaneously causes the formation of semi-whorled arrangement following helical initiation. The four and five appears as the dominant primordia number within a semi-whorl that are stable to parameters change, compared to other numbers. By counting of the frequency of floral organ number variation and calculating statistical quantities for them, I found an evidence of stable numbers within a species or genus, which can differ among species. The studies on variation also support the stable number within a semi-whorl, and showed a powerful variation source in the identity determination process.
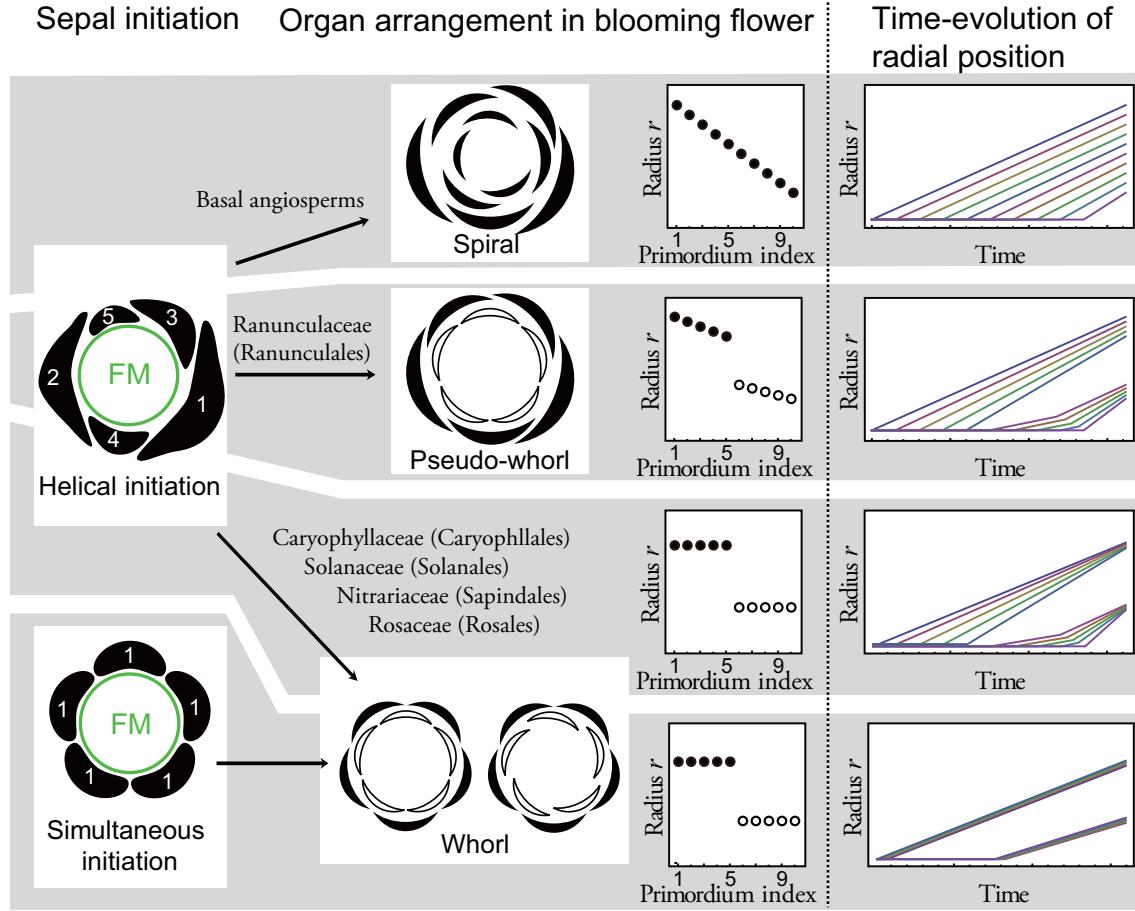
Figure 1.3: **Schematic diagram for pentamerous flower development.** Sepal initiation (the first row), arrangement of sepal (black) and petal (white) whorls in blooming flower (the second row). Green circle represents a floral meristem (FM). Index numbers indicate the initiation order of five sepals. The radial position of the organs (the third row), namely the distance between the organ and floral apex, is spaced regularly in a spiral arrangement, whereas it has a gap between the fifth and sixth organs in the pentamerous pseudo-whorled and whorled arrangement. Regarding the hypothetical time evolution of the radial position (the fourth row), in all arrangements, the radial position increases with the progression of floral development. In the spiral arrangement, the radial position of the organ is always spaced regularly. In the pseudo-whorled and whorled arrangement subsequent to helical initiation, the radial position of organs within a whorl becomes closer during growth. In the whorled arrangement following simultaneous initiation, the radial position of the organs within a whorl is always identical.

Organisation of this thesis The modelling of developmental process is described in section 2. the robustness of floral organ number is examined by the mathematical modelling approach, based on the phyllotaxis models that have been advanced over two centuries. With respect to the stochasticity, the variations of floral organ numbers observed by myself and prior researchers, including some studied that have been left behind for a century, and their statistical quantities are discussed for several clades in section 3. I applied four statistical models to those variations in floral organ numbers, and evaluated the best model by statistical model selection, which is discussed in section 4. I reviewed the plant morphology and the development of lateral organs in Appendices. The morphology of the plant aerial parts was captured the collection of unit structures, namely, the shoots consist of a stem and lateral

4

organs (Appendix A). The phyllotaxis, the arrangement of lateral organs around a stem in a shoot, is dispensable to discuss the floral organ number, hence I summarise the known phyllotactic pattern in the same section. In the second review, the modern knowledge of molecular development of plant shoots is reviewed (Appendix B).

Scientific names. The phylogeny and the taxonomic names were based on APGⅢ [15] for order-level phylogeny, and Angiosperm Phylogeny Group website (http://www.mobot.org/MOBOT/research/APweb/ at December 2014) for more detail. For the scientific names of species, I consulted The Plant List (http://www.theplantlist.org/) by major botanical gardens (the Royal Botanic Gardens, Kew and Missouri Botanical Garden, with many other collaborators). I also consulted for Integrated Taxonomic Information System (http://www.itis.gov/) to search the taxonomic information.

Symbols Throughout this thesis the following symbols are assigned to fixed meaning.
τ: the golden ratio $(1 + \sqrt{5})/2$ (τ is used for different meaning)
φ: the divergence angle
d: the divergence fraction (d_{ij} is used for the distance)
N/A means the data not available

Floral formulae and floral diagrams The way to describe the composition of flower has been developed in floral formulae [236]. It shows the structure of flower with the number of segments after abbreviated one-character symbol of floral organ type (Tab. 1.1).

Table 1.1: The names and abbreviations for major floral organs and bract [236].

Symbol	Whole	Part	Description
I	Involucre	Bract	Leaves subtend the flower
K	Calyx	Sepal	The outer (first) whorl, when the perianth whorls are differentiated into two types. Usually green in colour.
C	Corolla	Petal	A perianth whorl inside the calyx.
P	Perianth/Perigon	Tepal	Outer floral organs cannot distinguish into sepal and petal
N		Nectary	Nectar-secreting organ. Often it is a derivation or a part of a petal.
A	Androecium	Stamen	Male structure that produces pollen.
A°		Staminode	Stamen-like structure with imperfect male function.
G	Gynoecium	Pistil/carpel	Female structure that embraces ovules.
G°		Pistillode	Pistil- or carpel- like organ with imperfect female function.
	Pistil	Carpel	Fused carpel in syncarpous flower.

In this thesis I used curly bracket to show the variation range of the number (Table 1.2) in addition to typical use of floral formulae [236]. Using this formulae, we can treat the composition, modal number, and variation range of a species in a text line. For example, P5 means the flower contains five tepals, whereas A(3) indicates there are three carpels fused in a pistil. The positional relationship and spatial composition of floral organs are described by the floral diagrams (Fig. 1.2A,B) [83], representing each organ type by a symbol.

Table 1.2: The description for floral formulae.

Symbol	Description
( )	Fusion of organ within a whorl (sympetaly)
$a\{b - c\}$	mode number a, variation b to c

2 Developmental Model of Floral Organ Number

2.1 Abstract

How organisms determine particular organ numbers is a fundamental key to the development of precise body structures; however, the developmental mechanisms underlying organ-number determination are unclear. In many eudicot plants, the primordia of sepals and petals (the floral organs) first arise sequentially at the edge of a circular, undifferentiated region called the floral meristem, and later transition into a concentric arrangement called a whorl, which includes four or five organs. The properties controlling the transition to whorls comprising particular numbers of organs is little explored. I propose a development-based model of floral organ-number determination, improving upon earlier models of plant phyllotaxis that assumed two developmental processes: the sequential initiation of primordia in the least crowded space around the meristem and the constant growth of the tip of the stem. By introducing mutual repulsion among primordia into the growth process, I numerically and analytically show that the whorled arrangement emerges spontaneously from the sequential initiation of primordia. Moreover, by allowing the strength of the inhibition exerted by each primordium to decrease as the primordium ages, I show that pentamerous whorls, in which the angular and radial positions of the primordia are consistent with those observed in sepal and petal primordia in *Silene coeli-rosa*, Caryophyllaceae, become the dominant arrangement. The organ number within the outermost whorl, corresponding to the sepals, takes a value of four or five in a much wider parameter space than that in which it takes a value of six or seven. These results suggest that mutual repulsion among primordia during growth and a temporal decrease in the strength of the inhibition during initiation are required for the development of the tetramerous and pentamerous whorls common in eudicots.

2.2 Introduction

How to determine the numbers of body parts is a fundamental problem for the development of complete body structures in multicellular organisms. Digit numbers in vertebrates are evolutionarily optimized for the specific demands of the organism [271]; the body-segment number in insects is constant despite the evolutionarily diversified gene regulation in each segment [68, 200, 240]; and five petals are indispensable to forming the butterfly-like shape that is unique to legume flowers [209]. Studies of animal structures, such as vertebrate limbs and insect segments, strongly suggest that crosstalk between pre-patterns (e.g., morphogen gradients) and self-organizing patterns underlies the developmental process of organ-number determination [97, 101, 127, 190, 198, 249, 269, 296]. In plant development, a self-organization based on the polar transport of the phytohormone auxin [140, 228, 278] is conserved among seed plants [106] and seems to be the main regulator of the development of a hierarchical body plan, called a shoot, consisting of a stem and lateral organs such as leaves. The number of concentration peaks in most self-organizing patterns, such as Turing pattern and the mechanisms proposed for plant-pattern formation, is proportional to the field size [79, 140, 311]. Despite having a diversified field size for floral-organ patterning, the eudicots, the most diverged clade among plants, commonly have pentamerous or tetramerous flowers containing five or four sepals and petals (the outer floral organs), respectively, and rarely have other numbers of organs [91, 236]. Here, I focus on the developmental properties that so precisely and universally determine the floral organ numbers through self-organizing processes.

2.3 Background

Phyllotaxis, the arrangement of leaves around the stem, provides insight into floral development, because studies of floral organ-identity determination (see section B.5.3) [60] have verified Goethe's foliar theory (section A), which insists that a flower is a short shoot with specialized leaves [110]. The main phyllotactic patterns in the nature are spiral and whorled (section A). Phyllotaxis has been attracted many researcher especially in mathematics, physics, and and crystallography due to its capability and simplicity of mathematical expression (section A). In this section I overview the history of researches on phyllotaxis consulting following reviews: the mathematical representations summarised by Jean [137], the history of phyllotaxis theory by Adler [3], and modern reviews focusing on auxin [156, 305].

2.3.1 History of phyllotaxis studies

The history of the study of phyllotaxis is the history of the ideas of those who proposed them, and the history of the evolution of the ideas in the hands of those who exploited them. It is the history of the recognition of errors made, and their later detection and correction. It is a history of dialectical movement between experimental-observational and theoretical-mathematical viewpoints, between physical and chemical approaches, and the history of great trends initiated by the pioneers.—Adler, I., Barabe, D., Jean, R. V. [3]

Mathematicians, physicists, and even botanists have found that it is necessary to elaborate mathematical models based on botanical hypotheses in order to understand phyllotaxis. The spiral phyllotaxis is the most common type in plants, therefore it has been the main target of their discussion. The history of phyllotaxis, as the regular pattern of leaves, can be traced back to Greco-Roman period. Theophrastus (370 B.C. – 287 B.C.), who was a philosopher and scientist in the Aristotle school, and Plinius (23 A.D. – 79 A.D.), who was a statesman and scholar and is famous for his literary work Natural History, referred the regularity in leave arrangement as a primary feature of plants.

Golden ratio and Fibonacci numbers are indispensable for reviewing history of phyllotaxis models. The golden ratio τ was probably known in the Egypt or Greek, at latest 5th century B.C., and inherited to Greco-Roman sciences. τ is such number that, when we divide a segment into two parts, both the ratio between a long part and a short part of a segment and the ratio between the long part and whole segment become $1 : \tau$. A simple algebra gives the exact value $\tau = (1 + \sqrt{5})/2$, and applying this division to a circle, we obtain the golden angle of the smaller section as $360°/(1 + \tau) = 360°/\tau^2 = 360°(1 - 1/\tau) \sim 137.5°$. Meanwhile, Leonardo Fibonacci da Pisa (1175 – 1240) discussed the monthly growth of a population of rabbits and showed a sequence now called Fibonacci sequence: $1, 1, 2, 3, 5, 8, ...$ obtained by setting first two terms to 1 and summing two preceding terms for the rest ($F_0 = F_1 = 1$, $F_k = F_{k-1} + F_{k-2}$; F_k represents the k-th term of the sequence). The numbers within this sequence is called Fibonacci numbers. A sequence $2, 1, 3, 4, 7, 11, ...$ obtained by the same rule but another initial condition $F_0 = 2, F_1 = 1$ is known as Lucas sequence, also is associated with phyllotaxis together with $3, 2, 5, 7, 12, 19, ...$ The golden ratio mathematically relates to Fibonacci sequence as shown in formula $\tau = \lim_{k \to \infty} (F_{k+1}/F_k)$.

After the Renaissance. In the period of Renaissance, the famous Leonardo da Vinci (1452 – 1519) described some notes on the phyllotaxis. After this, the studies on phyllotaxis have been proceeded. As ever and after, phyllotaxis is not a field only for botanists. For example, Johannes Kepler (1571 – 1630), who was astronomer and fascinated by the number five, referred "the cycles of five leaves spiralling around a stem in plants, and the five parts to the seed-bearing core of an apple" [3].

In the middle of 18th century, the systematic classification of phyllotaxis has started. A naturalist **Bonnet (1754)** is designated as the first scientist who seriously studied the phyllotaxis [3]. He classified leaf arrangement into five categories, following Calandrini [37, p. 159–166 & Pl. XX]. He put *Alterne* as the first category, indicating the leaves are aligned in two lines on opposite sides of the stem, and if a leaf is at one of the line, the successive leaf is at another line. *Paires croisées* is the second category that have a pair of leaves at one point, and the pair is cross to the previous pair, what is now called decussate. The third category, *Feuilles verticillées*, is whorled pattern with three or more leaves at one point, which subdivided by the number of leaves in a whorl. *Quinconces* has the five lines along the stem, and if the first leaf is on the first line, the second leaf is on the third line, the third leaf is on the fifth line, the fourth leaf is on the second line, the fifth leaf is on the fourth line, and the sixth leaf is on the first line again. It can be expressed much simpler using what we call genetic spiral connecting the leaves by the initiation order, with divergence of 2/5 or 144° between successive leaves. The fifth category is *Spirales redoublées*, with several parallel spirals, which is subdivided by the number of spirals (what is known as parastichy, or can be jugy) and the number of leaves in each round of a spiral. He explained the cause of phyllotactic patterns by the function of leaves, insisting that the efficient transpiration of leaves requires the free circulation of air and the least overlapping of leaves.

At the same era, the taxonomist Linné and a medical doctor Sauvages also proposed the classification of leaf arrangement. Sauvages (in Mémoire sur une nouvelle méthode de connoitre les Plantes par les Feuilles, 1943, from [37]) proposed four classes: *Opposées* that has leaves two by two, *Verticillées* with whorls of set of three, four, etc. leaves, *Alternes* with alternate succession of leaves, and *Éparses* that lacks constant order. Linné listed several classes: *Stellata* that means whorled phyllotaxy with more than two leaves surround a stem at one point (further

divided into *Terna, Quaterna, Quina, Sena,* etc. by the number of the leaves within a whorl), *Opposita, Alterna* with leaves one after another,*Sparsa* that lacks constant order, *Conferta* that the stem is covered by leaves without space, *Imbricata* that the leaves crowded and erect to overlap others, *Fasciculata* having many leaves and shoots at one point, *Disticha* that the leaves on only two side of the stem [166, sect. 83,C,m]. They used these classes to the taxonomy of the plant species, since the leaves are the long-term characteristic, as opposed to flowers observed only seasonally [259].

First systematic theory. **Schimper (1830)** studied the spiral arrangement of leaves around a mature stem and introduced the concepts of genetic spiral, divergence angle and parastichy [3]. He insisted all divergence between succession leaves is able to be represented in rational numbers (divergence fraction d). He calculated the divergence fraction $d = n/m$ by starting with a leaf, counting the number of leaves (m) until it reaches another leaf directly above to the focusing one, and counting how many times round the stem (n). The rational fraction is obvious consequence from this definition. However, he found interesting properties of these fraction that the divergence angles are expressed by the ratio of two alternate terms of the Fibonacci sequence such as 1/3, 2/5 and 3/8. **Braun (1831, 1835)**, who was a friend of Schimper, followed the theory by Schimper. He examined whorled and spiral arrangement, and found what are now known as conspicuous parastichies, multiple spirals in clockwise and anticlockwise direction observed in many of phyllotactic patterns [42]. He stated, if the number of parastichy is m (m-parastichy) in one direction and n-parastichies in another direction, m and n are consecutive terms of the Fibonacci sequence. The observation Scimper and Braun that connected phyllotaxis to Fibonacci numbers are now together called Scimper-Braun's law.

Cylindrical-lattice representation. **Bravais brothers (1837)**, who was a botanist and an officer, respectively, represented leaf distribution as a point-lattice on a cylinder, which called cylindrical representation or Bravais-Bravais lattice. They emphasised the importance of genetic spirals as fundamental spirals, and demoted eye-catching spirals (parastichies) to the secondary spirals.

The Bravais-Bravais theorem states that the neighbouring two organs on n-parastichy differ n in the initiating order. Therefore in a (m, n) system, the difference in initiation order of two organs is represented by $tm + sn$, where t and s are integers. From this, they derived the relationship between the divergence angle in fraction d and parastichy pair. When the difference in initiation order (the number of organs between the two +1) between an organ at the origin and another organ almost above the origin is represented as $tm + sn$, $d(tm + sn)$ represents the distance of these two organs on the genetic spiral. Suppose that u and v are the integers respectively the nearest to md and nd, which can be obtained as the separation of the successive two organs on the Bravais-Bravais lattice. We obtain the approximation $d(tm + sn) \approx tu + sv$, which gives $d \approx (tu + sv)/(tm + sn)$, the relationship between divergence fraction and parastichies on Bravais-Bravais lattice. They also distinguished the number of genetic spirals J, which represents jugy (jugacy or jugacity). They proved that if the the greatest common divisor of m and n is greater than 1, there are more than one genetic spiral and the common divisor directly gives J. They named alternate with only one genetic spiral ($J = 1$) unijugate, and the phyllotaxis with two ($J = 2$) and multiple genetic spirals ($J > 2$) bijugate and multijugate, respectively [137, p. 141] (see section A.3). These theorem is summarised in representation, later by Adler (1974), as $J < 1, t, t + 1, 2t + 1, 3t + 2, ... >$, where $t > 1$ and the sequence in $<>$ gives convergence on specific divergence.

They insisted the irrational divergence angles, especially the golden ratio $360°/\tau^2$ corresponds to the system with $J = 1$ and $t = 2$ ($< 1, 2, 3, 5, 8, ... >$), are common in the nature instead of Schimper and Braun's rational divergence angles. They mentioned other irrational angles: approximately equal to $99.50155°$ corresponding to the sequence with $J = 1$ and $t = 3$ ($< 1, 3, 4, 7, 11, ... >$), and another one of $77.57°$ corresponding to the sequence $J = 1$ and $t = 4$ ($< 1, 4, 5, 9, 13, ... >$). The first two divergence angles can be expressed by a single formula: $\varphi = 360°(1/((t - 1) + \tau))$, though they did not reach this expression.

Wiesner's law — adaptive advantage of golden angle. Some researchers were suspicious of these mathematical ideas, such as **Sachs (1882)**, who stated "If it was possible to put all leaf positions into this rule of divergence angle, that is indeed a kind of natural law, which lacks any causal relationship, and is an unexplained wonder" in

his botanical textbook (Beziehungen ausgezeichnetem Lehrbuch der Botanik, from [329]). In the consequence, some attempts was made to show botanical advantages of golden spiral.

Wiesner (1875) showed relationship between divergence sequence $1/z, 1/(z+(1/1)), 1/(z+1/(1+1/1)), 1/(z+1/(1+1/(1+1/1))), ...$ and generalised divergence fraction $(2z-\sqrt{5}-1)/2(z^2-z-1)$, where z can be considered to be equivalent to above t in Adler's notation. In compliance with Sachs's question, he tried a functional explanation for the irrational divergence fraction, which is now known as Wiesner's law. He insisted that a spiral arrangement with smallest possible number of z ($z = 2$) is the most common and is optimised to cover the region around the axis (stem) with the least number of leaves [330]. It is in accord with Leonardo da Vinci and Bonnet, who claimed the teleological cause of phyllotactic pattern, though he did not mentioned these precursors.

Package efficiency. **Airy (1873)** gave the idea of packing efficiency [6]. Standing on Darwinian point of view, he stated the phyllotaxis must be the result of selection. The primary advantage to control the phyllotaxis is efficient capture of sunlight, but many plants such as elm with distichous phyllotaxy rotate the branch to satisfy this requirement. Hence he considered the advantage to operate the phyllotaxis should be in the earlier stage — inside the bud, rather than mature stem. He described the advantage of having order of leaf arrangement inside the bud as "economy of space, whereby the bud is enabled to retire into itself and present the least surface to outward danger and vicissitudes to temperature". Also he stated the $1/2$ phyllotaxy (distichy) is the ancestral pattern, since it is the simplest and is the least optimised for this packing advantage. He demonstrated his idea of packing efficiency aligning spheres representing leaf primordia along with stretched rubber band, and relaxing the tension. This simple demonstration leaded to a compact arrangement with Fibonacci-related divergence fraction, such as (nearly) $1/3, 2/5, 3/8$, and so on.

Later in 20th century, **Ridley (1982)** gave a mathematical treatment for the idea of packing efficiency in sunflower head [232]. Starting from Vogel's model [318] with two assumptions of the constant divergence angle and of equal-sized seeds, he calculated the packing efficiency. He defined packing is the most efficient when the density of the primordia is uniform for any local region in the capitulum, and analytically showed that the maximum of the packing efficiency is achieved if and only if the divergence fraction is $1/\tau^2$.

The centric representation: points on a disc. From the tip cut at right angles to the axis, we obtain the secret of phyllotaxis [3] — **Church (1904)** firstly proposed the centric representation, which expresses leaves as points inside a disc. Although the cylindrical representation and centric representation are mathematically equivalent, he rejected some precursor's idea. For example, he emphasised the importance of parastichies than the genetic spiral, insisting "that impulses of energy travel away from the centre of the disc in spiral paths, and that new leaves grow where the spirals intersect" [3]. Standing upon these concept, he found several important relationship between patterns and parameters. He found that the parastichy pair (m, n) always satisfies $n \leq m \leq 2n$, where the case $n = m$ indicates whorled phyllotaxis. Also he referred the importance of the ratio of the radius of the primordium assumed to be circular to the radius of the apex, and defined as the bulk ratio B [137, p. 89]. He studied the phenomenon of transitions between different sequence resulting in the change of jugy J, called discontinuous transitions [137, p. 164]. For example, Church observed $(8, 5)$ (unijugate spiral) and $2(5, 3)$ (bijugate) systems in the main axes of *Podocarpus japonica*. The transition to whorled or bijugate can be occurred by either adding or losing parastichy: for example. for system of $(7, 6)$, adding or losing a parastichy can lead to the transition to whorled phyllotaxy $(7, 7)$ or $(6, 6)$, or to bijugate phyllotaxy $(8, 6) = 2(4, 3)$ [137, p. 165]. He insisted that such change in parastichy is caused by the enlargement or contraction of circumference of the apex, as represented by B. In other words, Church's bulk ratio B acts as the key parameter of transitions between different phyllotactic patterns.

Richards (1948, 1951) defined plastochrone ratio R for the ratio of the distances of two successive leaves from the centre of the disc. He related this ratio to several other known indices, such as parastichy pair (m, n), γ, which the angle of intersection of the parastichy pair, and r, which is called rise corresponding to the internode length [137, pp. 77–79]. He further defined two indexes: Phyllotaxis index $P.I. = 0.379 - 2.3923 \log \log R$ and area ratio $A = 1/(2 \ln R)$, which are often used for quantify the phyllotactic patterns [137, p. 90].

Inhibitory field hypotheses from botanical observations. The inhibitory field hypotheses birthed from observation of shoot tip, has been experienced multiple revisions, and now is a widely accepted concept. **Hofmeister**

(1868) observed the shoot apical meristem (SAM) in plants with spiral phyllotaxis and found the developmental rules in the initiation of leaf primordia [131]. His observation can be summarised into three basic rules: the time periodicity of primordia initiation, the initiation of a primordium at the largest available space at the edge of the meristem, and the relative movement of primordia in a centrifugal direction from the apex due to the growth of the stem tip. The most important rule in these three is the initiation of a new primordia at the furthest place from pre-existing other primordia. Originally he stated it is "the least crowded space", but later in the middle 20th century, another idea was derived: "the largest available space".

Snow and Snow (1931) removed the rule for time-periodicity and expanded inhibitory field theory to whorled phyllotaxis. They suggested the rule of the furthest position is only a fundamental rule, and stated that, without any temporal-restriction, when there are enough space to initiate a primordium, then a primordium arises. They physically isolated a leaf primordium of *Lupinus albus*, and found that the initiating position of a new leaf primordium is influenced by the pre-existing leaf primordia adjacent to the site of initiation. This was confirmed later by the laser ablation that the most influential primordium is not temporally but spatially adjacent primordium [226].

Wardlaw (1949) studied the phyllotaxis in the fern using surgical techniques, and obtained substantially consistent results to Snows' observation. He suggested that young primordia are inhibited by older adjacent primordia, and that new primordia typically arise in regions of minimal stress [322].

Following these hypotheses, numerous mathematical models incorporating contact pressure [2, 265], chemical inhibitor [31, 263, 311], and mechanical buckling of the epidermis [112, 197] were proposed to explain the observed phyllotactic patterns.

Physical inhibitory field and contact pressure models: circles instead of points. The idea that the pressure of the growing leaves against each other would compel the divergence to shift toward the particular values that are observed in plants was developed by **Schwendener (1878)** [265] and van Iterson [313], which was rediscovered and extended by **Erickson (1973)**, and inherited into the Adler-Jean theorem.

van Iterson (1907) employed an idea of crystarography and constructed models of packing of circular or curved leaf primordia on a cylinder surface, disc, and cone surface. He recognised the pattern by the "contact spiral" (contact parastichy, see section A), not by the conspicuous parasitichy. He described the transition of phyllotactic pattern by change of parameter b, the ratio of the diameter of the circle representing organs to the circumference of the cylindrical surface [313, p. 26]. He stated the transitions are caused, not by the insertion of parastichy as Church, but by the change of contact between circles: depending on b, the number or the difference (in initiation order) of organs contacting to an organ changes. He also produced a phase-space diagram showing the relationship between parameter b and and divergence angle φ (α, in his notation) [313, Taf. II]. This phase-space diagram is inherited to show the model capacity in modern phyllotaxis studies.

Adler and Jean's fundamental theorem. **Adler (1974)** stated the Fundamental Theorem of Phyllotaxis (FTOP). He clarified the meaning of visible opposed parastichy pair in divergence fraction [2]. In the sequence of normal phyllotaxis with the Fibonacci-type sequence $J < 1, t, t + 1, 2t + 1, 3t + 2, 5t + 3, ... >$ ($t \geq 2$ and $J \geq 1$ are integers) and $N_{t,k} = F_k t + F_{k-1}$ is the general term (F_k is the k-th term of the Fibonacci sequence $< 1, 1, 2, 3, 5, 8, ... >$), the $(JN_{t,k}, JN_{t,k+1})$ is visible and opposed if and only if $F_k/JN_{t,k} < d < F_{k+1}/JN_{t,k+1}$. Calculation of the d for given t and J converges on a specific value of d as k increases. For example, d converges on $1/(1 + \tau)$, the golden angle, when $t = 2, J = 1$. He also gave the relationship between visible opposed parastichy pair and divergence fraction for the sequence of anomalous phyllotaxis in the form of $J < t, 2t + 1, 3t + 1, 5t + 2, ... >$.

The Fundamental Theorem of Phyllotaxis was reworked by **Jean (1984)**, and was given a specific formulation [3]. He formulated the FTOP as follows:

Let (m, n) be a parastichy pair, where m and n are relatively prime, in a system with divergence angle d. The following properties are equivalent:

(1) There exist unique integers $0 \leq v < n$, amd $0 \leq u < m$ such that $|mv - nu| = 1$ and $d < 1/2$ is in the closed interval whose end points are u/m and v/n;

(2) The parastichy pair (m,n) is visible and opposed

This theorem gives the general form of the relationship between observed parastichy counts and the divergence fraction.

Chemical inhibitory field. **Schoute (1913)** proposed the chemical inhibitory-field theory, which insists that the substance of inhibitory field is a chemical inhibitor secreted by pre-existing primordia.

In his celebrated work in 1952, **Turing** discussed the whorled phyllotaxis and floral organ number [311]. He demonstrated the stationary wave formation on the ring by the reaction between two diffusible chemicals, what he called morphogen, and stated this is what occurs around the meristem during the pattern formation in whorled phyllotaxy. On the other hand, he discussed that this is not directly applicable for floral whorls, because in his system all numbers should be occurred in the same frequency, contrary to the flowers that have high frequency on five. He said it requires the phyllotaxis theory to show the mechanism of the dominancy of pentamerous flower, and left some notes on phyllotaxis collaborating with Wardlaw [258].

One representative of Turing pattern is that generated by short-range activation and long-range inhibition [109], and the spot pattern of this system was compared to the phyllotactic pattern. For example, **Chapman and Perry (1987)** regarded the spots generated by reaction-diffusion system as primordia and found that the golden spiral appears on the advected cylinder mimicking growing stem.

Dynamic pattern formation. **Douady and Couder (1992, 1996)** performed an experiment of likening droplets of magnetic fluid to organ primordia. They showed that the constant drop of fluid to magnetic field spontaneously generates the phyllotactic spirals, and that the transition of phyllotactic pattern occurs by the change of the time interval of drip [245]. They performed a series of computer simulations in a developing field. From the first model based on Hofmeister's hypotheses, they found that one key parameter $G = V_0 T / R_0$ (V_0: the initial velocity of the centrifugal replacement of primordia, T: time interval of primordia initiation, R_0: the size of meristematic area where the primordia entering is forbidden), which is related to Richard's plastochrone ratio R, governs the transition between phyllotactic patterns [78]. From a computational model based on Snows' modification, they observed the alternate occurrence of spiral and spiral patterns depending on one parameter $\Gamma = l / R_0$, which is the ratio of the primordium size to R_0 similar to Church's bulk ratio B [79]. They found transition between multiple divergence angle φ by the above parameters, whose phase diagram is almost equivalent to that of van Itersons's. Some limitation are exist, however, for example it cannot reproduce a transient leaf lobed in two, which observed in the transition from trimerous whorl to tetramerous whorl in *Abelia* [80].

The message from phyllotaxis theories to contemporary plant sciences. As reviewed here, numerous theories have been applied for the phyllotaxis. Many assumptions, namely, assuming stem as a cylinder, a disk, or a cone, leaves as a points, circles, or spheres, interaction between primordia caused by physical touching, chemical signal, or energy, etc., have been examined; teleological or evolutionary explanations for sun-light capture or packing have been proposed; their mathematical or botanical aspects have been discussed. The history seems complicated, but the message from these studies is simple: The inhibition between primordia is the fundamental source of phyllotactic pattern. The molecular mechanism of inhibition has been sought since the latter part of 20th century, which was the dawn of the auxin-based theories.

Models for auxin distribution. The main substance that is required and sufficient for organ primordia positioning is auxin, the major phytohormone in plants (see Section B.2). The heterogeneous spatial-distribution of auxin, which is regulated both by directional transport and local biosynthesis, has been suggested as the leading candidate of substance of the inhibitory field. Computational biologists have focused on the polar transport of auxin, especially the polarisation of auxin efflux carrier, and two working hypotheses have been proposed.

Up-the-gradient/against-the-gradient hypothesis states that the the difference of auxin concentration among the cells causes the polarisation of auxin efflux carrier. Jönsson et al. [140] and Smith et al. [278] simulated the auxin concentration distribution and polarisation of auxin efflux carrier PIN1 on growing tissue in the computer and found that the PIN localisation depending on local auxin concentration is able to mimic the phyllotactic patterns. In their scenario, the difference of the concentration between neighbouring cells is sensed by individual cells, and the PIN1s are localised to the cell wall directing the neighbour with the highest auxin concentration. This simple local mechanism is sufficient to generate global phyllotactic pattern, including several common patterns such as golden spiral and decussate pattern. This Turing-like pattern [247] is unstable but can be stabilised if the

activities of influx carrier [19] or boundary factors [214] are taken into account. However, this hypothesis is plausible only at the meristem surface where the PIN1 expression is observed, and not for the other parts.

With-the flux/canalisation hypothesis proposes that auxin fluxes passing through their membranes causes the polarisation of efflux carriers. A positive feedback loop is formed by the concentration of the efflux carriers on the membranes with high flux, which enhances the flux. This hypothesis was firstly proposed by Sachs [246] for the patterning of veins in leaves and stems, and applied for phyllotactic patterns by Stoma et al. [290]. Although with-the-flux hypothesis can produce spatial periodicity, the primordia position corresponds to auxin minima [290], which is inconsistent with observations [28]. Since the with-the-flux mechanism can explain auxin drain from the epidermal layer of the primordia to internal pro-vascular tissue, a combination model applying two auxin-patterning hypotheses to two different tissues, i.e., up-the-gradient mechanism to epidermal phyllotactic pattern and with-the-flux mechanism to internal vascular and venational pattern, was suggested [25].

2.3.2 Floral organ positioning and phyllotaxis models

Similarity between phyllotaxis and floral organ patterning. Despite their simple rules and uncertain molecular basis, the phyllotaxis models can account for several of the quantitative properties observed in floral organ patterning. In the basal eudicots, spirals with Fibonacci sequence and the golden angle also appears in the floral organs of several Ranunculaceae species [188, 261]. The similarity also appears in core eudicots. For example, several models showed that the divergence angle between successive leaves is 180 degrees for the first and second leaves, 90 degrees for the second and third leaves, and oscillating thereafter, converging to the golden angle, 137.5 degrees, which agrees with the phyllotaxis of true leaves in *Arabidopsis thaliana* after the two cotyledons [80, 277]. Similar oscillatory convergence to a particular divergence angle occurs in the sepal primordia of the pentamerous flower of *Silene coeli-rosa*, Caryophyllaceae. In *S. coeli-rosa*, the divergence angle is 156 degrees at first, and then it oscillates, converging on 144 degrees [174]. The agreements between the phyllotaxis models and actual floral development suggest that mathematical models can give useful clues to the underlying mechanisms of not only phyllotaxis but also floral organ patterning.

Difference between phyllotaxis and floral organ patterning. There are at least three fundamental differences between real floral development and the phyllotaxis models. The first difference is the assumption of constant primordium displacement during tip growth, which comes from Hofmeister's hypothesis and has been incorporated into most phyllotaxis models. Although the helical initiation was thought to always result in spiral phyllotaxis, many eudicots form the whorled-type sepal arrangements in their blooming flowers subsequent to helical initiation [90] (Fig. 1.3; e.g., Caryophyllaceae [174], Solanaceae [130], Nitrariaceae [238], and Rosaceae [96]). The remnants of helical initiation are more obvious in the pseudo-whorls (e.g., Ranunculaceae [229]), where the distance between each organ primordium and the floral center varies slightly even in the whorls of mature flowers, which usually have more varied floral organ numbers [236, 261], suggesting that post-meristematic modifications of primordia positions [214] play an essential role in generating the whorled arrangement and determining the floral organ number during floral development. In contrast, most phyllotaxis models assume constant growth of the primordia, so that the whorls appear only after the simultaneous initiation of several primordia [79]. The second difference comes from the fact that floral development is a transient process, whereas most phyllotaxis models have focused on the steady state of the divergence angle. Although the golden angle (137.5 degrees) is quite close to the inner angle of regular pentagon (144 degrees), the developmental convergence from 180 degrees (cotyledon) to 137-144 degrees in phyllotaxis requires the initiation of more than five primordia, both in *A. thaliana* leaves and in the mathematical models [277, 278]. In contrast, the divergence angle between the second and third sepal primordia in pentamerous eudicot flower development is already close to 144 degrees [174]. The third difference comes from the accuracy of the floral organ number in many eudicots. Although the polar auxin-transport model reproduced both wild-type and mutant *A. thaliana* floral organ positioning [314], the organ number in the model was more variable, even with an identical parameter set (Fig. 3 in [314]), than that in experimental observations (Tab. 1 in [244]). Moreover, among eudicot species, the appearance of pentamerous flowers is robust, despite the diversity of the meristem size and the outer structures, including the number and position of outside organs such as bracts [236]. Together, the differences between real floral development and previous phyllotaxis models indicate that floral development requires additional mechanisms to determine the particular floral organ number.

12

2.4 Model

To resolve the inconsistencies between the earlier models and actual floral development, I set out a simple modelling framework, integrating Hofmeister's rules with two additional assumptions, namely, the repulsion between primordia that can repress primordium growth and the temporal decrease in initiation inhibition of new primordium, which were proposed independently in the contact pressure model [2,125,234] and the inhibitory field model [114,277,301], respectively, for phyllotaxis.
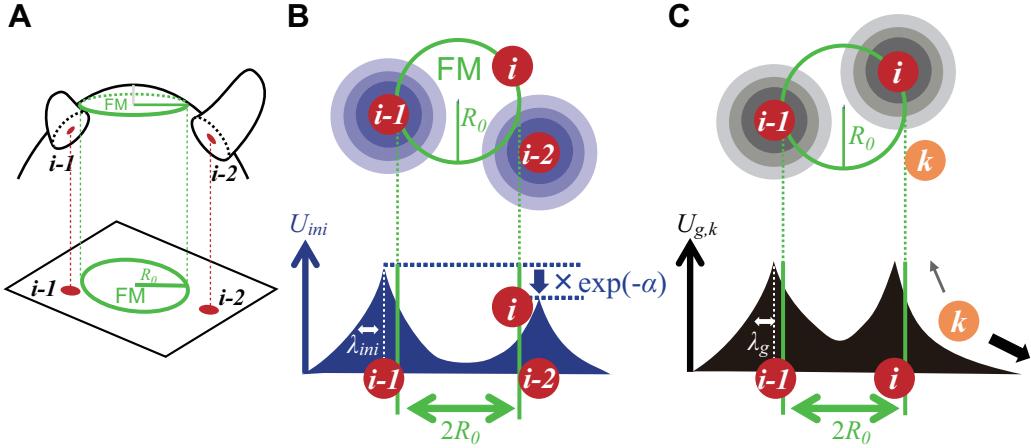

Figure 2.1: **Schematic diagram for the model. A.** Geometric assumptions of the model. The model illustrates the initiation (**B**) and growth (**C**) processes. **B.** A new primordium (i) is initiated at the edge of the floral meristem (FM; green circle) where the initiation potential U_{ini} takes the minimum value. i, $i-1$, and $i-2$ are the primordium indices that denote the initiation order. U_{ini} exponentially decreases with time (α) and the distance between primordia (λ_{ini}). **C.** Each primordium (k) moves at the outside of the circular FM, depending on the growth potential $U_{g,k}$. Primordium k rarely moves against the gradient (grey arrow), but mostly follows the gradient (black arrow; see the Model section).

Following Hofmeister's rules as mathematically interpreted by Douady and Couder [78], I focused on initiation and growth, the two processes of floral development. In the initiation process, each primordium emerges successively at the least crowded position, depending on a potential function [78]. I assumed periodic initiation to examine how the sequential initiation results in the whorled-type pattern. I allowed the primordia to move during the growth process in response to the repulsion among the primordia, unlike earlier studies that assumed constant growth depending only on the distance from the apex [31,78].

The initiation process Following the earlier models [78], I represented the meristem as a circular disc with radius R_0 and the primordia as points (Fig. 2.1A). A new primordium arises at the point along the edge of the meristem (R_0, θ), in polar coordinate with the origin at the meristem center, where θ gives the minimum value of the inhibition potential U_{ini}. As one of the simplest set-ups for sequential initiation [90], I followed the assumption of earlier models for spiral phyllotaxis [78], which stated that new primordia arise sequentially with time intervals τ, as opposed to the simultaneous initiation studied previously for whorled phyllotaxis [79] (Fig. 1.3). Although the structures outside of the flower, such as bracts and other flowers, as well as the position of the inflorescence axis, may affect the position of organ primordia, the pentamerous whorls appear despite their various arrangement [236]. Therefore, as the first step of modelling of floral organ arrangement, I assumed that whorl formation is independent of any positional information from structures outside of the flower. Thus, I calculated the inhibition potential only from other primordia.

The potential functions for the initiation inhibition by pre-existing primordia have been extensively analysed

in phyllotaxis models [78, 278, 301]. The potential decreases with increasing distance between an initiating primordium and the pre-existing primordia, which can account for the diffusion of inhibitors secreted by the pre-existing primordia [263, 322], and the polar auxin transport in the epidermal layer, as proposed in previous models of phyllotaxis [21, 140, 278] and the flowers [314]. I employed an exponential function

$$\exp\left(-d_{ij}/\lambda_{ini}\right) \tag{2.1}$$

as a function of θ, where d_{ij} denotes the distance between a new primordium i and a pre-existing primordium j at (r_j, θ_j) as

$$d_{ij} = \sqrt{R_0^2 + r_j^2 - 2R_0 r_j \cos\left(\theta - \theta_j\right)}. \tag{2.2}$$

The function decreases spatially through the decay length λ_{ini} exponentially, induced by a mechanism proposed for the polar auxin transport, i.e., the up-the-gradient model [140, 278]. Up-the-gradient positive feedback amplifies local auxin concentration maxima and depletes auxin from the surrounding epidermis, causing spatially periodic concentration peaks to self-organize [140, 278] and thus determine the initiation position of the primordia [28]. The amplification and depletion work as short-range activation and long-range inhibition, respectively [312], which are common to Turing patterns of reaction-diffusion systems [311]. Since the interaction of local maxima in the reaction-diffusion systems follows the exponential potential [82, 202], the up-the-gradient model likely explains the exponential potential between the auxin maxima. The decay length λ_{ini} depends not only on the ratio of the auxin diffusion constant and the polar auxin-transport rate [140] but also on other biochemical parameters for polar transport and the underlying intracellular PIN1 cycling [247]. The other mechanism, with-the-flux model, can be responsible for the auxin drain from the epidermal layer of the primordia to internal tissue [25]. Since the drain gets stronger as the primordia mature [25, 104], the auxin drain could cause decay of the potential depending on the primordia age. The auxin decrease in maturing organs can also be caused by controlling auxin biosynthesis [51, 217]. Therefore, I integrated another assumption that the inhibition potential decreases exponentially with the primordia age at the decay rate α (Fig. 2.1B). Temporally decaying inhibition was proposed previously to represent the degradation of inhibitors [114, 301] and account for various types of phyllotaxis by simple extension of the inhibitory field model [277].

Taken together, the potential at the initiation of the i-th primordium is given by

$$U_{ini}(\theta) = \sum_{j=1}^{i-1} \exp\left(-\alpha\left(i - j - 1\right)\right) \exp\left(-\frac{d_{ij}}{\lambda_{ini}}\right). \tag{2.3}$$

The growth process Most phyllotaxis models have assumed, based on Hofmeister's hypothesis, that the primordia move outward at a constant radial drift depending only on the distance from the floral center without angular displacement, which makes helical initiation result in spiral phyllotaxis [78]. I assumed instead that all primordia repel each other, even after the initiation, except for movement into the meristematic zone following observation of the absence of auxin ($DR5$ expression) maxima at the center of the floral bud [123] (Fig. 2.1C). The growth is not limited at the peripheral zone away from the meristem, therefore there is no upper limit for the distance between primordia and the center. The repulsion exerted on the k-th primordium is represented by another exponentially decaying potential when there are i primordia ($1 \leq k \leq i$):

$$U_{g,k}(r, \theta) = \sum_{j=1, j\neq k}^{i} \exp\left(-\frac{d_{kj}}{\lambda_g}\right), \tag{2.4}$$

where the decay length, introduced as λ_g, can differ from λ_{ini}. The primordia descend along the gradient of potential U_g to find a location with weaker repulsion. The continuous repulsion can account for post-meristematic events such as the mechanical stress on epidermal cells caused by the enlargement of primordia [116, 146] that is supported by the fact that the ablation of surrounding primordia can enlarge the primordium width [226], or the gene expression that regulates the primordial boundary [214]. The present formulation (Eq. 2.4) is similar to the contact pressure model, which has been proposed for re-correcting the divergence angle after initiation [2, 125, 234]. Another type of post-initiation angular rearrangement has been modelled as a function of the primordia age employed as $i - j - 1$ in

the present model (Eq. 2.3) and the distance between primordia with some stochasticity [189]. Eq. 2.4 accounts for not only the angular rearrangement but also the radial rearrangement with stochasticity in both directions as will be described in the next subsection.

Numerical experiments I modelled the initiation process numerically by calculating the potential U_{ini} (Eq. 2.3) for angular position θ incremented by 0.1 degree on the edge of the circular meristem. I introduced a new primordium at the position where the value of U_{ini} took the minimum, provided that the first primordium is initiated at $\theta = 0$. I modelled the growth process by using a Monte Carlo method [160] to calculate the movement of primordia in the outside of the meristem depending on the potential $U_{g,k}$ (Eq. 2.4, Fig. 2.1C). After the introduction of a new primordium, I randomly chose one primordium indexed by k from among the existing primordia and virtually moved its position (r_k, θ_k) to a new position (r'_k, θ'_k) in the outer meristem $(r_k, r'_k \geq R_0)$. The new radius r'_k and the angle θ'_k were chosen randomly following a two-dimensional Gaussian distribution whose mean and standard deviation were given by the previous position (r_k, θ_k) and by two independent parameters, $(\sigma_r, \sigma_\theta/r_k)$, respectively. Whether or not the k-th primordium moved to the new position was determined by the Metropolis algorithm [160]; the primordium moved if the growth potential (Eq. 2.4) of the new position was lower than that of the previous position (i.e., $U_{g,k}(r'_k, \theta'_k) < U_{g,k}(r_k, \theta_k)$). Otherwise, it moved with the probability given by

$$P_{MP} = \exp\left(-\beta \Delta U_g\right), \tag{2.5}$$

where $\Delta U_g = U_{g,k}(r'_k, \theta'_k) - U_{g,k}(r_k, \theta_k)$ and β is a parameter for stochasticity. This stochasticity represents a random walk biased by the repulsion potential. A case $P_{MP} = 0$ represents that primordia movement always follows the potential ($\Delta U_g < 0$). The first primordium stays at the meristem edge $r = R_0$ until the second one arises when $P_{MP} = 0$ because the growth potential is absent, while it can move randomly outside of the meristem when $P_{MP} \neq 0$. To maintain the physical time interval of the initiation process at τ steps for each primordium, the number of iteration steps in the Monte Carlo simulation during each initiation interval was set to $i\tau$, where i denotes the number of the primordia. All programs were written in the C programming language and used the Mersenne Twister pseudo-random number generator (http://www.math.sci.hiroshima-u.ac.jp/~m-mat/MT/emt.html) [181].

2.5 Results of numerical simulations

Because the initiation time interval is set as constant, one possible scenario for allowing a whorled pattern should involve decreasing or arresting the radial displacement of primordia (Fig. 1.3, forth row). Therefore, I focused on the change in radial position and velocity, while angular positions were not taken into account.

Mutually repulsive growth promotes a whorled arrangement from sequential initiation at the proper meristem size Numerical simulations showed that several whorls self-organised following the sequential initiation of primordia. Although several previous phyllotaxis models showed the transition between a spiral arrangement following sequential initiation and a whorled arrangement following simultaneous initiation [79,140,278], they were not able to reproduce the emergence of a whorled arrangement following sequential initiation, which is the situation observed in many eudicot flowers (see section B.5.2) [90,96,130,174,229]. In the present model, a tetramerous whorl appeared spontaneously that exhibited four primordia almost equidistant from the meristem center (Fig. 2.2A, left and middle), by arresting radial movement of the fifth primordium at the meristem edge until the seventh primordium arose (arrowhead in Fig. 2.2A, right). Likewise, subsequent primordia produced the same gap in radial distance for every four primordia (Fig. 2.2A, middle and right), leading to several whorls comprising an identical number of primordia (Fig. 2.2A). The radial positions of all primordia were highly reproducible despite stochasticity in the growth process (error bars in Fig. 2.2A–C, middle and right). Therefore, I identified the whorled arrangement by radial displacement arrest (arrowhead in Fig. 2.2A, right).

I also studied the movement following U_g by the ordinary differential equations to confirm the independence of the numerical methods (Fig. 2.3). The spontaneous emergence of whorled arrangement is also observed if the primordia displacement is calculated by the ordinary differential equations.

The initiation order and angle of the first tetramerous whorl in the model reproduced those observed in *Arabidopsis thaliana* sepals [279] (Fig. 2.4). The first primordium scarcely moved from the initiation point until the

15
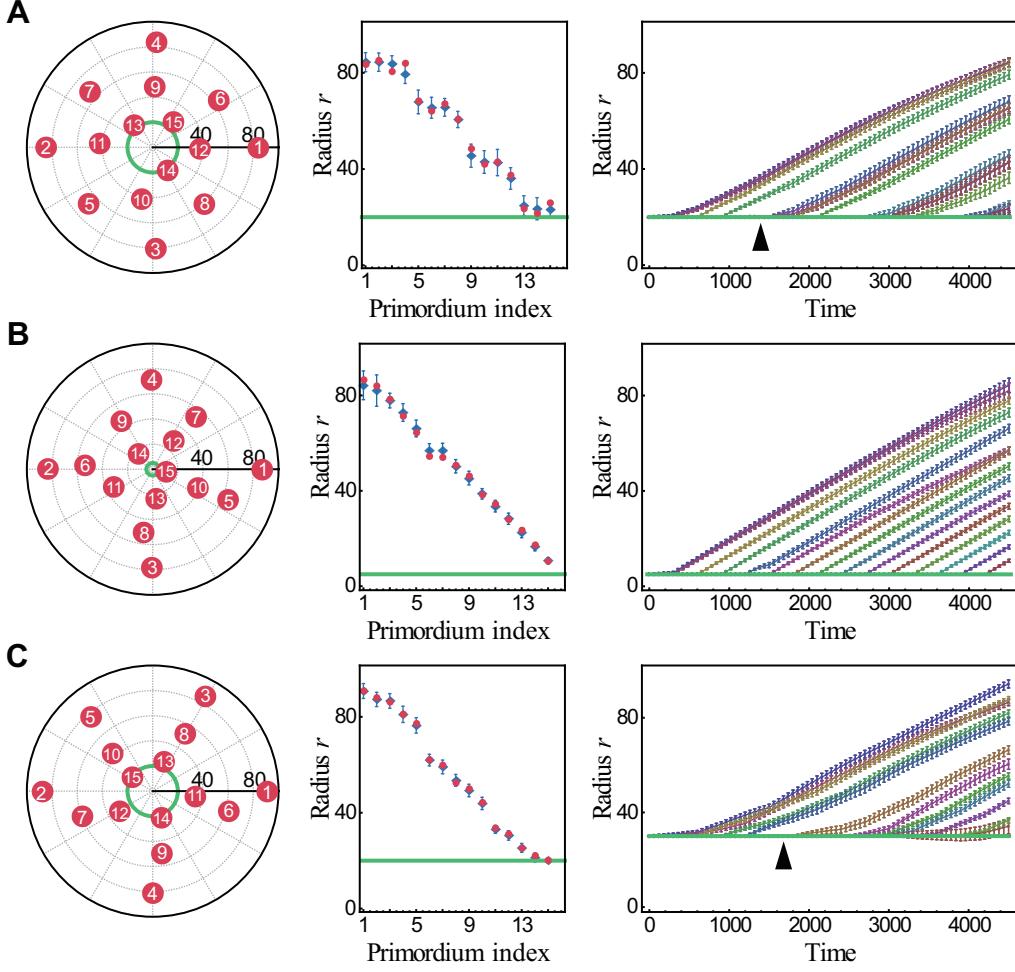
Figure 2.2: **The spontaneous emergence of whorled-type pattern with increasing meristem radius R_0 and temporal decay rate α.** Left panels: Spatial pattern after 15 primordia (red points) initiated in an indexed order at the meristem edge (green circle; $r = R_0$). Middle panels: Radial distance (blue) from the meristem center as a function of the primordium initiation index (left panel) averaged over 400 replicate Monte Carlo simulations. Error bars represent twice the S.D. Red points are a set of representative samples. Right panels: Time evolution of the radial coordinates of each primordium averaged over 400 replicates. Error bars show 2 S.D. The arrowheads in **A** and **C** indicate the growth arrest of the fifth and sixth primordia, respectively. Colours denote the index of the primordia. Green line in the left, middle and right panels denotes the meristem edge. $(R_0, \alpha) = (20.0, 0.0)$ in **A**, $(5.0, 0.0)$ in **B** and $(20.0, 2.0)$ in **C**. $\beta = 1.0 \times 10^4$, $\lambda_{ini} = \lambda_g = 10.0$, $\tau = 300$, and $\sigma_r = \sigma_\theta = 0.05$ in **A**–**C**.
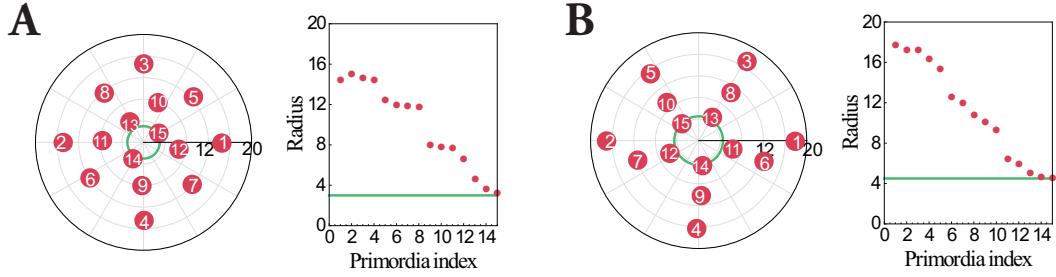
Figure 2.3: **The emergence of whorled-pattern using another method for numerical calculation of growth process.** The tetramerous (**A**) and pentamerous (**B**) pattern generated by numerical integration (fourth-order Runge-Kutta method) of the ordinary differential equation $dr_k/dt = -\partial U_{g,k}/\partial r_k$, $d\theta_k/dt = -(1/r_k)\partial U_{g,k}/\partial \theta_k$, which was used instead of the Monte Carlo method. I confirmed (1) the emergence of whorled arrangements as shown in this figure (consistent with Fig. 2.2) and (2) the dominance of the tetramery at $\alpha = 0$ and the pentamery at $\alpha > 0$ (consistent with Fig. 2.6). $\lambda_g = \lambda_{ini} = 2.5$. **A.** $R_0 = 3.0$, $\tau = 17.5$, $\alpha = 0.0$. **B.** $R_0 = 4.5$, $\tau = 25$, $\alpha = 2.0$.
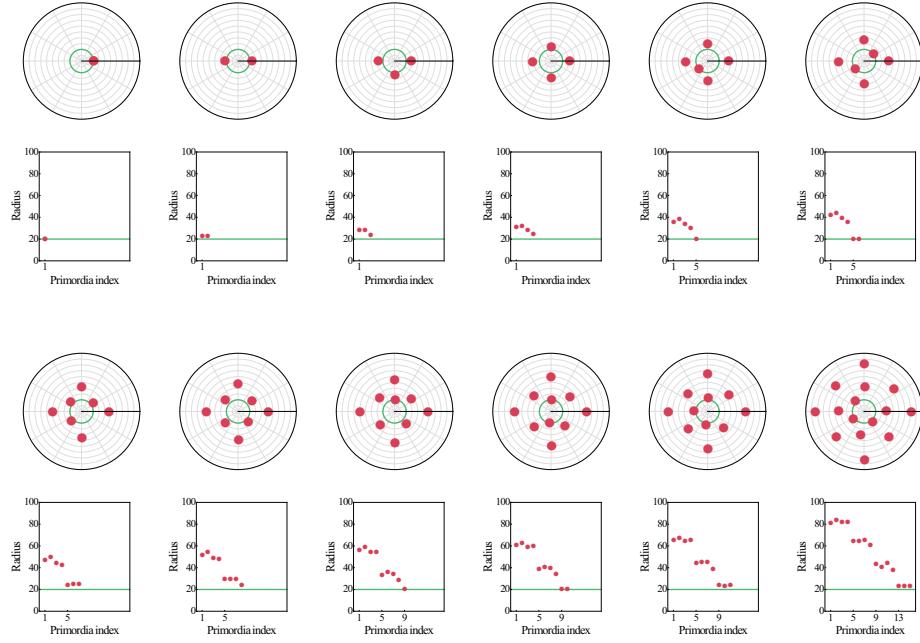
Figure 2.4: **The time-course of tetramerous whorl emergence in the model simulation.** Parameters are the same to Fig. 2.2A.

second primordium arose because growth repulsion was absent. The second primordium arose opposite the first, whereas the third and fourth primordia arose perpendicular to the preceding two. The angular position of the primordia did not change once the whorl was established because the primordia within a whorl blocked the angular displacement by the growth potential U_g (cf. Fig. 2.10 in the next section).

Introducing mutual repulsion among the primordia throughout the growth process caused the whorled arrangement to spontaneously emerge (Fig. 2.2A). This was in contrast to the model of constant growth in which all primordia arise depending only on the distance from the floral apex [78]. A study of post-meristematic regulation by the organ-boundary gene *CUC2* (section B.3.3) showed that the *Arabidopsis* plants up-regulating *CUC2* gene have an enlarged primordial margin and have whorled-like phyllotaxis following the normal helical initiation of primordia [214], suggesting that repulsive interactions among primordia after initiation are responsible for the formation of the floral whorls.

In the present model, the meristem size R_0 controls the transition from non-whorled (Fig. 2.2B) to whorled arrangement (Fig. 2.2A). Radial spacing of the primordia was regular when R_0 was small (Fig. 2.2B, middle) because the older primordia pushed any new primordium across the meristem (Fig. 2.2C, left), causing continuous movement at the same velocity (Fig. 2.2C, right). Above a threshold meristem size R_0, a tetramerous whorl appeared spontaneously via locking the fifth primordium at the meristem edge. The primordia number within each whorl increased with increasing R_0. In the *A. thaliana* mutant *wuschel*, which has a decreased meristem size, the pattern of four sepals does not have square positions at the stage when the wild-type plant forms a tetramerous sepal whorl [262]. Conversely, the *clavata* mutant, which has an increased meristem size, has excessive floral organs [262]. The present model consistently reproduced not only the transition from the non-whorled arrangement (Fig. 2.2B) to the tetramerous whorled arrangement (Fig. 2.2A) but also the increase in the primordia number within a whorl as the meristem size R_0 increased.
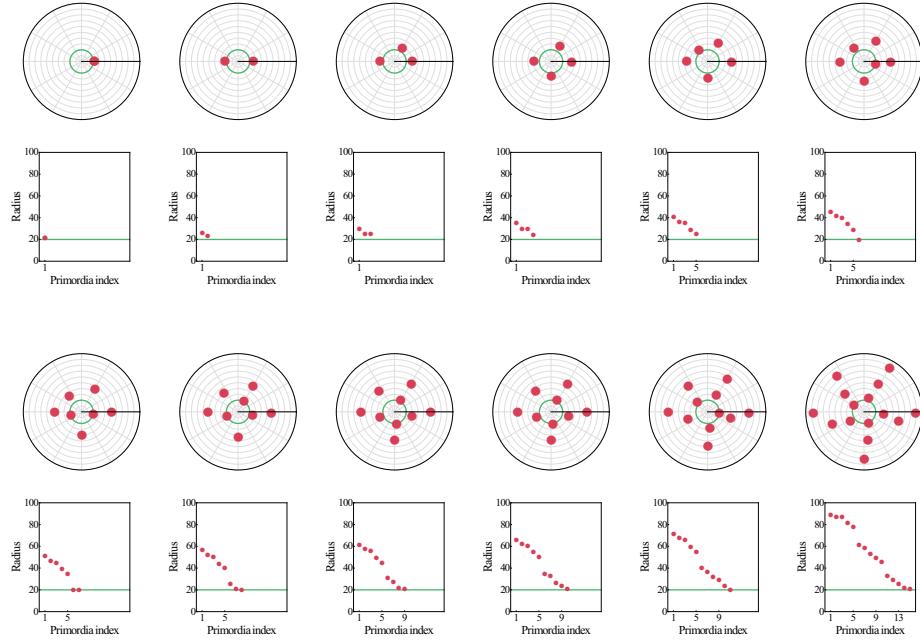

Figure 2.5: **The time-course of pentamerous whorl emergence in the model simulation.** Parameters are the same to Fig. 2.2C.

Developmental preference for particular organ number within a whorl In order to study the organ number within each whorl extensively, known as the merosity [239], I counted the number of primordia existing

18

prior to the arrest of primordium displacement, which corresponds to the merosity of the first whorl (arrowheads in Fig. 2.2A and C, right). I defined arrest of primordium displacement as occurring when the ratio of the initial radial velocity of a new primordium immediately after initiation to that of the previous primordium was lower than 0.2. The definition does not affect the following results as long as the ratio is between 0.1 and 0.6. I found that the key parameter for merosity is the relative value of R_0 normalized by the average radial velocity V (see Appendix) and the initiation time interval τ (Fig. 2.6). The arrest of radial displacement did not occur below a threshold of $R_0/V\tau$ (the left region coloured red in Fig. 2.6A, red circles), whereas the whorled arrangement appeared above the threshold value of $R_0/V\tau$. As $R_0/V\tau$ increased further, tetramery, pentamery, hexamery, heptamery, and octamery appeared, successively (Fig. 2.6A).

The present model showed dominance of special merosity, i.e., tetramery and octamery in the absence of temporal decay of inhibition ($\alpha = 0$ in Eq. 2.3; Fig. 2.6A); pentamery in the presence of temporal decay ($\alpha > 0$; Fig. 2.6B and C), in contrast to previous phyllotaxis models for whorled arrangement in which the parameter region leading to each level of merosity decreased monotonically with increasing merosity [79]. The major difference between $\alpha = 0$ and $\alpha > 0$ was that θ_3, the angular position of the third primordium, took an average value of 90 degrees when $\alpha = 0$ (arrowhead in Fig. 2.6A bottom magenta panel) and decreased significantly as α increased (arrowhead in Fig. 2.6A bottom cyan panel). In a pentamerous flower *Silene coeli-rosa*, the third primordium is located closer to the first primordium than the second one [174]. This is consistent with the third primordium position at $\alpha > 0$, indicating the necessity of α, as I will discuss in the next section. We divided R_0 by the average radial velocity V (see the next section) and the initiation time interval τ to make a dimensionless parameter $R_0/V\tau$. The parameter region $R_0/V\tau$ for pentamery expanded with increasing α, whereas the border between the whorled and non-whorled arrangements was weakly dependent on α (Fig. 2.6C). The tetramery, pentamery, and octamery arrangements were more robust to $R_0/V\tau$ and α than the hexamery and heptamery arrangements. Dominance of the particular number also appears in the ray-florets within a head inflorescence of Asteraceae [170], in which radial positions show the whorled-type arrangement [24]. Meanwhile, the leaf number in a single vegetative pseudo-whorl transits between two to six by hormonal control without any preference [158].

Moreover, the transition between the different merosities occurred directly, without the transient appearance of the non-whorled arrangement. This is in contrast to an earlier model [79] in which the transition between different merosity always involved transient spiral phyllotaxis. The fact that the merosity can change while keeping its whorled nature in flowers (e.g., the flowers of *Trientalis europaea* [182]) supports my results. To my knowledge, this is the first model showing direct transitions between whorled patterns with different merosities as well as preferences for tetramery and pentamery, the most common merosities in eudicot flowers.

Reconstructing the *Silene coeli-rosa* pentamerous whorl arrangement To further validate the present model of the pentamerous whorl arrangement, I quantitatively compared its results with the radial distances and divergence angles in eudicot flowers. Here I focus on a Scanning Electron Microscope (SEM) image of the floral meristem of *S. coeli-rosa*, Caryophyllaceae (Fig. 2.7A–C) [174], because *S. coeli-rosa* exhibits not only five sepals and five petals in alternate positions, which is the most common arrangement in eudicots, but also the helical initiation of these primordia, which I targeted in the present model. In addition, to my knowledge, this report by Lyndon is the only publication showing a developmental sequence for both the divergence angle $\Delta\theta_{k,k+1} = \theta_{k+1} - \theta_k$ ($0 \leq \Delta\theta_{k,k+1} < 360$) and the ratio of the radial position, r_k/r_{k+1}, referred to as the plastochrone ratio [230], in eudicot floral organs. Reconstructing such developmental sequences of both radial and angular positions is an unprecedented theoretical challenge, while those which describe the angular position alone for the ontogeny of spiral phyllotaxis (180 degree, 90 degree and finally convergence to 137 degree [277, 278]; the 'M-shaped' motif, i.e., 137, 275, 225, 275 and 137 degrees [32, 113]) have been reproduced numerically.

By substituting the initial divergence angle between the first and second sepals of *S. coeli-rosa* into $\Delta\theta_{1,2} = 156$ but not any plastochrone data into the simulation ($\theta_1 = 0$ and $\theta_2 = 156$ degree), I numerically calculated the positions of the subsequent organs (Fig. 2.7D). The observed divergence angle $\Delta\theta_{2,3} = 132$ degree indicates $\alpha > 0$, because $\Delta\theta_{2,3} = \Delta\theta_{1,3} = (360 - 156)/2 = 102$ degree at $\alpha = 0$, in the present model setting $r_1 \cong r_2$. Even when $r_1 > r_2$, the divergence angle was calculated as $\Delta\theta_{2,3} = 113$ degree ($r_1 = R_0 + 2V\tau$, $r_2 = R_0 + V\tau$, $R_0 = 1$, $V\tau = 0.14$, and $\lambda_{ini} = 0.05$ estimated from the *S. coeli-rosa* SEM image [174]; see Fig. 2.8 for detail), which is still less than the observed value. As α became larger, the inhibition from the second primordium became stronger than that from the first one, making $\Delta\theta_{2,3}$ consistent with the observed value in *S. coeli-rosa* (Fig. 2.7E, top).

19
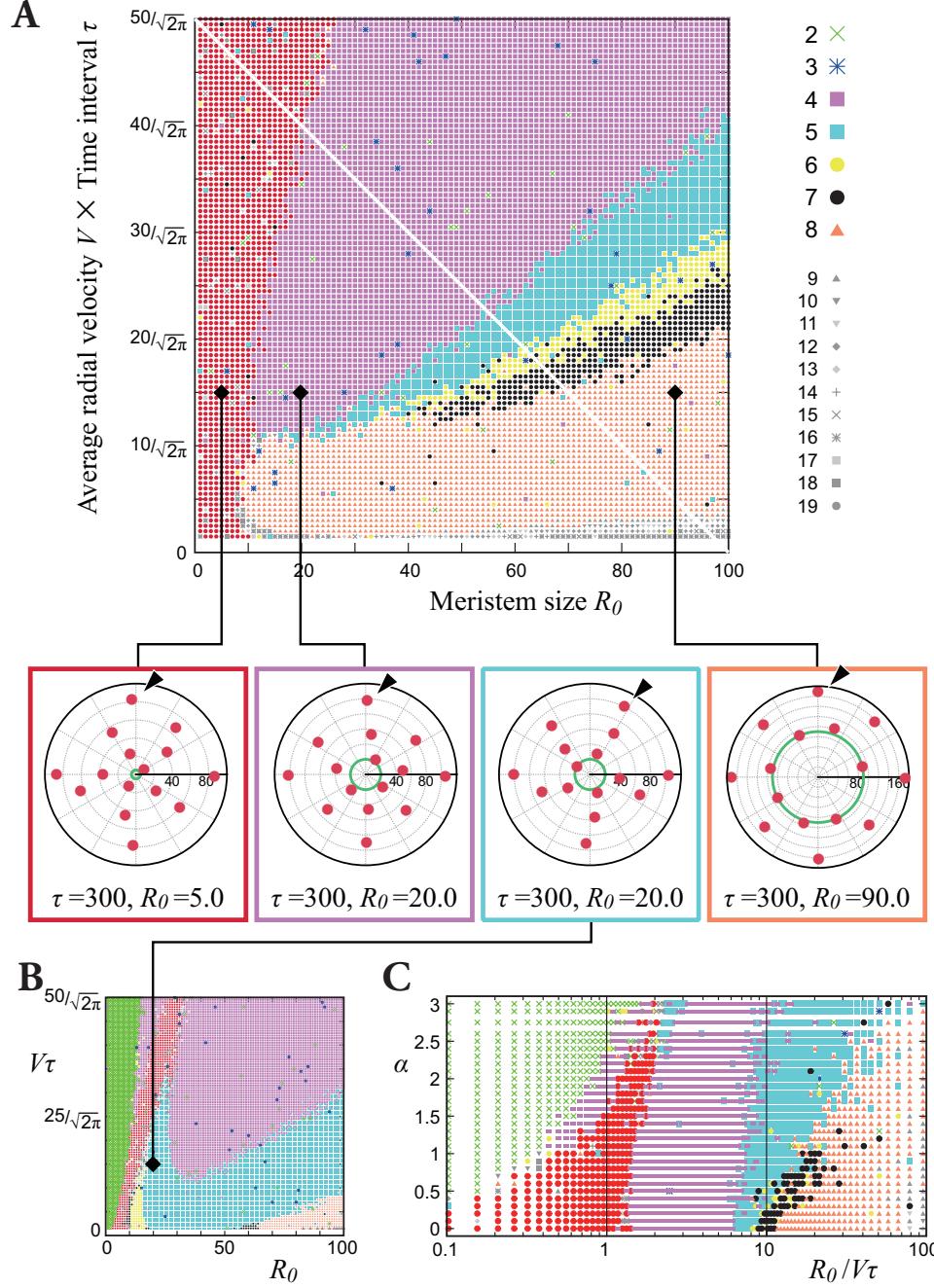
Figure 2.6: **Merosity of the first whorl. A, B.** The number of primordia before the first arrest (arrowheads in Fig. 2.2A and C) is depicted by colors in the legend. The red region indicates a non-whorled pattern. For simplicity, I set $P_{MP} = 0$ (Eq. 2.5) so that primordia could not move against the potential gradient $U_{g,k}$. $\lambda_{ini} = \lambda_g = 10.0$, $\sigma_r = \sigma_\theta = 0.05$. $\alpha = 0.0$ (**A**) and $\alpha = 2.0$ (**B**). The four panels between **A** and **B** are representative examples of each merosity where the arrowhead indicates the third primordium. **C.** Phase diagram of the first-whorl merosity according to α and $R_0/V\tau$ at $V\tau = (-0.5R_0 + 50)/\sqrt{2\pi}$ (white line in **A**). The color code is the same as that in **A** and **B**. The region of dimerous arrangement (green) increases as α increases, because the previous primordium becomes the most dominant inhibitor so that the new primordium initiates just opposite to the previous one and its growth is arrested by the second previous one.
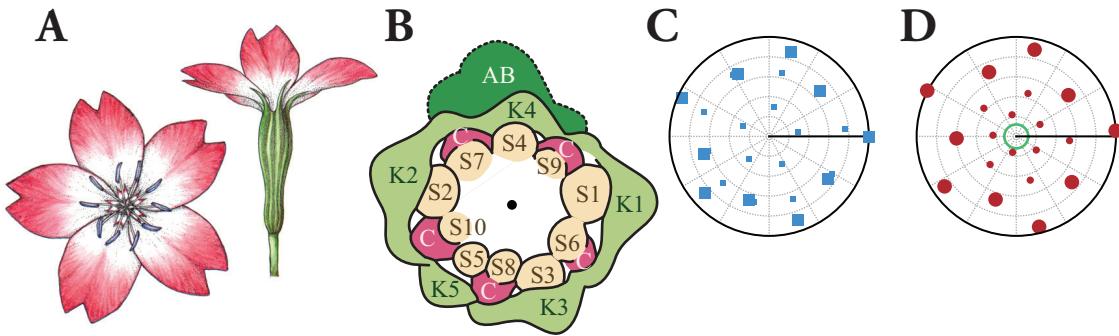
Figure 2.7: **Reconstructing pentamerous floral development. A.** Flower of *Silene coeli-rosa* (Caryophyllaceae). **B.** Reproduction of the *S. coeli-rosa* floral meristem traced from an SEM image by Lyndon [174]; the colors were modified. Numbers indicate the initiation order. K (sepals), C (petals), S (stamens), AB (axillary bud). **C.** Average position of the *S. coeli-rosa* floral primordia reconstructed from the divergence angle and plastochrone ratio measured by Lyndon (Table 1 in [174]). The smallest number of measured apices is $N = 9$ for sepals, 5 for petals, 7 for stamens, and 2 for carpels. The positions of sepals and petals are depicted in large squares, and those of stamens and carpels are depicted in small squares. **D.** Spatial pattern of the model simulation. The first ten primordia are shown by large circles, and the subsequent ten primordia are shown by small circles. $\tau = 600$, $R_0 = 30.0$, $\alpha = 3.0$, $\sigma_r = 0.05$, $\sigma_\theta = 5.0$, $\lambda_{ini} = \lambda_g = 20.0$, $P_{MP} = 0$. The green line in **D** indicates the meristem boundary in the simulation.
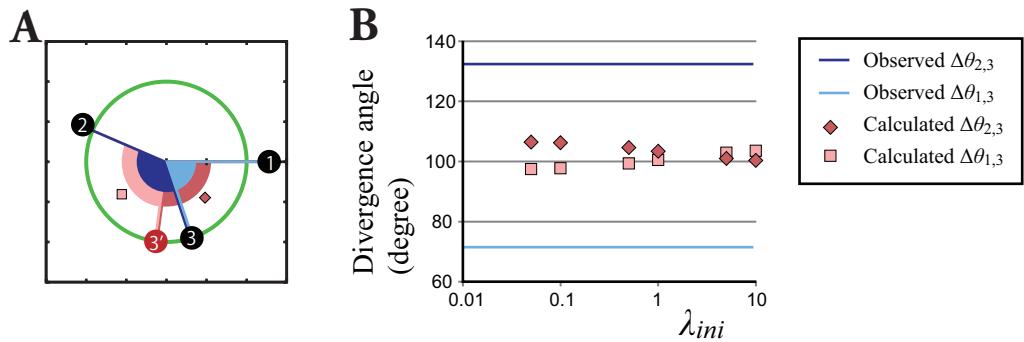
Figure 2.8: **Analytical calculation at $\alpha = 0$ could not account for the third primordium position of *Silene coeli-rosa*. A.** Black circles 1–3 demonstrate the positions of the first to third primordia. The angles were from experimental observation [174] and radii were estimated as $r_1 = R_0 + 2V\tau$, $r_2 = R_0 + V\tau$, and $r_3 = R_0$. $R_0 = 1.0$ and $V\tau = 0.14$ were obtained from the radius of the centermost carpel, which I assumed as the meristem edge and average of the radial difference between successive sepals, respectively, normalized by the radius of the centermost carpel. A red circle 3′ shows the position of the third primordium analytically calculated from the observed positions of the first and second ones at $\alpha = 0$. $\lambda_{ini} = 0.05$. **B.** The divergence angle between the third and second ($\Delta\theta_{2,3}$), as well as third and first primordia ($\Delta\theta_{1,3}$), as a function of λ_{ini}. In **A** and **B**, the observed $\Delta\theta_{2,3}$ and $\Delta\theta_{1,3}$ are represented in blue and pale blue, respectively, whereas the calculated $\Delta\theta_{2,3}$ and $\Delta\theta_{1,3}$ are depicted in pale red and red, respectively.

21
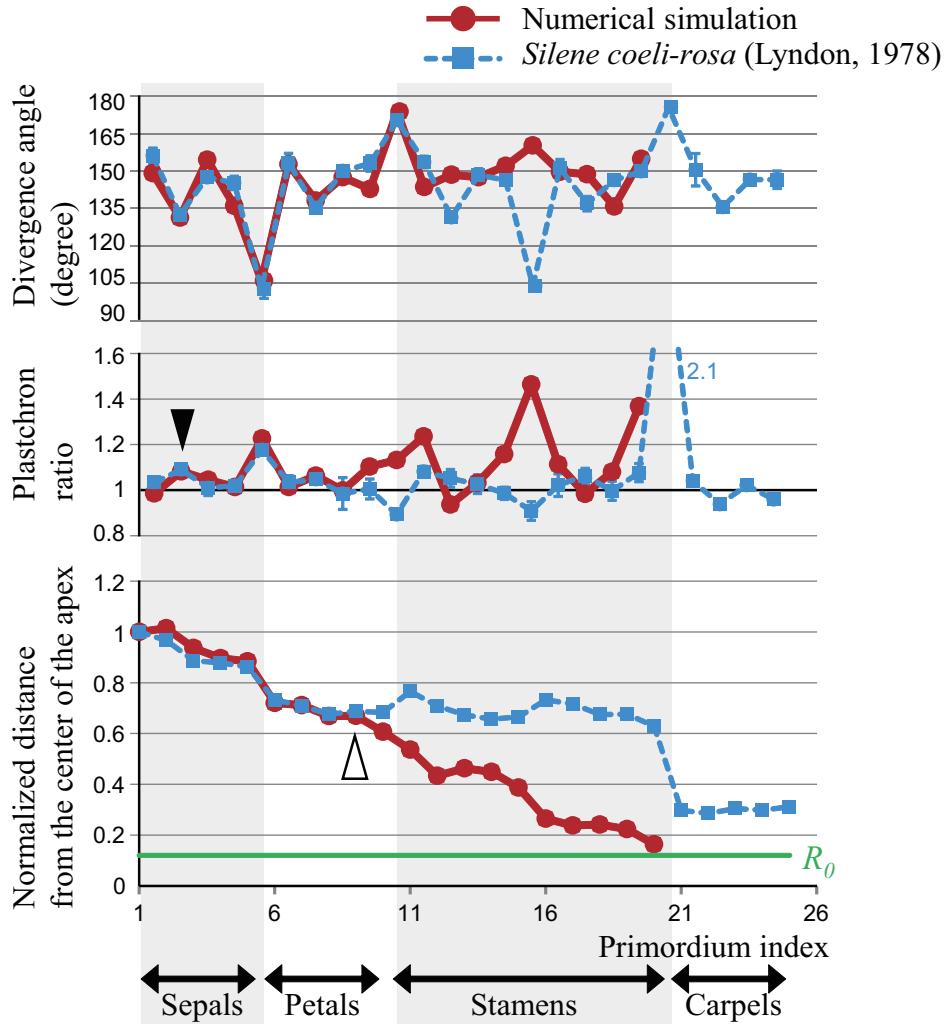
Figure 2.9: **The comparison of phyllotactic values between the numerical result and the real floral development.** Divergence angle (top panel) and plastochrone ratio (middle) between two succeeding primordia, and the distance from the center of the apex (bottom panel) in *S. coeli-rosa* (blue squares) and in the model simulation (red circles). The order of petal initiation was estimated from that of the adjacent stamens (S6-S10 in Fig. 2.7**B**) following the experimental report [174]. The measurements agree with the model until the ninth primordium (open arrowhead). Error bars for the divergence angle and plastochrone ratio of *S. coeli-rosa* denote the standard errors. Because the absolute values of the *S. coeli-rosa* primordia radii were not published, the distance from the center is normalized by the radius of the first sepal. The values of the parameters are the same as those in Fig. 2.7**D**. The green line in the bottom panel indicates the meristem boundary in the simulation.

For the subsequent sepals and petals, the model faithfully reproduced the period-five oscillation of the divergence angle and the plastochrone ratio until the ninth primordium (Fig. 2.9), notably in the deviation of the divergence angle from regular pentagon (144 degree) and the increase of plastochrone ratio at the boundary between the sepal and petal whorls. Moreover, a similar increase in the plastochrone ratio occurred weakly between the second and third primordia in the first whorl (closed arrowhead in Fig. 2.9), indicating a hierarchically whorled arrangement (i.e., whorls within a whorl). Such weak separation of the two outer primordia from the three inner ones within a whorl is consistent with the quincuncial pattern of sepal aestivation that reflects spiral initiation in most eudicots with pentamerous flowers (e.g., Fig. 2D–E in [91]). Even with an identical set of parameters, the order of initiation in the first pentamerous whorl can vary depending on the stochasticity in the growth process. The variations of the initiation order in simulations may be caused by the absence of the outer structure, because the axillary bud seems to act as a positional information for the first primordia (Fig. 2.7B). The positioning of the five primordia in the first whorl was reproducible in 70% of the numerical replicates, within less than 20 degrees of that in *S. coeli-rosa* or that of the angles in a regular pentagon. Mismatches in the inner structure (from the tenth primordium, i.e., the last primordium in petal whorl) might be due to an increase in the rate of successive primordia initiation later in development [261], which I did not assume in the present model. The agreements between the present model and actual *S. coeli-rosa* development of sepals and petals in both the angular and the radial positions suggests that the *S. coeli-rosa* pentamerous whorls are caused by decreasing inhibition from older primordia.

2.6   Analytical results

Mechanism for the tetramerous whorl emergence.   A possible mechanism to arrest the radial displacement of a new primordium, a key process for whorl formation (arrowheads in Fig. 2.2A,C), involves an inward-directed gradient of the growth potential $U_{g,k}$ (Eq. 2.4) of a new primordium so that its radial movement is prevented. To confirm this for tetramerous whorl formation (Fig. 2.6A), I analytically derived the parameter region such that the radial gradient of the growth potential at the angle of the fifth primordium $U_{g,5}$ (Eq. 2.4), which is determined by the positions of the preceding four primordia, is inward-directed. For ease in the analytical calculation, I set $\alpha = 0$ and $P_{MP} = 0$.

Analytical derivation of the average radial velocity during growth.   The radial velocity of primordia averaged over the growth process is approximately derived by integrating Monte Carlo steps. The radial displacement of the primordium k in a single Monte Carlo step given by $x = r'_k - r_k$ follows a Gaussian distribution (see Numerical experiments in the Model section) given by

$$\frac{1}{\sqrt{2\pi\sigma_r^2}} \exp\left(-\frac{x^2}{2\sigma_r^2}\right),$$

where the average and the standard deviation are zero ($r_k = r'_k$) and σ_r, respectively. At $P_{MP} = 0$, when the radial gradient of the growth potential $U_{g,k}$ is negative, the Metropolis method always selects outward movement (see Numerical experiments in the Model section) so that the actual movement follows a one-sided truncated Gaussian distribution ($x \geq 0$). The average radial velocity V is approximated as the expected value given by

$$V = \int_0^\infty \frac{x}{\sqrt{2\pi\sigma_r^2}} \exp\left(-\frac{x^2}{2\sigma_r^2}\right) dx = \frac{\sigma_r}{\sqrt{2\pi}}. \tag{2.6}$$

Hence, during the time interval τ of primordia initiation, all primordia move radially a distance of $\tau\sigma_r/\sqrt{2\pi}$ on average.

Intuitive estimation of first four primordia.   Because I set the angular position of the first primordium to zero ($\theta_1 = 0$), the second primordium arose at the opposite side of the meristem ($\theta_2 = 180$) farthest from the first primordium. The third and fourth primordia were initiated at the middle positions relative to the preceding primordia (i.e., at $\theta_3 = 90$ and $\theta_4 = 270$ degrees, respectively) at $\alpha = 0$ due to symmetric repression by the first and second primordia. Regarding the radial direction, the first primordium was not affected by any other primordia

until the second primordium arose; therefore, the first primordium stayed at the meristem edge R_0 at $P_{MP} = 0$ (see the Model section). After initiation of the second primordium, the primordia repelled each other symmetrically following the growth potential (Eq. 2.4). Thus, the times spent for movement until the fifth primordium arose were 3τ for the first and second primordia and 2τ and τ for the third and fourth primordia, respectively. The average velocity of radial movement from the meristem edge was $V = \sigma_r/\sqrt{2\pi}$ (Eq. 2.6) for these four primordia after initiation of the second primordium. Since the fourth primordium is in the local minimum in the angular direction (Fig. 2.10), the angular position will not be changed until the fifth primordium arises. Thus, the positions of these four primordia (r_i, θ_i) in polar coordinates are given by

$$
\begin{aligned}
r_1 &= R_0 + 3\tau\sigma_r/\sqrt{2\pi}, \ \theta_1 = 0 \\
r_2 &= R_0 + 3\tau\sigma_r/\sqrt{2\pi}, \ \theta_2 = 180 \\
r_3 &= R_0 + 2\tau\sigma_r/\sqrt{2\pi}, \ \theta_3 = 90 \\
r_4 &= R_0 + \tau\sigma_r/\sqrt{2\pi}, \quad \theta_4 = 270,
\end{aligned}
\tag{2.7}
$$

which agreed with the numerical results with an error of less than several percent regardless of the parameter spaces.
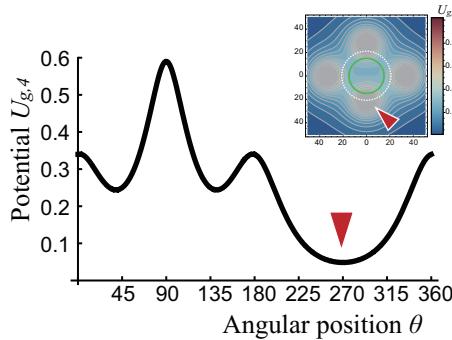
Figure 2.10: The growth potential $U_{g,4}$ is shown as a function of the angular position θ at the radius of the fourth primordium in Fig. 2.12B. The small panel shows the landscape of potential $U_{g,5}$ at the corresponding time (identical to the upper panel of Fig. 2.12B). Arrowheads indicate the position of the fourth primordium.

The angular position of the fifth primordium. Hereafter I demonstrate a case $V\tau = 6.0$. By substituting Eq. 2.7 into the function for the initiation potential Eq. 2.3, the function becomes

$$
U_{ini}(\theta) = \sum_{j=1}^{4} \exp\left(-\frac{d_{5j}}{\lambda_{ini}}\right) = \sum_{j=1}^{4} \exp\left(-\frac{\sqrt{r_j^2 + R_0^2 - 2r_j R_0 \cos(\theta_j - \theta)}}{\lambda_{ini}}\right),
\tag{2.8}
$$

The angle θ_{min} taking the local minimum of the potential yielded the angular position of the fifth primordium, i.e., $\theta_5 = \theta_{min}$. The angle θ_{min} underwent a pitchfolk bifurcation at $R_0 = 2$ and $\tau = 300$ and split from 90 degrees into 45 and 135 degrees (Fig. 2.11). At $R_0 > 2$, the minimum around ~ 135 degrees was selected instead of ~ 45 degrees as the initiating position of the fifth primordium without losing the generality because the potential was symmetrical around $\theta = 90$ at $\alpha = 0$. Thus the position of the fifth primordium becomes $\theta_5 = 90$ when $R_0 \leq 2$, whereas $\theta_5 \sim 135$ when $R_0 > 2$.

Calculation of potential gradient in radial direction that can cause the arrest of primordium displacement. I calculated the potential for the fifth primordium in radial direction by substituting Eq. 2.7 and
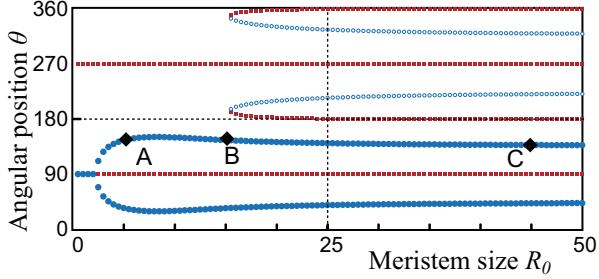
Figure 2.11: **The minima and maxima of U_{ini} when the fifth primordium arises.** After the initiation of four primordia at the positions given by Eq. 2.7, the angular positions that occupy the local minima (blue) and maxima (red) of potential U_{ini} at the edge of the meristem (Eq. 2.8) are plotted as a function of R_0. Blue solid circles denote the global minima, which represent the position of the fifth primordium, whereas the blue open circles around 200 and 340 degrees at $R_0 > 15$ signify the local minima. Solid black diamonds correspond to Fig. 2.12**A**–**C**.

the position of the fifth primordium θ_5 into Eq. 2.4. The function becomes

$$U_{g,5}(r, \theta_5) = \sum_{j=1}^{4} \exp\left(-\frac{d_{5j}}{\lambda_g}\right) = \sum_{j=1}^{4} \exp\left(-\frac{\sqrt{r_j^2 + r^2 - 2r_j r \cos(\theta_j - \theta_5)}}{\lambda_g}\right). \tag{2.9}$$

The potential exhibited a uni-modal ($2 < R_0 < 10$; Fig. 2.12A) or bi-modal ($R_0 < 2, R_0 > 10$; Fig. 2.12B and C) shape. At $R_0 < 10$, the potential gradient at the initiation position of the fifth primordium $\partial U_{g,5}(r, \theta_5)/\partial r\big|_{r=R_0}$ is outward-directed (Fig. 2.12A), providing almost constant growth resulting a non-whorled arrangement in the simulations (Fig. 2.6A, red region). At $R_0 > 10$, I defined the radial position of the local maximum closest to the fifth primordium as r_{max} (open arrowhead in Fig. 2.12B and C; red squares in the upper half of Fig. 2.12D) and the local minimum as r_{min} (blue circles in Fig. 2.12D; $0 < r_{min} < r_{max}$). The potential gradient $\partial U_{g,5}(r, \theta_5)/\partial r\big|_{r=R_0}$ has a negative value when $R_0 < r_{min}$ or $r_{max} < R_0$ (Fig. 2.12C), causing the fifth primordium to constantly move outward. On the other hand, the potential gradient was positive, i.e., directed inward (Fig. 2.12B), when $r_{min} < R_0 < r_{max}$ (between the two solid arrowheads in Fig. 2.12D), causing the arrest of radial movement of the fifth primordium. The values of r_{min} and r_{max}, analytically calculated as function of R_0 and τ (solid black line in Fig. 2.12E), were faithfully consistent with the parameter boundaries between the non-whorled pattern and the tetramerous-whorled pattern and between the tetramerous-whorled and pentamerous-whorled patterns, respectively, in the numerical simulations (Fig. 2.12E). Thus the inward-direct gradient of the growth potential (Eq. 2.4), which works as a barrier to arrest the outward displacement of the fifth primordium, causes the formation of tetramerous whorl.

Mechanism for the pentamerous whorl emergence The inward radial gradient of the potential $U_{g,k}$ (Eq. 2.4) also accounted for the emergence of pentamerous whorls at $\alpha > 0$. Unlike the case of $\alpha = 0$, the angular position of the third primordium θ_3 at the global minimum of U_{ini} deceased from 90 degrees as α increased (Fig. 2.13A). For example, the recursive calculations for the minimum of U_{ini} gave the angular positions of the two subsequent primordia, $\theta_3 \cong 62$ and $\theta_4 \cong 267$, respectively, at $\alpha = 2.0$ ($\tau = 300$, $R_0 = 20.0$, and $P_{MP} = 0$). Those angular positions are consistent with the numerical results (e.g., Fig. 2.2C and 2.5). The gradient of the growth potential $\partial U_{g,5}(r, \theta_5)/\partial r$ at the edge of the meristem for the fifth primordium that arose at $\theta_5 \cong 129$ was negative (Fig. 2.13B). Therefore, the fifth primordium moved outward at constant velocity so that the tetramerous whorl was unlikely to emerge. The inward-directed potential at the position of the new primordium first appeared when the sixth primordium arose around 343 degrees which was derived by the recursive calculation (Fig. 2.13C). The

25
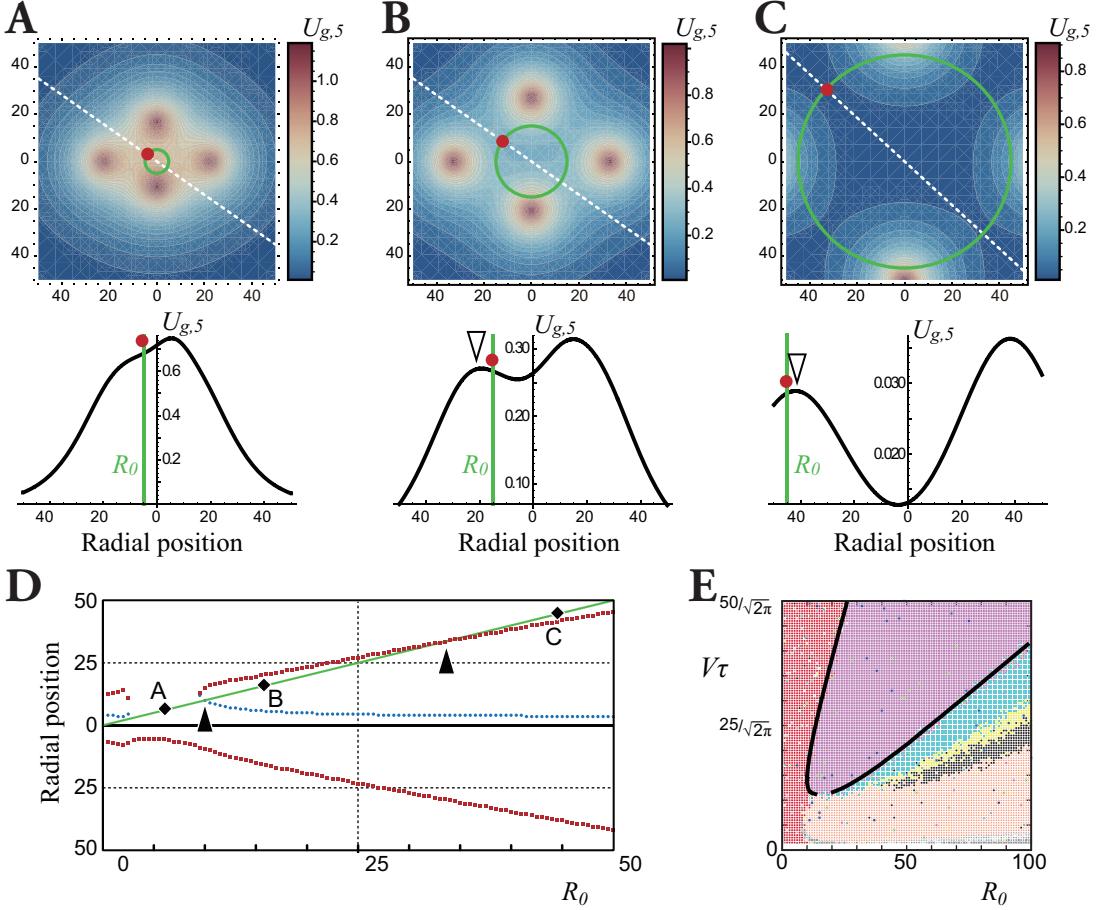
Figure 2.12: **The potential landscape captures tetramerous whorl formation. A–C.** Colour-coded potential landscape (upper panel; legend) and the section (bottom panel) at the angle where U_{ini} takes the global minimum so that the fifth primordium arises (white dashed line in upper panel; Eq. 2.9). The green line shows the meristem edge with a diameter of R_0. The direction of the potential at the position where the fifth primordium arises, denoted by the red circle, is inward in **B** but outward in **A** and **C** (bottom panel). $R_0 = 5.0$ (**A**), 15.0 (**B**), 45.0 (**C**). **D.** Radial positions that take the local minima (r_{min}, blue circles) and maxima (r_{max}, red squares) of potential $U_{g,5}$ (Eq. 2.9). Between $R_0 = r_{min}$ and r_{max}, indicated by the two arrowheads, the potential at the meristem edge decreases inward as in **B**. Black diamonds correspond to the initiating position of the fifth primordium of **A–C**. $P_{MP} = 0$, $\tau = 300$, $\sigma_r = 0.05$, $\sigma_\theta = 0.0$ in **A–D**. **E.** Superposition of the analytical result onto the numerical results (Fig. 2.6A). Solid lines show the crossovers $r_{min} = R_0$ and $r_{max} = R_0$, respectively (arrowheads in **D**). $P_{MP} = 0$, $\sigma_r = 0.05$. $\sigma_\theta = 0.05$ for numerical result, $\sigma_\theta = 0.0$ for analytical result.

first primordium (the rightmost potential peak in Fig. 2.13C) prevented the outward movement of the sixth primordium (red point in Fig. 2.13C). Arrest of radial displacement of the sixth primordium was maintained until the seventh primordium arose to allow the radial gap between these primordia to appear (i.e., a pentamerous whorl emerged). Likewise, the other merosities can be explained by similar recursive calculations of the angular position from the initiation potential (Eq. 2.3) and the radial gradient of the growth potential (Eq. 2.4).

26
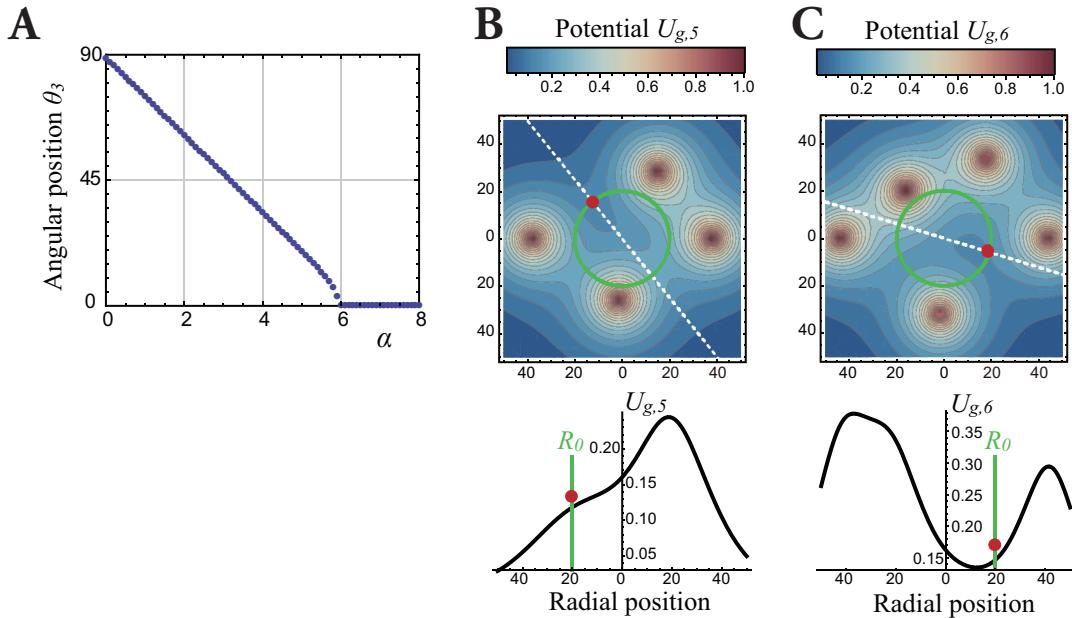
Figure 2.13: **The potential landscape captures pentamerous whorl formation. A.** The angular position of the third primordium as a function of α. **B–C.** Colour-coded growth-potential landscape (top) and the section (bottom) at the angle where the fifth (**B**) and the sixth (**C**) primordia arise (white dashed line in the top panel). $\alpha = 2.0$, $\tau = 300$, $R_0 = 20.0$, $\sigma_\theta = 0$, $\sigma_r = 0.05$, $\lambda_{ini} = \lambda_g = 10.0$, and $P_{MP} = 0$ in **A–C.**

2.7 Discussion

2.7.1 Relevance and difference to phyllotaxis models

Based on these analytical results (Fig. 2.12 and 2.13) and the dimensionless parameter $G = \tau V/R_0$, which represents the natural logarithm of the Richard's average plastochrone ratio R [78, 230], I quantitatively compared the present model against previous phyllotaxis models assuming simultaneous initiation based on the initiation potential [79]. The tetramerous and pentamerous whorls appeared in, at most, 1.3-fold and 1.2-fold ranges of G, respectively, in the earlier studies (Fig. 4D in [79]); however, they appeared in much wider ranges in the present model (i.e., 3-fold to 5-fold and 1.2-fold to 5-fold ranges of G, respectively; Fig. 2.6C). Here, another key parameter is the temporal decay rate of the initiation inhibition α that shorten the transient process approaching to the golden angle (Fig. 2.13A) than those of spiral phyllotaxis [80, 277]. λ_{ini}, representing the gradient of the initiation potential (Eq. 2.3), little affects the border between the whorled and non-whorled arrangements at $\alpha = 0$ (Fig. 2.14A and B); λ_{ini} affects the border only when $\alpha \neq 0$ (Fig. 2.14C and D). The independency of λ_{ini} at $\alpha = 0$ is consistent with the result shown by the previous model, which did not incorporate temporal decay of the potential and indicated that the phyllotactic pattern depends little on the functional type of initiation potential [78]. On the other hand, the gradient of the growth potential (Eq. 2.4) regulated by λ_g causes a drastic transition between the whorled and non-whorled arrangements (Fig. 2.14E and F). Unlike G, λ_{ini}, and α (Fig. 2.13A), λ_g hardly affects the angular position, as demonstrated in the previous sections, but it controls how far the growth potential works as a barrier to determine the merosities of the whorls (Fig. 2.14E and F). Thus, λ_g, α, and G differentially regulate phyllotaxis of the floral organs, suggesting the involvement of distinct molecular or physiological underpinnings.

2.7.2 Propriety of assuming two inhibitions

We employed two inhibitory potentials between the primordia dividing the primordial development into two stages. The first is the initiating stage represented by the initiation potential U_{ini}. Since the plant hormone auxin is both required and sufficient for the initiation of organ primordia at the periphery of meristem (Appendix B.2), spatial distribution of auxin should be the substance of the initiation potential. Then, is it proper to assume the inhibition on initiation site by pre-existing auxin maxima and organ primordia? The computational models based on the polar transport of auxin have properties similar to spot-type of Turing-type reaction-diffusion pattern [247]. Therefore it can be thought as Turing-pattern formation, which produces new spot(s) in new region expanded by growth of the tissue [50]. In this pattern formation, the new spot(s) are made with specific distance from pre-existing spots. Although it is different from the present model in the time-periodicity, the resulting spiral patterns are equivalent between with and without time-periodicity [78, 79]. Therefore I equated the inhibition represented as initiation potential U_{ini} with the spatial distribution of auxin.

In phyllotaxis models, the auxin patterning is usually thought as only one source of primordia pattern formation at the periphery of the meristem (e.g. [140]). However, there is an evidence of the post-meristematic modification of organ position by the boundary gene expression such as *CUP-SHAPED-COTYLEDON* (*CUC*) [214]. Peaucelle et al. showed that the inadequate expression of boundary genes causes the disruption of phyllotactic pattern without affecting the initial position of primordia [214]. Therefore there is another determination process of organ position that independent from the auxin patterning, as I expressed as the growth potential U_g. Of course the boundary gene expression is the strong candidate for the U_g. Also the contact-pressure between primordia, which is caused by physical contact, is a candidate for U_g since the efficient packing of growing organs in a floral bud should affect the toughness of the bud that required for protection of reproductive structure [6].

2.7.3 The initiation potential and the temporal decay of initiation inhibition

We have seen that both the temporal decay of initiation inhibition controlled by α and the mutual repulsion of growth regulated by λ_g are responsible for the formation of tetramerous and pentamerous whorls following sequential initiation. These mechanisms can be experimentally verified by tuning α and λ_g. Here, I discuss several candidates for the molecular and physiological underpinnings.

The temporal decay of the initiation inhibition α is probably caused by the transient expression of genes in incipient primordia, which transiently increase the auxin level in the incipient primordia and decrease it in the
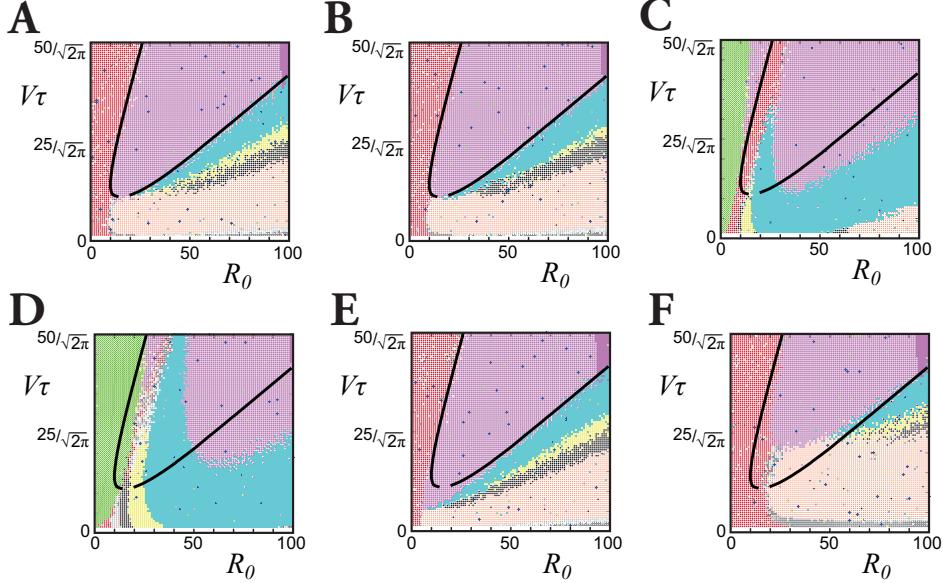
Figure 2.14: **Effects of λ_{ini}, λ_g, and α on merosities.** Superposition of the analytical result (the solid lines are identical to Fig. 2.12E: $\lambda_{ini} = \lambda_g = 10.0$, $\alpha = 0.0$, $\sigma_\theta = 0.05$, $\sigma_r = 0.05$, $P_{MP} = 0$) and the numerical result (the following parameters are different from the solid line: **A.** $\lambda_{ini} = 5.0$, **B.** $\lambda_{ini} = 20.0$, **C.** $\alpha = 2.0$ **D.** $\alpha = 2.0$, $\lambda_{ini} = 20.0$, **E.** $\lambda_g = 5.0$, **F.** $\lambda_g = 20.0$). The colors follow Fig. 2.6. λ_g and α affect the boundary lines between each whorl as well as that between non-whorls and tetramerous whorls (**E** and **F**), whereas λ_{ini} hardly affects at $\alpha = 0$ (**A** and **B**). At $\alpha \neq 0$, α and λ_{ini} synergistically affect the phase boundaries (**C** and **D**).

maturing primordia. This activity decreases the involvement of older primordia in competing for auxin at the initiation site, leading to decreased initiation inhibition by the older primordia. The following two gene families of *Arabidopsis* controlling the depletion and biosynthesis of auxin exhibit transient expression and affect floral organ arrangement, thus satisfying the requirements for α.

Auxin drain into inner tissue. *NAKED PINS IN YUC MUTANTS* (*NPY*) gene families control auxin-mediated organogenesis [53,103]. The transient expression of *NPY1 / MACCHI-BOU 4* (*MAB4*), *NPY3*, *NPY5* in the incipient primordia in wildtype plants (Fig. 2E in [52]; Fig. 3A-B in [53]) indicates that auxin depletion is stronger in maturing primordia, which corresponds to $\alpha > 0$ in the present model. In the *mab4/npy1 npy3 npy5* triple mutants, loss of PIN1 localization towards the inner tissue leads to suppressed auxin drain such that the auxin level becomes rather flat regardless of primordia age (Fig. 1L-M in [104]), indicating $\alpha \cong 0$. Wild-type flowers, which corresponds to $\alpha > 0$, have a tetramerous arrangement, whereas the mutants, corresponding to $\alpha \cong 0$, show randomized flowers, e.g., the *mab4/npy1* mutant possesses a disrupted tetramerous sepal whorl (Fig. 1N and Table 2 in [103]), and the *npy1 npy5* double mutant exhibits more severe defects with more petals and fewer sepals (Fig. 3 and Fig. S2 in [53]).

Auxin local biosynthesis. *AINTEGUMENTA / PLETHORA* (*ANT/PLT*) genes up-regulate local auxin biosynthesis via the *YUCCA* pathway [217,222]. The *AINTEGUMENTA-like 6* (*AIL6*)/ *PLT3* expression decreases as the primordium ages (Fig. 1J in [154]; Fig. 1B-C in [195]), suggesting that auxin polar transport is much weaker in the maturing floral organ primordia, as represented by $\alpha > 0$. The *ant4 ail6* double mutant produces disrupted tetramerous whorls with a random number of floral organs (Fig. 2 and Table 1 in [154]).

Validity of the parameters. The dimensionless parameter $R_0/V\tau$ of *Arabidopsis* was estimated to be around or more than 10 (from Fig. 2D in [279]). As shown in the phase diagram (Fig. 2.6C), the present model consistently predicted that the decrease in α in *Arabidopsis* caused a transition from tetramerous whorl to a fuzzy border consisting of tetramerous and pentamerous whorls, indicating that the organ number in each whorl was random. I predict that mutation in other genes with such properties (i.e., transient expression that increases the auxin level in younger primordia and decreases it in older ones) would also lead to randomized flower formation. Thus, positive α is a key factor for stabilizing floral organ number in *Arabidopsis*.

2.7.4 The growth potential and its biological source.

Because the gradient of the growth potential is the main cause of the whorl formation in the present model (Fig. 2.12 and 2.13), experimentally manipulating the potential decay length λ_g can induce the transition between the different whorl arrangements. There are two biological properties that could account for the inhibitory distance λ_g: mechanical contact pressure between primordia and gene expression that establishes the floral organ boundary.

Mechanical contact pressure between primordia. Surface buckling could account for the former [112], with a wavelength regulated by mechanical properties [197] such as the expansibility of the cell wall [95].

Gene expression that establishes the floral organ boundary. NAM-ATAF-CUC (NAC) domain transcription factors, including *CUC1*, *CUC2*, and *No Apical Meristem* (*NAM*), are expressed at the organ boundaries and play a central role in establishing and maintaining organ boundaries [4] (Appendix B.3.3). In gain-of-function mutants of both *CUC1* and *CUC2*, their expression domain became enlarged (e.g., Fig. 5C and D in [273]) and the whorled arrangement was disrupted with extra sepals and petals [177, 273, 324, 332]. The expression breadth of *NAC* genes which establish the boundary between organs can be represented as λ_g in the present model. In model simulations, doubling λ_g consistently disrupts the tetramerous whorls, producing a non-whorled or octamerous arrangement (Fig. 2.14F; the tetramerous region at $\lambda_g = 10.0$ bounded by the solid lines turns red at $\lambda_g = 20.0$, indicating a non-whorled arrangement, or orange, indicating an octamerous arrangement). The present model further predicts that the tetramerous arrangement will be maintained even when λ_g decreases by half (Fig. 2.14E; the tetramerous region at $\lambda_g = 10.0$ bounded by solid lines is included in tetramerous region at $\lambda_g = 5.0$ denoted by the magenta points in Fig. 2.14E), corresponding to the *A. thaliana* loss-of-function *cuc* mutant that shows no changes in sepal position [4]. Those consistencies suggest predictions for pentamerous flowers: weakening the post-meristematic interactions between organs will not change the merosity (the region just below the bottom solid line Fig. 2.14E), whereas enhancing them will disrupt the whorls or increase the merosity (Fig. 2.14F). Intriguingly, in the pentamerous flower tomato *Solanum lycopersicum* and *Petunia* (Solanaceae), the role of a member of the NAC transcription factor family *NAM* seems consistent with the prediction: a *Solanum* mutant suppressing NAM expression exhibits fused sepals and fused whorls with keeping merosity (Fig. 2 and 3 in [126]), whereas a *Petunia num* mutant exhibits extra petals (Fig. 3B and 4B in [282]). Further investigation of other species [1, 173] is an interesting topic for future research.

2.8 Future plan

Future studies should also clarify the limits and applicability of the common developmental principle elucidated here by exploring more complex development in a wide variety of flowers.

Co-initiation of primordia. Because the present model assumes sequential initiation of the primordia, it does not cover the floral development of all eudicots; sepal primordia arise simultaneously in some eudicot taxa (Fig. 1.3; e.g., mimosoid legume [225], Appendix. B.5). Likewise, in later development, several primordia arise at once in the stamen and carpel whorls (e.g., Ranunculaceae [261]). The transitions between simultaneous and sequential development have two additional intriguing implications for evolutionary developmental biology. First, the initiation types may affect the stochastic variation of floral organ numbers, possibly caused by the absence or presence of pseudo-whorls (Fig. 1.3) and the noisy expression domain of homeotic genes, as will be described in later in Sec. 4. Second, such transitions occur even in animal body segmentation [68, 240], possibly caused by evolution of both

gene regulatory network topologies and embryonic growth [97, 101, 249, 296]. The limitations of the model can be reduced by introducing initiation whenever and wherever the potential (Eq. 2.3) is below a threshold, allowing simultaneous as well as sequential initiation [79]. The threshold model exhibiting both types of initiation does not by itself result in the dominance of particular merosities [79]. Incorporating two mechanisms, mutual growth repulsion and temporally decreasing inhibition at the point of initiation, into the threshold model could explain the dominance of particular merosities following both the sequential and the simultaneous initiation of floral organ primordia (Fig. 1.3).

Adaxial-abaxial polarity and positional information from the bracts. The change of adaxial-abaxial polarity and bract position sometimes associates with the change of floral organ number (Appendix B.5.4). For example, *cyc/dich* mutant of *Antirrhinum* that misses adaxial-abaxial polarity of floral bud has six petals instead of five petals in wild type [172], and *Arabidopsis bop1 bop2* mutant that gains a bract at the abaxial base of flower has five sepals instead of four sepals in wild type. The striking phenotype of these mutants is the change of symmetry: *cyc/dich* mutant shows radial symmetry but wild type has zygomorphic flower. *bop1 bop2* mutant shows zygomorphy instead of disymmetric composition of wild type. Therefore the number can be influenced by the adaxial-abaxial polarity of the floral bud bract position, which involve the transition between radial symmetry and zygomorphy that have occurred multiple times during angiosperm phylogeny.

Trimery The trimerous whorls that common in monocots and magnoliids are absent in the present model (Fig. 2.6). The transition between the trimery and tetramery or pentamery, and vice versa, occurred multiple times during the evolution of angiosperms. Therefore, trimerous flowers are scattered across the basal angiosperms, monocots, and a few families of eudicots [88, 89]. Elucidating the developmental mechanisms underlying the transitions between the different merosities, as well as those between sequential and simultaneous initiation, will be an important avenue for future studies.

2.9   Partial conclusion

One problem in determining floral organ number is how to generate whorls comprised of a specific number of organs. By introducing a growth assumption (i.e., continuous repulsion among primordia throughout development, which was originally proposed as the contact pressure model [2, 125, 234] and is supported by experimental observations [214]) into a dynamical model of phyllotaxis [78], I showed that the whorled arrangement arises spontaneously from sequential initiation. Moreover, when I allowed the inhibition to decay over time [114, 277, 301], pentamerous whorls became the dominant pattern. The merosity tended to be four or five in much larger parameter spaces than those in which it tended to be six or seven. The emergence of tetramerous and pentamerous whorls could be verified experimentally by tuning the two parameters α and λ_g.

3 Variation Curves and Their Statisticval Quantities in Floral Populations of Asteracae and Ranunculaceae

3.1 Abstract

The variation in floral morphologies contributes to speciation of flowering plants by testing various phenotypes that may have higher adaptability, eventually leading to their phylogenetic diversity. However, the diversity has been apprehended mostly by the modal morphologies where the variation is averaged out so that little is known about the relation between variation and diversity. Here I comprehensively analysed the intra-specific variation of floral organ number within a flower of Ranunculaceae, which has branched near the monocot-eudicot bifurcation, and flower number in an inflorescence of Asteraceae, which is one of the most diversified family in eudicots, using elementary statistical quantities: the mean and the standard deviation (SD). We found three types of clade- or organ-type-specific relationship between mean and SD of organ numbers: In Asteraceae ray florets and Ranunculaceae stamens and carpels, the SD is proportional to the mean. In Ranunculaceae petals and sepals, SD is proportional to square root of mean in several genera, e.g., *Ranunculus* and *Anemone*, with special robustness in three and five organs, whereas SD is not correlated with mean in some species, e.g., *Eranthis* nectaries. The variation-types quantitatively indicate the morphological robustness and variation at genus- to family-level. The difference in variation-types suggests that the floral developmental processes regulating the variation are different among the clades in angiosperms, which may affect the phylogenetic diversification.

3.2 Background

3.2.1 Statistical quantities and biological process

Biological systems ubiquitously exhibit stochasticity in traits from the molecular to the multicellular level. The stochasticity in the numbers of protein molecules within single cells has been extensively analysed in species ranging from bacteria to mammals [85, 184, 208, 256]. Statistical noise at the molecular level can be transmitted to other levels of organization via biochemical reaction networks [85, 215, 270, 292]. During multicellular development, the variation in molecular concentrations is transmitted to macroscopic characteristics of organs and tissues, such as the domain size of gene expression [178] or the number of organs, e.g., body segments in vertebrates [8, 231] and Myriapoda [145, 316], tentacles [12], and floral organs in plants [129].

The contribution of biochemical processes to phenotypic noise was studied both theoretically [297] and experimentally with bacterial species *Bacillus subtilis*, which showed varied expression level among cells in a population of isogenic strain [206]. The simple theoretical model for gene expression with essential features of transcription and translation showed that the Fano factor ratio (phenotypic noise strength; defined as variance/mean) is dependent on the translational efficiency but not on the transcriptional efficiency [297]. This result was supported by the experiment, which showed that the phenotypic noise strength for the four different translational mutants is clearly dependent on translational efficiency, whereas the transcriptional efficiency does not significantly affect noise strength [206]. These results suggest that the same average level of gene expression can be achieved controlling either translation or transcription, but the degree of fluctuation would be different depending on the employed way [297]. Moreover, several plausible models for transcription noise yielding a characteristic dependency of noise strength on average protein amount were suggested [141]. Thus, focusing on the dependency of noise strength on the average might allow us to distinguish different biological processes that cause phenotypic variations.

3.2.2 Floral organ number variations

Although the floral organ number is a hallmark of eudicot species, it can distribute stochastically, even within an individual plant (Fig. 3.1A) or a continuous population of a single species (Fig. 3.1B, C). Statisticians in old days put the variation of floral organ numbers as a subject of their discussion. Around the end of 19th century, de Vries and Ludwig found several features for the variation in floral organ numbers. At the beginning of the 20th century, a periodical named *Biometrika* was founded, in which the discussion on various natural variation took place.

The stochasticity has been quantified by the frequency distributions of floral organ numbers in wild populations, including that of the floret numbers in Asteraceae, since the end of 19th century [70, 170]. de Vries (1895,1899)

found three types of curves in the variations: The symmetric curve (*Galton Kurven*), negatively and positively skewed curve (*halbe Galton-Kurven* [70]; Fig. 3.1B, C), and bimodal curve (*zweigipflige Variationskurven* [71]). He performed a sequence of selection of the plants by petal number for several generations, and observed the transition between these curve types [70, 72]. Ludwig described multi-modal variation-curves in Asteraceae florets numbers with more than one peak in a population, and stated that the modal number is related to Fibonacci numbers, namely, $8, 13, 21, 34, ...$, and the sum (e.g., $8 + 21 = 29$) or multiple (e.g., $8 \times 2 = 16$) of them (Ludwig's law). The counting of daisy florets in Europe made by de Vries agreed with the Ludwig's law [72], but the exception was soon found by Lucas in American daisy population [94], which was later supported by Shull [272] and Tower [304].
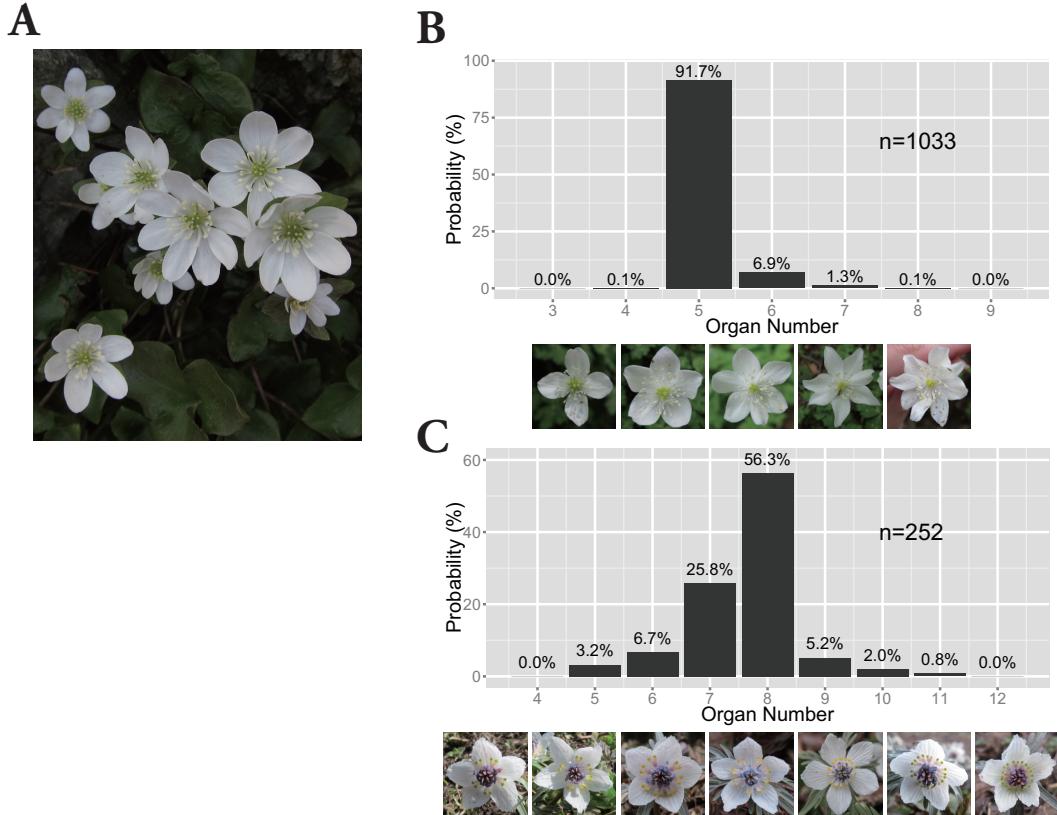

Figure 3.1: **Floral organ number variation in Ranunculaceae. A.** An individual plant of *Hepatica nobilis* var. *japonica* that has flowers with seven to nine tepals. **B, C.** Asymmetric variation in the Ranunculaceae floral organ number. The sample size *n* and the probability (%) are given on the bar chart. **A.** Right-tailed variation in the tepal number in *Anemone flaccida*. The photographs show the flowers with four to eight tepals (the white, petal-like organs). **B.** Left-tailed variation in the nectary number in *Eranthis pinnatifida*. The photographs show flowers with five to 12 nectaries (the yellow, forked organs).

In journal *Biometrika*, researchers described many variations in flower-related organ numbers, such as petal and sepal numbers in Adoxaceae and Ranunculaceae, ovule and seed numbers in Malvaceae, and floret numbers in an inflorescence in Asteraceae. They have tried to understand these variations in the words of statistics. For example, Karl Pearson, one of the founders and editors of the journal, calculated statistical quantities such as mean, standard deviation, and skewness for them. But no unified view for the variations in floral organ numbers has been made.

In this section, I ask two questions: Does the statistical quantities imply the unified law, or different sources for floral organ number variation? Is there any number, such as Fibonacci-related number, that is especially preferred?

3.3 Method

To describe the features of the floral-organ number variation quantitatively, I calculated the five basic statistical quantities, namely, mode, mean, standard deviation, skewness, and kurtosis.

3.3.1 Five basic statistical quantities

Using the statistical quantities [138], it is able to quantitatively describe the shape of variation curve. I calculated these quantities for each variation curve with sample size n (≥ 50) by myself and others.

Mode, Mo, is a state (in this case, specific organ number) that appears at the highest frequency in the population. Mean is the primary moment around 0 calculated as follows:

$$Mean = \frac{1}{N}\sum_{i=1}^{N} x_i.\tag{3.1}$$

Standard deviation describes the degree of variation.

$$s^2 = \frac{1}{N}\sum_{i=1}^{N}(x_i - Mean)^2.\tag{3.2}$$

Since the data was sampled from a fraction of a population, unbiased estimation should be used.

$$SD^2 = \frac{1}{n-1}\sum_{i=1}^{n}(x_i - Mean)^2.\tag{3.3}$$

Skewness is the tertiary moment about the mean $Mean$ divided by s^3 and gives the degree of asymmetry. The skewness is zero in the symmetric variation such as the standard Gaussian distribution. If it is positive, it has heavier tail on the side larger than the mean, whereas the negative skewness means the longer tail on the side smaller than the mean.

$$skewness = \frac{1}{Ns^3}\sum_{i=1}^{N}(x_i - Mean)^3.\tag{3.4}$$

Unbiased estimation is:

$$skewness = \frac{n}{(n-1)(n-2)SD^3}\sum_{i=1}^{n}(x_i - Mean)^3.\tag{3.5}$$

Kurtosis is the quaternary moment about the mean $Mean$ divided by s^4 and represents the steepness of the curve. High kurtosis appears when the variation curve has extraordinary high frequency on its mode and wide tail around it.

$$kurtosis = \frac{1}{Ns^4}\sum_{i=1}^{N}(x_i - Mean)^4 - 3.\tag{3.6}$$

Reduction of 3 is to set the kurtosis of standard Gaussian distribution to 0. The unbiased form is:

$$kurtosis = \frac{n(n+1)}{(n-1)(n-2)(n-3)SD^4}\sum_{i=1}^{N}(x_i - Mean)^4 - \frac{3(n-1)^2}{(n-2)(n-3)}.\tag{3.7}$$

3.3.2 Plant samples

Populations of flowers of Asteraceae and Ranunculaceae were studied in natural and cultivated environments. The sampling of each floral population was limited both temporally (1–8 days) and spatially (diameter up to 100 m), because seasonal [327] as well as geographical effects [171] on floral organ numbers can be significant. Except for plants in my own field, to avoid injuring plants, counting an individual twice, and miscounting superposed organ, I took one to three (from different direction: when the number is not obvious) photographs for each flower along with a path in a population. I also used published data sets whose sources are written in corresponding sections.

34

3.4 Results

3.4.1 Floral organ number variation in Ranunculaceae flowers

As reported earlier [70], the asymmetric distribution of floral organ numbers appears in many of Ranunculaceae species. There are two types of the asymmetric distribution: positively and negatively skewed distributions. In a positively skewed distribution, as in the tepals of *Anemone flaccida* (Fig. 3.1B), the organ number often increases from the mode *Mo* but rarely decreases. In a negatively skewed distribution, as in the nectaries (located in the second whorl; petal-derived) of *Eranthis pinnatifida* (Fig. 3.1C), the organ number often decreases from the mode *Mo* but rarely increases. In most cases, the asymmetric distribution is species-specific and organ-specific, and follows either of the two types. For example, *A. flaccida* tepals have a right-tailed distribution, not only in my and collaborators' observations made at different locations but also in previously published data [201], whereas *E. pinnatifida* nectaries sampled in various locations have a left-tailed distribution. In addition, the probability of the modal organ number is extraordinarily high in the floral populations compared with that in the Gaussian distribution, indicating the robustness of particular organ numbers. The extraordinary probability of the modal number is statistically represented by the high positive value of kurtosis, which the standard Gaussian distribution cannot account for [280]. To quantitatively describe the properties of these variation curves, I calculated the degree of variation (SD), of asymmetry (skewness), and of steepness (kurtosis) of the curves for floral organs in Ranunculaceae.

Since Ranunculaceae is a gigantic family in basal eudicots, I treat the data sets dividing into several groups according to phylogenetic relationship of Ranunculaceae. The effort to clarify the phylogeny in family Ranunculacae has been made using morphology [295], chloroplast DNA [139], Nuclear 26S Ribosomal DNA [235], and so on. This family is divided into subfamilies, Glaucidioideae (consists of only one Japanese endemic species; Shirane-aoi), Hydrastidoideae (*Hydrastis*), Coptoideae (*Coptis*), Thalictroideae (*Thalictrum* and *Aquilegia*), Ranunculoideae (*Ranunculus, Delphinium, Aconitum, Clematis, Anemone* s.l.) [289, Dec. 2014]. All genera I examined here for the perianth-segment (petal, sepal, and tepal) number variation are classified as Ranunculoideae and subdivided into three tribes. First is the Ranunculeae, including *Ranunculus* (*R. arvensis* [45], *R. bulbosus* [70], *R. cantoniensis*, *R. ficaria* [17, 171, 176, 251, 327], *R. japonicus, R. parviflorus* [253], *R. repens* [218, 250], and *R. silerifolius*). The second is Anemoneae, including *Anemone* (*A. flaccida* [201], *A. hupehensis* var. *japonicus, A. narcissiflora, A. nemorosa* [334], *A. nikoensis*) and *Hepatica* (*H. nobilis* var. *japonica*). The third tribe is the Helleboreae, including *Eranthis* (*E. hyemalis* [255], *E. pinnatifida*). In addition to above species (including data from other articles for *Ranunculus* [254, 255]), I examined two more genera, namely, *Aquilegia* (*A. vulgaris* [251]) that belongs to Thalictroideae and *Clematis* (*C. vitalba* [252]) in Anemoneae, for stamen and carpel number variation.

The perianth-organ number of *Ranunculus* (tribe Ranunculeae) showed strong stability on $3, 5, 8$**.** *Ranunculus* is a type genus of Ranunculaceae. Their perianth consists of two whorls with distinct morphology. Outer sepals are green, whereas inner petals are usually yellow. The floral organ number of these two whorls are usually five, but in some species such as *R. ficaria*, which are sometimes treated as an independent genus *Ficaria* [133], the number is different. Using floral formulae, the petal and sepal number can be represented as follows:

Ranunculus	(buttercup)	K5C5 ,
Ficaria	(lesser celandine)	K3C8 ,
Ficaria	(in Swiss population [171])	K5C8 .

The statistical quantities of *Ranunculus* revealed that their standard deviation (SD) reaches to zero only when the mean is close to three, five, and eight, and it is higher between these numbers (Fig. 3.2). The points in the mean-SD chart (Fig. 3.2 left) is on a curve, which seems like a function as $SD = \sqrt{|Mean - d|}, (d = 3, 5)$, when the mean is smaller than 6. The skewness is the highest when the mean is three, and decreases across zero until the mean reaches five. It discontinuously soars again when the mean exceeds five, and decreases as mean increases. Kurtosis has the peaks where the mean is three, five, and eight. These findings provide an unified view for how the mean number changes between two modes, which may reproduce the evolutionary change between two average phenotype: The variation curve is tight and steep at the first mode (three), gets broader as mean increases changing its shape from right-tailed curve to symmetric curve, is broadest and symmetric at the median of the two mode, gets tighter via left-tailed curves, and again becomes tight and steep at the next mode (five).
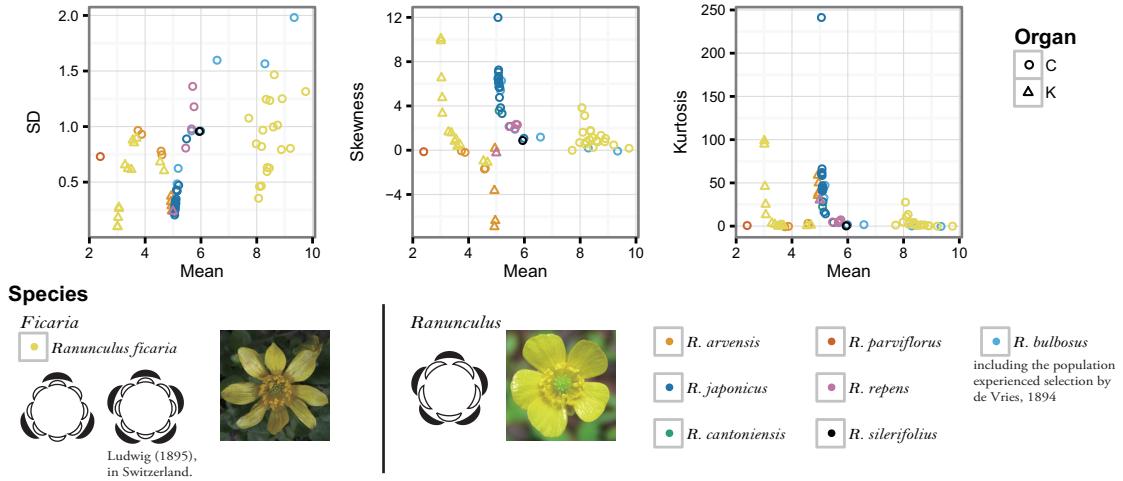
Figure 3.2: **Statistical quantities in *Ranunculus*.** I and collaborator collected the data for *R. cantoniensis*, *R. japonicus*, *R. silerifolius*, and *R. ficaria*. Other species were from previous works: *R. arvensis* [45], *R. bulbosus* [70], *R. ficaria* [17, 171, 176, 251, 327], *R. parviflorus* [253], *R. repens* [218, 250]

All of the three quantities showed unique features on three, five, and eight, which can be regarded as preferred modes with high stability for this genus. I would suggest these stable numbers are their original modal numbers hidden by stochasticity in biological processes, and refer these numbers as hidden modal number(s) of the species, genus, or family, which can differ from conventional modal number defined in a pictorial book without comprehensive investigation, or from superficial modal number appears as peak(s) of a variation curve in a population.

The tepal number in tribe Anemoneae showed stability on 5 **or** 6. The Anemoneae is attractive target for the study on floral organ number, because it includes species with dimerous, trimerous, and pentamerous flowers [229]. Schöffel [261] described the floral organ number of several European species of *Anemone* s.s. as:

A. ranunculoides	(terminate)	P6A50{45-59}G28{23-38}
A. ranunculoides	(lateral)	P5A45{40-56}G17{12-21}
A. nemorosa		I3P6

I and collaborators observed variation in tepal numbers of Eastern Asian species *A. flaccida* (Fig. 3.1B), *A. hupehensis* var. *japonica*, and *A. nikoensis*. Their superficial modal number is usually five, but occasionally it can be six or seven, depending on the location or cultivated variety. For example, in *Anemone hupehensis* var. *japonica*, two populations showed pentamerous flower as their mode, but the modal number of one population was seven.

I also observed tepal number variation in *Hepatica*, which is closely related genus to *Anemone* and *Clematis* [48]. Their flower usually consists of two tepal whorls, many stamens and carpels (Fig. 3.1). The colour, number, and even the types of floral organs are extremely variable. For example, cultivated plants show blue, red, green, pink, and purple tepals and stamens. Moreover, in some cultivated varieties, some or all stamens becomes narrow petal-like organs without anther, which is sometimes observed even in wild plants. This intermediate morphology between tepal and stamen occurs in whole whorl(s), i.e., additional whorl(s) of narrow petal-like organ is observed inside the second tepal whorl. The flower composition is in trimerous mode:

H. nobilis	I3P6A∞G∞.

Likewise the *Ranunculus*, SD approaches to zero when mean is five. However, the SD-mean relationship is split into several groups: The majority are on almost linear line starting from $(Mean, SD) = (5, 0)$, but some others, namely, *A. nemorosa*, *H.* nobilis, and some of *A. hupehensis* and *A. nikoensis*, forms another cluster (solid arrowhead in Fig. 3.3). The absolute value of skewness and kurtosis have the peaks around 5 for the former group, whereas
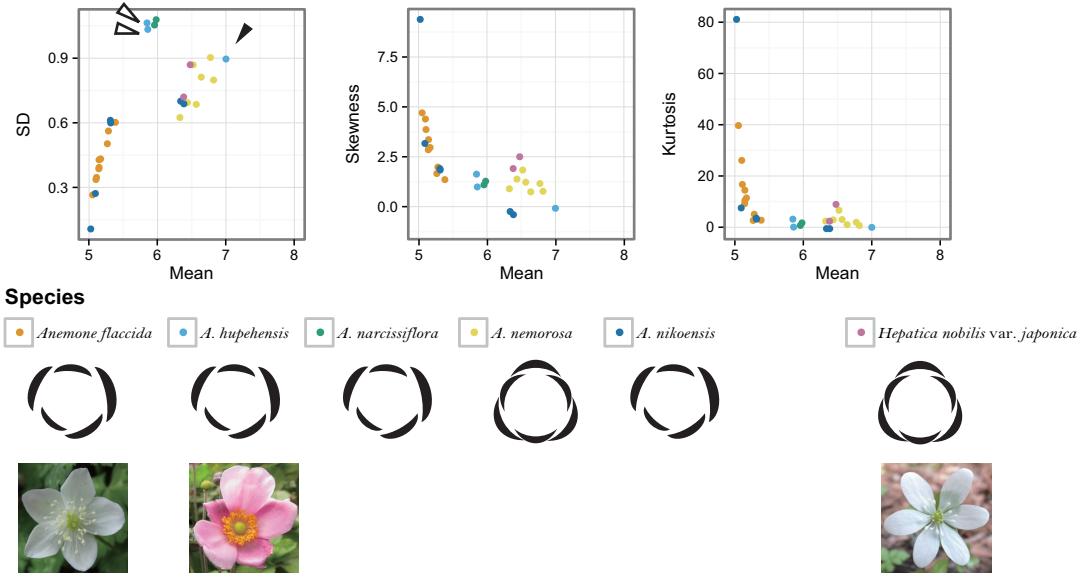
Figure 3.3: **Statistical quantities in *Anemone*.** The datasets of *A. flaccida*, *A. hupehensis*, *A. narcissiflora*, *A. nikoensis*, and *Hepatica nobilis* were collected by myself or by collaborator. The data sets of *A. nemorosa* are from Yule (1902) [334] and one of *A. flaccida* is from Ohno [201].
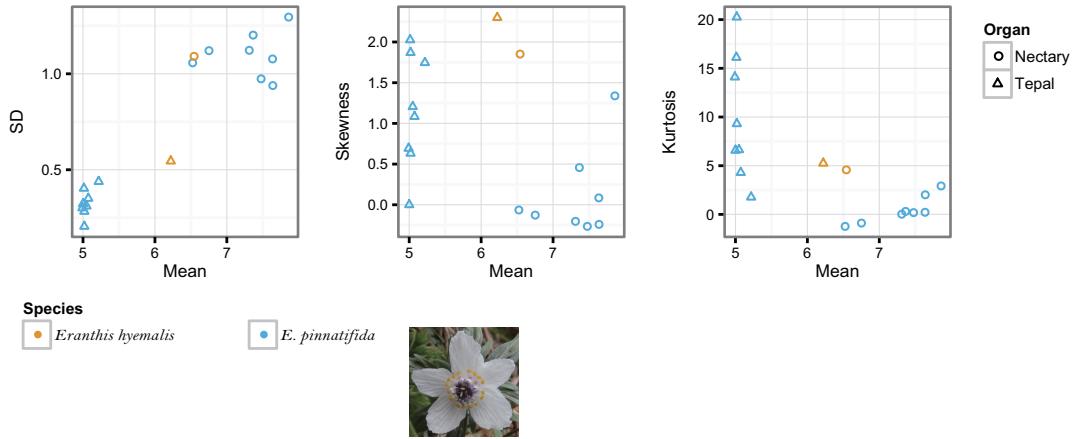

Figure 3.4: **Statistical quantities in *Eranthis*.** The variation curves of *Eranthis pinnatifida* were obtained through my field observations. The variation curve of trimerous-flower species *Eranthis hyemalis* [251] might have similar statistical quantities to that of trimerous-flower species of *Anemone*. However, the insufficiency of the data prevent the further discussion.

the peak is around 6.5 for the latter.

Interestingly, the two groups appear in the SD-mean diagram almost correspond to the conventional merosity (Floral diagram in Fig. 3.3). Pentamerous species *A. flaccida* are in the first group and has peak on five in the absolute value of skewness and kurtosis. The trimerous species *A. nemorosa* and *H.* nobilis belong to the latter group and have peak around 6.5. *A. nikoensis* and *A. hupehensis* tepal number belong to either group. In *A. hupehensis*, two out of three populations, which have usually five pink tepals, form a cluster with the five-mode species (open arrowheads in Fig. 3.3), while the rest one population with white tepals having seven as the superficial mode is in the cluster of trimerous (or hexamerous) species (solid arrowhead in Fig. 3.3). Therefore, although this population of the white-tepal form of *A. hupehensis* has the mode on seven, I expect the true mode of this species is six and the counting of larger population will show the mode at six.

SD does not correlate with mean in the variation in *Eranthis* nectary numbers. I observed the variation in *Eranthis pinnatifida* nectary and tepal number (Helleboreae), and compared to the European species *E. hyemalis*. These two species have different features, and some researchers treated these species in two different genera: genus *Eranthis* that distributes in Europe and North America, and *Shibateranthis* in Asia. For example, Japanese endemic species *E. pinnatifida*, Korean endemic species *E. byunsanensis* are classified into genus *Shibateranthis* by Nakai (1937) and Tamura (1987), which was supported by molecular phylogeny that showed they make a sister group to *E. hyemalis*, an European species [162]. Hence we often find the name *Shibateranthis pinnatifida* in Japanese books, but here I refer this species as *Eranthis pinnatifida* and treat *Shibateranthis* as a section in genus *Eranthis*.

Tepals are usually white in section *Shibateranthis*, contrary to yellow tepals in section *Eranthis*. The conventional modal number is different between the sections:

E. pinnatifida	P5N8A∼20G{2-5},
E. hyemalis	P6N6.

Nectaries of *E. pinnatifida* are bifurcated, reddish purple at the bifurcation point, yellow or green at the two round tips, which are derived from petals to attract insects. Stamens have purple anther and white (sometimes red) filaments. The tip of apocarpous pistils is bent outward, and the pistils are longer than stamens. The superficial modal number of pistils is different among populations. It is two or three in a population in Hyogo prefecture, whereas five in a population in Shiga prefecture.

For variation curves of *E. pinnatifida* tepal number, SD increases and kurtosis decreases with increasing mean (Fig. 3.4). Therefore, the variation type of tepal number is similar to that of *Ranunculus*. SD of variation curves of their nectary number does not show the clear dependence on the mean. It spreads out as mean increases without any correlation. The kurtosis slightly increases as mean increases, in the opposite way to *Ranunculus* petal numbers.

The SD of nectary number variation of *E. hyemalis* belongs to the same group to that of the *E. pinnatifida*. However, kurtosis and skewness of nectary number variation, and also the all quantities of tepal number variation of *E. hyemalis* did not form a group with *E. pinnatifida*. It can be the shift from five to six as found in *Anemone*, but I don't have enough data to discuss.

Ranunculaceae stamen and carpel number variation. Ranunculaceae flowers have multiple stamens and carpels in apocarpous gynoecia, and the numbers vary remarkably. The SD of stamen and carpel number variation monotonically increases with increasing mean. The skewness and kurtosis do not show clear peak, and roughly convergent on zero as mean increases (Fig. 3.5).

3.4.2 Floral organ number variation in other clades

In Ranunculaceae, I found three types of variation curves distinguished from statistical quantities. The first is found in *Ranunculus*, *Anemone*, and *Eranthis* perianth segments (tepal, sepal, petal). In this *Ranunculus*-perianth type, SD reaches to zero when the mean is near to certain numbers specific to the genus or species, what I call hidden modal numbers. Absolute value of skewness and kurtosis take the local maxima on these hidden modal number, and monotonically decreases between these numbers. The *Eranthis*-nectary type is found in the variation in *Eranthis* nectary number, whose SD shows no clear dependence on mean, and kurtosis slightly increases as mean. The large-mean type whose SD shows monotonic increase depending on the mean was found in variations of carpel
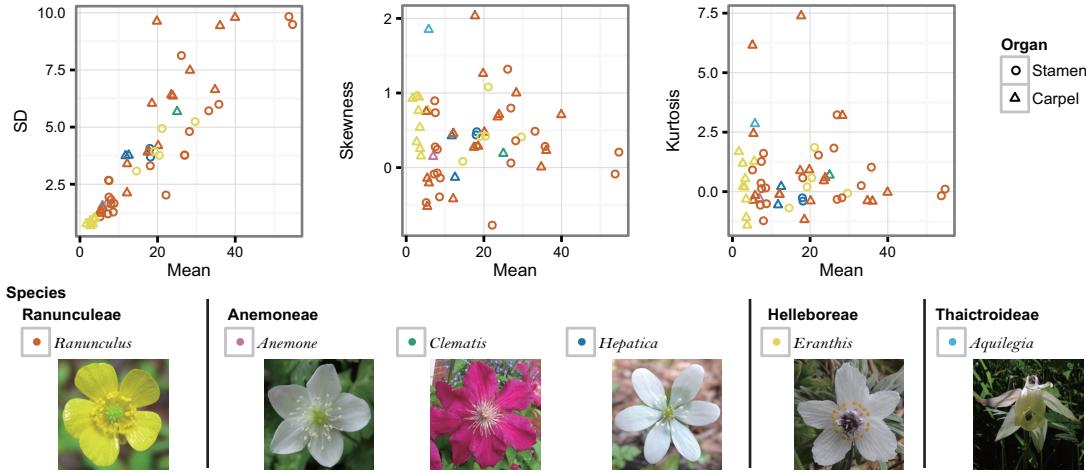
Figure 3.5: **Statistical quantities of stamen and carpel number variation in Ranunculaceae population.** Each circle corresponds to a variation of stamen number in a population, and each triangle corresponds to a variation of carpel number in a population.

and stamen number, which have rather larger mean (> 10). I examined whether the statistical quantities of other clades fall into three types of SD-mean relationship in Ranunculaceae.

Petal number in Papaveraceae. Papaveraceae is a basal eudicot family, which belongs to Ranunculales. In petal number variation in *Sanguinaria canadensis*, SD is close to zero on eight, and increases with increasing mean. Skewness and kurtosis are highest on eight, and decreases as mean increases. Therefore it is the same type to perianth segment number variations in Ranunculaceae, as expected by the close relationship of these two families.
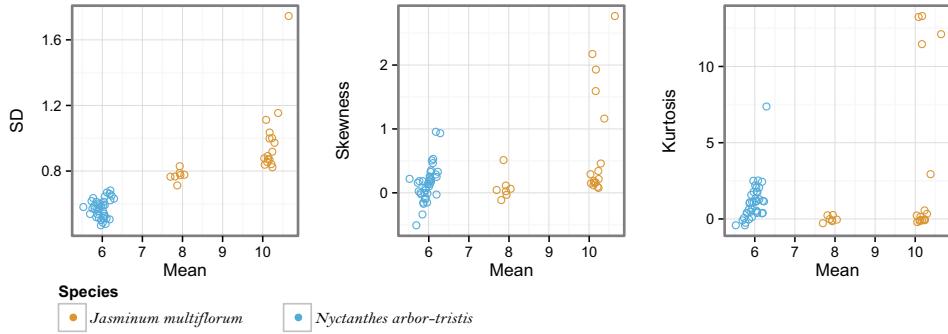
Figure 3.6: **Statistical quantities of petal number variation in Oleaceae population.**

Petal number in Oleaceae. The petal number variation of three groups of Oleaceae, *Nyctanthes arbor-tristis* and two varieties of *Jasminum multiflorum*, was measured by Roy (1963) [241]. The modal number is 6 in *N. arbor-tristis*, 8 in *J. multiflorum* var. *alba*, and 10 in *J. multiflorum* var. *rubescens*. The degree of variation indicated by SD gets larger with increasing mean, when we see the three groups together. The skewness of some populations of *J. multiflorum* var. *rubescens* is larger than *N. arbor-tristis* and *J. multiflorum* var. *alba*, reflecting longer right

tail of the distribution than the left tail in some of the *J. multiflorum* var. *rubescens* data sets, in contrast to the symmetric variation in *N. arbor-tristis* and *J. multiflorum* var. *alba*.

For the whole Oleaceae petal number, the SD-mean relationship is similar to that of large-mean type since SD monotonically increase according to mean, but if we see these statistical quantities for each species and variety, SD does not correlate with mean but just spreads out as mean increases (e.g. see only the blue circles in Fig. 3.6), as in *Eranthis* nectary number variation. Also, the kurtosis of *N. arbor-tristis* increases with increasing mean similarly to *Eranthis* nectary number.

Pappus part number in *Microseris* hybrids (Asteraceae). The inter-specific hybrid of the *Microseris*, *M. pygmaea × M. bigelovii*, showed larger SD than the genuine species (Fig. 3.7). Its skewness gradually decreases as mean increases. Among the *Microseris* species, the kurtosis is the highest on five, and also slightly higher on ten, than the other numbers between five and ten. These features are close to that of the variation in perianth segment numbers of Ranunculaceae.
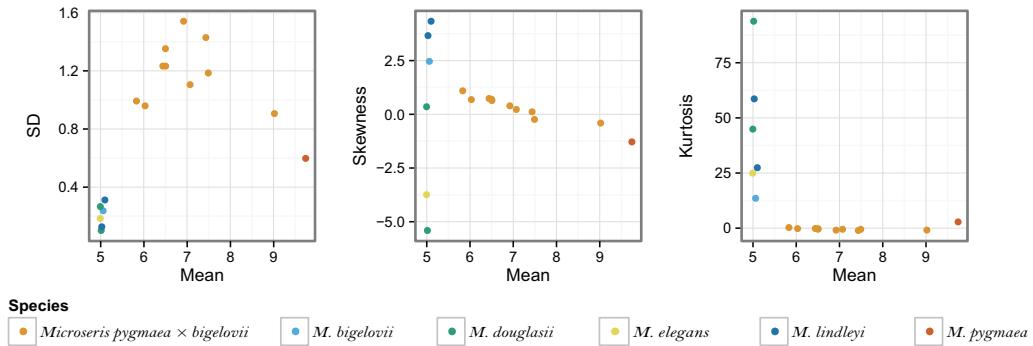

Figure 3.7: **Statistical quantities of pappus part numbers in *Microseris* species.**
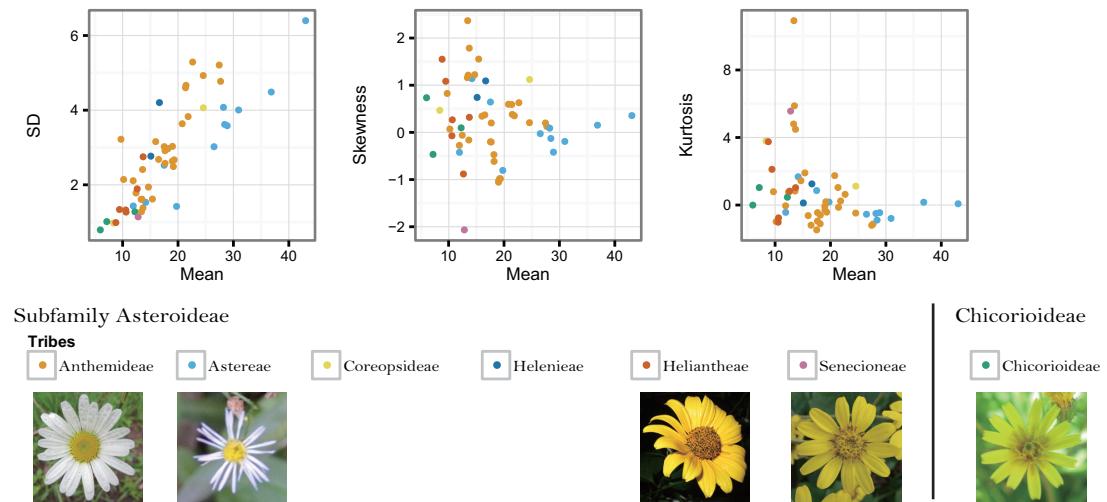
Figure 3.8: **Statistical quantities in variations of ray floret number in Asteraceae.** The colour represents the tribes, and the photographs show a species included in each section. SD is almost proportional to mean, whereas skewness and kurtosis are convergent to zero as mean increases.

Flower number variation in capitulum in Asteraceae (Asterales)   All Asteraceae plants develop capitulum inflorescences. The composition of florets is differ between Asteraceae subfamilies. Subfamily Asteroideae includes tribes Anthemidae (*Leucanthemum*; ox-eye daisy and *Chrysanthemum*), Astereae (*Aster*), Coreopsideae (*Cosmos* and *Dahlia*), Helenieae (*Gaillardia*), Heliantheae (*Helianthus*; sunflower), Senecioneae (*Senecio*), which heads have both ligulate and tubular florets. On the other hand, heads of subfamily Cichorioideae (dandelion) consist of only ligulate florets.

The floret number in Asteraceae flowers has been a subject of the studies of the organ number variation [70,170] The point of contention was whether or not the modal numbers of ray floret number in *Leucanthemum vulgare* (syn. *Chrysanthemum leucanthemum*) follows the Fibonacci sequence [23, 23, 94, 170, 211, 304]. The ray floret number of *Leucanthemum* varies about from ten to 50, and often has several peaks in a variation in a population. For instance, Ludwig reported the variation with peaks on 21 and 34.

The calculation of statistical quantities of Asteraceae ray floret numbers for multiple populations revealed that the SD is almost proportional to the mean (Fig. 3.8). It means the degree of variation increases as the average number increases. The proportionality constant is slightly different between tribes Helenieae (dark orange in Fig. 3.8; *Helianthus*, *Rudbeckia*, Anthemideae (light orange in Fig. 3.8; *Anthemis* [170], *Glebionis* [70, 170], *Cota* [170], and *Leucanthemum* [23, 23, 94, 170, 211, 304]), and Astereae (blue in Fig. 3.8; *Aster* [115, 272], *Callistephus* [124], *Symphyotrichum* [272]), and the former is larger.

Ovule and seed number variation.   Ovules and seeds are not the lateral organs of floral bud as perianth, stamens, and carpels, hence I examined the variation curves of them to know whether they are different from the lateral organs (Fig. 3.9). The SD is almost proportional to mean, with different gradient depending on families. In Papaveraceae (basal eudicots), the degree of variation is almost the same between ovules and seeds, whereas the variation of seed number is larger than that of ovule number in Malvaceae and Fabaceae (core eudicots), indicating different pollination efficiency between these families. The features of skewness and kurtosis are hardly found. These features are similar to Ranunculaceae stamens/carpels and Asteraceae ray florets, indicating the proportional relationship between SD and mean appears in the variation with large mean (> 10).
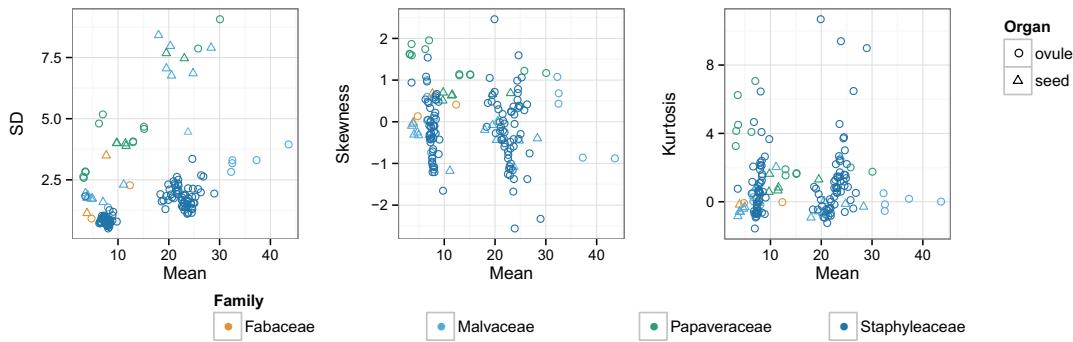
Figure 3.9: **Ovule and seed number variation.**

3.4.3   Relationship between SD and mean

To quantitatively examine the relationship between SD and mean, I calculated the correlation coefficient for the above species and organs, and applied two functions for the relationship.

Correlation.   The Pearson product-moment correlation coefficient for several species (Tab. 3.1) shows quantitative expression of the qualitatively described in previous sections. Majority of the species show the correlation between SD and mean (> 0.4). On the other hand, some species and organ such as *Eranthis pinnatifida* nectary

number does not show correlation between them (< 0.2). The correlation coefficient changes depending on the extent of the group to calculate, for instance, there are no correlation if only the data sets of *Nyctanthes arbor-tristis* are includes, but strong correlation is found if the data sets of *Jasminum multiflorum* are also included.

Table 3.1: **Correlation coefficient between SD and mean.** References are cited in Refs column, and data set number is in Data column. $*1$ [94,170,211,304], $*2$ [70,94,170,211,304], $*3$ [17,171,176,251,327], $*4$ [176,255,327], $*5$ [17,45,70,171,176,218,250,251,253]

Family	Species	Organ	Data	Refs	Mode	Corr. coef.
Asteraceae	*Glebionis segetum*	ray floret	17	[70, 170]	13, 14, 21	0.72
	Leucanthemum vulgare	ray floret	9	$*1$	16, 21, 22, 33	0.75
	family Asteraceae	ray floret	56	$*2$	6–43	0.83
Oleaceae	*Nyctanthes arbor-tristis*	petal	36	[241]	6	0.17
	family Oleaceae	petal	61	[241]	6, 8, 10	0.85
Malvaceae	*Hibiscus syriacus*	ovule (per locule)	5	[119]	6, 8	0.60
	H. syriacus	seed (per locule)	5	[119]	4, 5	-0.80
	genus *Hibiscus*	seed (per locule)	8	[119]	4–25	0.88
Papaveraceae	*Sanguinaria canadensis*	petal	9	[283]	8	0.67
Ranunculaceae	*Anemone flaccida*	tepal	11	[201]	5	0.97
	A. nemorosa	tepal	7	[334]	6,7	0.71
	genus *Anemone*	tepal	32	[201, 334]	5–12	0.58
	Eranthis pinnatifida	tepal	8		5	0.63
	E. pinnatifida	nectary	8		7, 8	0.15
	Ranunculus ficaria	petal	19	$*3$	8, 9, 10	0.42
		sepal	13	$*3$	3, 5	0.58
		stamen	7	$*4$	21–33	0.96
		carpel	7	$*4$	15–27	0.63
	R. japonicus	petal	17		5, 6	0.93
	genus *Ranunculus*	sepal	18	$*5$	3, 5	-0.012
	genus *Ranunculus*	petal	53	$*5$	3–10	0.49

Some group, such as the sepals in genus *Ranunculus*, does not have correlation (Tab. 3.1) but their relationship is highly non-random (Fig. 3.2). Therefore next I examined the fitting of two functions to the relationship.

The function that explains the relationship between SD and mean. Since the relationship between SD and mean seems like as following $SD = c\sqrt{|Mean - d|}$ in *Ranunculus* and $SD = a * Mean - b$ in the variations with large mean, I applied these two functions to the SD-mean relationship by non-linear least square method and compare them by the residual sum of squares (RSS; Tab. 3.2.

Indeed the *Ranunculus*-perianth-type variation such as *Anemone flaccida* tepals, *Ranunculus ficaria* sepals, and *R. japonicus* petals, the relation $SD = c\sqrt{|Mean - d|}$ is much proper than $SD = a * Mean - b$. In these species, $c = 1$ and d corresponds to the hidden modal number, namely, $d \simeq 5$ in *A. flaccida* tepals and *R. japonicus* petals, and $d = 3$ in *Ranunculus ficaria* sepals. Although the large-mean type variation, such as in Asteraceae ray florets and *R. ficaria* stamens and carpels, showed high correlation between SD and mean, it was not fit by the $SD \propto \sqrt{|Mean - c|}$. SD of the *Eranthis*-nectary-type variation was almost constant for the mean, as indicated by small correlation coefficient and proportionality coefficient a.

Table 3.2: **mean-SD relationship.** * $P < 0.01$, ** $P < 0.001$. RSS is the residual sum of squares. See Tab. 3.1 for references and number of data sets. *1 data sets whose mean is smaller than four.

Family	Genus/ Species	Organ	Mode	$SD = a * Mean - b$			$SD = c\sqrt{Mean - d}$		
				a	b	RSS	c	d	RSS
Asteraceae	*Glebionis segetum*	ray floret	13,14 ,21	0.178*	0.445	2.81	0.904**	8.71**	2.82
	Leucanthemum vulgare	ray floret	16,21, 22,33	0.205	0.256	2.68	1.41**	12.8*	2.30
Papaveraceae	*Sanguinaria canadensis*	petal	8	0.989	7.30	0.117	1.46*	7.90**	0.110
Ranunculaceae	*Anemone flaccida*	tepal	5	1.14**	5.48**	0.0119	0.980**	4.97**	0.00264
	A. nemorosa	tepal	6,7	0.420	1.99	0.0315	0.813 *	5.67**	0.0305
	Eranthis pinnatifida	tepal	5	0.618	2.79	0.0221	0.658	4.80**	0.0225
		nectary	7,8	0.0364	-0.832	0.0918	0.279	-8.14	0.0918
	Ranunculus ficaria	petal	8,9,10	0.281	1.48	1.53	0.699*	6.79**	1.55
		sepal *1	3,5	1.14**	3.27**	0.0697	1.07**	3.00**	0.0391
		stamen	21–33	0.130	-1.46	13.9	1.15	8.00	13.8
		carpel	15–27	0.267	-0.415	18.8	1.76	8.67	18.1
	R. japonicus	petal	5,6	0.854**	4.00**	0.101	1.08**	4.97**	0.0417

3.5 Discussion on floral organ number variation and statistical quantities

From the calculation of statistical quantities of floral-organ number variation in multiple populations, I found three types of relationships between mean and other statistical quantities. The *Ranunculus*-perianth-type showed high correlation between SD and mean, whose relation is on the function as $SD = c\sqrt{|Mean - d|}$. As the mean increases, the $SD = c\sqrt{|Mean - d|}$ relation becomes less obvious, but still the correlation between SD and mean is highly prominent. This large-mean type includes stamen, carpel, ovule, and seed number variations in various families, and ray floret number variations in Asteraceae. Although the above two types continuously can appear with increasing mode, there is another totally different type. It is the *Eranthis*-nectaries, which shows no correlation between the SD and mean. These three types of SD-mean relationship imply there are at least three sources of stochasticity in biological process. SD-mean relationship can be a indicator of stochasticity in floral development, likewise the Fano factor ($\sigma^2/mean$) in stochastic gene expression in which the different biological processes are reflected [141,206,297].

In the *Ranunculus*-perianth-type, SD falls to zero at specific numbers d indicating high stability of that numbers. The preference for specific numbers was insisted by Ludwig for Asteraceae floret number [170]. Shull, who was sceptical about the Luwig's law, referred the Lucas's result that has 22 as mode [94] and stated it implies the modal number changes depending on the location not following the Fibonacci-related numbers [272]. He criticized the Ludwig's law since if we consider the Unterzahlen (the product or sum of Fibonacci numbers; e.g. 5×2) and Scheingipfel (the fake mode appears between close Fibonacci-related numbers because it is adjacent to two "true" modes; e.g. 9, the number between Fibonacci number 8 and Unterzahlen 10) as Ludwig insisted, large proportion of natural numbers can be included in the Fibonacci-related numbers. In this point I agree with Shull, and not with Ludwig's law from a view that the superficial modal numbers are related to the Fibonacci number.

On the other hand, the stability on specific numbers, aside from whether they are Fibonacci numbers or not, is exist as the hidden modal number. In the variations of *Ranunculus* petals, the standard deviation is convergent to zero and the absolute value of skewness and kurtosis are considerably large when the mean of the population is near to three, five or eight, indicating high preference for these numbers (Fig. 3.2). Are these stable numbers, what I called hidden modal number, specific to the species, genus, or higher clade, or conserved among angiosperms? The fact that the especial stability on five-numbered perianth shown by the relationships between mean and SD, skewness, and kurtosis, respectively, are similar between two genera *Ranunculus* (Fig. 3.2) and *Anemone* (Fig. 3.3)

seems to indicate that five is conserved as the stable organ number for these two genera. However, there are two points that reject the conservation of stable number among species. First, SD-mean relationship in some species in Anemoneae such as *A. nemorosa* and *Hepatica nobilis* is slightly shifted indicating the mode number of the species is not five but six (Fig. 3.3). Second, in *Ranunculus bulbosus* generations which experienced selection by de Vries [70], SD monotonically increases as mean gets larger, and skewness and kurtosis monotonically falls to zero with increasing mean. This indicates that the hidden modal number of *Ranunculus ficaria*, eight, is not the hidden modal number of *Ranunculus bulbosus*.

In the perianth segment number of Ranunculaceae, except for some *Anemone* species, the hidden modal number is agreed with the superficial modal number appeared in the variation curve of each population, therefore the advantage of usage of the statistical quantities to find the hidden modal number is not clear. On the other hand, such species that the superficial modal number differ among population as *Leucanthemum* [94, 170, 272], it can be a powerful tool to find the original mode of the species. Taking the idea that the hidden mode appears as the high absolute-skewness and kurtosis into consideration, we find hidden modal numbers around 8, 13, and 20 in the ray-floret number variation (Fig. 3.8) although it needs further verifications. The discussion on Ludwig's law would be advanced by employing the hidden modal number for each species.

3.6 Partial conclusion

Using the statistical quantities, I found three types of SD-mean relationship in the floral organ number, depending on floral-organ types and taxonomic clades. These types of SD-mean relationship can be an indicator of different sources of stochasticity in the developmental processes. The relationship between mean and skewness and kurtosis shows how the variation changes between mean phenotypes, and gives a novel way to find a hidden mode phenotype of the species. What developmental process determine the hidden mode phenotype and how the variation is generated is the further problem to solve the affect of the developmental process to evolution.

4 Statistical Model Selection for Variation Curves of Floral Organ Numbers

4.1 Abstract

Stochasticity ubiquitously inevitably appears at all levels from molecular traits to multicellular, morphological traits. Intrinsic stochasticity in biochemical reactions underlies the typical inter-cellular distributions of chemical concentrations, e.g., morphogen gradients, which can give rise to stochastic morphogenesis. While the universal statistics and mechanisms underlying the stochasticity at the biochemical level have been widely analysed, those at the morphological level have not. Such morphological stochasticity is found in floral organ numbers. Although the floral organ number is a hallmark of floral species, it can distribute stochastically even within an individual plant. The probability distribution of the floral organ number within a population is usually asymmetric, i.e., it is more likely to increase rather than decrease from the modal value, or vice versa.

I combined field observations, statistical analysis, and mathematical modelling to study the developmental basis of the variation in floral organ numbers among species mainly from Ranunculaceae and several other families from core eudicots. I compared four hypothetical mechanisms and found that a modified error function reproduced much of the asymmetric variation found in eudicot floral organ numbers. The error function is derived from mathematical modelling of floral organ positioning, and its parameters represent measurable distances in the floral bud morphologies. The model predicts two developmental sources of the organ-number distributions: stochastic shifts in the expression boundaries of homeotic genes and a semi-concentric (whorled-type) organ arrangement. Other models species- or organ-specifically reproduced different types of distributions that reflect different developmental processes. The organ-number variation could be an indicator of stochasticity in organ fate determination and organ positioning.

4.2 Introduction

The developmental bases of stochasticity in the discrete traits, such as that in organ numbers has been little examined in animals [16] and plants [18]. Do universal statistical laws govern the stochasticity appearing at the morphological level? If the answer is yes, then how do stochasticity at the molecular level and developmental properties regulate those laws? In section 3, I showed three types of SD-mean relationship, which might imply the different developmental bases of the stochasticity. Here I discuss the application four models that produces characteristic distribution to floral organ number, and which model is the most plausible for each species- and organ-type-specific variation.

To account for the right-tailed asymmetric distribution found in the Ranunculaceae, Pearson proposed the beta distribution [210]; however, there are three fundamental problems with that idea. First, the beta distribution requires continuous variables and is therefore not well suited to discrete organ numbers. Second, the beta distribution has not been examined in other species for over a century. Third, the beta distribution hardly gives a developmental underpinning. The floral organ numbers are determined during the initiation and fate determination of the floral organs. Scanning electron microscopic studies of the initiations of floral organs revealed that the sepal primordia initiate in sequential, helical order in the Ranunculaceae [229], the main target of the present paper, and in several other families such as the Caryophyllaceae [174] and the Oleaceae [67]. These species exhibit considerable variation in floral organ numbers, as I will show. The identity of the organ primordia is determined after initiation by the so-called ABC genes [60]. These two processes, the sequential initiation and subsequent determination of organ identity, are the candidate sources of the stochasticity in the floral organ numbers. The helical initiation order is similar to spiral phyllotaxis. Stochasticity in the angular and radial positioning of spiral phyllotaxis [78, 230] has been studied both experimentally [32, 214, 222] and theoretically [113, 189]. No model has been proposed, however, for the stochasticity in the organ positioning and the spatial expression pattern of fate determination genes during floral development.

I performed a review and statistical comparison of four hypothetical mechanisms for the stochastic determination of floral organ numbers in eudicots. I combined field observations, statistical analysis, and mathematical modelling to study the developmental basis of variation in floral organ numbers. The statistical selection of the best model to describe the observed variation in floral organ numbers clarified that a distribution based on a homeosis, which

is derived from mathematical modelling of the floral organ positioning and its parameters represent measurable distances on the floral bud morphologies, widely reproduced the asymmetric variation found in nature. Moreover, the model predicts several mechanisms for the observed distributions (e.g., stochastic shifts in the expression boundaries of genes). The homeosis model requires a semi-concentric organ arrangement (i.e., the whorled-type arrangement) to give an asymmetric distribution, whereas it does not require such an arrangement to give a symmetric distribution. The organ-number variation could be an indicator of stochasticity in organ fate determination and organ positioning during floral development.

4.3 Method

4.3.1 Plant materials

In addition to the species used in section 3, I used published data for Papaveraceae [118, 283], hybrid of Asteraceae [18], and Oleaceae [241], because these data show the features I cannot found in my own field works.

4.3.2 Models and their biological bases

Floral organ arrangement (FOA) model based on dynamic phyllotaxis model. In the previous section I showed that the three parameters, $R_0/V\tau$ representing the ratio of the meristem size and average deviation distance of primordia, repulsive range λ_g, and temporal decay α, control the transition between merosities. Since natural variation of floral meristem sizes is observed and the increase of the floral meristem sizes (R_0) associates with the increase of floral organ number variation [58], I assumed $R_0/V\tau$ varies following standard Gaussian distribution with μ_R and σ_R (Fig. 4.1). Cumulating the probability that $R_0/V\tau$ is in the region of X-merous arrangement, I obtained the probability of each floral organ number X (Fig. 4.1B–D).
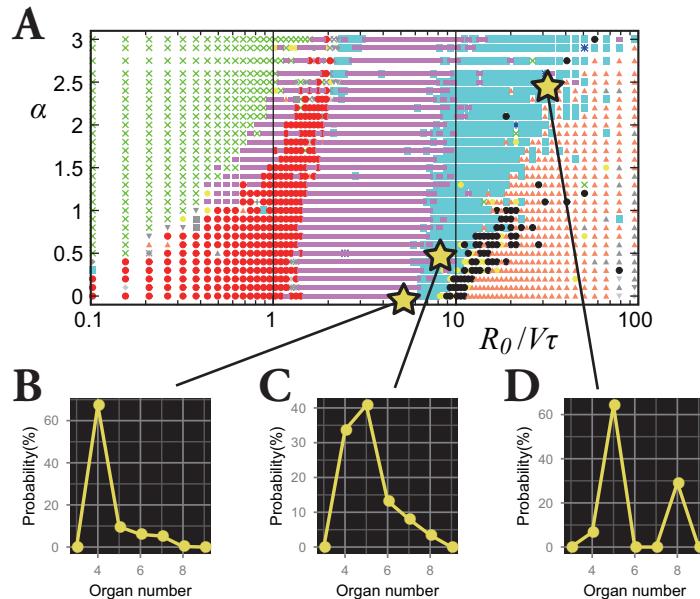

Figure 4.1: **Floral organ arrangement model. A.** The phase diagram obtained as a result of floral organ arrangement model (Section 2). Stars represent $(R_0/V\tau, \alpha) = (\mu_R, \alpha)$ of B–D. **B–D.** Examples of variation curves of floral organ numbers generated by the FOA model. A. $\mu_R = 5.0$, $\sigma_R = 2.5$, and $\alpha = 0.0$. B. $\mu_R = 8.0$, $\sigma_R = 2.5$, and $\alpha = 0.5$. C. $\mu_R = 30.0$, $\sigma_R = 5.0$, and $\alpha = 2.5$.

46

Poisson model. Suppose that each flower has a special number c of candidate sites that usually grow one primordium but rarely have two primordia. When the probability of having two primordia is very low but not negligible (i.e., the average value of λ in Eq. 4.1 below is on the order of unity or more and is given by $c \times n \times p$, where p is the probability that the rare event occurs and n is the number of counted flowers), the organ number satisfies the condition for the Poisson distribution. [18] predicted this as the developmental source for the Poisson distribution of floral organ-number variation. If a candidate site can have one or two primordia, the distribution becomes right-tailed (Fig. 4.2A, B); whereas if a site can have one or no primordium, the distribution becomes left-tailed (Fig. 4.2C). A stochastic increase in the number of primordia is reminiscent of reaction-diffusion-like patterning: a single concentration peak (e.g., a peak in phytohormone auxin concentration) preceding the emergence of a primordium sometimes splits into two primordia due to expansion of the space (Fig. 4.2A). Such organ splitting was observed in *Abelia* leaves [80] and tomato floral organs upon exposure to low temperature [169]. A stochastic decrease in the number of primordia can be induced by the fusion of two primordia that results no primordium in a candidate site (Fig. 4.2C). The difference between the actual organ numbers and the mode c follows the Poisson distribution when the probability of a stochastic increase or decrease is very low but not negligible.
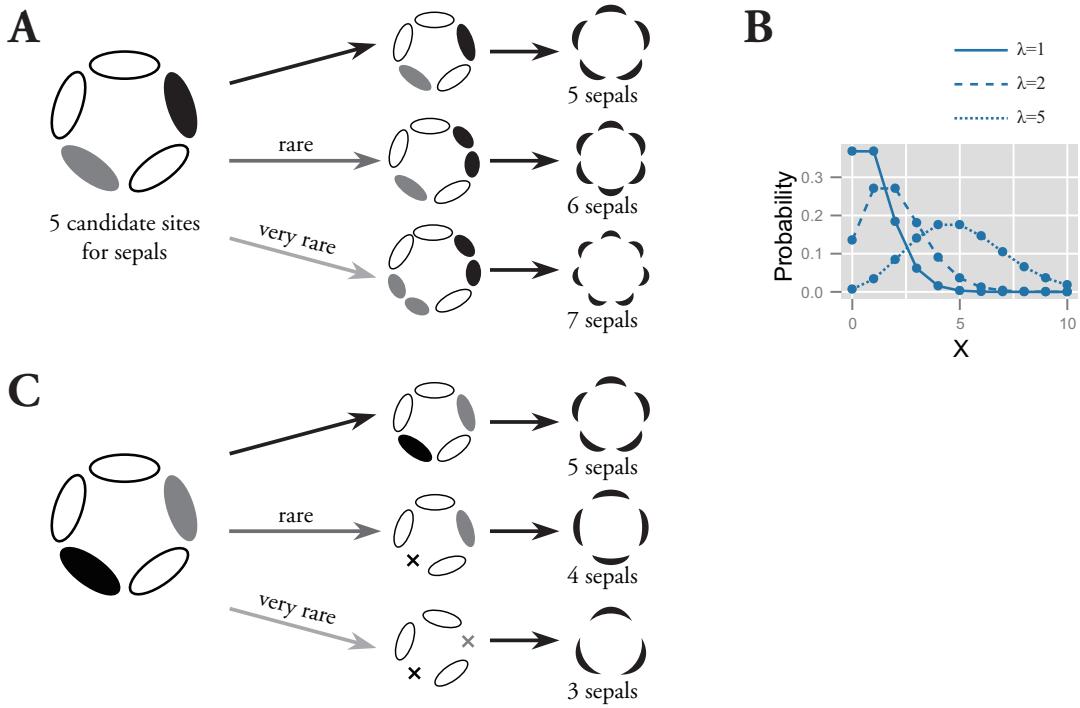

Figure 4.2: **The idea to apply the Poisson distribution to the variation in floral organ numbers [18]. A, B.** The Poisson model for positively skewed variation. **C.** The Poisson model for negatively skewed variation.

The probability density function of the Poisson distribution is given by

$$P_{Po}(X; \lambda) = \frac{\lambda^X}{X!} \exp(-\lambda), \tag{4.1}$$

where the parameter λ corresponds to the mean (Fig. 4.2B). By introducing the parameter representing the mode c, the equation is modified to

$$P_{mPo}(X; \lambda, c) = P_{Po}(X - c; \lambda). \tag{4.2}$$

Standard homeosis model. Some of the stochasticity in floral organ numbers is induced by so-called homeotic transformations, i.e., the variations in the determination of floral organ identities [110]. For example, in a natural population of Ranunculaceae, the nectary-like or stamen-like narrow tepals, bract-like green tepals, or petal-like stamens that lack the anther sporadically appear (Fig. 4.3A). Also, the increase in perianth organ number accompanied by disruption of the perianth/stamen boundary was observed experimentally by silencing the homeotic gene *APETALA3* paralogue in *Nigella damascena*, Ranunculaceae [111]. Therefore, I constructed a model of homeotic transformations targeting the outer organs, such as the sepals, petals, and tepals, derived from the floral meristem.
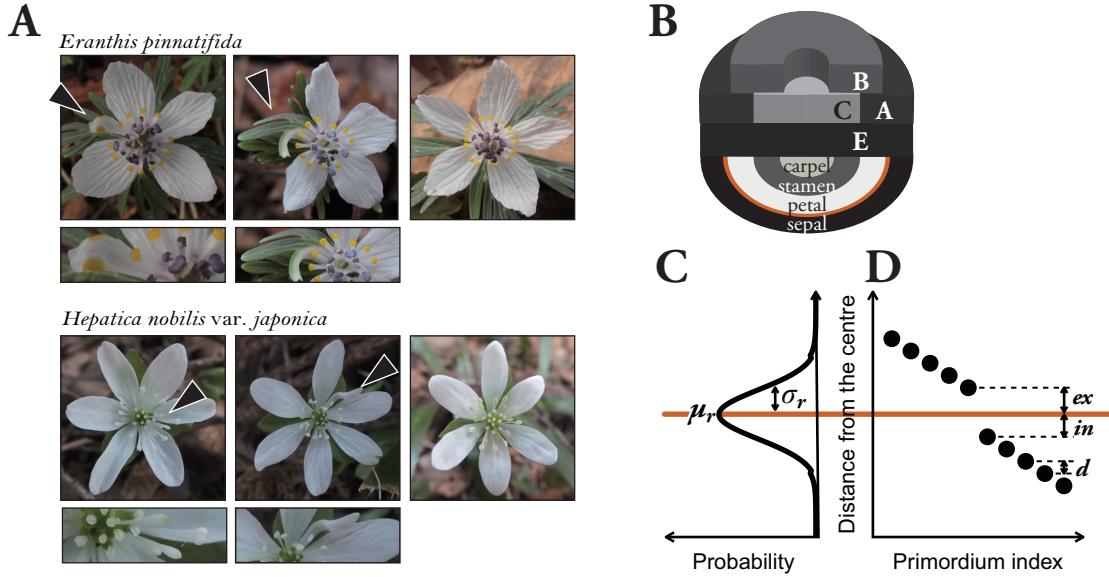

Figure 4.3: **Developmental model for the based on homeosis. A.** Examples of homeosis, where the typical flowers are shown at the right and the flowers with homeosis are shown in the left and middle panel. The bottom small panels shows the magnification of transformed organs indicated by the arrowheads in the top panel. **A.** Schematic illustration of the ABC model. A flower separated into four regions according to the expression of the ABC genes. **B.** The assumption for the variation of the boundary. The variation in the position of the expression boundary of the B gene follows a normal Gaussian distribution with average μ_r and standard deviation σ_r (Eq. 4.3). **C.** Schematic diagram of the assumption of the primordia position proposed in the homeosis model. In a single whorl, all primordia have an identical radial distance d from the previous primordia. The distance gap between successive whorls is given by $ex + in$, where ex and in denote the distance from the average boundary μ_r to the last (innermost) primordium of the first whorl and the first (outermost) primordium of the second whorl, respectively (Eq. 4.5).

Floral organ identities are determined by homeotic genes, referred to as the ABC genes, which are expressed in a concentric manner (Fig. 4.3B) [60]. For example, in the concentric region where only gene A is expressed (i.e., the region outside the expression boundary of gene B indicated by orange line in Fig. 4.3B), the primordia differentiate into sepals. The homeotic transformations are observed even in an individual plant, indicating that it occurs non-genetically. The non-genetic homeotic transformations are explained by the variation of expression boundary of ABC genes, that is to say, when the expression boundary varies within a floral population, the number of sepals is variable. Similar variation in expression boundaries has been extensively studied in fruit fly *Drosophila* embryos. The boundary where the concentration of morphogens such as the Bicoid and Hunchback proteins exceeds a threshold value varies among individual embryos [30, 134]. In such cases, the threshold position can follow a

Gaussian distribution if the concentrations of mRNA molecules, the concentration of morphogen degrading enzyme (which is usually proportional to enzyme degradation rate), and other molecular properties also follow a Gaussian distribution. Although quantitative studies of the ABC genes have not yet been reported, as an initial step, I assumed that the expression boundary positions of a gene determining floral identity follow a Gaussian distribution (e.g., B gene in Fig. 4.3B). The probability density that the boundary is at radial position r is given by

$$P_{gene}(r; \mu_r, \sigma_r) = \frac{1}{\sqrt{2\pi}\sigma_r} \exp\left(-\frac{(r - \mu_r)^2}{2\sigma_r^2}\right).$$ (4.3)

where r, μ_r, and σ_r denote the radial distance from the meristem center and the average and standard deviation of the distance within the population, respectively (Fig. 4.3C). The probability of having X organs (e.g., sepal in Fig. 4.3) is given by the integral of the probability that the boundary is located between the radial positions of X-th and $X + 1$-th primordia. The probability of the organ number being X is calculated by integrating the probability of the boundary position given by Eq. 4.3 for this region

$$P_{er}(X) = \int_{r_{X+1}}^{r_X} P_{gene}(r)\, dr.$$ (4.4)

where r_{X+1} and r_X are the radial positions of the $X + 1$-th and X-th primordia, respectively (Fig. 4.3).

In addition to the boundary variation, I assumed that the organs take on the semi-whorled arrangement that is widely observed in the Ranunculaceae [236] and the Caryophyllaceae [174] (Fig. 4.3C). The semi-whorl stands for the small variation among the radial positions within an apparent whorl. For simplicity, I assumed that the distances from the floral apex are regularly spaced within a whorl with an interval d (Fig. 4.3C that represents a pentamerous whorl, i.e., the modal organ number $Mo = 5$, as an example). I defined the radial gap between two semi-whorls as $ex + in$, where the average position of expression boundary μ_r is located between the Mo-th and $(Mo + 1)$-th (e.g. the fifth and sixth when $Mo = 5$) primordia at distances ex and in, respectively.

From this assumption of semi-whorled arrangement, the position of X-th primordium r_X is written as follows by the four parameters of the floral whorl: μ_r (the average boundary position), ex (the radial distance between μ_r and the interior edge of the exterior whorl), in (the radial distance between μ_r and the exterior edge of the interior whorl), and d (the radial distance between two successive primordia within each whorl)

$$r_X = \begin{cases} \mu_r + ex + d(Mo - X) & (X \leq Mo) \\ \mu_r - in + d(Mo - X + 1) & (X > Mo), \end{cases}$$ (4.5)

where Mo is the mode defined by the most frequent number of floral organs (e.g., $Mo = 5$ for sepals in Fig. 4.3D). By substituting Eq. 4.5 into Eq. 4.4, the probability of sepal number X becomes

$$P_{er}(X) = \begin{cases} \int_{\mu_r+ex+d(Mo-X-1)}^{\mu_r+ex+d(Mo-X)} P_{gene}(r)\, dr & (X < Mo) \\ \int_{\mu_r-in+d(Mo-X)}^{\mu_r-in+d(Mo-X+1)} P_{gene}(r)\, dr & (X > Mo) \\ \int_{\mu_r-in+d(Mo-X)}^{\mu_r+ex+d(Mo-X)} P_{gene}(r)\, dr & (X = Mo). \end{cases}$$ (4.6)

Using Eq. 4.3 and the variable transformation $z = (r - \mu_r)/\sqrt{2}\sigma_r$, Eq. 4.6 is rewritten as

$$P_{er}(X) = \begin{cases} \frac{1}{\sqrt{\pi}} \int_{\frac{ex+d(Mo-X-1)}{\sqrt{2}\sigma_r}}^{\frac{ex+d(Mo-X)}{\sqrt{2}\sigma_r}} \exp\left(-z^2\right) dz & (X < Mo) \\ \frac{1}{\sqrt{\pi}} \int_{\frac{\mu_r-in+d(Mo-X)}{\sqrt{2}\sigma_r}}^{\frac{\mu_r-in+d(Mo-X+1)}{\sqrt{2}\sigma_r}} \exp\left(-z^2\right) dz & (X > Mo) \\ \frac{1}{\sqrt{\pi}} \int_{\frac{-in}{\sqrt{2}\sigma_r}}^{\frac{ex}{\sqrt{2}\sigma_r}} \exp\left(-z^2\right) dz & (X = Mo) \end{cases}$$ (4.7)

The Gaussian integral with finite range is rigorously represented by the error function (ERF) given by

$$\mathrm{erf}(z) = \frac{2}{\sqrt{\pi}} \int_0^z \exp\left(-z^2\right) dz.$$ (4.8)

49
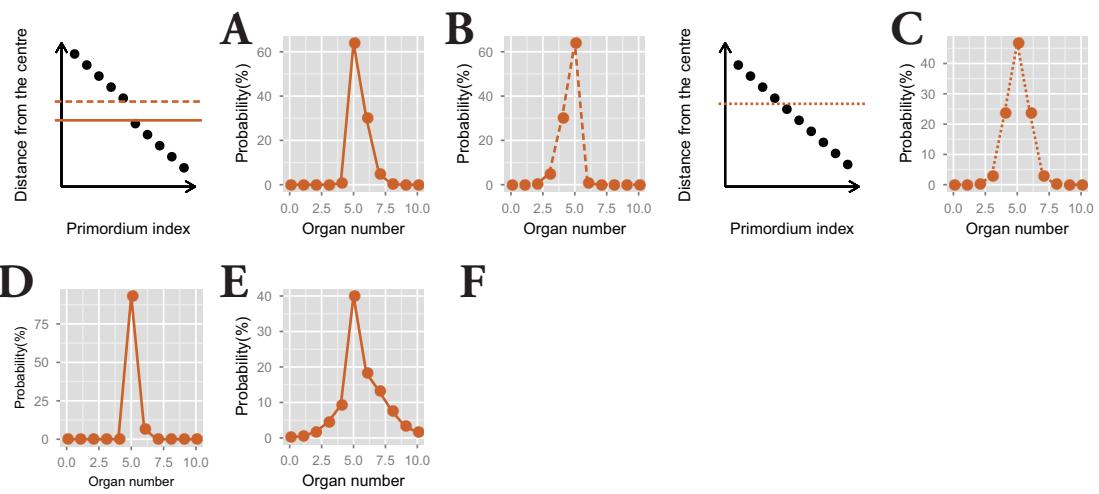
Figure 4.4: **Organ number distribution generated by the homeosis model. A–C.** Three different forms (skewness) of modified homeosis calculated by the integrals using the NORM.DIST function in Microsoft Excel, which is the cumulative distribution function of the Gaussian distribution. $ex > in$ causes a right-skewed distribution (**A**; $ex = 2.0$, $in = 0.3$, $\sigma = 0.8$), whereas $in > ex$ causes a left-skewed distribution (**B**; $ex = 0.3$, $in = 2.0$, $\sigma = 0.8$). If $ex = in = d/2$, the distribution of the organ numbers becomes symmetric (**C**; $ex = 0.5$, $in = 0.5$, $\sigma = 0.8$). $d = 1.0$ for **A–C. D, E.** The distribution with different kurtosis with different σ. The kurtosis is about 9 when $\sigma = 0.2$ (D), whereas it is about 6 when $\sigma = 2.0$ (E). The primordia position and the average position of expression boundary is the same to A.

By substituting Eq. 4.8 into Eq. 4.7 and normalizing parameters as

$$ex_d = \frac{ex}{d}, in_d = \frac{in}{d}, \sigma_d = \frac{\sigma}{d},\qquad(4.9)$$

the probability of floral organ number X becomes

$$P_{er}\left(X; ex_d, in_d, \sigma_d\right) = \begin{cases} \frac{1}{2}\mathrm{erf}\left(\frac{ex_d + Mo - X}{\sqrt{2}\sigma_d}\right) - \frac{1}{2}\mathrm{erf}\left(\frac{ex_d + Mo - X - 1}{\sqrt{2}\sigma_d}\right) & (X < Mo) \\ \frac{1}{2}\mathrm{erf}\left(\frac{in_d - (Mo - X)}{\sqrt{2}\sigma_d}\right) - \frac{1}{2}\mathrm{erf}\left(\frac{in_d + (Mo - X + 1)}{\sqrt{2}\sigma_d}\right) & (X > Mo) \\ \frac{1}{2}\mathrm{erf}\left(\frac{ex_d}{\sqrt{2}\sigma_d}\right) - \frac{1}{2}\mathrm{erf}\left(\frac{in_d}{\sqrt{2}\sigma_d}\right) & (X = Mo) \end{cases}.\qquad(4.10)$$

The first line of Eq. 4.10 ($X < Mo$) integrates the probability that the expression boundary is located within the exterior whorl, resulting in a decrease in the organ number. The second line ($X > Mo$) integrates the probability that the expression boundary is within the interior whorl. The third line ($X = Mo$) integrates the probability that the expression boundary is located within the gap between the two whorls.

The homeosis model is able to manipulate the skewness (by ex_d and in_d; Fig. 4.4A, B, C) and kurtosis (by σ_d and $ex_d + in_d$; Fig. 4.4A, D, E), hence it can account for two ubiquitous properties of floral organ-number variation (i.e., the asymmetry and the extraordinary mode probability). The skew to larger values of X becomes prominent as the difference $ex_d - in_d$ increases (Fig. 4.4A), whereas the skew to smaller values of X grows as $in_d - ex_d$ increases (Fig. 4.4). Symmetric variation is reproduced by two scenarios: $ex_d = in_d$ and/or $in_d + ex_d = 1$. When $ex_d = in_d$ and $in_d + ex_d > 1$, the kurtosis is larger than 0 (kurtosis of standard Gaussian distribution). $in_d + ex_d = 1$ indicates an equal radial distance between all successive primordia, as in spiral phyllotaxis [131], and the probability distribution becomes symmetric irrespective of other parameters (Fig. 4.4C). Thus, the homeosis model predicts that symmetric organ-number variation with low kurtosis indicates the spiral arrangement, or the discordant between position of the whorls and the expression boundary of ABC genes.

Homeosis model with boundary following log-normal distribution (log homeosis model). To test a possibility that the boundary of gene expression (Eq. 4.3) does not follow the standard Gaussian distribution but follows another function, I employed log-normal distribution for the boundary as a representative of heavy right-tail distribution that decreases as increasing from the mode more gradually than the standard Gaussian (Fig. 4.5A).

The probability density function of the log-normal distribution is given by

$$P_{ln}(r; \mu, \sigma) = \frac{1}{\sqrt{2\pi}\sigma r}\exp\left(-\frac{(\ln r - \mu)^2}{2\sigma^2}\right),\qquad(4.11)$$

where r represents the radial position in the floral bud. This function represents a Gaussian distribution when r is on a logarithmic scale, but it is skewed to larger values of r on a linear scale (Fig. 4.5A). The origin of the probability variable $r = 0$ can be shifted using another parameter c:

$$P_{mln}\left(r; \mu, \sigma, c\right) = P_{ln}\left(r - c; \mu, \sigma\right).\qquad(4.12)$$

When Eq. 4.12 was employed as the boundary of the expression gene in the homeosis model, there are four parameters. For easiness of calculation, I separately treated the gene-boundary parameters μ, σ, and c from the whorl indicator, namely, $gap = ex_d + in_d$.

Beta distribution Since Pearson [211] applied beta distribution for variation of petal number of *Ranunculus bulbosus* [70], I also tested beta distribution for that variation, in addition to above three models. Although the values of the probability variable X are continuous, I assumed that they represent the organ number.

The probability density function of the beta distribution is given by

$$P_\beta(X; \alpha, \beta) = \frac{X^{\alpha-1}\left(1 - X\right)^{\beta-1}}{\mathrm{B}\left(\alpha, \beta\right)},\qquad(4.13)$$
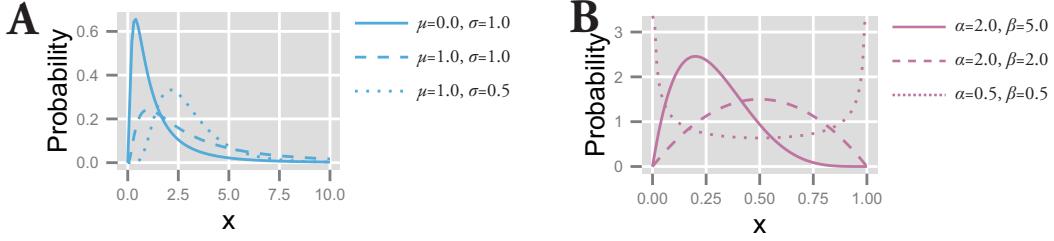
Figure 4.5: **Log-normal (A) and beta (B) distributions with various parameters.**

where $B(\alpha, \beta)$ is the beta function. The function is not only skewed to either larger or smaller values of X but also bimodal, depending on the two shape parameters α and β (Fig. 4.5B). Because the domain of the beta distribution is restricted to values between $X = 0$ and $X = 1$, in order to apply the beta distribution to floral organ numbers, the domain should be expanded between two real-number parameters c_{max}, i.e., the maximum organ number, and the minimum organ number c_{min} ($c_{max} > c_{min}$). By normalizing the factor $c_{max} - c_{min}$, the probability density function of the modified beta distribution can be represented by

$$P_{m\beta}(X; \alpha, \beta, c_{max}, c_{min}) = \frac{P_\beta\left(\frac{X - c_{min}}{c_{max} - c_{min}}; \alpha, \beta\right)}{c_{max} - c_{min}}, \tag{4.14}$$

where X denotes the organ number and $\frac{X - c_{min}}{c_{max} - c_{min}}$ is bounded by 0 and 1. We estimated this functional form of Eq. 4.14 from Pearson's original paper (equation in the middle of p. 401 in [210]).

4.3.3 Model fitting and selection

Model fitting (parameter selection) The fitting of the measured probability distribution to four models was determined using the non-linear least-square (NLS) method, where the probability of each organ number was a single data point. Because the organ number in each population does not distribute to a very large number of states (e.g., five states in Fig. 3.1B), convergence is difficult to obtain using NLS. To improve the convergence, I adopted the Levenberg-Marquardt algorithm [193]. For the Levenberg-Marquardt NLS fitting, I custom-designed a program using the R interface (http://www.r-project.org) with nlsLM function provided by the minpack.lm package [86]. The initial parameters were set arbitrarily to avoid parameter divergence during the NLS fitting, and three initial parameter sets were tested for each model.

Statistical model selection by AIC One of the most popular and statistically rigorous criteria for selecting the best-fit model is the Akaike-Information Criterion (AIC), which is represented by the parameter number of the model k minus the natural logarithm of the maximum likelihood L [Eq. 4.15; [7, 46, 248]].

$$\text{AIC} = -2\ln(L) + 2k. \tag{4.15}$$

The AIC can be used to autonomously select the best-fit statistical distribution, which gives the minimum value of the AIC. When the number of states M denoting the number of the organ number with non-zero frequency (e.g., $M = 5$ in Fig. 3.1B) is not very large compared with those of the parameters k, as in the present study, it is better to adopt the corrected AIC (AICc) given by

$$\begin{aligned}
\text{AICc} &= -2\ln(L) + \frac{2kM}{M - k - 1} \\
&= \text{AIC} + \frac{2k(k+1)}{M - k - 1},
\end{aligned} \tag{4.16}$$

which must satisfy $M > k + 1$ and converges to the AIC at the upper limit of M [291]. I computed the AICc for each combination of probability distribution and fitting function. Because the absolute value of the AICc does not

have any meaning, I used ΔAICc, which is defined as the difference in AICc between a given model and the best model [47], for ease of model comparison. Thus, the fitting function indicating ΔAICc = 0.0 is the best model, whereas models giving larger values are not as good. Generally, models with ΔAICc < 2.0 have the potential to be the best model, and those with ΔAICc < 7.0 cannot be easily rejected [47].

4.4   Results

4.4.1   Selection of the best statistical model of the perianth-lobe number variation in Ranunculaceae

To find the best model for each pattern of floral organ-number variation and to elucidate whether there is any common law that unifies the patterns, I performed non-linear least-square fitting of each data set containing more than five states (histogram in Fig. 3.1B,C) to three models based on different developmental process, and beta distribution proposed by Pearson. For each data set, the best-fit distribution was selected by the AICc (Eq. 4.16), which determines the best-fit distribution, even when the number of parameters differs among the fitting functions [7, 291]. In many cases, the ranking of the models based on the ΔAICc values were reproducible among different data sets representing the same organ in a given species (see the Methods section for definitions of AICc and ΔAICc).

|	A (n=1033)	B (n=252)	C (n=5160)	D (n=222)
FOA	39.49	8.00472	54.52	15.04
Poisson	26.55	27.60556	77.33	10.34
Homeosis (s)	0.00	0.00	8.36	0.00
Homeosis (l)	N/A	13.5987	0.00	22.49
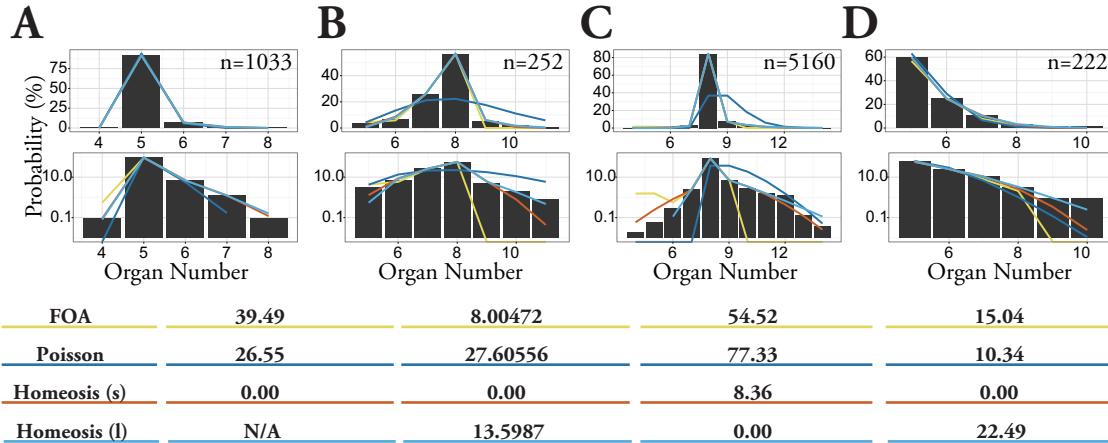
Figure 4.6: **The result of model fitting and selection for Ranunculaceae species.** The bar chart shows the observed frequency of each organ number, whereas the lines show the result of non-linear least-square fitting for four models. The numbers below each graph show the ΔAICc values for FOA model (phyllotaxis-model based floral organ arrangement model), Poisson model, homeosis model with standard Gaussian (s) and log-normal (l) boundary. **A.** *Anemone flaccida*, **B.** *Eranthis pinnatifida*, **C.** *Ranunculus ficaria* [17], and **D.** *Ranunculus bulbosus* [70].

The standard homeosis model could account for an extraordinarily high mode and asymmetric tails on both sides of the distribution.   The standard homeosis model was the best fit for the outer floral organs in three-fourths of the Ranunculaceae data sets (Tab. 4.1). The features of the variation that were best fit by the standard homeosis model were the high modal probabilities and the two-sided asymmetric tails, which FOA and Poisson models could not simultaneously account for (Fig. 3.2). The next dominant model was the log homeosis model. The data sets with the larger modal number were selected by log homeosis model in higher frequency. The majority of mode of tepal, petal, sepal number of Ranunculaceae species I examined is five, whereas it is larger in species best fit by log homeosis model (6 or 7 in *A. nemorosa*, 6 to 8 in *E. pinnatifida*, and 8 to 10 in *R. ficaria*). Also the tendency was found that the right tail follows log homeosis and the left tail follow standard one, in several data sets (Fig. 3.2C), indicating the variation curve becomes closer to log normal distribution than standard Gaussian distribution as the organ number increases.

Table 4.1: **The result of statistical model selection for Ranunculaceae perianth organs (petal, sepal, tepal).** Four models, namely, floral organ arrangement (FOA) model, Poisson model, and Homeosis models (two types of boundary with standard Gaussian and log-normal distribution), were compared by AICc. The denominators show the number of data sets, whereas numerators indicate how many times the model gave the smallest AICc values. * indicates original data collected by myself or my collaborators.

Species	Organ	Refs	FOA	Poisson	Homeosis Standard	Log
Anemone flaccida	tepal	[201]*	0/10	1/10	9/10	0/10
A. hupehensis var. *japonica*	tepals	*	0/3	0/3	3/3	0/3
A. narcissiflora ssp. *nipponica*	tepals	*	0/2	1/2	1/2	0/2
A. nemorosa	tepal	[334]	0/7	0/7	5/7	2/7
A. nikoensis	tepal	*	0/2	0/2	2/2	0/2
A. raddeana	tepal	*	0/	0/1	1/1	0/1
genus *Anemone*			0/25	2/25	21/25	2/25
Eranthis hyemalis	tepal	[251]	0/1	0/1	0/1	1/1
E. hyemalis	nectary	[251]	0/1	0/1	1/1	0/1
E. pinnatifida	tepal	*	0/1	0/1	1/1	0/1
E. pinnatifida	nectary	*	0/7	2/7	3/7	2/7
genus *Eranthis*			0/10	2/10	5/10	3/10
Hepatica nobilis var. *japonica*	tepals	*	0/1	0/1	1/1	0/1
Ranunculus arvensis	sepal	[45]	0/4	0/4	4/4	0/4
R. arvensis	petal	[45]	1/4	1/4	2/4	0/4
R. bulbosus	petal	[70]	0/6	0/6	5/6	1/6
R. cantoniensis	petal	*	0/1	0/1	1/1	0/1
R. ficaria	sepals	[17, 171, 176]	0/5	0/5	5/5	0/5
R. ficaria	petal	[17, 171, 176, 251, 327]*	0/18	1/18	12/18	5/18
R. japonicus	petal	*	0/15	2/15	13/15	0/15
R. parviflorus	petal	[253]	0/1	0/1	1/1	0/1
R. repens	sepal	[218]	0/1	0/1	1/1	0/1
R. repens	petal	[218, 250]	0/4	0/4	2/4	2/4
R. silerifolius	petal	*	0/1	0/1	1/1	0/1
genus *Ranunculus*			1/60	4/60	47/60	8/60
Trollius europaeus	nectary	[261]	0/1	0/1	1/1	0/1
T. europaeus	tepal	[261]	0/1	0/1	1/1	0/1
Total			1/98	8/98	76/98	13/98

Table 4.2: **The ΔAICc of four models applied for petal-number variation of *Ranunculus bulbosus* by de Vries [70].**

n	FOA	Poisson	Homeosis		Beta
			Standard	Log	
222	15.04	10.34	0.00	22.49	25.57
128	6.49	16.57	N/A	0.00	8.97
214	36.65	33.90	0.00	13.29	16.41
1130	56.75	56.82	5.62	23.48	0.00
337	7.59	2.04	0.00	N/A	N/A
380	12.90	21.55	0.00	14.16	14.67

Homeosis model accounted for the petal number variation of *Ranunculus bulbosus* better than the beta distribution. Pearson applied the beta distribution to petal number variation in *R. bulbosus* [210]. In addition to three models based on different developmental process, I compared beta model. I statistically revisited the six original data sets of *R. bulbosus* measured by de Vries (2894), which include two natural populations, one cultivated population, and three populations selected over several generations for greater petal number by the author [70]. Contrary to Pearson's results, three out of four data sets, which were able to find convergence of fitting parameters, were best fit by Homeosis (Tab. 4.2). Beta distribution was selected only for one data sets, suggesting that the Homeosis model is more plausible for the petal number variation in *Ranunculus bulbosus* than the beta distribution.

4.4.2 Selection of the best model for variation curves of other clades and organs

The variation curves with larger mode tend to be well-explained by the log homeosis model. The statistical model selection for variation curves with larger mode, such as stamen, carpel, ovule, seed, and ray-floret number variation, exhibited a little different results. The homeosis model was still the likeliest model, but the boundary function P_{gene} (Eq. 4.3) is more likely to follow log-normal distribution (Fig. 4.7).

The Poisson distribution fits the distributions of pappus part numbers of hybrid of *Microseris*, Asteraceae. The Poisson distribution of floral organ numbers was originally proposed for inter-specific hybrids of *Microseris* [18]. The pappus is homologous to sepal and, as in other eudicot species, the basic number is multiple of five in *Microseris*. Because the modal organ (pappus parts) numbers of the two parental species are different, namely, 5 in *M. bigelovii* and 10 in *M. pygmaea*, the organ number of the hybrids varies between the two parental modes [18].

We statistically tested the distributions of pappus part numbers in nine of the inter-specific hybrid populations of the genus *Microseris* published by Bachmann et al. [18]. Consistent with the earlier studies, 5/9 data sets for the hybrids generated by *M. pygmaea* × *M. bigelovii* crosses were best fit by the Poisson distribution, and 4/9 by the standard homeosis model (Fig. 4.8A). On the other hand, all of the pappus-number distributions in the three genuine species *M. douglasii*, *M. lindleyi*, and *M. pygmaea* best fit the standard homeosis model as species in other clades rather than the Poisson model (Tab. 4.3), suggesting that the hybrid populations whose parental species have different modal organ numbers show the Poisson-type variation, contrary to the majority of perianth organ number variation.

4.4.3 The parameters of the homeosis model

Since the Homeosis model with standard Gaussian boundary was the most dominant in the four models I compared as indicated by AIC_c, it is worth to examine the relevance of the parameters fit by the least square method, and their difference between clades and organs. This model has three parameters: The gap between whorls $ex_d + in_d$, the position of the boundary as the distance from the innermost primordium of the first whorl ex_d, and the
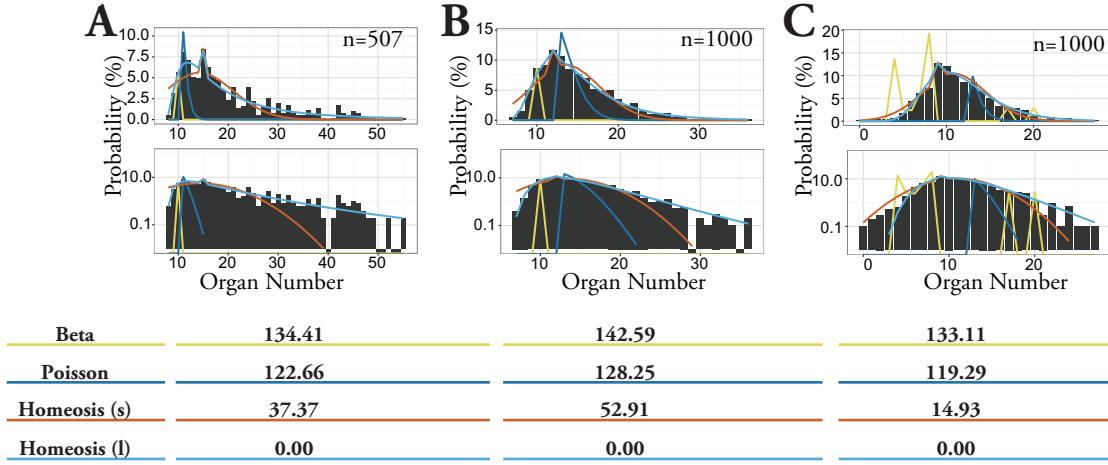
Figure 4.7: **Selection of the best model for variation curves with larger mode.** The bar chart shows the observed frequency of each organ number, whereas the lines show the result of non-linear least-square fitting for six models. The numbers below each graph show the ΔAICc values. **A.** Carpel number variation of *Ranunculus ficaria* [255], **B.** ovule number variation of *Sanguinaria canadensis* [118], and **C.** seed number of *Sanguinaria canadensis* [118].
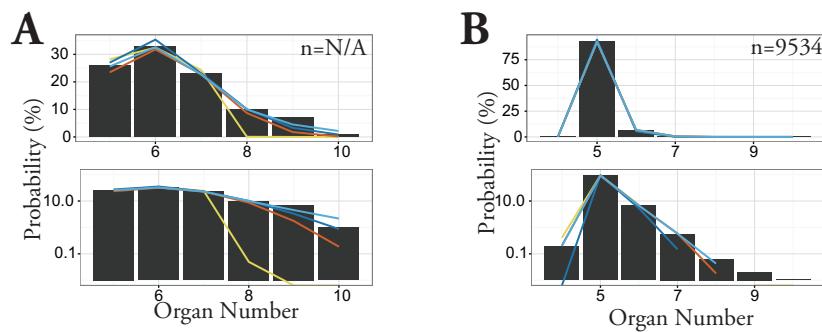

Figure 4.8: **The result of model fitting and selection for *Microseris*.** The bar chart shows the observed frequency of each organ number, whereas the lines show the result of non-linear least-square fitting for six models. The numbers below each graph show the ΔAICc values. **A.** *M. pygmaea* $\times$ *M. bigelovii* (corresponds to the seventh data in Tab. 4.3) [18], **B.** genuine species of *Microseris* (*Microseris lindleyi*) [18]

Table 4.3: The ΔAICc of four models applied for variation of *Microseris* pappus part numbers [18].

Species	n	FOA	Poisson	Homeosis normal	log-normal
M. douglasii	2514	18.94	30.03	0.00	27.64
M.lindleyi	9534	33.63	44.97	0.00	7.07
M. pygmaea	632	68.59	54.95	0.00	21.90
M. pygmaea × *M. bigelovii*	N/A	5.80	0.00	4.69	NA
	N/A	31.32	4.88	0.00	N/A
	N/A	23.42	0.00	12.68	33.86
	N/A	22.25	0.00	13.77	34.37
	N/A	21.22	17.83	0.00	17.97
	N/A	12.79	0.00	2.84	34.22
	N/A	17.63	2.58	0.00	32.50
	N/A	16.45	3.91	0.00	29.24
	N/A	15.22	0.00	3.30	25.94

standard deviation of boundary stochasticity σ_d. Biologically, $ex_d + in_d$ indicates the arrangement of the floral organ arrangement, whereas ex_d and σ_d are the properties of boundary.

The comparison between experimental data and parameters obtained by the fitting. Since I have data both for the developmental positions [174] and floral organ number variation [76]. From Lyndon [174], if we assume the average interval of successive sepals and petals within each whorl as $d = 1$, we can calculate the value $ex_d + in_d = 3.19$. Homeosis model fit by the non-linear least square method gave $ex_d + in_d = 4.83$, which agreed in the order but 1.5 times larger than the real floral parameters (Tab. 4.4).

Table 4.4: The ΔAICc of four models applied for variation curves of perianth of Caryophyllaceae, and the parameters of the homeosis models. The floral organ number variation of *Silene coeli-rosa* was measured by [76]. The asterisk ∗ indicates $Pr < 0.05$, ∗∗ $Pr < 0.01$.

Species	Organ	n	FOA	Poisson	Homeosis standard	log	Homeosis (standard) parameters ex_d	in_d	σ_d
Silene coeli-rosa	sepal	964	3.83	17.18	0.00	N/A	1.50 ∗	3.34	1.40 ∗
Silene coeli-rosa	petal	661	1.05	N/A	0.00	13.64	2.65	10.00	4.37
Moehringia lateriflora	petal	550	25.50	2.37	0.00	N/A	2.65 ∗∗	0.99 ∗∗	0.93 ∗∗

As in the two species in Tab. 4.4, the values of one species can several times larger than the other. However, among several data sets of the same organ of the same species, these values are close each other. The large gap corresponds to the extraordinary high probability on the mode, whereas the small gap indicates it is close to standard Gaussian (Fig. 4.9). These values can be thought as another representation of kurtosis that has botanical meaning as a indicator of floral organ arrangement.

Features of data sets with non-semi-whorled arrangement I compared the mean and standard deviation (SD) of $ex_d + in_d$, ex_d, and σ_d between the multiple data sets, if there are more than eight data sets for the same species and organ-type (Tab. 4.5).

Perianth segments numbers usually showed large $ex_d + in_d$. Only the variation curves of Oleaceae petal numbers, *Eranthis pinnatifida* nectary numbers, and also Primulaceae petal and sepal numbers showed small gap parameter
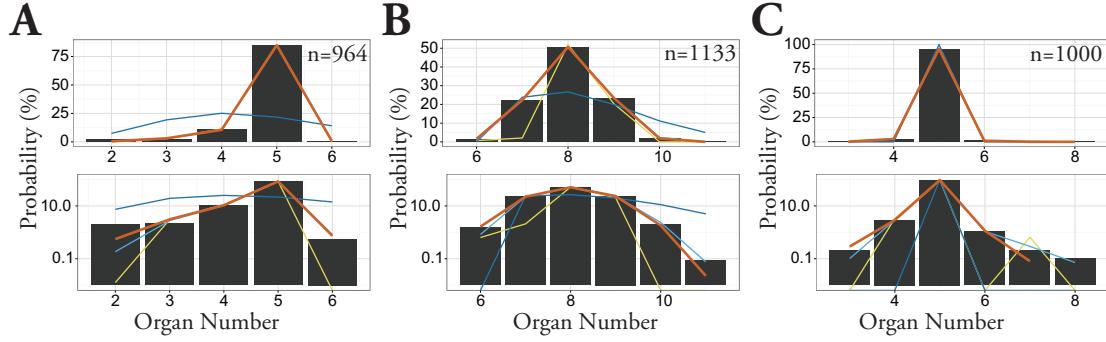
Figure 4.9: **The relationship between the homeosis model parameters and properties of variation curves.** The bar chart shows the observed frequency of each organ number, whereas the lines show the result of non-linear least-square fitting for the homeosis model. core eudicots. **A.** *Silene coeli-rosa*, **B.** *Jasminum multiflorum* var. that showed small gap parameter, **C.** . All datasets are from Roy (1963) [241].

Table 4.5: **The parameters of the homeosis model.** For each variation curve of perianth segments, the homeosis model was fit by the non-linear least square method. The parameters were then averaged for the same species and organ-type. The references are cited in the column (** see Tab. 4.1)

Family	Species	Organ	data	Refs	$ex_d + in_d$ mean	SD	ex_d mean	SD	σ_d mean	SD
Oleaceae	*Jasminum multiflorum*	petal	22	[241]	1.05	0.129	0.572	0.194	0.852	0.148
	Nyctanthes arbor-tristis	petal	36	[241]	1.28	0.248	0.620	0.276	0.605	0.0975
Papaveraceae	*Sanguinaria canadensis*	petal	9	[283]	8.74	4.23	5.70	2.49	2.88	1.28
Polemoniaceae	*Linanthus androsaceus*	petal	15	[135]	4.71	1.63	2.02	0.636	1.09	0.239
Ranunculacae	*Anemone flaccida*	tepal	10	**	3.64	0.916	2.53	0.524	0.961	0.125
	A. nemorosa	tepal	7	**	1.64	0.451	1.43	0.570	0.794	0.166
	Eranthis pinnatifida	nectary	7	**	1.36	0.422	0.417	0.288	1.12	0.103
	Ranunculus ficaria	petal	18	**	2.95	2.65	1.90	1.53	1.37	0.620
	R. japonicus	petal	14	**	6.31	2.11	3.88	1.37	1.47	0.352

$(ex_d + in_d < 1.5)$. In Ranunculaceae, 4/25 in *Anemone* and 9/57 data sets in *Ranunculus* had $ex_d + in_d < 1.5$. Interestingly, the modal number of almost all of Ranunculaceae data sets with small gap differ from other data sets of the same species (only one exception with $ex_d + in_d = 1.47$ and two lack any other data to compare).

4.5 Discussion

4.5.1 Developmental bases of the homeosis model

The homeosis model requires three properties during floral development: 1) the concentric expression of homeotic genes, 2) a stochasticity in the gene expression boundary, and 3) a semi-whorled arrangement. Here I discuss the biological bases of these three assumptions.

The concentric gene expression during flower and inflorescence development. The identity of floral organs of eudicots is determined by MADS-box genes expressed in concentric manner, which is known as the ABC model (Fig. 4.3B; Appendix B.5.3). For example, I assumed that the number of sepals is determined by the expression boundary of B class gene. The association between perianth organ number and B class gene was demonstrated in a Ranunculaceae species *Nigella damascena* [111]. Taken together with other B class gene expression in Ranunculales that is known to be considerably variable [153], my results proposes the strong contribution of B class gene on the variation in perianth-organ numbers.

Such concentric expression appears even in the inflorescences of the Asteraceae. The *TCP* family *CYC/DICH* genes, which determine the fates of the floret primordia, are expressed concentrically to the inflorescence apex in the radiate heads of the Asteraceae. For example, in *Gerbera hybrida*, the expression of *GhCYC2* follows a gradient along the radial axis of the inflorescence [44]. Similarly in *Senecio vulgaris*, *RAY1* and *RAY2*, the homologues of *GhCYC2*, are expressed in the outer floret primordia [147]. Thus, the concentric expression of organ-fate determinants is widespread among eudicots, not only in flowers but also in inflorescences.

The Gaussian distribution of the gene-expression boundary. Little is known about the stochastic variation in MADS-box and *TCP* gene-expression boundaries ($P_{gene}(r)$ in Eq. 4.3), in contrast to the morphogen gradients in *Drosophila* embryogenesis [30, 134]. Although I assumed a Gaussian distribution for the variation, when the expression boundary follows other types of probability distributions (e.g., the log-normal or gamma distributions), the functional form of Eq. 4.10 should be improved by integrating the probability (see Eq. 4.4 in Appendix). In addition to the noisy spatial patterns, the noisy temporal sequences of the fate determination gene expression [9] could be another future problem for the floral organ number variation.

The semi-whorled arrangement of the floral organs. Many Ranunculaceae species such as *Ranunculus* exhibit semi-whorled arrangements (Fig. 4.3D; sometimes referred as false-whorls or pseudo-whorls) in their flowers [261]. Even in some whorled flowers, the primordia initiation is sequential; in other words, their positional arrangement is transiently semi-whorled [e.g., Caryophyllaceae [174] and Oleaceae [67]]. In the Caryophyllaceae species *Silene coeli-rosa*, the positions of the primordia were measured quantitatively in the early stage of floral development, showing that the sepals took on a semi-whorled arrangement [174]. If the ABC genes determine the organ fate at that stage, the homeosis distribution is valid even for the whorled flowers.

4.5.2 Counter examples of the homeosis model

The easiest way to confirm such a model based on homeotic stochasticity (Fig. 4.3A) is to find a negative correlation between the organ numbers of successive whorls. Although the homeosis model fit much of the observed floral organ variation well, there are some counter examples that do not exhibit such strong negative correlations. For example, there is no correlation between the numbers of tepals and nectaries in *Eranthis pinnatifida*. The absence of a negative correlation is partially explained by the MADS-box genes affecting not only the organ-identity determination but also the organ numbers, which the ABC model does not take into account: mutations in the ABC genes result in the partial loss of some organs or whorls (e.g., the partial or complete loss of the organs of the second and third whorls caused by mutations in the A gene, *APETALA2*, in *Arabidopsis thaliana* [40,157]). In addition, merosity variation,

where the numbers of sepals, petals, and stamens are strongly and positively correlated, was found in Ranunculaceae flowers (e.g., *Hepatica nobilis*) and is common among Primulaceae flowers (e.g., *Trientalis europaea*; [302]), indicating that homeotic variation is not the sole source of floral organ-number variation. Therefore, the variation should be represented by the sum of two or more distributions. Because the homeosis model was selected as the best model for Primulaceae flowers (*Primula×julianna* and *T. europaea*), we cannot distinguish between merosity and homeotic variation from the model selection. However, the gap parameter was small for Primulaceae petals and sepals, suggesting it can be distinguished by the gap parameter, and merosity variation as the source for Oleaceae petal and *Eranthis* nectary number variation that have similar gap parameter values.

Another source of variation can be the fusion of the flowers. It was often observed in *Myosotis* sp. (Boraginaceae), and none of two data sets were best-fit by the homeosis model with standard Gaussian boundary, but Poisson and homeosis model with log-normal boundary were better. Therefore the variation caused by the fusion follows different variation curve to that generated by the four model presented in this thesis. The fusion of flowers may be under hormonal control by cytokinins [284], suggesting that the examination of the fused flowers in the laboratory will give clues to how to construct a model for the multi-modal distribution.

4.6 Future problems

4.6.1 Improvement of the models.

In some variation, the right-tail and left-tail separated by the mode followed different models (Fig. 4.3C). There is a possibility for the summation of two or more distributions caused by different developmental sources of stochasticity. One simple idea to confirm this possibility is to fit a limited range of the distribution, such as the right-tail and the left-tail, which would clarify whether the same or different laws govern decreases and increases, respectively, in the organ number relative to the mode.

I hardly discussed multi-modal distributions, which have attracted some researchers who suggest that there is a relation between peak organ numbers and the Fibonacci series, especially among Asteraceae heads [170]. There seem to be at least two different sources of multi-modal distributions. One is stochastic changes in the number of whorls that differentiate into identical organs. Suppose that, for example, there are two whorls comprising eight and five organ primordia, respectively. If only the whorl with eight primordia differentiates into ray florets, there will be eight ray florets; whereas if both whorls become ray florets, there will be 13 ray florets. By assuming such multiple semi-whorls, the present homeosis model could be improved for the multimodal distributions. The other source of multimodal distributions may be the fusion of the flowers, which is not accounted for by any of the present models. For example in *Myosotis* sp. (Boraginaceae), the mode of the petal number is five, but the distribution has a second peak at 10. The flowers with 10 petals seem to be generated by the fusion of two flowers, which may be under hormonal control by cytokinins [284], suggesting that the examination of the fused flowers in the laboratory will give clues to how to construct a model for the multimodal distribution.

4.7 Partial conclusion

The variation in the floral organ numbers of various eudicot species was fit to six statistical models. Statistical model selection revealed that the selection of the best model was reproducible for each species and organ. The homeosis model, which I first proposed by assuming a semi-concentric arrangement of organ primordia following helical initiation and stochasticity in the concentric determination of organ fate during floral development, was widely selected for the perianth organs of eudicots, and even for the stamens and ray florets of some core eudicots. The standard Gaussian and log-normal distributions were selected, respectively, for the Oleaceae petals, which show the simultaneous initiation of the primordia, and the Papaveraceae ovules, which have a totally different developmental process compared with the perianth organs. I showed that the different distributions of morphological traits reflect different developmental processes. The modelling of developmental process of these organs and the statistical analyses of other species and organs will shed more light on the developmental and evolutionary sources of morphological variation.

5 General Conclusion and Relevance Between Chapters

How plants determine the floral organ number precisely is a fundamental problem to understand the relationship between evolution and development, since the organ number involves the branching of major clades of angiosperms. I accessed this question from two sides: the developmental origin of the robustness and stochasticity in the floral organ number. I constructed a mathematical model for floral development, and found that the mutual repulsion among primordia after initiation was essential to form whorled-type arrangement following helical initiation as observed in many eudicots. The arrangement with four or five sepals were more robust to change of model parameters than other arrangements with more or less sepals. The field observation and calculation of statistical quantities of multiple wild-plant populations revealed that there are at least three sources of the organ number variations. Moreover, the statistical quantities provided the existence of hidden modal numbers, which cannot be found only by the averaged phenotype, suggesting the importance to focus on the variation to discuss the phenotype. Four possible model for the variation curves was tested by statistical model selection, and it was shown that the selected model is retained for the same species and organ type. Statistical model selection showed that different developmental process can be reflected to the shape of variation curve, consistently to the result indicated by statistical quantities that different species and organ type can have different sources for organ number variation.

The preference to specific number is in the developmental process. The model in section 2 explained the reason of the dominance of the four and five in the nature from the developmental process. I examined whether the variation of parameters in FOA model can explain the variations observed in natural population. It was not as plausible as the alternative model constructed from field observation, because it was too stable to explain the extent of natural variation. Therefore, the pattern formation of floral organ arrangement is considered as very stable process, and the variation source should be in other processes.

Three types of variation curves were found both in the statistical quantities and statistical model selection I found three types of variation in the two studies (Sec. 3,4). The mean-SD relationship follows $SD = \sqrt{|Mean - d|}$ in many of variations in perianth-segment numbers in Ranunculaceae, whereas it was not explained by $SD = \sqrt{|Mean - d|}$ though SD and Mean showed high correlation in those of large-mean type (Sec. 3). The transition from standard-Gaussian type variation source to log-normal type variation source was observed along with the increase of mode and mean (Sec. 4). It is consistent each other for the large-mean type if $SD \propto Mean$, because if the variation is generated by log-normal type stochasticity, it should show $SD \propto mean$ because the mean of log-normal distribution is $\exp(\mu + \sigma^2/2)$, standard deviation is $\sqrt{\exp(\sigma^2) - 1}[\exp(\mu + \sigma^2/2)]$, and thus $SD \propto Mean$. The next curious point is, whether the homeosis model with standard-Gaussian boundary can explain the relationship $SD \propto \sqrt{Mean}$ or not.

The variation in perianth segment numbers is commonly found in basal eudicots such as Ranunculales (including Ranunculaceae and Papaveraceae) and basal core-eudicots such as Caryophyllaceae, but rare in other core eudicot species (Oleaceae in Lamiales, Polemoniaceae and Primulaceae in Ericales are exceptional). One of the major differences in floral development between core and basal eudicots is the B class gene expression (Appendix B.5.3), which can be the clue for the molecular underpinning of variation in perianth segment numbers. The copy number and expression domain of B gene, namely, the homologues of *APETALA3* (*AP3*) and *PISTILLATA* (*PI*), is considerably variable among species in basal eudicots [153] and Caryophyllaceae [237]. For example, the expression of two *AP3* homologues and two *PI* homologues are variable in *Ranunculus ficaria* but rather uniform in *R. bulbosus* [153] . Since the variation properties of *R. ficaria* petals shown by statistical quantities was intermediate between *Ranunculus*-perianth type and large-mean type (Sec. 3), in contrast to *R. bulbosus* petals showing typical *Ranunculus*-perianth type variation, various expression of B gene can be a source for the large-mean type variation. In the homologues of *AP3* and *PI*, *AP3-3* seems to have especial importance on the floral organ number determination, since it is expressed only in petals contrary to other B class genes that specify petals and stamens [268,335]. Therefore *AP3-3* can cause two types of homeosis in two boundaries: the homeosis between sepal and petal as expected for the usual B class gene, and the boundary between perianth (corolla) and androecium. The latter is likely to cause the drastic variation of total number of perianth segment, since the modal number changes between 14 and 22 in the forms associating with different *NdAP3-3* expression, and the degree of number variation associates

with *NdAP3-3* expression domain in *Nigella damascena* (Ranunculaceae) [111]. Thus the variation in expression domain of *AP3-3* can be related to the perianth-segment number variation.

Another mean-SD relationship, which were found in the *Eranthis pinnatifida* nectary number, has no obvious correlation between mean and SD but the SD spreads in wider range as mean increases. This relationship was also observed in Oleaceae petal number variation. In the statistical model selection, these variation showed common features: one-thirds of their data sets were selected by the log-normal homeosis model, and the gap parameter of the standard Gaussian homeosis model were close to zero. The common botanical features of *Eranthis pinnatifida* nectary and Oleaceae petal is only they are located at the second whorl. They are distantly related each other in phylogeny, but their variation are in the similar manner, indicating similar development. Oleaceae floral development was observed and reported for the sepal [67, 266], whose initiation and number influence the petal number because sepals are adjacent to petals (remember phyllotaxis studies that showed primordium position is determined by the adjacent primordia): In addition to the four coincident sepals common in Oleaceae flowers, the *N. arbor-tristis* flower develops two extra sepals [266]. On the other hand, the sepal initiation in genus *Jasminum* is much more complicated. *J. nudiflorum* develops six sepal primordia in the same order as *N. arbor-tristis*, whereas *J. fruticans* shows pentamerous helical initiation but stochastically develops four or six sepals [67, 266]. Thus, there are three patterns of Oleaceae sepal initiation: the simultaneous initiation of four sepals, the extra two sepals $(4 + 2)$ found in *N. arbor-tristis* and some *Jasminum*, and the sequential helical initiation of five sepals similar to that in the basal eudicots [229]. The situation in *N. arbor-tristis* is much different from the assumptions of the homeosis model: primordia arise coincidently, indicating the formation of a "true" whorl in a concentric circle immediately after the initiation. Therefore we need to suspect another source this type of variation with $ex_d + in_d \simeq 1$. In the statistical model selection, Primulaceae petal and sepal numbers showed similar value of the gap parameter, although there is not enough data sets to examine the mean-SD relationship. If the mean and SD has no correlation in Primulaceae, we can propose the variation source for *Eranthis*-nectary-type variation as the merosity change without preference for the specific number and that can take any number depending on flower size, which is common type of variation in floral organ numbers in Primulaceae.

In summary, both studies indicated three types of the variation curves. The first type has the mode on small number, the SD is proportional to square root of mean, and well-explained by the homeosis model with standard-Gaussian type boundary whose gap parameter $ex_d + in_d$ is larger than 1. The second type has the mode on larger number and the SD is proportional to mean, consistently to the statistical model selection that selected log-normal type Homeosis model. The third type does not show correlation between mean and SD, and if fit by the standard Homeosis model, the gap parameter is close to 1 indicating non-whorled arrangement.

The semi-whorled arrangement and hidden modal numbers. These works indicate an importance of the semi-concentric arrangement. Since the variation was suggested to be originated from the homeosis in the semi-whorled arrangement, the hidden mode is the number within each semi-whorl. The variation can be divided into intra-mode variation that shares the same semi-whorl construction and inter-mode variation. For example, all *Ranunculus* perianth-love variation can be explained from a single semi-whorl construction if we assume $3 + 2 + 3$ construction, namely, there are three primordia in the first whorl, two primordia in the second whorl, and three primordia in the third whorl. On the other hand, the mode-on-six and mode-on-five *Anemone* species cannot be explained from a single semi-whorl construction.

Transition between stable modes and the evolution of angiosperms. Finally I insist that, if we want to understand the change of merosity associated with the branching of eudicots and monocots, we need to examine the semi-whorl construction, not only the change of the primordia number within a single semi-whorl. Returning to the FOA model, the next key-point is the primordia number within successive semi-whorls. In *Ranunculus*, the gradual change of number between three and five was found, but that species does not have $3 + 3$ construction, namely, two whorls containing three tepals each, as in monocots and some *Anemone* species. If mode-on-five species of *Anemone* have $3 + 2$ as proposed for *Ranunculus*, we need to know the transition between $3 + 3$ and $3 + 2$. Finding the factor that stabilise the trimerous arrangement and the key parameter that change the semi-whorl construction between $3 + 3$ and $3 + 2$ will elucidate the difference of programme of floral development between eudicots and monocots.

Appendix

A The Morphology of Angiosperm Aerial Parts

A.1 Phylogeny of angiosperms

Angiosperms are in division of seed-producing plants Spermatophyta (as opposed to spore-producing plant, e.g., Bryophyta) and in subdivision Angiospermae (as opposed to Gymnospaermae). The term angiosperm originates from Greek *angeion* and *sperma*, meaning a container of a seed, together indicating enveloped seed or carpel closure.

The traditional morphological and anatomical classification, such as the taxonomy by Engler [92] and Cronquist (1968, 1988) [63, 64], divided angiosperms into two clades by the number of cotyledons: dicotyledons (dicots) and monocotyledons (monocots). One can easily tell the differences of these two clades. For example, the number of cotyledons is two in the former and one in the latter; the leaf venation pattern is reticular in the former whereas it is parallel in the latter; and the basic number of floral organs is five or four in the former but three in the latter. This traditional classification has been refined by Angiosperm Phylogeny Group (APG), who has integrated the molecular phylogeny and anatomical or morphological taxonomy [13–15]. The newest version of APG classification, APG III, was published in 2009 [15] (Fig. 1.1), and is widely accepted by botanists, while the efforts to improve the phylogeny has been made constantly [289].

In APG phylogeny, monocots form a closely related group consistently to the classical classification. However, classical dicots fall into two groups. The majority of classical dicots, which accounts for 75% of angiosperms, is put into a monophyletic group eudicotyledons (eudicots; with Greek *eus* that means good). Eudicots is divided into core eudicots, a monophyletic group with rather uniform morphology, e.g., the petal number is restricted to four or five, and basal eudicots represented by Ranunculales, which is paraphyly branched early in the eudicot evolution and has varied morphology with three to eight or more perianth segments. Two major monophyletic groups in core eudicots are called rosids and asterids, represented by two famous species, namely, rose (*Rosa*) and aster (*Aster*), respectively. The remaining part or dicots, which holds 3% of angiosperms, is informally called palaeodicotyledons or basal dicotyledons (basal dicots). Basal dicots further falls into a monophyletic group magnoliids that occupies the majority of basal dicots, and the others which called basal angiosperms. The basal angiosperms contain several orders, which form the sister clades to all other angiosperm species, such as the most basal genus *Amborella*.

A.2 Shoot, basic structure of aerial part of angiosperms, and the foliar theory

Die geheime Verwandtschaft der verschiedenen äussern Pflanzentheile, als der Blätter, des Kelchs, der Krone, der Staubfäden, welche sich nach einander und gleichsam aus einander entwickeln, ist von den Forschern im allgemeinen längst erkannt, ja auch besonders bearbeitet worden, und man hat die Wirkung, wodurch ein und dasselbe Organ sich uns manigfaltig verändert sehen lässt, die Metamorphose der Pflanzen genannt.— Goethe, Johann Wolfgang von [110]

Although the angiosperms species have diverged morphologies range from tiny herbs to giant trees and from flexible ivy to stiff wood, their aerial parts consist of a common unit. In 18th century, Goethe insisted the foliar theory that the all plant organs are transformed leaves [110]. This concept is basically accepted in modern biology, modifying the terms and definitions. The transformed leaf, or an organ homologous to a leaf, is now referred to as a lateral organ, which is defined by their developmental origin that is produced from and around an apical meristem at the stem tip (arrowheads in Fig. A.1A) as the stem undergoes tip growth. A set of a stem and lateral organs generated from the stem is referred to as a shoot, which is regarded as a unit of plant architecture (Fig. A.1A).

The plant architecture is composed of hierarchical axes built up by shoot(s). The main (primary) axis is the stem firstly arises from the seed, which is usually vertical to the ground. Each lateral organ in the primary axis can subtend axillary bud(s), which grows as the secondary axis, at the boundary of the stem and leaf called axil (Fig. A.1A). The lateral organs in the secondary axis can generate tertiary shoots. The higher-degree shoots can be generated in the same manner. Thus branching at the axils forms the hierarchical architecture of plant. These axes can be either monopodial or sympodial. In monopodial axis, the growth of an apical meristem construct a whole linear axis, therefore the linear axis is composed of a single shoot (Fig. A.1B). The sympodial axis is built up with a linear series of shoot units (sympodial units) (Fig. A.1C).
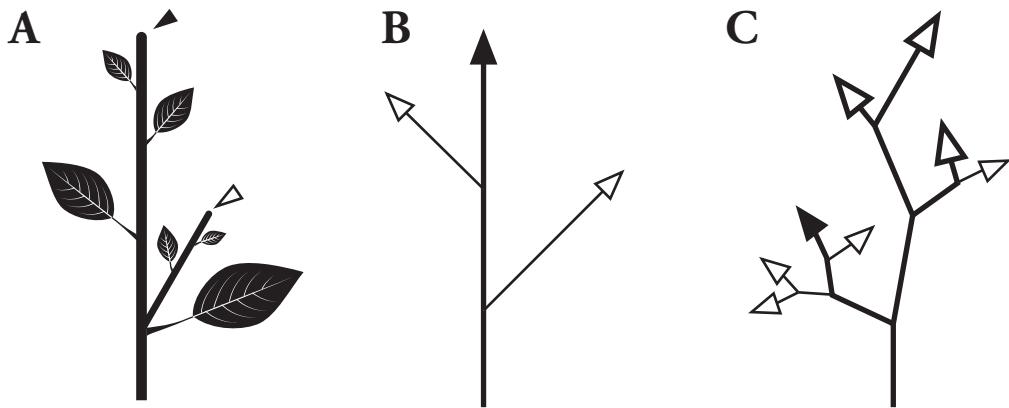
Figure A.1: **Schematic representation of shoot, the fundamental unit of hierarchical architecture of plant aerial parts. A.** The primary and secondary shoots. The solid arrowhead indicates the apical meristem of the primary shoot, whereas the open arrowhead shows the apical meristem of the secondary shoot. The secondary shoot develops from the axil of the main shoot. **B-C.** Schematic diagram for monopodial (B) and sympodial (C) shoots. Black solid triangle denotes the primary meristem, whereas the open triangles represent the other meristems.

Hereafter I describe the major structures of angiosperm aerial body, but it should be noted that plants show various exceptions. For example, in the branching manner, some species develop adventitious bud at unfixed location on the stem.

Three types of shoots. According to the developmental stage in the plant ontogeny, shoots are divided into vegetative state that generates leaves and reproductive state, which is further divided into an inflorescence and flower. The inflorescence bears flowers at the axil, whereas the flower contains floral organs such as petals.

Stem Stem is a cylindrical shape structure supporting the architecture of plant body. It has radial symmetric composition of three types of tissues, named epidermis, cortex, and stele, from outside to inside. Stem is essential for producing lateral organs, transportation of water and nutrients, and mechanical support for all other structures. To satisfy these functions, the stem contains an apical meristem at the tip and vascular bundles in the stele. The apical meristem is a stem cell region with frequent cell division and certain population of undifferentiated cells, which is responsible for the terminal growth (tip growth; the common growth manner in plants [62]) and for producing lateral organs. The geometric form varies from conical or dome-shaped to flat or even slightly depressed, and the diameter ranges from 50 μm to 3500 μm among species [285, p. 47]. The vascular bundles (xylem and phloem) are responsible to conduct water and minerals to the leaves, and to transport photosynthetic products from the leaves to other parts of the plant. Also, the tough structure of xylem is responsible for the support of plant structure.

Lateral organs All lateral organs initiate as dome-shaped primordia at the periphery of the apical meristem. These lateral organs are usually bilateral symmetry with two symmetry axes: a top-bottom axis and an adaxial-abaxial (dorsi-ventral) axis (see section A.4.1). The lateral organs take various forms depending on the developmental stage of the plant, such as leaves in the vegetative shoot, bracts in the inflorescence shoot, and floral organs in the flower.

64

A.3 Phyllotaxis

Phyllotaxis (from Greek *phyllon* meaning leaf and *táxis* meaning arrangement) stands for the arrangement of repeated units such as lateral organs around a stem and florets in a head inflorescence of Asteraceae. In most cases the phyllotaxis appears as the regular spacing of the repeated units, thus it can be thought as "living crystals" whose pattern formation occurs on the growing tissue. Although some species show chaotic or random organ pattern whose regularity is not found, the majority have regular spiral or whorled phyllotaxy. Since phyllotaxis is constrained evolutionarily by at least developmental and ecological factors [62, p. 116], it can be discussed from several points of views such as development, environment, heredity, and evolution. Here I describe the morphological properties on phyllotaxis, whereas the theoretical perspectives are summarised in Sec. 2.3.1.
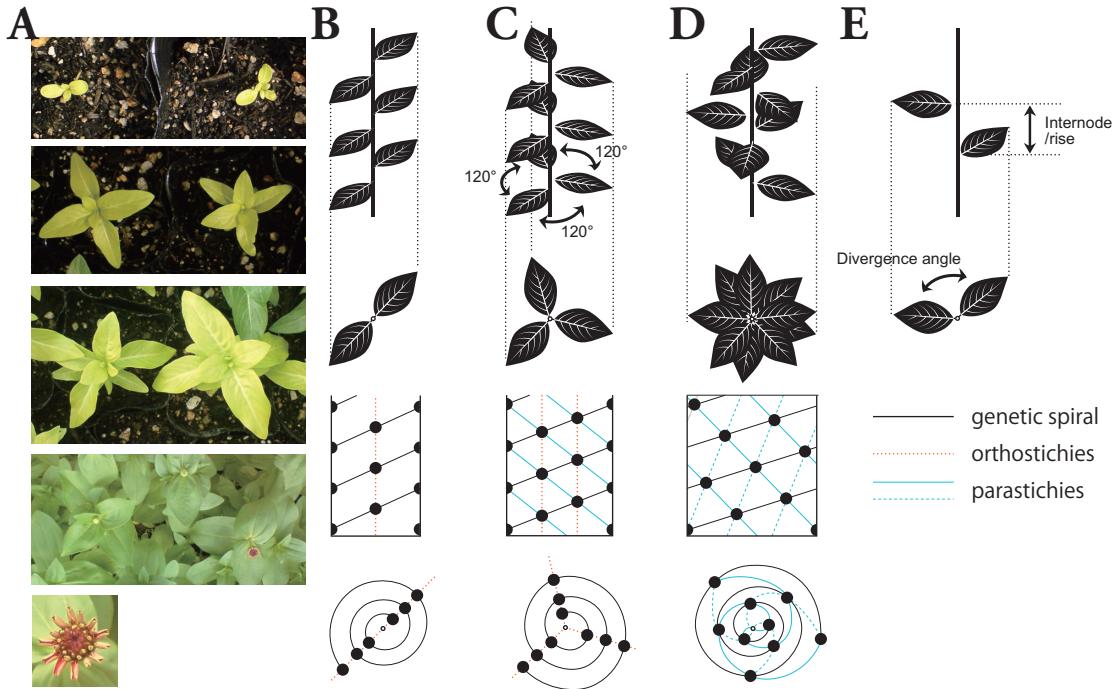
Figure A.2: **Representative patterns of phyllotaxis. A.** The phyllotaxis in the ontogeny of *Zinnia elegans* (Asteraceae). The left individual showed typical development of eudicots that started from two cotyledons, produced leaves in a decussate manner and florets in a spiral arrangement. The right individual sprouted with three cotyledons, produced three leaves in a whorl, and then changed into spiral phyllotaxis. **B–D.** Alternate phyllotaxis. Each phyllotactic pattern is also represented by corresponding cylindrical (middle row) and centric representation (bottom row). Black solid lines denote genetic spirals, orange dotted lines indicate orthostichies, and blue lines represent parastichies (see legend at the bottom-right). The divergence angle is $\varphi = 180°$ (**B**), $\varphi = 120°$ (**C**), $\varphi = 137.5°$ (**D**). **E.** Internode length (the vertical length, top) and divergence angle (the projection angle, bottom).

A.3.1 Classifying phyllotaxis

There are many different types of phyllotaxis, and the type can be different depending on the species and developing stage. In eudicots, the development starts off with two cotyledons that are positioned opposite to one another and the following vegetative phyllotaxis is often decussate or spiral. The inflorescence phyllotaxis is often different from the vegetative stage, and floral organs are arranged in concentric whorls (Fig. A.2A). These phyllotactic pattern is able to describe and classify by mathematical terms because of their regularity.

The basic values for evaluating phyllotaxis. The phyllotactic patterns are usually described in two-dimensional system in cylindrical representation (Fig. A.2B–D, middle row) or in centric representation (Fig. A.2B–D, bottom row; see Sec. 2.3.1 for the history of these representations). The cylindrical representation, which has developed from the observation of mature shoot, describes the position of organs by rolling out the cylindrical stem with angular position θ and longitudinal position L. The centric representation describes the pattern in circular plane with polar-coordinate system (r, θ) since it has developed with the observation on the section of the immature stem tip. In both representations, the angular position is described by divergence angle φ, the projection angle between two successive organs (Fig. A.2E). In the cylindrical representation, the longitudinal position is characterised by internode length or rise, the difference of longitudinal position between two successive organs (Fig. A.2E). In the centric representation, plastochrone ratio R, the ratio of radii of two successive organs, is employed for describing the phyllotactic patterns. Although the term plastochrone itself means the time interval for the primordia succession, plastochrone ratio is calculated from the spatial distance from the apex.

Alternate phyllotaxy. In Alternate phyllotaxis, lateral organs are regularly arranged with constant internode length or constant plastochrone ratio R (Fig. A.2B–D).

Alternate phyllotaxis with orthostichies. If the divergence angle φ is constant for every successive leaves and divides exactly into $360°$, the organs are aligned in row(s) along the stem, which are called orhostichies [62, p. 116]. When $\varphi = 180°$ it is distichous (two-ranked) phyllotaxis, because it has two orthostichies (Fig. A.2C). When $\varphi = 120°$, it has three orthostichies and is called tristichous (three-ranked; Fig. A.2D).

Spiral phyllotaxis. Spiral is the most common phyllotactic pattern. In the spiral phyllotaxis, spiral lines that connect "closest" primordia are visible (Fig. A.2D). The spirals are defined in three ways.

The first is contact parastichies, which are spiral lines connecting the contact points between organs. For example in transversal section of dense leaves and sunflower seeds, each organ usually contact with four or six neighbouring organs. If an organ contacts with four organs, the organ is in quadrilateral shape, and two pair of contact gives the direction for two spirals. The parastichies with the same direction compose a family of contact parastichies, and a pair of such families winding to opposite direction in respect to the shoot axis is called a contact parastichy pair. When one of the pair comprises m parastichies and its pair contains n parastichies, they are called m-parastichy and n-parastichy, respectively, and the pattern is expressed as (m, n) system. In the case with hexagonal shape in transversal section, we find three families of parastichies, therefore there are three families in the "pair" [137, p. 13].

The second way to find the spirals is used when only the centre positions of organs are obtained. In this case many spirals can be depicted. Visible opposed parastichy pair is a pair of parastichy families in the opposite direction, which always intersect on the organ centres. If there are plural such pairs, a pair whose intersection angle between the opposite parastichies is the closest to $90°$ is selected as the visible opposed parastichy pair. Similarly to the contact parastichies, the system of phyllotaxis is described as (m, n), with the number of parastichies composing each parastichy family.

The third way to line spirals is connecting the temporally closest organs. The spiral depicted by connecting organs in initiation order is called genetic spiral (also known as generative, fundamental, or ontogenic spiral). The number of genetic spirals, jugy, is also used for characterising phyllotactic pattern. The alternate phyllotaxis always has only one genetic spiral, and is called unijugate system (black lines in the bottom row in Fig. A.2B–D). It has been suggested that the divergence angle on the genetic spiral takes close value to golden angle, $360°/\tau^2 \simeq 137.5°$, in most species with the spiral phyllotaxis.

***Orixa*-type phyllotaxis** is a representative of non-spiral alternate phyllotaxis. The leaves form two lines on the opposite sides, but differently from distichous phyllotaxis, they are arranged two by two.

Whorled phyllotaxy. The phyllotactic pattern is called opposite if two leaves attached to opposite sides at the same level, or a node, of the stem (Fig. A.3A,B), and whorled if there are more than two leaves at a node (Fig. A.3C,D). Decussate phyllotaxis is a special opposite phyllotaxis whose divergence angle between successive nodes is $\varphi = 90°$ (Fig. A.3B). The whorled phyllotaxis with three organs at a node is trimerous-whorled (Fig. A.3C,

D), and if the successive whorls are in alternate relationship with $\varphi = 60°$, the pattern is tricussate (Fig. A.3D). The whorled phyllotaxis has multiple genetic spirals and thus it is multijugate system (solid lines in Fig. A.3A–D). The opposite phyllotaxis is bijugate system with two genetic spirals (Fig. A.3A,B), whereas the trimerous-whorled phyllotaxy is a trijugate system with three genetic spirals (Fig. A.3C,D).
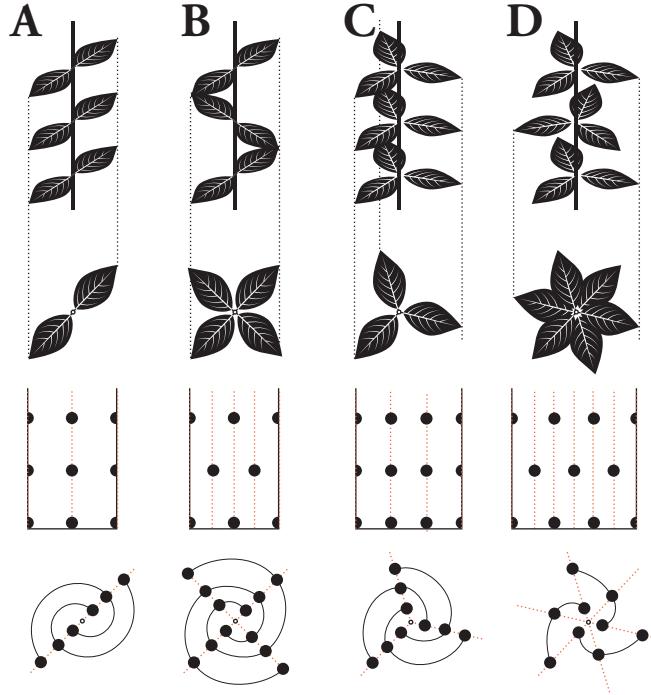

Figure A.3: **Whorled phyllotaxis. A.** Opposite pattern. **B.** Decussate. **C.** Trimerous-whorled. **D.** Tricussate. Black solid lines denote genetic spirals, whereas orange dotted lines indicate orthostichies.

When we carefully observe whorled-type phyllotaxis in some species, the members in a "whorl" are not precisely attached to the same level of the stem. Such pattern is expressed as pseudo-whorled or false-whorled. On the other hand, if the internode is strictly zero throughout the development, the whorl is referred to as a true-whorl. However, there is no clear criteria for distinguishing true- and pseudo-whorls, and many eudicot flowers are recognised as "whorled arrangement" despite their primordia show spiral pattern in early stages of development.

A.4 Vegetative Shoots

Plants undergo vegetative and reproductive stages in their ontology. In the vegetative stage, the shoot apical meristem produces leaves that are responsible for photosynthesis.

A.4.1 Basic leaf structure

A simple leaf is composed of a set of a petiole/stalk and a lamina/leaf blade (Fig. A.4A). The base of leaf stalk surrounds the stem and forms a sheath, and usually associates with an axillary bud. Many monocots lack the petiole and their laminae directly form the sheath.

Leaves are bilateral symmetric with top-bottom axis and adaxial-abaxial axis (Fig. A.4A). In the bifacial leaves that are the most common among the species, the two sides differentiate into different tissue specialised for light capture in the adaxial (ventral) face and gas exchange with stomata in the abaxial (dorsal) side.
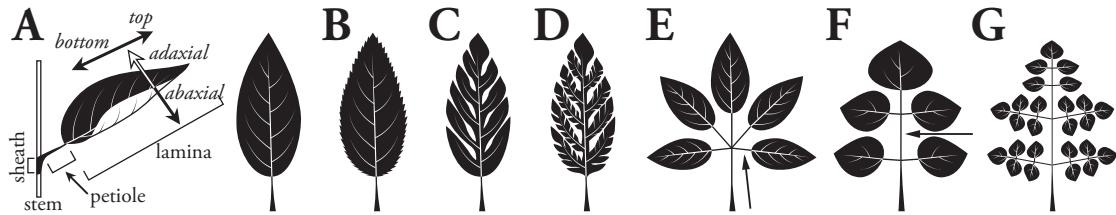
Figure A.4: **Variety in the leaf shape. A.** Basic leaf structure with entire margin. Lamina (leaf blade), petiole (stalk), and sheath compose a leaf. Leaf is bilateral symmetric with top-bottom axis and adaxial-abaxial axis. **B–D.** Leaves with serrated (**A**), dissected (**C**), or secondary dissected (**D**) margin. **E–F.** Compound leaves. **E.** Palmate leaf with five leaflets. **F.** Pinnate leaf with five leaflets. This leaf ends with a leaf (odd pinnate), as opposed to the even pinnate leaf whose tip ends with two leaves. **G.** Bipinnate leaf. Arrows in **E** and **F** indicate rachis.

A.4.2 Variations in leaf shape

To adapt diverse condition, plants have evolved a variety of leaves with different shapes, sizes, and arrangements [49] (Fig. A.4). For example, dissected or compound leaves (Fig. A.4C–G) have adaptive values for heat dissipation and resistance to high winds. Leaves with different characteristics are categorised by several criteria, such as the shape, serration, faciality, and complexity [259].

Complexities. Leaves can be distinguished into simple and compound leaves according to their degree of complexity of the shape [34,49]. Simple leaf has a continuous margin, which can be entire, serrated, or dissected by lobes. Entire leaves have smooth margin without indentations (Fig. A.4A). Serrated leaves have jagged edge (Fig. A.4B). Dissected or lobed leaves have deep incisions of the margin that reach the main leaf axis (Fig. A.4C). Each lobe can be further dissected as in secondary dissected leaf (Fig. A.4D).

Compound leaf is a cluster of leaf-like structures (leaflets), which are distinguished from leaves by the lack of potential to subtend axillary buds. The difference between compound leaves and dissected leaves is the rachis, which the multiple leaflets are attached to (arrows in Fig. A.4E, F). Compound leaves are subdivided by the number of leaflets, arrangement of leaflets on the rachis, and the order of complexity [49]. Bifoliate compound leaf has two leaflets, whereas trifoliolate or ternate leaf has three leaflets, as in clover *Trifolium*. The compound leaves with more than three leaflets are divided into palmate and pinnate. The leaflets of Palmate leaves are borne at the tip of a rachis (Fig. A.4E), whereas those of Pinnate leaves are in succession along a rachis, as seen in Fabaceae (Fig. A.4F). The leaflet can be divided into secondary leaflets (e.g. bipinnate leaf in Fig. A.4G), and thus the compound leaves can be close to fractal shape when the degree of complexity is increased.

Two hypotheses have been proposed for the homology between simple and compound leaves [49]. The first hypothesis equates a leaflet with a simple leaf, and regards a compound leaf as a shoot. The second hypothesis equates the entire compound leaf with a simple leaf, hence the compound leaf is put after a sequence from a simple leaf with entire margin, serrated, and dissected margin. Largely the latter is supported, but it has not been settled and the similarity of gene set in the compound leaf growth and the shoot apical meristem is discussed [49].

Facialities. In contrast to conventional leaves that have bifacial parts specialised for gas exchange and light capture, several types of facialities are known (reviewed in [98, 306]). Unifacial (cylindrical) leaves have a radial transectional symmetry differently from flattened conventional leaves [98]. The secondarily flattened unifacial leaves are called ensiform, and to distinguish from this, the radial-symmetric unifacial leaves are called terete leaves.

Equifacial (isobilateral) leaves indicate flat leaves with the same anatomy in the both faces, but the internal structure has the adaxial-abaxial asymmetry. The equifacial leaves are thought to have been evolved to optimise the efficiency of capturing sun-light entering with low angle, as in *Eucalyptus*.

A.5   Inflorescence

Inflorescence stands for the way the flowers are arranged in a flowering branch. The whole inflorescence is composed of a single or multiple inflorescence shoots, flowers, and leaves at the base of flowers (bracts), which is lacked in some species such as the model plant *Arabidopsis thaliana*.

Many efforts have been made for the typology of inflorescence to distinguish them by the bifurcation pattern of the stem, the arrangement of flowers, and the direction of the growth. However, many combinations and intergradations between types make it complicated.

A.5.1   Classification of inflorescence

The typology of inflorescence can be traced back to Greco-Roman, but here the work of Linné (1751) is noted as the founder of modern taxonomy. He developed a system to classify plant species depending on several plant parts, and employed the modes in which the flowers are borne on the stem as one of the criteria [166, sect. 82,D]

Linné's classes of inflorescence modes.   In the first part of his list for inflorescence modes, he listed classes divided by the number of the flowers in an inflorescence. He called an inflorescence with only one flower as *uniflorus*, that with two flowers as *biflorus*, that with three as *triflorus*, etc. The inflorescences with many flowers was called *Multiflorus*, and they were further classified into several types. A bunch inflorescence was called *fasciculus*. The term capitulum was used when many flowers are clustered in a spherical head (Fig. A.5A). *Spica* (spike) was for a branch with sessile flowers on the two sides (Fig.   A.5B), and subdivided into *secunda* if flowers are only on one side, and *disticha* if flowers are borne alternately to the two sides of the stem. *Corymbus* denoted an inflorescence whose stalk lengths are different among flowers and the lower flower has longer stalk. *Panicula* (panicle) was used when the flowers or flowering branches are dispersed and variously subdivided, and subdivided into *diffusa* if the branches spread into various direction, and *coarctata* if the stalks are located closely one another. *Thyrsus* was also a panicle contracted in a egg-shaped cluster. *Racemus* (raceme) was used for a branch bearing flowers with a short lateral stalk (Fig.   A.5C). Finally he listed *verticillus* for subsessile flowers ringing around a stem. Usually this term indicates the whorled phyllotaxy with several flowers, but from his illustration, we can guess he applied this term for the inflorescence that have many flowers surrounding one point of stem like a cloud.

Classical classification by de Candolle.   de Candolle (1827) was the forerunner of systematic typology. He proposed four categories by the determinacy: axillary, terminate, mixed, and anomalous inflorescences [69, pp.395–430]. His terminology (written in *italic*) is almost equivalent to what we use now (written in sans serif), and his definition is basically the idea to divide into indeterminate "racemose" and determinate "cymose" inflorescences.

The first category was axillary or indefinite inflorescence that blooms in centripetal order. In *spica* (spike), flowers are born in the leaf axils or sessile or carried on an inconspicuous pedicel (Fig. A.5B). *Racemus* (raceme) bears flowers in the axils of bracts, but differs from the spica in the lengths of stalks, which are more elongated (Fig. A.5C). *Umbella* (*ombelle*, umbel) is an assembly of flowers whose pedicels are attached to the tip of a peduncle (Fig. A.5D; can be *ombelle simple* also called *sertule*, or can be *ombelle composée*, depending on its complexity). *Tête* (capitulum) is a branch with tightly gathered flowers (florets) with zero-length pedicels (Fig. A.5E).

The second class *cime* (cyme) terminates with a terminal flower and blooms in centrifugal order (Fig. A.5E). He called all of terminate inflorescences as cyme, and listed several subclasses. *Cimes dichotomes* has two bracts and generates two branches on opposite sides of the terminal flower. This type of inflorescence continues the bifurcation around the terminated branch in repeated manner. *Cimes scorpioïdes* gives rise to the lateral branch always the same direction. It is a Monochasial cyme inflorescence that shows sympodial growth [27, p.173], which can be also called a rhipidium and a sickle-shaped cyme (Fig. A.5F). *Cime contractée*, or fasciculus, is combination of different types of cyme. *Glomerule*) is a kind of cyme with inconspicuous branching that looks like a capitulum.

He named two types of mixed inflorescence of above two categories: *Thyrses* (thyrsus) for the inflorescence whose central axis gives rise to lateral axes in an indeterminate manner but the lateral axes are determinate, and *Corymbes* (corymb) for the inflorescence whose central axis follows terminal manner but the lateral axes follows indeterminate fashion. Finally he mentioned several anomalous inflorescences representing exceptions of above three.
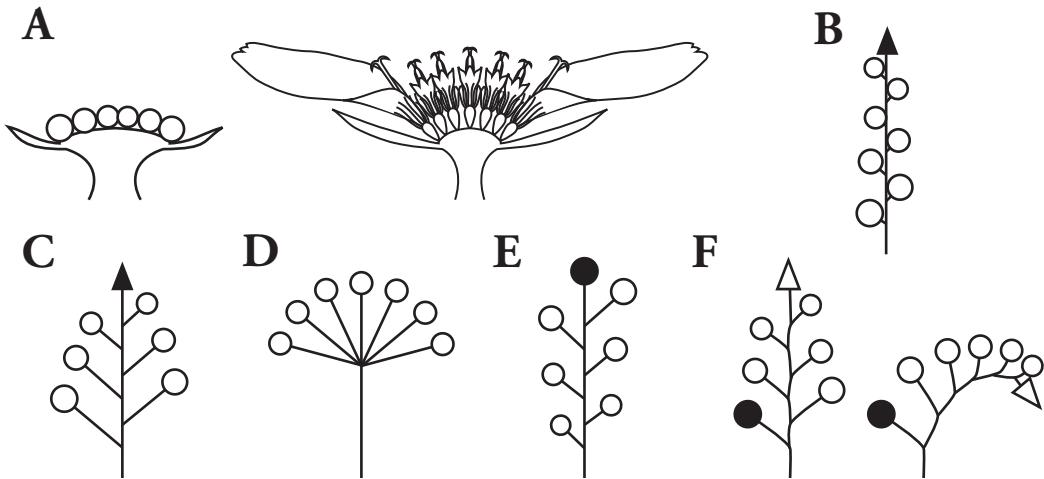
Figure A.5: **Schematic diagrams for the inflorescence structures.** Circles indicate the flowers and the triangle represent the apical meristem. **A.** Capitulum/head looks like a large flower and is common in Asteraceae. The right panel shows Asteroideae heads with vivid and large ray florets (ligulate flowers) to attract pollinators, and disc/disk florets (tubular flowers) to develop seeds. Asteraceae subfamily Cichorioideae heads only have ray floretsm, whereas Carduoideae have only discs. **B.** Spike. **C.** Raceme. **D.** Umbel inflorescence. It can be either terminate or indeterminate, and even if it is terminate, it is difficult to distinguish the terminal flower. **E, F.** Cyme. It can be either monopodial (E) or sympodial (F). The solid circle denotes the terminal flower.

A.5.2 Criteria for systematic classification

Troll started systematic classification of the inflorescence since the middle of the 20th century, by setting the terminal flower as a primary feature of inflorescence mode. He showed several criteria for assessing the inflorescence, such as the existence of bract (bracteate/ebracteate), whether the termination of inflorescence meristem is programmed or not (terminate/indeterminate), and complexity (simple/compound).

Determinate and indeterminate inflorescence In determinate inflorescence, the inflorescence meristem produces several lateral structures, i.e., lateral flowers or partial inflorescences, and finally transforms into a terminal flower [323]. Sometimes it is observed that the terminal flower and side flower have different morphology, for example the floral organ number and the symmetry (e.g. the terminal flower of *Adoxa* has four petals, whereas lateral flower has five petals [328]). The blooming order is usually centrifugal, that is, the terminate flower first blooms.

The inflorescence meristem in indeterminate inflorescence only produces lateral structures. The inflorescence ends with an incomplete lateral structure, or ends between the uppermost lateral structure [323]. Usually the bottom flower blooms at first, and the later-formed upper flowers follow in centripetal order.

Simple and compound inflorescence In the simple inflorescence (Fig. A.5), the lateral structure developed from the axil of the main axis is only the flowers. If the primary axis generates secondary, ternary, or higher inflorescence shoots, it is called compound inflorescence.

A.6 Flower

Flower is a short shoot specialised for reproduction, which contains floral organs that derived from a meristem (floral meristem). Most angiosperm flowers are hemaphroditic (bisexual) with perianth (sepals and petals, or tepals),

stamens (male organs), and carpels (female organs). However, unisexual flower in which the male organs and female organs are separated into staminate and pistillate flowers, occur in many different angiosperm lineage [99, p. 9].

A.6.1 Components of flower: floral organs

Several types of floral organs compose a flower. The arrangement of floral organs is whorled in many of angiosperms, and the organs composing a whorl are the same type. Although the number of whorls is varied among species, the general order of the whorls is conserved: Gynoecium is located at the centre, surrounded by the stamens, and perianth segments (Fig. A.6A–D). The order is highly conserved except only for two genera (*Lacandonia* [10] and *Trithuria* [243]) that have male-organ inside and female-organ outside [242].
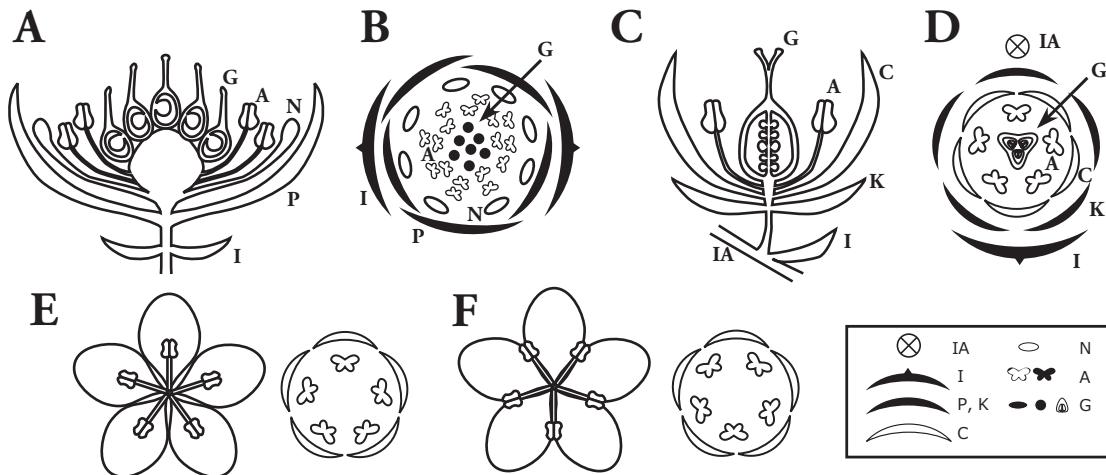
Figure A.6: **Floral organs and floral diagram.** The symbols are listed in the legend on the right bottom, with the one-character abbreviation (IA: inflorescence axis, I: bract, P: tepal, K: sepal, C: petal, N; nectary, A: stamen, G: carpel). **A, B.** Longitudinal (**A**) and floral diagram (**B**) of a Ranunculaceae flower, which consists of tepals (P), nectaries (N), stamens (A), and multiple carpels (G). **C, D.** Longitudinal (**C**) and floral diagram (**D**) of a typical core-eudicot flower, which consists of sepals (K), petals (C), stamens (A), and a syncarpous gynoecium (G). **F and G.** The angular-positional relationship between petals and stamens. In opposite relationship each stamen overlaps a petal (**F**), whereas in alternate arrangement each stamen locates at the middle of two petals (**G**).

Female organs.   A female organ equivalent to a leaf is a carpel, which contains ovule(s), which develops into seeds after pollination, inside the ovary. In multiple-carpel flowers, the gynoecia (the collective of carpels) is classified into apocarpous whose carpels are separated each other (Fig. A.6A,B), and syncarpous whose carpels are fused (Fig. A.6C,D). Apocarpous gynoecia are common in extant basal angiosperms and some basal eudicots, whereas syncarpous gynoecia are common in core eudicots and monocots. The whole syncarpous gynoecium is termed pistil.

Male organs.   An androecium consists of a number of stamens to product and disperse pollen. Each stamen is composed of an anther that contains pollen in pollen sacs and support stalk called filament. Stamens show various adnation (the union of different organs) to other floral organs, mainly to petals. For example, each stamen is connate to a petal at their base in Primulaceae, thus the stamen and petal number are exactly the same (Fig. A.6E).

Perianth organs.   Perianth, sensu lato, is the general term for outer whorls of flower, with variable number of variously coloured (petaloid) or green segments. There are two types of perianth, namely, simple and double perianth. The latter has whorls of distinctly different perianth segments [323]. Perianth, sensu strico, or perigon,

stands for the simple perianth, and its parts are called tepals (Fig. A.6C, D). Double perianth has two distinct types of segments in different whorls, and are often found in in eudicot flowers. The inner more distal components, the petals, constitute the corolla, and the outer more proximal components, sepals that are usually green-coloured and have leaf-like morphology, constitute the calyx (Fig. A.6A, B).

Bracteoles. Additional leaf-like structures may exist proximal to calyx. They may take the form of bracteoles, and a single whorl of bracteoles inserted closely below the calyx is termed an epicalyx.

A.6.2 Positional relationship between floral components

Positional relationship between adjacent whorls. There two types of positional relationship between whorls. Opposite relationship between whorl is the case such as in Primulaceae stamens and petals: looking from the floral apex, each stamen is overlapped with a petal (Fig. A.6E). If petals and stamens are in alternate relationship, each stamen is located at the middle of two petals (Fig. A.6F).

Aestivation. Aestivation represents the folding or packing of floral organs, mainly perianth, in a bud. It also mentions the positional relation to the supporting stem axis and bract(s), and the side of the flower nearest to the axis is referred to as posterior, that nearest the bract is anterior.

 The aestivation is classified by the touch between nearest organs, and the overlapping order in a whorl. If the margin of the organs do not reach each other, the aestivation is open (apart), which is common type in calyx (Fig. A.7A). If they only touch, it is called valvate. If they pass over each other, the aestivation is imbricate (Fig. A.7B–F). The imbricate aestivation is further classified into quincuncial, contort (twisted), and cochleate [323, pp. 13–16] The quincuncial aestivation is directly accomplished by 2/5 phyllotaxy (Fig. A.7B). There are two types of contort, namely, right-handed and left-handed (Fig. A.7C). In left-handed contort aestivation (e.g. *Oxalis*), each organ is outside of the left neighbour and inside of right neighbour, and vice versa in right-handed one (Gentianaceae). Cochleate means snail-shape, and this type occurs commonly in pentamerous corollas (Fig. A.7D–F). In this type, one segment lies entirely outside, one segment lies completely inside, and the other three with one margin in and the other out. The inmost and outermost segments are in the relationship of angle 144° in the basic form of coheleate. When the innermost segment is the closest to the axis, the aestivation is ascending cochleate (Fig. A.7D), whereas the inmost organ is the farthest from the axis, the aestivation is the descending cochleate (Fig. A.7E). Another type of cochleate aestivation is proximal-cochleate (paratact), where the innermost segment is next to the outermost segment, as *Drosera* and *Jasminum* flowers show (Fig. A.7F).
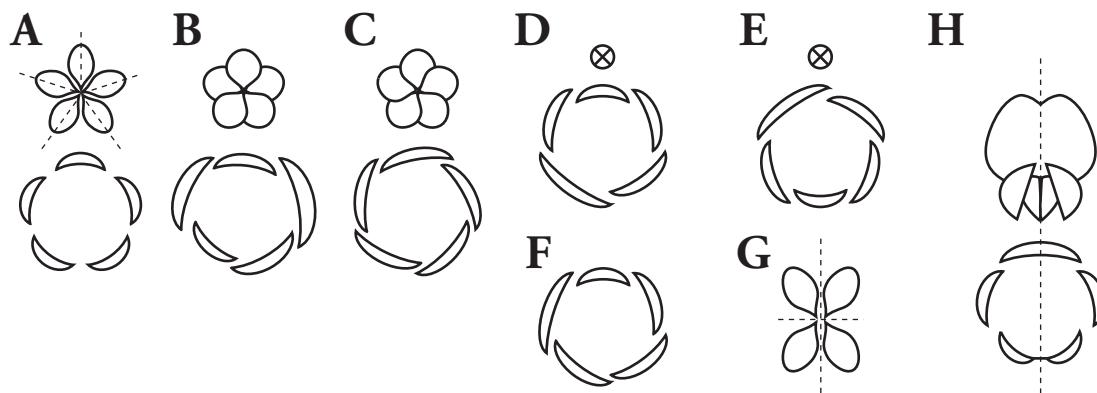

Figure A.7: **Schematic representation of aestivation and symmetry of flower. A.** Open flower in pentaradial symmetry. **B.** Quincuncial. **C.** Left-handed contort. **D.** Ascending cochleate. **E.** Descending cochleate. **F.** Proximal-cochleate (paratact). **G.** Disymmetric flower. **H.** Zygomorphic flower of Fabaceae. **A,G,H.** Dashed lines show the symmetry axes.

A.6.3 Symmetry

The majority of flowers show either radial symmetry, disymmetry, or zygomorphy [323]. Zygomorphic flowers have advantages since they can designate specific species of pollinators such as bumblebee and increase pollination efficiency, by restricting the entry of nectar-seeking insects into the flower to one direction and precisely placing anthers and stigma on pollinators' body. Probably this advantage causes the evolution of zygomorphic flowers from ancestrally radial-symmetric flowers, independently and multiple times in different taxa.

Radial symmetry (actinomorphy). Flower is called as radial symmetry, or actinomorphy, when floral organs, which are identical each other in shape within each whorl, are arranged around a central axis (e.g. Fig. A.7A). If there are five identical parts in a whorl such as five petals in a corolla, the corolla is in pentaradial symmetry. The number of floral organs can be different between whorls within a flower. For example, in a pistillate flower of *Euphorbia* flower, sepal and petal whorls are pentaradial symmetric, but there are three carpels in triradial symmetric position [236]. The different number of symmetric axis is found frequently also in hermaphroditic flowers, e.g., Saxifragaceae flower has two to three carpels, although others organs are in pentaradial symmetry (cf. Fig. A.6B).

Disymmetry. Disymmetric flower has two symmetry axis (Fig. A.7G). The adaxial side and abaxial side is symmetric, as in *Arabidopsis thaliana*.

Zygomorphic (dorsi-ventral, monosymmetric) Zygomorphic flower has only one axis of symmetry (Fig. A.7H). Majority of zygomorphic flower in a Asteridae have two adaxial petals, two lateral petals, and an abaxial petal. The forms of zygomorphic flowers are classified by how many petals differentiate into the adaxial (upper) shape from the abaxial (lower) side. A study on Asteridae showed three common forms in zygomorphy [77]: The 2:3 form is the type in *Antirrhinum*, in which the two adaxial petals are differentiated from the three other petals. In the second 4:1 pattern, four adaxial petals are differentiated from an abaxial petal. The 5:0 pattern, which all five petals are shifted towards the abaxial side of the flower, is relatively rare [77].

Fabaceae in Rosidae (sister clade of Asteridae) is upside-down to zygomorphic flowers of Asterids, having an adaxial petal, two lateral petals, and two abaxial petals (Fig. A.7H). The zygomorphy in basal eudicots, such as *Aconitum* flower (Ranunculaceae) which is hooded by a large adaxial tepal, is totally different form those in core eudicot because it has a simple perianth in contrast to double perianth in core eudicots. In Orchidaceae, the largest zygomorphic group in monocots, an adaxial petal (or inner tepal) differentiates into labellum, an organ specific to orchids. Taken together, although zygomorphy evolved individually, the underlying mechanism is similar among angiosperms in terms of "specialisation of adaxial side".

B Development of Lateral Organ

Shoot, the basic unit of aerial part of plant consist of stem and lateral organs, is developed through the tip growth. The development occurs around the differential stem cell region called apical meristem, which generates lateral organ primordia around it. The position of organ primordia is prescribed by the spatial distribution of phytohormone auxin, which is regulated by the its polar transport and local synthesis. The organ primordia further continue the outgrowth and establish the boundary around them, and set up adaxial-abaxial pattern. Flower primordium, one type of axillary buds, works itself as a meristem and produces floral organ primordia around it. Floral organ primordia undergo the specification of their fate, namely, one of the sepal, petal, stamens, and so on. Here I review modern biology knowledge on these developmental processes.

B.1 Meristem

The apical meristem locates at the shoot apex and produces the primordia of lateral organs. It is a small mound of undifferentiated dividing cells, which can be classified as stem cells based on the ability to proliferate, to maintain themselves, to give rise to a variety of differentiated cell types, and to regenerate a new meristem if damaged [221].

Generally there are three types of meristem corresponding to three three types of shoot (section A); shoot apical meristem (SAM) gives rise to leaves, inflorescence meristem (IM) produces flowers, floral meristem (FM) generates floral organs. In dicotyledonous plants, the primary SAM is formed between the two cotyledons during embryogenesis, and secondary (lateral) shoot meristems are formed at leaf axils. These meristems are considered to be homologous each other since they are regulated by similar set of genes. However, the pattern (whorled or spiral) and number (fixed or not) of lateral organs, and the fate (terminate or indeterminate) of the meristems are different depending on species and their ontogenic stage. For example, although *Arabidopsis thaliana* SAM is indeterminate and gives rise to leaves in spiral phyllotaxis, FM gives rise to fixed number of floral organ in whorled arrangement and terminate. On the other hand, *Anemone* FM forms unfixed number of organs but terminate.

B.1.1 Organization

Clonal domain. The attempt to distinguishing the meristematic region started in the latter half of 19th century. Hanstein stated three-histogen hypothesis through his works on 46 species of angiosperms, which distinguished three histogenic regions in the shoot apex: The dermatogen as an histogen for an outermost layer of cells (epidermis), the periblem for one or more underlying layers of cells (cortex), and the plerome that forms the central core (the stele or central cylinder), which is covered by the first two histogens.

However, Hanstein's theory is not applicable to all higher plants because the number of germ layers is different among different species. For example, Schmidt have reported that Hanstein's histogens are distinguishable in some plants, but it is unable to find a distinction between periblem and plerome in some other plants. Satina [257] studied periclinal chimera in *Datura* and found that there are three independent germ layers, where the number is in accord with Hanstein's theory of three histogens in plants, and the outermost germ layer in *Datura* primordia corresponds to Hanstein's dermatogen. However, periblem and plerome shows paradox: In the Hanstein's theory the central core should be initiated from the plerome, but in fact it is a derivative of the third germ layer that is classified into periblem in Hanstein's criteria. Barton (1993)'s observation [22] in *Arabidopsis* is consistent with *Datura*: The outer two layers are direct derivatives of the epidermal and upper hypodermal layers of the embryo, respectively, and the third layer and the central core are the derivatives of the lower hypodermal layer.

Schmidt (1924) divided meristem into two anatomically distinct regions: tunica and corpus. In his theory, the tunica and the corpus differ in the manner of growth (orientation of cell division) and in the arrangement of the cells. Tunica is composed of one or more superficial cell layers of the apex that cover underlying corpus. The number of tunica layers ranges from one to five, where the two-layered tunica as in *Datura* [257] and *Arabidopsis* [22] is the most common. The layered arrangement of the tunica is maintained by the anticlinal division of tunica cells, allowing an increase of the surface of the apex. Corpus locates beneath the tunica, and cells of the corpus divide in irregular direction, resulting in an irregular arrangement of cells. As a result, the apex increases in volume [285].

In the species with two-layered tunica, the meristem has three superimposed separate layers: a superficial epidermal L1, a subsurface L2, and a deeper L3 layer. L1 and L2 are equated to two tunica layers [22].

Functional domain. The meristem organization is also described with three functional domains. CZ is the central zone located at the very summit of the apical meristem, where the cells divide relatively infrequently to keep a specific population of pluripotent cells. CZ is surrounded by PZ (peripheral zone)/flank meristem with rapidly dividing cells, where lateral organ primordia are initiated . RM/Rib meristem is a zone underneath the CZ, whose cells also rapidly divide and develops into the pith.

B.1.2 Initiation

The meristem are observed under three conditions: (1) the primary shoot apical meristem that formed during embryogenesis, (2) lateral meristems or floral meristems at the axils of leaves, and (3) adventitious meristem, such as from a callus or somewhere else where the meristem usually does not arise.

Initiation of SAM in seedlings. In *Arabidopsis*, The SAM arises from the central part of the upper hemisphere of the torpedo stage embryo, which consists of three layers named as epidermal layer and the upper and lower hypodermal layers. Cells in the epidermal and upper hypodermal layer divide anticlinally, whereas cells in the lower hypodermal layer show divisions in various directions. The former two layers form tunica (L1 and L2), whereas the latter forms the corpus (L3 and central core). The embryonic SAM is slightly domed and has 7-8 cells in diameter in the fully formed embryo [22].

Class 1 *KNOTTED* class homeobox (*KNOX1*) genes are required for the acquisition of meristematic fate. *KNOX1* genes [144, 320], such as Maize *KNOTTED-1* (*KN1*), *Arabidopsis SHOOTMERISTEM* (*STM*) and *KNAT1*, are required for SAM formation during embryogenesis [22], and their expression is kept in the apical meristems after the germination [168, 276]. The studies of loss-of-function mutations [168, 319] and overexpression of the *KNOX1* genes [55, 275] showed that *KNOX1* genes are able to switch the cell fate from determinate to indeterminate, and ectopic expression of *STM* suppresses the cell differentiation in leaf primordia. However, the ectopic expression of *KNOX1* cannot induce the expression of the stem cell marker *CLAVATA3* (*CLV3*) [165] and it is not sufficient for complete activation of cell division [105].

WUSCHEL (*WUS*) expression is the first indication of stem cell niche during *Arabidopsis* embryogenesis. Expression of another homeobox gene *WUS* is also detected continuously at the centre of top of the embryo [183]. The ectopic expression of *WUS* is able to induce stem cell identity as indicated by the expression of stem cell marker *CLV3*, acting independently each other to *STM* gene (*KNOX1* family) [165]. Combined expression of *KNOX1* and *WUS* can trigger the initiation of meristem activity as indicated by meristematic marker *CLV1* and initiation of a new outgrowth on the differentiated tissue, but the meristem is only transient and cannot keep the meristematic state [105], suggesting that the *KNOX1* and *STM* genes are responsible for initiation of the meristem in different pathways, but are not sufficient for the maintenance.

ARGONAUTE (*AGO*) family genes, especially *ZWILLE/PINHEAD/AGO10* (*ZLL*), are required for maintaining expression domain of *KNOX1* in embryogenesis. AGO proteins play central role in all known small RNA-directed regulatory pathways, such as miRNA and siRNA cleavage [315]. In *Arabidopsis thaliana*, *ZLL* is essential for restricting the expression domain of *KNOX1* in the embryo [175, 194]. In the *zll* mutant, *KNOX1* gene *STM* express correctly at first, but cannot maintain the expression at the central dome when the first two true leaves are initiated [194], and the mutant embryos form differentiated cells and organs instead of shoot meristematic cells [175, 194]. These mutant seedlings eventually produce adventitious meristems, therefore they are fertile with indeterminate inflorescences [308], indicating that *ZLL* is required specifically for embryonic (primary) shoot meristem development but not for post-embryonic (secondary) meristem maintenance. *ZLL* is also likely to influences the function of *WUS* in promoting stem cell identity, and is in a linear sequence with *AGO1* [309].

Initiation of axillary meristem. The shoot branching is triggered by the formation of new lateral meristems, which recapitulate the function of the SAM, at leaf axils. They can either grow out as shoots or remain dormant depending on their position along the shoot axis, their seasonal or ontogenic phase, and environmental factors [187].

The expression of meristematic factors, such as *KNOX1* and *WUS*, newly establishes in axillary meristem separately from the SAM [183]. In *Arabidopsis*, the interplay between adaxial factors and boundary determiners such as *LATERAL SUPPRESSOR* (*LAS*), *REGULATOR OF AXILLARY MERISTEMS1, 3* (*RAX1, 3*), *RAX3*, *NAC* gene family such as *CUP-SHAPED COTYLEDON1–3* (*CUC1–3*), and miR164 plays the central role in the axillary meristem formation (see also Appendix B.3.3). *AGO1* also works in the axillary meristem formation in *Arabidopsis*, indicated by loss-of-function mutant *ago1* that rarely develops axillary meristems [36, 175].

The development of compound leaves is somewhat similar to the axillary meristem establishment [49]. In the incipient primordia, *KNOX1* genes are down-regulated in all types of leaf. Despite this down-regulation is permanent in simple leaves, it is re-established later in compound leaves, such as in *Lepidium* (Brassicaceae), but not in Fabaceae [33]. Additionally, over-expression of *KNOX1* genes can increase the complexity and leaflet number of compound leaves, but it has no dramatic effect for simple leaves [117].

B.1.3 Maintenance.

Specific population of stem cell needs to be protected in CZ against the differentiation that occurs around the organ initiating region in PZ. In *Arabidopsis* SAM and FMs, the *WUS* gene is required to keep undifferentiated state of stem cells, whereas the *CLV1, 2*, and *3* genes regulate the *WUS* activity. A feedback loop between *WUS* in the underlying organizing centre and *CLV* in the stem cells is responsible for keeping specific population of stem cell.

Size. In *Arabidopsis*, *WUS* is required to maintain an undifferentiated state of a small cell group underneath the CZ termed the organising centre (OC) [183], and *wus* mutant shows small meristem [262]. In contrast, the loss-of-function mutants *clv1* [58] and *clv3* [59] show enlarged meristems. *CLV3* is a signal peptide that is expressed in stem cells and restricts *WUS* transcription via the CLV1/CLV2 receptor kinase signalling cascade [41]. *CLV* activity negatively regulate proliferation of the central meristem, forming negative feedback loop with *WUS* [262]. This feedback loop between the OC containing *WUS* activity and stem cells with *CLV* expression mainly controls the size of the stem cell pool, although several parallel pathways have been identified.

Undifferentiated state. To keep the undifferentiated state of stem cells in the apical meristem, the *KNOX1* family gene and *WUS* genes, which express differently each other, are required. For example in *Arabidopsis*, *STM* (*KNOX1* family) expresses in SAM and FMs [168], and suppresses differentiation of stem cells. STM competitively regulate its antagonist *CLV* gene that promotes organ initiation [57], independently to that by *WUS*. *WUS* is expressed in a small subdomain of the SAM, but disappears in the differentiating organs and maturing flowers. *WUS* requires *AITEGUMENTA* (*ANT*) and *AIL6* to keep the indeterminacy of stem cell pool [154].

Termination. Meristem of determinate shoot terminates with a terminal flower in a determinate inflorescence, or carpel(s) in a flower. In flowers, central cells of floral meristem are consumed and *WUS* expression decreases to become undetectable when the carpel primordia emerged [183]. For this down-regulation of *WUS* expression and termination of the meristem, *AGAMOUS* (*AG*) is required [164].

B.2 Lateral organ formation at the concentration maximum of plant hormone auxin

The organ primordia initiation occurs in PZ at the concentration maxima of plant hormone auxin, a small molecules represented by indole-3-acetic-acid (IAA; Tab. B.1. Auxin is both required and sufficient for lateral organ initiation, as demonstrated by *pin-formed1* (*pin1*) mutant of *Arabidopsis* with defect in auxin polar transport whose inflorescence grows continuously without flowers [203], and the rescue of this phenotype by micro-application of the IAA to the apex [227]. The heterogeneous distribution of auxin concentration is generated both by directional transport and local biosynthesis of auxin in the shoot apex, which loss leads to pin-like inflorescence.

B.2.1 Auxin polar transport

The major form of auxin in plants, IAA, is not able to diffuse across membranes. Especially it hardly goes out from the cell, because it is in acid form (IAA$^-$) in the cytoplasm. Therefore IAA transporters localised at cell membranes

Table B.1: **Molecules that can act as auxin in plants.**

Abbreviations	Name	Description
IAA	indole-3-acetic acid	Plant endogenous, the most abundant
NAA	naphthalene-1-acetic acid	does not require carrier to enter the cell
NOA	naphthoxy-1-acetic acid	Inhibitor of the carrier-mediated influx
NPA	N-1-naphthylphthalamic acid	Auxin polar transporter inhibitor
2,4-D	2,4-dichlorophenoxyacetic acid	

are responsible for inter-cellular transport and spatial distribution that required for correct organ positioning. On the other hand, the pH is more neutral in the extracellular space such that IAA can take IAAH form. Since this neutral form is easier to pass through the membranes, the influx carrier is considered to be less important for auxin active transport but required for stabilising spatial auxin distribution.

Auxin efflux carrier PIN1 (PIN-FORMED1). PIN1 and its localization is responsible for phyllotactic pattern [107, 228]. The auxin flux indicated by sub-cellular polarisation of PIN1 protein directs the incipient primordia in the epidermal L1 layer, and in the primordia, it directs to the base forming a connection to the vascular tissue of the stem [28]. Therefore the primordia can be thought as auxin sinks that transport auxin into the pro-vascular tissues and depleting auxin from surrounding cells. This polar transport and accumulation of auxin have been suggested to be responsible for the heterogeneous auxin distribution and formation of the auxin concentration maxima in regular spatial-interval [140, 278].

Auxin influx carriers *AUXIN1/LIKE-AUX1* (*AUX1/LAX*). *AUX/LAX*s, which belong to the auxin amino acid permease (AAAP) family, are proposed to stabilize the phyllotactic pattern in *Arabidopsis* and tomato [19, 207]. The first *AUX/LAX* gene was found as a regulator of root gravitropism [29], and now four *AUX/LAX* genes are known in *Arabidopsis*. The function of AUX1 as an import carrier was suggested by the fact that the *aux1* mutant was sensitive only for NAA, which enters the cells by passive diffusion [73], but not for 2,4-D nor IAA that require the influx carrier to enter the cells [179], and was confirmed by the isotope-labelled auxin ^{3}H$-$IAA [333]. AUX/LAXs are transmembrane protein that actively transport auxin into cells [293, 333], and are considered to be present on all membranes of L1 cells, in contrast to the polarised localisation of efflux carrier *PIN1*. The mutant of *AUX1* does not show any defect in the shoot. However, application of NOA, the inhibitor of the carrier-mediated influx [136], leads to the formation of organs that occupy a larger segment of the meristem [207]. Moreover, the phyllotaxis of triple or quadruple mutants of four influx carriers is irregular, or in severe phenotype, it cannot form clear auxin concentration maxima [19]. Thus these influx carriers redundantly control the correct leaf positioning [207].

B.2.2   Auxin biosynthesis

The auxin biosynthesis is also necessary to control the auxin level and spatial pattern formation at the apical meristem besides the auxin transport. To synthesize an endogenous auxin IAA, plants use multiple L-Tryptophan (Trp)-dependent pathways and a Trp-independent pathway [331]. Four Trp-dependent pathways have been suggested: The indole-3-pyruvic acid (IPA, IPyA) pathway, the indole-3-acetamide (IAM) pathway, the indole-3-acetaldoxime (IAOx) pathway, and the tryptamine pathway.

IPA pathway. In IPA pathway, Trp is sequentially catalysed by L-tryptophan aminotransferase, indole pyruvate decarboxylase (PDC), and aldehyde oxidase (AO). It was well-defined in microbes, and has been thought to be the same in plants [151]. Indeed in tomato, isotope-labelling study showed that IPA acts as a precursor to IAA [61]. Moreover, in *Arabidopsis thaliana*, *TRYPTOPHAN AMINOTRANSFERASE OF ARABIDOPSIS1* (*TAA1*) [287] and *Arabidopsis Aldehyde Oxidase* (*AAO*) [267] were predicted to responsible for the first and last steps, respectively. Taken together, the pathway was hypothesised as:

$$\text{Trp} \quad -\text{CH}_2-\underset{\underset{\text{NH}_2}{|}}{\overset{\overset{\text{H}}{|}}{\text{C}}}-\text{COOH} \xrightarrow{TAA1} \quad -\text{CH}_2-\text{CO}-\text{COOH} \quad \text{IPA}$$

$$\xrightarrow{(PDC)} \quad -\text{CH}_2-\text{CH}{=}\text{O} \quad \text{IAAld} \xrightarrow{AAO} \quad -\text{CH}_2-\text{COOH} \quad \text{IAA}$$
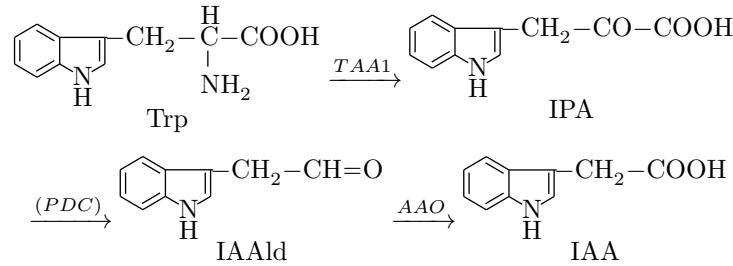
However, there is no *in planta* evidence indicating that PDCs and AAOs are working in this pathway. Since new evidences of catalysis from IPA to IAA by YUCCA (YUC), a flavin monooxygenase (FMO)-like enzyme, and successive catalyses by TAA1 and YUC in a linear pathway have been shown [180, 288], the pathway was updated:

$$\text{Trp} \xrightarrow{TAA} \text{IPA} \xrightarrow{YUC} \text{IAA}$$

YUC-family genes are known to be important in organ initiation [51] and *Arabidopsis yuc* dominant mutant show elevated levels of free auxin [336]. The *YUC* genes are expressed both in the center of the inflorescence meristem and in organ primordia, indicating the region where this pathway works [51]. The orthologue of *YUC* in *Petunia, FLOZZY* (*FZY*), is expressed similarly to that of *YUC* in the center of young floral meristematic dome, the base of floral organs, and later localised on the stamens and carpels, but it is not detectable in inflorescence meristem [51, 303]. Mutants in *YUC* homologues of several species both in eudicots and monocots [303] exhibited similar developmental defects, indicating that the auxin biosynthesis via YUC is conserved in angiosperms.

TAA1 and its paralogue (*TRYPTOPHAN AMINOTRANSFERASE RELATED* or *TAR*) affect the spatial regulation of auxin biosynthesis. The double mutant *taa1 tar2* (*wei8 tar2*) displays a auxin-related phenotype [287]. *TAA1* expresses similarly to *YUC* in the central part of L1 in floral meristem in early stage of floral development, and later moves inwards to the base of gynoecia [287], suggesting the collaboration of TAA1 and YUC.

IAM pathway. IAM pathway converts Trp to IAM by a tryptophan-2-monooxygenase IaaM, and then hydrolyse IAM to release IAA by a hydrolase IaaH [152], in plant pathogens such as Agrobacterium [325] and *Erwinia* [56].

$$\text{Trp} \xrightarrow{(IaaM)} \quad -\text{CH}_2-\text{CO}-\text{NH}_2 \quad \text{IAM} \xrightarrow{(IaaH)} \text{IAA}$$
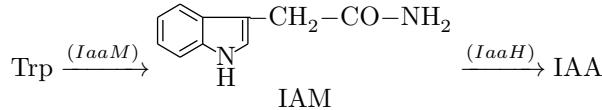
The reports on the occurrence of IAM in plants leaves a room for a microbial contribution [220]. However, IAM was shown as endogenous metabolite in *Arabidopsis thaliana* whose level varies with developmental stage of the plants [219]. The genome of *Arabidopsis thaliana* contains a small family of genes encoding amidase-like proteins (*AMI1* to *AMI4*), and one of them (*AMI1*) encodes an amidase with significant sequence similarity to the bacterial *IaaH*, and expression of its cDNA in *E. coli* yielded a functional enzyme with substrate specificity for IAM [220]. These evidences support IAM pathway in plants, but no *IaaM*-like sequence in plant genomes has been reported.

IAOx pathway. NITs are suggested to be able to convert indole-3-acetnitrile (IAN) to IAA or to IAM.

$$\text{L}-\text{Tryptophan} \xrightarrow{CYP79B2, CYP79B3} \quad -\text{CH}_2-\underset{\underset{\text{H}}{|}}{\text{C}}{=}\text{N}-\text{OH}$$

$$\xrightarrow{CYP71A13} \text{IAN } or \text{ IAM} \xrightarrow{(NITs)} \text{IAA}.$$
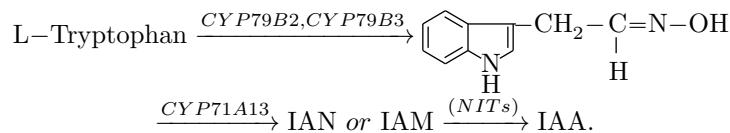
Tryptamine pathway Since *Escherichia coli*-produced YUC protein could catalyse the conversion of tryptamine into N-hydroxyl tryptamine (NHT), classically this pathway was suggested as follows. However, recent studies have shown that the YUC works in IPA pathway, leading to less trust on this pathway.

$$\text{L−tryptophan} \xrightarrow{(TDC)} \underset{\underset{\text{tryptamine}}{\text{H}}}{\overset{\text{−CH}_2\text{−CH}_2\text{−NH}_2}{\boxed{}}} \xrightarrow{YUC} \underset{\underset{\text{NHT}}{\text{H}}}{\overset{\text{−CH}_2\text{−CH}_2\text{−NH−OH}}{\boxed{}}} \longrightarrow \longrightarrow \text{IAA.}$$
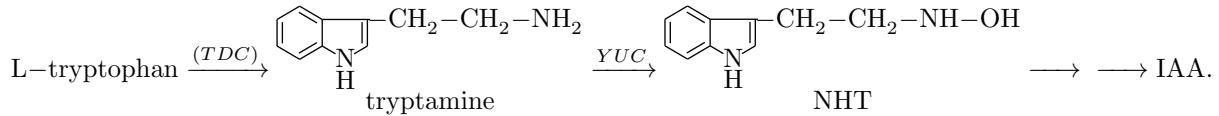
Trp-independent IAA biosynthesis. Using Tryptophan Synthase mutants, namely, *trp3-1* that has mutation in Tryptophan Synthase α [224] and *trp2-1* that has mutation in Tryptophan Synthase β [161], the Trp-independent IAA biosynthesis pathway has been shown [199]. These mutants have defects in Trp biosynthetic pathway as follows:

$$\text{IGP(Indole−3−glycerolphosphate)} \xrightarrow{trp3} \underset{\underset{\text{Indole}}{\text{H}}}{\boxed{}} \xrightarrow{trp2} \text{Tryptophan.}$$
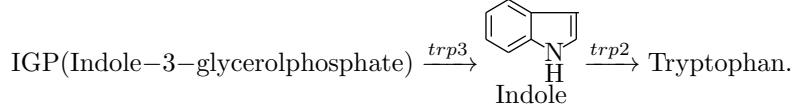
Since IAA can be synthesised even if the downstream of the IGP is impaired, IGP has been suggested as a branch-point compound to enter a Trp-independent IAA biosynthetic pathway from Trp biosynthesis pathway [205].

B.3 Downstream of the auxin signalling

Auxin concentration maxima triggers development of organ. The cells in organ primordia lost their undifferentiated state and differentiate into determinate fate. The incipient primordia start to swelling and increase the volume. The boundary and The adaxial-abaxial pattern are established to form the shape of bifacial lateral organs.

B.3.1 Switch to determinate state

After the launch of differentiation programme specified for organ primordia, it cannot be returned to the undifferentiated state of stem cells during normal development. The first event is the local down-regulation of expression of meristematic factors. The meristematic factor *KNOX1* genes, such as *BREVIPEDICELLUS* (*BP*), are repressed independently by the auxin activity and by the evolutionary conserved MYB factors encoded by the *ASYMMETRIC LEAVES1/ROUGH SHEATH2/PHANTASTICA* (*ARP*) genes such as the *Arabidopsis ASYMMETRIC LEAF1* (*AS1*), the *Zea mays ROUGH SHEATH2* (*RS2*), and the *Antirrhinum PHANTASTICA* (*PHAN*) genes [121]. The repression of meristematic factors allow the primordia to differentiate as organs.

B.3.2 Cell division and organ swelling

The first morphological feature that indicates the formation of a new leaf is the formation of a new mound at the place determined by the concentration maxima of auxin. The periclinal cell divisions, which forms a new cell wall parallel to the organ surface, firstly occurs in the tunica layers, in contrast to anticlinal division in meristem, and allowing these layers to grow in a new direction [66, 257]. After the formation of a mound, the primordium expands to form leaf blade at the marginal region between adaxial and abaxial sides, which called marginal meristem.

Several regulators of the organ growth are known, such as *AP-2*-like gene *ANT*, *ARGOS* (*Auxin-Regulated Gene involved in Organ Size*), and *AUXIN-RESISTANT1* (*AXR1*). They are suggested to work in a linear sequence:

$$\text{AXR1} \longrightarrow \text{ARGOS} \longrightarrow \text{ANT.}$$

The loss-of-function mutant of *ANT* show reduced number of floral organs in all four whorls in *Arabidopsis* [84, 150] with decreased size and cell number in organs [191], and its ectopic expression causes increase of organ size [155, 191]. The *ANT* expression is detected in very early stage of the initiation of all lateral organs [84], and is repressed in maturing organs by *AUXIN RESPONSE FACTOR* (*ARF2*), a negative regulator of organ growth [264]. Other members of *ANT* family, such as *AINTEGUMENTA-like6* (*AIL6*), also promotes floral organ growth [154].

B.3.3 Boundary establishment and post-meristematic modification of organ position

After the initiation of lateral organ primordia in the PZ of the apical meristem, boundaries that separate primordia from the meristem and adjacent primordia are established [5]. Several NAC (NAM/ATAF1,2/CUC2) domain transcription factors, one of the largest families of plant-specific transcription factors, is necessary for the separation [5].

The spatial expression pattern of NAC domain transcription factors cleaved by miR164 determines the organ boundary. *CUC* genes of *Arabidopsis thaliana* encoding NAC domain transcription factors are involved in the establishment of lateral organ boundaries, as indicated by the fused cotyledons and floral organs in their loss-of-function mutants [4]. *Arabidopsis thaliana* has three *CUC* genes, *CUC1*, *2*, and *3*, which have partially redundant functions in cotyledons, for example *CUC3* works during axillary meristem development, whereas the *CUC2* contribute to embryogenesis greater than *CUC1*.

The expression of *CUC1* and *CUC2* are restricted to the boundary around the primordia by the regulation by microRNA164 (miR164), which is essential for keeping the angular position of organs and correct interval of internodes [214]. In *Arabidopsis* genome, three members of miR164 family have been identified: *MIR164A*, *MIR164B*, and *MIR164C*. *eep1*, a loss-of-function mutant of *MIR164C*, leads to the formation of extra petal primordia, which arise adjacent to normal four petals in various size, in early arising flowers [20]. This defect is enhanced by the mutations in *MIR164A* and *MIR164B* [20], indicating functional redundancy of these three members.

The functional conservation of NAC domain transcription factors. The role of *CUC* in SAM function and organ separation is evolutionarily conserved among eudicots, as indicated by mutants of the *CUC* homologues, *NO APICAL MERISTEM* (*NAM*) in *Petunia hybrida*, *CUPULIFORMIS* (*CUP*) in *Antirrhinum majus*, and *GOBLET* (*GOB*) in *Solanum lycopersicum*, which show similar developmental defects in organ separation. These factors are also required in leaf development for regulation of leaf margin serration or dissection, and for the formation of leaflets, suggesting that the function as the separator is also conserved among the developmental stages, from the lateral organ primordium boundary to the leaflet margins [35]. The regulation of spatial expression domain of *NAC*s by the miRNA is also conserved among species and developmental stages.

The evolution of NAC domain transcription factors. The phylogeny *NAC* genes has two clades which divided predating the monocot-eudicot divergence. *CUC3* clade is a single copy gene in all the species that were examined so far, whereas the copy number of *NAM/CUC1/CUC2* clade in a species is more variable [337]. In *NAM/CUC1/CUC2* clade, only one member has been identified in tomato (*GOB*) and *Antirrhinum* (*CUP*) [326], and the strong phenotype of their mutations with fused cotyledons, floral organs, and leaves, associating with fasciated apical meristem, suggests that there is no redundant gene. In *Zea mays* and *Pisum sativum*, two paralogues probably duplicated recently are found [337]. *Arabidopsis* also has two copies, but *CUC1* and *CUC2* only show limited conservation outside the NAC domain. Since *CUC1* of *Arabidopsis* and another Brassicaceae species *Cardamine hirsuta* form a sub-clade separated from the other genes of the *NAM/CUC1/CUC2* clade, the duplication occurs probably before the speciation of these two species.

B.3.4 Adaxial-abaxial patterning

After the initiation of organ primordia in spherical geometry, the margin between the two sides, namely, the adaxial side directly adjacent to the apical meristem and the abaxial side distant from the meristem (Fig. A.4A), is fixed on the continuous surface of primordia. The margin works as a marginal meristem, which is required for the outgrowth of leaf blade, therefore the loss of adaxial-abaxial polarity results in filamentous radially symmetric organs.

The establishment of abaxial-adaxial polarity in lateral organs involves factors both intrinsic and extrinsic to the primordia [39]. Several transcription factors and small RNAs are identified as the adaxial and abaxial factors, which mutually exclusively interact and specify the adaxial and abaxial domains.

The signal from the apical meristem and members of HD-ZIPIII gene family act as the adaxial factors. The adaxial factors provide the fate to be adaxial side, thus their loss leads to the abaxialisation of leaves. Abaxialised leaf can be induced by micro-surgical techniques, such as physical separation of a leaf primordium from the shoot apex and ablation of L1-layer cells around a leaf primordium [226]. Since the laser ablation of L1 layer between swelling primordium and SAM causes the abaxialisation in high frequency [226], the leaf primordia are hypothesized that they receive positional information of mobile signal(s) from the the apical meristem from which they are derived through the L1 layer after their initiation, and that abaxial identity is a default state.

Adaxial specialisation involves some members of the class III homeodomain-leucine zipper (HD-ZIP). In *Arabidopsis thaliana*, three HD-ZIP III family genes, namely, *PHABULOSA* (*PHB*), *PHAVOLUTA* (*PHV*), and *REVOLOTA*

(*REV*), are proposed to work as the adaxial factors [223], since *PHB* and *PHV* genes express adaxial side [186] and their dominant mutant shows the radial adaxialised leaves [185,186], and *REV* is first expressed in L3 layer and moves to the adaxial domain preceding axillary meristem formation [204] and its loss-of-function mutant lacks the axillary meristems [294]. Their redundancy in the regulation of the adaxial fate was suggested from their double [223] and triple mutant [87]. Their gain-of-function mutants with adaxialised leaves have mutation in the region complementary to microRNAs miR165 and miR166 [87], suggesting regulation of their expression domain by miR165/166-guided mRNA cleavage. In accord with this, miR165/166 are transcribed in the abaxial side and move towards the adaxial side by the inter-cellular movements that common in plant small RNAs [192]. The tight regulation by these microRNAs is conserved among angiosperms, as indicated by adaxialised leaves in miRNA-resistant HD-ZIP Ⅲ mutants in *Arabidopsis*, *Zea mays*, and *Nicotiana sylvestris*.

MYB family transcription factors of *ARP* orthologues group affect the adaxial-abaxial patterning in some species, but their function is not conserved among angiosperms. The defects in some members of *ARP* genes encoding MYB transcription factor, such as the *AS1* in *Arabidopsis* and the *PHAN* in *Antirrhinum majus*, show the abaxialisation in leaves, bracts, and petals [321]. In *Arabidopsis*, *AS1* and its interactor *AS2* are likely to activate HD-ZIP Ⅲ transcription factors via miR165/166 regulation [100]. Although the function to down-regulate the *KNOX1* is common to the *AS1* and *PHAN* in maize orthologue *RS2*, its mutant do not show clear phenotype in adaxial-abaxial patterning [307], indicating the different regulatory mechanism of adaxial-abaxial patterning among plant species and different leaf development programme between eudicots and monocots [102,307].

YABBY (*YAB*) and *KANADI* (*KAN*) genes are the abaxial factors. The *YAB* gene family is a small plant-specific gene family encoding transcription factors with a zinc finger and HMG-related domains [38,260], which is responsible for the specification of abaxial cell fate in lateral organ primordia. The *Arabidopsis YAB* gene family is composed of six members, namely, *CRABS CLAW* (*CRC*) [38,93], *FILAMENTOUS FLOWER* (*FIL/YABBY1/AFO*) [260,274], *YABBY2* [274], *YABBY3* [274], *INNER NO OUTER* (*INO/YABBY4*) [317], and *YABBY5*. Each of the family members is expressed in abaxial side in cotyledons and lateral organ primordia [38,93,260,274,317] overlapping with other members of the family [93] or organ-type specifically [38,317]. Expression of *YAB* genes correlates with abaxial cell fate even in the mutation of adaxial-abaxial polarity [274], and ectopic expression of family members is sufficient to develop ectopic abaxial tissues in lateral organs [260] and in cotyledons [274], whereas the loss of these *YAB* genes results in a loss of polarity [93,260,274]. Thus the primary function of *YAB* gene family members is to specify abaxial cell fates in lateral organs and cotyledon [39].

The *KAN* genes encode GARP family of transcription factors, expressing complementary to adaxial factors *AS1*, *AS2*, and HD-ZIP Ⅲ genes in *Arabidopsis* [87]. *KAN* represses adaxialisation in the abaxial side, associating with *ARF4* and *ETTIN/AUXIN RESPONSE FACTOR3* (*ETT/ARF3*), which physically interact with *KAN* [143]. The spatial expression of *ETT/ARF3* and of *ARF4* is regulated by tasiR-ARF, a member of a class of endogenous small RNA called trans-acting small-interfering RNA (tasiRNA) [108]. A gradient of tasiR-ARF is formed by the transcription of precursor in the adaxial side and the inter-cellular movement of mature tasiR-ARF towards the abaxial side [54], resulting in the localisation of *KAN* in the abaxial side.

B.4 Contribution of mechanical properties for organ development

Since plant cell are rigid structure, the molecular networks must interfere with the physical properties of cells to shape lateral organs. Cell walls, which are made with a dense network of cellulose and cross-linking by hemicellulose and pectin, contribute the physical properties of plant cells. Plant cells have high internal turgor pressure, which is oppressed by a rigid cell wall, therefore controlling elasticity and amount of cell wall causes both expansion and elongation of the cells (turgor pressure-driven cell growth). For example, when the cell increase its size, the cell wall is loosened and the spaces between microfibres are expanded, and new polysaccharides are synthesised and inserted. The cell wall loosening is known to be caused by auxin or acid that triggers the secretion of protons into the cell wall, and by two groups of enzymes, namely, xyloglucan endotransglycosylase (XTH) and expansins, which cause loosening of cross-linking glycan (hemicellulose and pectin) and trigger the separation of cellulose fibres. These factors involves with early organ outgrowth and phyllotaxis, such as the methylesterification level of pectin affect the stability of golden divergence angle in spiral phyllotaxis [212,213].

The direction of cell elongation depends on the anisotropic properties of the cell wall, especially on the orientation of cellulose perpendicular to the growth axis. The cellulose orientation is strongly correlated with cortical microtubules, leading to the alignment hypothesis stating that cortical microtubules guide the synthesis and orientation of cellulose microfibrils. In accord with this hypothesis, rosette-like structures of heteromeric cellulose synthase (CESA) complexes at the plasma membrane co-align and move along with cortical microtubules. CESA and cortical microtubules is suggested to bind directly through CELLULOSE SUNTHASES INTERACTING1 (CSI1) protein [43], which loss shows thick and short root caused by the defect of anisotropic growth [120].

The orientation of microtubules is also aligned with auxin-efflux carrier PIN1 polarity [122]. PIN1 is localised at the edge parallel to the microtubule orientation, but it is not directly depend on the microtubules [122]. The auxin distribution and the physical properties of cell walls can interact to generate heterogeneous tension in the tissue that can be a principal factor for the morphogenesis, but it is still under discussion.

B.5 Floral development

The floral development has unique features differently from vegetative development. First, the floral organ position can be affected by bracts at the base of flowers. Second, the initiation order of floral organ primordia is different among species, and is not always centripetal as in the vegetative shoot. Third, floral organ primordium needs to be specified its fate and developed into a specific floral organ to carry out the function as a reproduction organ.
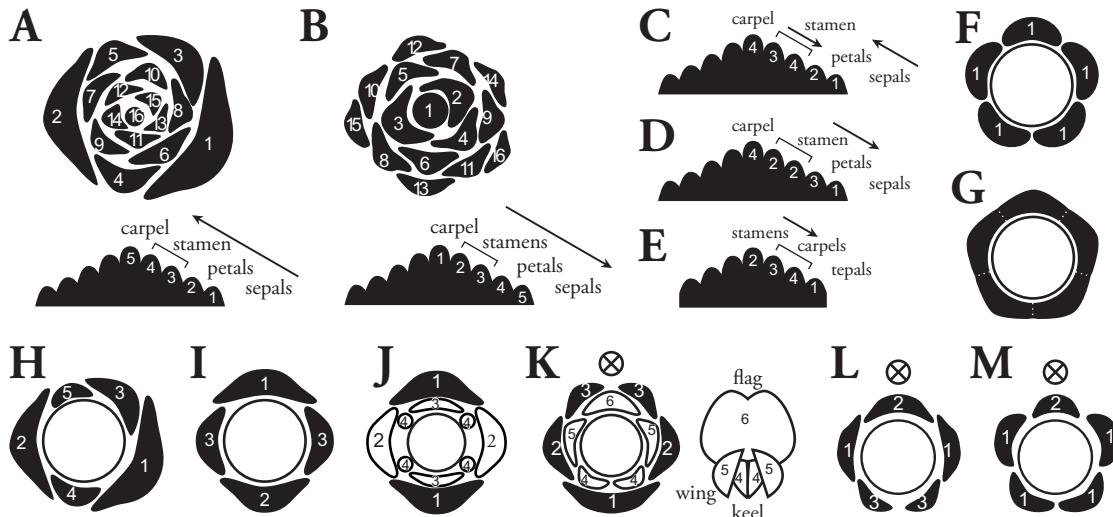
Figure B.1: **Initiation order of floral organ primordia.** Numbers and arrows show the initiation order. **A.** Centripetal organ initiation in transversal section (top) and vertical section (bottom) of floral bud. **B.** Centrifugal initiation. **C.** The intrazonal centrifugal development in two stamen whorls. **D.** The interzonal centrifugal development between stamen and petal whorls. **E.** The initiation order of inside-out flower. **F–L.** Initiation order in perianth (calyx) whorls. **F.** Simultaneous initiation of five primordia. **G.** Ring meristem. **H.** Helical initiation. **I.** Sepal initiation order of the *Arabidopsis*. **J.** Sepal and petal initiation of *Sanguinaria canadensis*. **K.** The butterfly-shape flower of Fabaceae. The numbers in the right panel correspond to the initiation order in the left panel. **L,M.** Bidirectional initiation in Mimosoideae (L) and *Antirrhinum* (M).

B.5.1 Bracts

In the typical form of angiosperm inflorescence, each flower has one or more bracts at the base. It is lacked in *Arabidopsis*, since the outgrowth of potential bract that appears as a local auxin maximum at the abaxial base

of flower is suppressed by several genes. Mutants of these gene, such as *bop1 bop2*, have bract and the bilateral pentamerous flowers, contrary to dilateral tetramerous flowers in wild type [128]. Thus the bracts can affect the floral organ number and arrangement, but their influence is largely unknown.

B.5.2   Initiation order of organ primordia

The order of floral organ initiation influences the number and arrangement of floral organs. The order of initiation is usually consistent within a species, but sometimes different initiation orders are observed among species within a genus- or family-level clade.

Developmental order in radial symmetric flower.   Centripetal/acropetal and centrifugal/basipetal represent two major types of the initiation order of floral-organ primordia along inside-outside axis of a flower. The centripetal development means that the outer organs are initiated first and the central organ is formed at last, as in the developing vegetative apex (Fig.   B.1A). By contrast, organs develop from the centre to periphery in centrifugal development. The centripetal organ initiation is considered as ancestral in angiosperms because of the absence of records of centrifugal development, and centrifugal initiation has evolved many times in angiosperm phylogeny [242].

The centrifugal development is subdivided into intrazonal and interzonal centrifugal development. Intrazonal centrifugal development indicates that the organ primordia within a "zone" show centrifugal initiation, for example, primordia in androecium zone initiate in a centrifugal sequence, and the last-formed (outermost) stamen whorls and the carpel whorls appear at the same time, as observed in large flowers with relatively high stamen number (polyandry) [242] (Fig.   B.1C). Interzonal centrifugal development means an entire organ zone initiate after the zone inside it, for example stamen initiation earlier than petal emergence is commonly found [242] (Fig.   B.1D).

Two genera that have inside-out flowers whose stamens are surrounded by the carpels, namely, monocot *Lacandonia* (Triuridaceae) [10] and the early-divergent angiosperm *Trithuria* (Hydatellaceae), show centrifugal development. In *Lacandonia*, three common primordia formed at first at the summit of floral meristematic dome. A stamen is formed at the top each common primordium, and then the foot of the common primordia are divided into several carpel primordia [10]. In *Trythuria*, two central stamens are formed in different size, and then the surrounding pistil are formed from top (centre) to bottom (periphery) [243] (Fig.   B.1E).

Intrazonal initiation order.   The initiation order within a zone composed of the same type organs is different among eudicot species, especially the sepal whorl. In some clades such as Asteraceae and some species in Mimosoideae (Fabaceae), sepal primordia within a whorl initiate at once. The coincident initiation can be either simultaneous initiation of several primordia (Fig.   B.1F), or ring meristem that will be dissected into several lobes of calyx (Fig.   B.1G). In pentamerous flowers of Ranunculaceae [229], Caryophyllaceae [174], and Solanaceae [130], the sepal primordia initiate one-by-one in helical order, which is obtained from 2/5 spiral phyllotaxis as in quincuncial aestivation (Fig.   B.1H). In the tetramerous flower of *Arabidopsis*, the adaxial sepal primordia swell at first, abaxial sepal appears the next followed by the lateral two sepals [279] (Fig.   B.1I). *Sanguinaria canadensis* also has tetramerous flowers, whose petals initiate differently from *Arabidopsis*. The two sepals and eight petals transition from decussate to tetramerous whorl: two sepal primordia are initiated opposite to the floral apex, two outer petals and two inner petals follow the sepals in a decussate manner, then four additional petals initiate simultaneously in alternate position to four pre-existing petals [163] (Fig.   B.1J). The fast succession or simultaneous initiation of primordia is commonly observed in the later stage of development in eudicots, regardless of the sepal initiation order [225,279]. The switch from helical initiation (Fig.   B.1H) to directional initiation (Fig.   B.1K,L) can associate with the evolution of zygomorphy as observed in Fabaceae [225], as will be touched upon in section B.5.4.

B.5.3   ABCE model and its evolutionary conservation

In floral development, different organ fate is assigned to floral organ primordia arose from one floral meristem, depending on expression of genes belong to ABCE classes.

ABCE model.   A model of organ-fate determination named as ABC model insisted that the doughnut-shape expression of B class gene and the mutual inhibition between A and C class genes divide the floral bud into four

concentric regions, corresponding to four whorls of floral organs: sepals, petals, stamens and carpels [60]. Since the loss of *SEPALLATA* genes leads to the sepal-like (*sep1 sep2 sep3* triple mutant [216]) or leaf-like floral organs (*sep1 sep2 sep3 sep4* quadruple mutant [75]), these genes are treated as E class (because D class was already assigned for genes required for ovule development), and the model is now known as ABCE model [216, 300] (Fig. B.2A).

MADS box genes. Most of the ABCE class genes are members of MIKC^c-type genes in type II MADS box (for MCM1, AG, DEFA, and SRF), which encode transcription factors [26] (Table B.2). MADS box genes are defined by a highly conserved 180-bp long DNA sequence, the MADS box, encoding the DNA-binding domain [26]. Type I and type II are divided by the sequence phylogeny and structural properties of the proteins they encode, and may evolved multiple times within different kingdoms of eukaryotes.

All plant type II MADS-box genes contain domains responsible for both DNA binding and dimerisation, namely, an I (Intervening) domain, a K (Keratin-like) domain, and a C (C terminal) domain, together known as MIKC-type MADS-box genes [298]. The I domain is only weakly conserved, and is involved in selective formation of DNA-binding dimers [233]. The K domain is plant specific, and contains hydrophobic amino acids at regular intervals and generates an amphipathic helix involved in protein-protein functions. The C terminus is the most variable, and it may be involved in cell's core transcriptional machinery, or may be necessary for the formation of multi-protein complexes required for transcriptional activation [81]. The plat type II MADS boxes are farther divided into two types, known as the MIKC^c and MIKC* types, and MIKC^c type is divided into 13 clades, including ABCE classes named *SQUA-* (A class), *DEF-* (B class), *GLO-* (B class), *AG-* (C class), and *AGL2*-like (E class) genes [26].
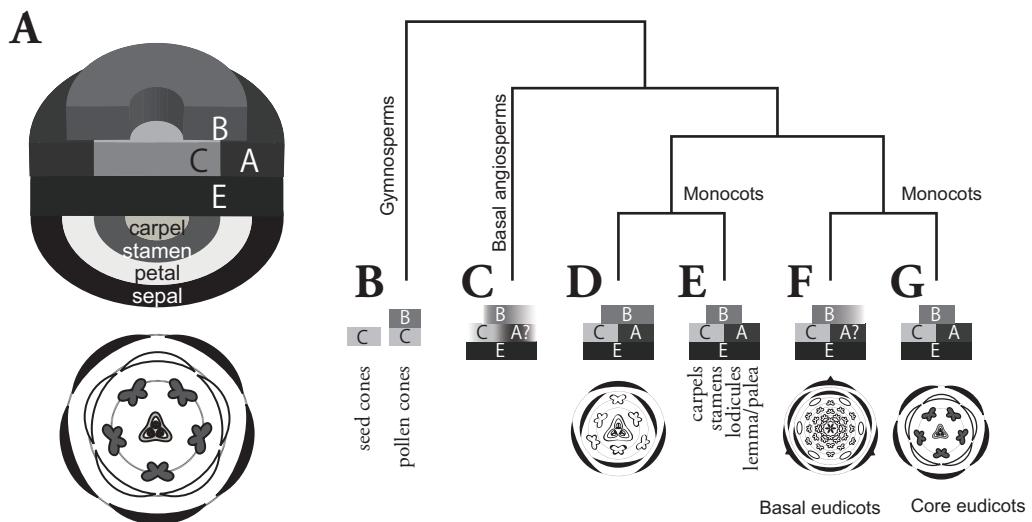
Figure B.2: **The ABCE model and its application to other clades. A.** The ABCE model developed in core-eudicots species. **B–G.** The schematic diagram showing evolutionary diversification of ABCE model [281]. **B.** Gymnosperms. **C.** magnoliids. **D.** Petaloid monocots such as lilies. **E.** Grass monocots such as rice and maize. Their ancestral flower is thought to have three sepals, three petals, three stamens and three carpels. One of the sepals differentiates into a lemma and the rest two sepals are fused to form a palea (this is suggested by the fact that the palea has two vascular strands). The petals develop as lodicules, and the adaxial lodicule is suppressed in most grass species [11]. **F.** Basal eudicots such as Ranunculales. **G.** Core eudicots.

AP2/ERF family. *Arabidopsis* A class gene *AP2* belongs to *AP2/ERF* family, which is a large gene family of DNA-binding proteins with AP2/ERF (ethylene-responsive element-binding factor) domain. There are three

Table B.2: MADS-box genes

Abbrev.	Name	Class	Description
AP1	*APETALA1*	*A*	*Arabidopsis thaliana*
SQUA	*SQUAMOSA*	*A*	*Antirrhinum majus* ortholog of *AP1*
AP2	*APETALA2*	*A*	*Arabidopsis thaliana*
PI	*PISTILLATA*	*B*	*Arabidopsis thaliana*
GLO	*GLOBOSA*	*B*	*Antirrhinum majus* ortholog of *PI*
AP3	*APETALA3*	*B*	*Arabidopsis thaliana*
DEF	*DEFICIENS*	*B*	*Antirrhinum majus* ortholog of *AP3*
Silky1 [11]	*Si1*	*B*	*Zea mays*, high sequence similarity to *AP3* and *DEF*
AG	*AGAMOUS*	*C*	*Arabidopsis thaliana*
SEP	*SEPALLATA*	*E*	*Arabidopsis thaliana*

classes in the family: *AP2*-like, *ERF*-like, and *RAV*, where the flower-related genes *AP2* and *ANT* [84, 150] are included in *AP2*-like class. The phylogeny of *AP2*-like transcription factors has two clades; *euAP2* lineage and *ANT* lineage [149], and latter is further divided into *PLT* clade and *ANT* clade.

Floral quartet model. The fact that all MADS-domain proteins bind to DNA sequence-specifically as dimers leads an idea that they bind to DNA as heterodimers, such as a heterodimer between A and B as ABCE model expected for petals. However, the MADS proteins bind to DNA only as AP1-AP1 homodimers (A-A homodimer), AG-AG homodimers (C-C homodimer), and AP3-PI heterodimers (B-B heterodimer), but not as AP3/PI-AP1 (B-A heterodimer) nor AP3/PI-AG (B-C heterodimer) [233]. A report from *Antirrhinum majus* showed that the protein complex actually binds to DNA as a protein tetramer (A-A-B-B tetramer), composed of a DEF-GLO heterodimer (B-B heterodimer) and a SQUA-SQUA homodimer (A-A homodimer) [81]. After a report of E-class genes [216], "floral quartet model" was suggested, stating that tetramers of ABCE class proteins composed of two protein dimers recognise two different sites on DNA and specify floral organ identity [300]. The formation of the complexes AP3/PI/AG/SEP3 (BCE) and AP3/PI/AP1/SEP3 (ABE), which are postulated for stamens and petals, respectively, was supported in yeast three- and four-hybrid assays [132]. Moreover, over-expressing PI + AP3 (B) with AP1 (A) or SEP3 (E) leads to the transformation of vegetative leaves to petaloid organs, over-expressing PI + AP3 with AG + SEP3 (CE) transforms into staminode organs [132]. Although there is no *in planta* evidence of multimeric complexes of these proteins, the floral quartet model has been widely accepted as the basic model of molecular mechanism underlying the fate determination of floral organ primordia [299].

Application of ABCE model to other species. ABCE model has been developed focusing mainly on core eudicot species *Arabidopsis thaliana* and *Antirrhinum majus*, and has been shown it is applicable to other clades.

Gymnosperms. B and C class genes have been identified in gymnosperms such as conifers, which develop male and female cones separately as their reproductive structure without any perianth organs. B class genes are expressed only in male cones, whereas C class genes are expressed in both male and female cones (Fig. B.2B). Hence the last common ancestor of gymnosperms and angiosperms had B and C class genes, and their function is common to extant eudicots: C class gene confers a reproductive identity, and B class gene specifies male organ.

Basal dicots. *AP3* and *PI* (B class) genes are isolated in magnoliids and some species from the basal angiosperms, namely, Austrobaileyales, Nymphaeales, and Piperales [286]. The expression of MADS genes are observed in the most basal angiosperm genus *Amborella*, in addition to above basal dicot orders, and have been shown that they express in broader region compared to eudicots and monocots [148] (Fig. B.2C).

Monocots. There are two main floral forms in monocots, namely, animal-attracting petaloid type and wind-pollinated type, each quite distinct from most eudicot flowers. The petaloid monocots, such as the tulip, iris, and lily, produce flowers with very unified structure, with trimerous gynoecium and surrounded by two whorls trimerous stamens and two whorls three petaloid perianth organs that called tepals. ABCE model is also applicable to petaloid monocots whose perianth whorls have similar appearance in contrast to core eudicots that have clear difference between green sepals and coloured petals. The striking difference between monocots and eudicots is found in the expression of *B* genes (Fig. B.2D). In *Tulipa gesnerriana* (Liliacee) [142] and *Agapanthus praecox* ssp. *orientalis* (Agapanthaceae; Amaryllidaceae in APG) [196], *B* genes (*ApGLO* and *ApDEF* in *Agapanthus*) are expressed in not only the second and the third whorls as in *Arabidopsis*, but also in the first whorl. These results agree with the concept of ABCE model, since A and B class genes that specify petals in eudicots are expressed in the first and the second whorl in petaloid monocots, leading to development of petaloid tepals in these two whorls.

The other group, the wind-pollinated monocots, including the grasses such as maize, rice, and wheat, produce male and female flowers separately. They have a lemma and a palea in the first whorl instead of sepals, which protect the developing flower. In the second whorl, a pair of small globular structures called the lodicules is often found, which forces the palea and lemma to open and allows reproductive organs, stamens or carpels in the centre of the flower, to access the wind. In grass plants, the combination of the MADS boxes is the same to those in eudicots, where the lemma and palea are equivalent to the sepals, and lodicules correspond to petals [167].

Basal eudicots. The expression of B gene was examined in basal eudicots such as Ranunculales and shown that it is not as uniform as in core eudicots. For example in *Papaver nudicaule*, two B class genes *PnPI-1* and *PnAP3-1* are expressed in the petal primordia until the initiation of stamen primordia, whereas another B class gene, *PnAP3-2*, is expressed at low level in the petals until stamens arise, once disappears, and turns on later in development along the petal edges [153]. *Ranunculus* species have two AP3 and two PI, whose expression patterns considerably vary among species. In *R. bulbosus*, all four genes are expressed in low level in petal primordia when the stamens start to mature, and increases in later stages. These genes also show high levels of expression in the stamens. On the other hand, in *R. ficaria*, *RfAP3-1* has extremely low petal expression until blooming time, whereas *RfAP3-2* is expressed at low levels earlier in petal development and vanish earlier than *R. bulbosus*, and also expressed in high levels in stamens. The expression of the *RfPI-1* and *RfPI-2* genes is comparatively low in both petal and stamen primordia [153]. These variation might be a cause of diverse floral composition in Ranunculales.

B.5.4 Development of zygomorphic flowers

The transition between radial symmetry and zygomorphy has occurred multiply during the evolution of angiosperms. The studies on Fabaceae showed the difference of the initiation order of the floral-organ primordia between zygomorphic and radial symmetric flowers, whereas studies on "peloric" mutants of *Antirrhinum* shows a group of genes represented by *CYCLOIDEA* (*CYC*) play central roles in the molecular mechanism of zygomorphic development.

The initiation order of floral-organ primordia in Fabaceae. The floral development in Fabaceae (FABALES) species show several different types of the organ initiation order, correlating with the symmetry.

Subfamily Faboideae. Subfamily Faboideae have specific butterfly-shaped zygomorphic flowers. Five petals differentiate into three distinct morphologies, depending on the position in the flower. A single adaxial petal forms a banner with two lobes, lateral two petals form wings, and abaxial two petals are fused together and make up a keel (Fig. B.1K, right). The floral organs of *Glycine max* cv. Ransom initiate in unidirectional order: One abaxial sepal primordium appears first, followed by two lateral sepals, and then two adaxial sepals (Fig. B.1K, left). Petal primordia arise in the same direction but the alternate position to the sepals, i.e., two abaxial petals, two lateral petals, and one adaxial petal [65]. This initiation order is observed in several other species in Faboideae [310], suggesting the conservation in legume flowers. The unidirectional initiation order leads to the different maturity of primordia in adaxial and abaxial side of a flower, thus it can be considered as one of the sources of zygomorphy.

Subfamily Mimosoideae. Mimosoideae have tetramerous or pentamerous radial symmetric flowers with many stamens. This subfamily is subdivided into four tribes: Acacieae, Ingeae, Mimoseae, and Mimozygantheae,

and shows various initiation order ranges from helical initiation common in other eudicots to directional initiation as in zygomorphic flowers of Faboideae. In tribe Mimoseae, sepals initiate either helically (Fig. B.1H), simultaneously (Fig. B.1F), or in ring meristem (Fig. B.1G) [225]. In tribe Acacieae, sepals initiate in helical order [74], but some species exceptionally show bidirectional initiation [225] (Fig. B.1L). In tribe Ingeae, helical initiation is majority but a few species show simultaneous initiation [225]. On the other hand, petals initiate simultaneously in above three tribes, except for a few species that occasionally show helical initiation [225]. The radial symmetry in this family can be considered as an atavism since the other subfamilies with zygomorphic flowers forms a paraphyly to Mimosoideae in the phylogeny of Fabaceae [289]. The complication of several types of initiation order may reflect the intermediate stage of transition between zygomorphic flower associating with unidirectional initiation and actinomorphic flower with helical initiation.

The molecular basis of floral development with zygomorphy. The genes involving zygomorphy were firstly identified in *Antirrhinum*, which has pentamerous-zygomorphic flower with one adaxial (dorsal) sepal. The initiation order of their sepal is bidirectional, but it is different from bidirectional initiation in Mimosoideae (Fig. B.1L,M). The wild type *Antirrhinum* flower have two adaxial petals considerably larger than the two lateral and one abaxial petals, whereas in the peloric mutant the all petals become the same size, and also the number of petals and sepals increases to six. The plants with this phenotype have mutation in *CYC/DICH* family genes, which expresses adaxial petal primordia and causes the differentiation into adaxial fate [172].

CYC/DICH family genes are also responsible for the differentiation of florets in Asteraceae capitulum. *CYC*-like genes in Asteraceae, such as the *GhCYC2* in *Gerbera hybrida*, and the *RAY1* and *RAY2* in *Senecio vulgaris*, are expressed only in outer floret primordia that differentiate into ligulate florets [147, 159]. The function of *GhCYC2* can be explained by an analogy with MADS boxes in floral development, because of the concentric expression and the capacity for homeosis indicated by transformation of disk into ray-like florets by over-expression of *GhCYC2* [44].

These two floret types in Asteraceae are different in symmetry: tubular florets have radial symmetry, whereas the ligulate florets are in zygomorphy. Together with *Antirrhinum* results, *CYC/DICH* family genes are key factor for controlling zygomorphy, widely in core eudicots.

Acknowledgement

References

[1] Adam, H., Marguerettaz, M., Qadri, R., Adroher, B., Richaud, F., Collin, M., Thuillet, A.-C., Vigouroux, Y., Laufs, P., Tregear, J. W., and Jouannic, S. Divergent expression patterns of *miR164* and *CUP-SHAPED COTYLEDON* genes in palms and other monocots: Implication for the evolution of meristem function in angiosperms. *Molecular Biology and Evolution 28*, 4 (2011), 1439–1454.

[2] Adler, I. A model of contact pressure in phyllotaxis. *Journal of Theoretical Biology 45*, 1 (1974), 1–79.

[3] Adler, I., Barabe, D., and Jean, R. V. A history of the study of phyllotaxis. *Annals of Botany 80* (1997), 231–244.

[4] Aida, M., Ishida, T., Fukaki, H., Fujisawa, H., and Tasaka, M. Genes involved in organ separation in *Arabidopsis*: an analysis of the *cup-shaped cotyledon* mutant. *The Plant Cell Online 9*, 6 (1997), 841–857.

[5] Aida, M., and Tasaka, M. Genetic control of shoot organ boundaries. *Current Opinion in Plant Biology 9*, 1 (2006), 72–77. Growth and development / edited by David R Smyth and Thomas Berleth.

[6] Airy, H. On leaf-arrangement. *Proceedings of the Royal Society of London 21* (1873), 176–179.

[7] Akaike, H. A new look at the statistical model identification. *Automatic Control, IEEE Transactions on 19*, 6 (1974), 716–723.

[8] Allen, E., and MacDowell, E. C. Variation in mouse embryos of 8 days gestation. *The Anatomical Record 77*, 2 (1940), 165–173.

[9] Alvarez-Buylla, E. R., Azpeitia, E., Barrio, R., Benítez, M., and Padilla-Longoria, P. From ABC genes to regulatory networks, epigenetic landscapes and flower morphogenesis: Making biological sense of theoretical approaches. *Seminars in Cell & Developmental Biology 21*, 1 (2010), 108–117. Tumor-Stroma Interactions Flower Development.

[10] Ambrose, B. A., Espinosa-Matías, S., Vázquez-Santana, S., Vergara-Silva, F., Martínez, E., Márquez-Guzmán, J., and Alvarez-Buylla, E. R. Comparative developmental series of the mexican triurids support a euanthial interpretation for the unusual reproductive axes of *Lacandonia schismatica* (Triuridaceae). *American journal of Botany 93*, 1 (2006), 15–35.

[11] Ambrose, B. A., Lerner, D. R., Ciceri, P., Padilla, C. M., Yanofsky, M. F., and Schmidt, R. J. Molecular and genetic analyses of the *Silky1* gene reveal conservation in floral organ specification between eudicots and monocots. *Molecular Cell 5*, 3 (2000), 569 – 579.

[12] Amui-Vedel, A.-M., Clancy, L., and Arthur, W. Developmental plasticity in a meristic character: the number of tentacles in the lophophore of a bryozoan species. *Biological Journal of the Linnean Society 104*, 3 (2011), 541–551.

[13] Angiosperm Phylogeny Group. An ordinal classification for the families of flowering plants. *Annals of the Missouri Botanical Garden* (1998), 531–553.

[14] Angiosperm Phylogeny Group. An update of the angiosperm phylogeny group classification for the orders and families of flowering plants: Apg ii. *Botanical Journal of the Linnean Society 141*, 4 (2003), 399–436.

[15] Angiosperm Phylogeny Group. An update of the angiosperm phylogeny group for the orders and families of flowering plants: Apgiii. *Botanical Journal of the Linnean Society 161* (2009), 105–121.

[16] Arthur, W., and Farrow, M. The pattern of variation in centipede segment number as an example of developmental constraint in evolution. *Journal of theoretical biology 200*, 2 (1999), 183–191.

[17] Babington, C. C. On the supposed generic distinction of *Ranunculus ficaria* of Linne. *Magazine of Natural History and Journal of Zoology, Botany, Mineralogy, Geology and Meteorology 7* (1834), 375–378.

[18] Bachmann, K., and Chambers, K. Pappus part number in annual species of *Microseris* (Compositae, Cichoriaceae). *Plant Systematics and Evolution 129*, 1-2 (1978), 119–134.

[19] Bainbridge, K., Guyomar'h, S., Bayer, E., Swarup, R., Bennett, M., Mandel, T., and Kuhlemeier, C. Auxin influx carriers stabilize phyllotactic patterning. *Genes & Development 22* (2008), 810–823.

[20] Baker, C. C., Sieber, P., Wellmer, F., and Meyerowitz, E. M. The *early extra petals1* mutant uncovers a role for MicroRNA miR164c in regulating petal number in *Arabidopsis*. *Current Biology 15*, 4 (2005), 303 – 315.

[21] Barbier de Reuille, P., Bohn-Courseau, I., Ljung, K., Morin, H., Carraro, N., Godin, C., and Traas, J. Computer simulations reveal properties of the cell-cell signaling network at the shoot apex in *Arabidopsis*. *Proceedings of the National Academy of Sciences 103* (2006), 1627–1632.

[22] Barton, M. K., and Poethig, R. S. Formation of the shoot apical meristem in *Arabidopsis thaliana*: an analysis of development in the wild type and in the *shoot meristemless* mutant. *Development 119*, 3 (1993), 823–831.

[23] Baten, W. D. Constancy in the number of ligulate flowers of *Crysanthemum leucanthemum*, variety *pinnatifidum*, during the flowering season. *Biometrika 27* (1935), 260–266.

[24] Battjes, J., Vischer, N. O., and Bachmann, K. Capitulum phyllotaxis and numerical canalization in *Microseris pygmaea* (Asteraceae: Lactuceae). *American journal of botany* (1993), 419–428.

[25] Bayer, E. M., Smith, R. S., Mandel, T., Nakayama, N., Sauer, M., Prusinkiewicz, P., and Kuhlemeier, C. Integration of transport-based models for phyllotaxis and midvein formation. *Genes & development 23*, 3 (2009), 373–384.

[26] Becker, A., and Theissen, G. The major clades of MADS-box genes and their role in the development and evolution of flowering plants. *Molecular Phylogenetics and Evolution 29*, 3 (2003), 464 – 489. Plant Molecular Evolution.

[27] Bell, A. D., et al. *Plant form. An illustrated guide to flowering plant morphology.* Oxford University Press, 1991.

[28] Benková, E., Michniewicz, M., Sauer, M., Teichmann, T., Seifertová, D., Jürgens, G., and Friml, J. Local, efflux-dependent auxin gradients as a common module for plant organ formation. *Cell 115* (2003), 591–602.

[29] Bennett, M. J., Marchant, A., Green, H. G., May, S. T., Ward, S. P., Millner, P. A., Walker, A. R., Schulz, B., and Feldmann, K. A. *Arabidopsis AUX1* gene: A permease-like regulator of root gravitropism. *Science 273*, 5277 (1996), 948–950.

[30] Bergmann, S., Sandler, O., Sberro, H., Shnider, S., Schejter, E., Shilo, B.-Z., and Barkai, N. Pre-steady-state decoding of the bicoid morphogen gradient. *PLoS biology 5*, 2 (2007), e46.

[31] BERNASCONI, G., AND BOISSONADE, J. Phyllotactic order induced by symmetry breaking in advected turing patterns. *Physics Letters A 232*, 3?4 (1997), 224–230.

[32] BESNARD, F., REFAHI, Y., MORIN, V., MARTEAUX, B., BRUNOUD, G., CHAMBRIER, P., ROZIER, F., MIRABET, V., LEGRAND, J., LAINÉ, S., ET AL. Cytokinin signalling inhibitory fields provide robustness to phyllotaxis. *Nature 505* (2013), 417–421.

[33] BHARATHAN, G., GOLIBER, T. E., MOORE, C., KESSLER, S., PHAM, T., AND SINHA, N. R. Homologies in leaf form inferred from *KNOXI* gene expression during development. *Science 296*, 5574 (2002), 1858–1860.

[34] BLEIN, T., HASSON, A., AND LAUFS, P. Leaf development: what it needs to be complex. *Current Opinion in Plant Biology 13*, 1 (2010), 75 – 82.

[35] BLEIN, T., PULIDO, A., VIALETTE-GUIRAUD, A., NIKOVICS, K., MORIN, H., HAY, A., JOHANSEN, I. E., TSIANTIS, M., AND LAUFS, P. A conserved molecular framework for compound leaf development. *Science 322*, 5909 (2008), 1835–1839.

[36] BOHMERT, K., CAMUS, I., BELLINI, C., BOUCHEZ, D., CABOCHE, M., AND BENNING, C. *AGO1* defines a novel locus of *Arabidopsis* controlling leaf development. *The EMBO journal 17*, 1 (1998), 170–180.

[37] BONNET, C. *Recherches sur l'usage des feuilles dans les plantes : et sur quelques autres sujets relatifs à l'histoire de la vegetation.* A Gottingue & Leide :Chez Elie Luzac, fils, imp.-lib.,, 1754. http://www.biodiversitylibrary.org/bibliography/95922.

[38] BOWMAN, J., AND SMYTH, D. *CRABS CLAW*, a gene that regulates carpel and nectary development in *Arabidopsis*, encodes a novel protein with zinc finger and helix-loop-helix domains. *Development 126*, 11 (1999), 2387–2396.

[39] BOWMAN, J. L. The YABBY gene family and abaxial cell fate. *Current Opinion in Plant Biology 3*, 1 (2000), 17 – 22.

[40] BOWMAN, J. L., SMYTH, D. R., AND MEYEROWITZ, E. M. Genes directing flower development in *Arabidopsis*. *The Plant Cell 1*, 1 (1989), 37–52.

[41] BRAND, U., FLETCHER, J. C., HOBE, M., MEYEROWITZ, E. M., AND SIMON, R. Dependence of stem cell fate in *Arabidopsis* on a feedback loop regulated by *CLV3* activity. *Science 289*, 5479 (2000), 617–619.

[42] BRAUN, A. Dr. Carl Schimpers Vortäge über die Moglichkeit eines wissenschafillchen Verständniss der Blasttstellung. *Flora, oder allgemeine botanische Zeitung 18* (1835), 145–192.

[43] BRINGMANN, M., LANDREIN, B., SCHUDOMA, C., HAMANT, O., HAUSER, M.-T., AND PERSSON, S. Cracking the elusive alignment hypothesis: the microtubuleellulose synthase nexus unraveled. *Trends in Plant Science 17*, 11 (2012), 666 – 674.

[44] BROHOLM, S. K., TAHTIHARJU, S., LAITINEN, R. A. E., ALBERT, V. A., TEERI, T. H., AND ELOMAA, P. A TCP domain transcription factor controls flower type specification along the radial axis of the *Gerbera* (Asteraceae) inflorescence. *Proceedings of the National Academy of Sciences 105*, 26 (2008), 9117–9122.

[45] BURKILL, I. On the variation of the flower of *Ranunculus arvensis*. *Journal of the Asiatic Society of Bengal 71* (1902), 93–120.

[46] BURNHAM, K. P., AND ANDERSON, D. R. *Model selection and multimodel inference: a practical information-theoretic approach.* Springer, New York, 2002.

[47] BURNHAM, K. P., ANDERSON, D. R., AND HUYVAERT, K. P. AIC model selection and multimodel inference in behavioral ecology: some background, observations, and comparisons. *Behavioral Ecology and Sociobiology 65*, 1 (2011), 23–35.

[48] CAI, Y.-F., LI, S.-W., LIU, Y., QUAN, S., CHEN, M., XIE, Y.-F., JIANG, H.-Z., WEI, E.-Z., YIN, N.-W., WANG, L., ET AL. Molecular phylogeny of Ranunculaceae based on internal transcribed spacer sequences. *African Journal of Biotechnology 8*, 20 (2009).

[49] CHAMPAGNE, C., AND SINHA, N. Compound leaves: equal to the sum of their parts? *Development 131*, 18 (2004), 4401–4412.

[50] CHAPMAN, J., AND PERRY, R. A diffusion model of phyllotaxis. *Annals of botany 60* (1987), 377–389.

[51] CHENG, Y., DAI, X., AND ZHAO, Y. Auxin biosynthesis by the YUCCA flavin monooxygenases controls the formation of floral organs and vascular tissues in *Arabidopsis*. *Genes & Development 20*, 13 (2006), 1790–1799.

[52] CHENG, Y., QIN, G., DAI, X., AND ZHAO, Y. NPY1, a BTB-NPH3-like protein, plays a critical role in auxin-regulated organogenesis in *Arabidopsis*. *Proceedings of the National Academy of Sciences 104*, 47 (2007), 18825–18829.

[53] CHENG, Y., QIN, G., DAI, X., AND ZHAO, Y. *NPY* genes and AGC kinases define two key steps in auxin-mediated organogenesis in *Arabidopsis*. *Proceedings of the National Academy of Sciences 105*, 52 (2008), 21017–21022.

[54] CHITWOOD, D. H., NOGUEIRA, F. T., HOWELL, M. D., MONTGOMERY, T. A., CARRINGTON, J. C., AND TIMMERMANS, M. C. Pattern formation via small RNA mobility. *Genes & Development 23*, 5 (2009), 549–554.

[55] CHUCK, G., LINCOLN, C., AND HAKE, S. *KNAT1* induces lobed leaves with ectopic meristems when overexpressed in *Arabidopsis*. *The Plant Cell Online 8*, 8 (1996), 1277–1289.

[56] CLARK, E., MANULIS, S., OPHIR, Y., BARASH, I., AND GAFNI, Y. Cloning and characterization of *iaaM* and *iaaH* from *Erwinia herbicola* pathovar *gypsophilae*. *Phytopathology 83*, 2 (1993), 234–240.

[57] CLARK, S., JACOBSEN, S., LEVIN, J., AND MEYEROWITZ, E. The *CLAVATA* and *SHOOT MERISTEMLESS* loci competitively regulate meristem activity in *Arabidopsis*. *Development 122*, 5 (1996), 1567–1575.

[58] CLARK, S., RUNNING, M., AND MEYEROWITZ, E. M. *CLAVATA1*, a regulator of meristem and flower development in *Arabidopsis*. *Development 119* (1993), 397–418.

[59] CLARK, S., RUNNING, M., AND MEYEROWITZ, E. M. *CLAVATA3* is a specific regulator of shoot and floral meristem development affecting the same processes as *CLAVATA1*. *Development 121* (1995), 2057–2067.

[60] COEN, E., AND MEYEROWITZ, E. M. The war of the whorls: genetic interactions controlling flower development. *Nature 353* (1991), 31–37.

[61] COONEY, T., AND NONHEBEL, H. Biosynthesis of indole-3-acetic acid in tomato shoots: Measurement, mass-spectral identification and incorporation of ^{-2}H from $^{-2}H_2O$ into indole-3-acetic acid, d- and l-tryptophan, indole-3-pyruvate and tryptamine. *Planta 184*, 3 (1991), 368–376.

[62] CRONK, Q. *The Molecular Organography of Plants.* Oxford Biology. OUP Oxford, 2009.

[63] Cronquist, A. *The evolution and classification of flowering plants, 2nd ed.* New York Botanical Garden, 1988.

[64] Cronquist, A., et al. *The evolution and classification of flowering plants.* Thomas Nelson & Sons Ltd., London, 1968.

[65] Crozier, T. S., and Thomas, J. F. Normal floral ontogeny and cool temperature-induced aberrant floral development in *Glycine max* (Fabaceae). *American journal of Botany* (1993), 429–448.

[66] Cunninghame, M. E., and Lyndon, R. F. The relationship between the distribution of periclinal cell divisions in the shoot apex and leaf initiation. *Annals of Botany 57*, 6 (1986), 737–746.

[67] Dadpour, M. R., Naghiloo, S., and Neycharan, S. F. Inflorescence and floral ontogeny in *Jasminum fruticans* (Oleaceae). *Australian Journal of Botany 59*, 5 (2011), 498–506.

[68] Davis, G., and Patel, N. Short, long, and beyond: molecular and embryological approaches to insect segmentation. *Annual Review of Entomology 47* (2002), 669–699.

[69] de Candolle, A. P. *Organographie végétale, ou Description raisonnée des organes des plantes; pour servir de suite et de développement a la théorie élémentaire de la botanique, et d'introduction a la physiologie végétale et a la description des familles.* ParisDeterville, 1827. http://www.biodiversitylibrary.org/bibliography/20679.

[70] de Vries, H. Ueber halbe Galton-Curven als Zeichen discontinuirlicher Variation. *Berichte der Deutschen Botanischen Gesellschaft 12* (1894), 197–207.

[71] de Vries, H. Eine zweigipflige Variationskurve. *Development Genes and Evolution 2*, 1 (1895), 52–64.

[72] de Vries, H. Ueber Curvenselection bei *Chrysanthemum segetum*. *Berichte der Deutschen Botanischen Gesellschaft. 17* (1899), 84–98.

[73] Delbarre, A., Muller, P., Imhoff, V., and Guern, J. Comparison of mechanisms controlling uptake and accumulation of 2, 4-dichlorophenoxy acetic acid, naphthalene-1-acetic acid, and indole-3-acetic acid in suspension-cultured tobacco cells. *Planta 198*, 4 (1996), 532–541.

[74] Derstine, K. S., and Tucker, S. C. Organ initiation and development of inflorescences and flower of *Acacia baileyana*. *American journal of botany* (1991), 816–832.

[75] Ditta, G., Pinyopich, A., Robles, P., Pelaz, S., and Yanofsky, M. F. The *SEP4* gene of *Arabidopsis thaliana* functions in floral organ and meristem identity. *Current Biology 14*, 21 (2004), 1935 – 1940.

[76] Donnison, I. S., and Francis, D. Models of floral pattern in detached flowers of silene coeli-rosa (l) godr. (caryophyllaceae). *Botanical Journal of the Linnean Society 140*, 3 (2002), 229–235.

[77] Donoghue, M. J., Ree, R. H., and Baum, D. A. Phylogeny and the evolution of flower symmetry in the Asteridae. *Trends in Plant Science 3*, 8 (1998), 311 – 317.

[78] Douady, S., and Couder, Y. Phyllotaxis as a dynamical self organizing process part I: The spiral modes resulting from time-periodic iterations. *Journal of Theoretical Biology 178*, 3 (1996), 255–273.

[79] Douady, S., and Couder, Y. Phyllotaxis as a dynamical self organizing process part II: The spontaneous formation of a periodicity and the coexistence of spiral and whorled patterns. *Journal of Theoretical Biology 178*, 3 (1996), 275–294.

[80] Douady, S., and Couder, Y. Phyllotaxis as a dynamical self organizing process part III: The simulation of the transient regimes of ontogeny. *Journal of Theoretical Biology 178*, 3 (1996), 295–312.

[81] Egea-Cortines, M., Saedler, H., and Sommer, H. Ternary complex formation between the MADS-box proteins SQUAMOSA, DEFICIENS and GLOBOSA is involved in the control of floral architecture in *Antirrhinum majus*. *The EMBO Journal 18*, 19 (1999), 5370–5379.

[82] Ei, S.-I. The motion of weakly interacting pulses in reaction-diffusion systems. *Journal of Dynamics and Differential Equations 14*, 1 (2002), 85–137.

[83] Eichler, A. W. *Blu?thendiagramme /construirt und erla?utert.* Engelmann, Verlag von Wilhelm, Leipzig, 1875.

[84] Elliott, R. C., Betzner, A. S., Huttner, E., Oakes, M. P., Tucker, W., Gerentes, D., Perez, P., and Smyth, D. R. *AINTEGUMENTA*, an *APETALA2*-like gene of *Arabidopsis* with pleiotropic roles in ovule development and floral organ growth. *The Plant Cell Online 8*, 2 (1996), 155–168.

[85] Elowitz, M. B., Levine, A. J., Siggia, E. D., and Swain, P. S. Stochastic gene expression in a single cell. *Science 297*, 5584 (2002), 1183–1186.

[86] Elzhov, T. V., Mullen, K. M., Spiess, A.-N., and Bolker, B. *minpack.lm: R interface to the Levenberg-Marquardt nonlinear least-squares algorithm found in MINPACK, plus support for bounds*, 2013. R package version 1.1-8.

[87] Emery, J. F., Floyd, S. K., Alvarez, J., Eshed, Y., Hawker, N. P., Izhaki, A., Baum, S. F., and Bowman, J. L. Radial patterning of *Arabidopsis Shoots* by class III HD-ZIP and *KANADI* genes. *Current Biology 13*, 20 (2003), 1768 – 1774.

[88] Endress, P., and Doyle, J. Floral phyllotaxis in basal angiosperm: development and evolution. *Current Opinion in Plant Biology 10* (2007), 52–57.

[89] Endress, P., and Doyle, J. Reconstructing the ancestral angiosperm flower and its initial specializations. *American Journal of Botany 96* (2009), 22–66.

[90] Endress, P. K. Floral phyllotaxis and floral evolution. *Botanische Jahrbücher für Systematik, Pflanzengeschichte und Pflanzengeographie 108* (1987), 417–438.

[91] Endress, P. K. Evolutionary diversification of the flowers in angiosperms. *American Journal of Botany 98*, 3 (2011), 370–396.

[92] Engler, A., Krause, K., Pilger, R. K. F., and Prantl, K. A. E. *Die Natürlichen Pflanzenfamilien nebst ihren Gattungen und wichtigeren Arten, insbesondere den Nutzpflanzen, unter Mitwirkung zahlreicher hervorragender Fachgelehrten*, vol. Teil 2, Abt. 1. Leipzig, W. Engelmann, 1889. http://www.biodiversitylibrary.org/bibliography/4635.

[93] Eshed, Y., Baum, S. F., and Bowman, J. L. Distinct mechanisms promote polarity establishment in carpels of *Arabidopsis*. *Cell 99*, 2 (1999), 199 – 209.

[94] FC, L. Variation in the number of ray-flowers in the white daisy. *The American Naturalist 32* (1898), 509.

[95] Fleming, A., McQueen-Mason, S., Mandel, T., and Kuhlemeier, C. Induction of leaf primordia by the cell wall protein expansin. *Science 276* (1997), 1415–1418.

[96] FOSTER, T., JOHNSTON, R., AND SELEZNYOVA, A. A morphological and quantitative characterization of early floral development in apple (*Malus×domestica* Borkh.). *Annals of Botany 92*, 2 (2003), 199–206.

[97] FRANÇOIS, P., HAKIM, V., AND SIGGIA, E. D. Deriving structure from evolution: metazoan segmentation. *Molecular Systems Biology 3*, 1 (2007), 154.

[98] FRANCK, D. H. The morphological interpretation of epiascidiate leaves: An historical perspective. *The Botanical Review 42*, 3 (1976), 345–388.

[99] FRIIS, E., CRANE, P., AND PEDERSEN, K. *Early Flowers and Angiosperm Evolution*. Cambridge University Press, 2011.

[100] FU, Y., XU, L., XU, B., YANG, L., LING, Q., WANG, H., AND HUANG, H. Genetic interactions between leaf polarity-controlling genes and *ASYMMETRIC LEAVES1* and *2* in *Arabidopsis* leaf patterning. *Plant and Cell Physiology 48*, 5 (2007), 724–735.

[101] FUJIMOTO, K., ISHIHARA, S., AND KANEKO, K. Network evolution of body plans. *PLoS ONE 3*, 7 (07 2008), e2772.

[102] FUKUSHIMA, K., AND HASEBE, M. Adaxial-abaxial polarity: The developmental basis of leaf shape diversity. *genesis 52*, 1 (2014), 1–18.

[103] FURUTANI, M., KAJIWARA, T., KATO, T., TREML, B. S., STOCKUM, C., TORRES-RUIZ, R. A., AND TASAKA, M. The gene *MACCHI-BOU 4/ENHANCER OF PINOID* encodes a NPH3-like protein and reveals similarities between organogenesis and phototropism at the molecular level. *Development 134*, 21 (2007), 3849–3859.

[104] FURUTANI, M., NAKANO, Y., AND TASAKA, M. MAB4-induced auxin sink generates local auxin gradients in *Arabidopsis* organ formation. *Proceedings of the National Academy of Sciences 111*, 3 (2014), 1198–1203.

[105] GALLOIS, J.-L., WOODWARD, C., REDDY, G. V., AND SABLOWSKI, R. Combined SHOOT MERISTEMLESS and WUSCHEL trigger ectopic organogenesis in *Arabidopsis*. *Development 129*, 13 (2002), 3207–3217.

[106] GALVÁN-AMPUDIA, C. S., AND OFFRINGA, R. Plant evolution: AGC kinases tell the auxin tale. *Trends in Plant Science 12*, 12 (2007), 541–547.

[107] GÄLWEILER, L., GUAN, C., MÜLLER, A., WISMAN, E., MENDGEN, K., YEPHREMOV, A., AND PALME, K. Regulation of polar auxin transport by AtPIN1 in *Arabidopsis* vascular tissue. *Science 282*, 5397 (1998), 2226–2230.

[108] GARCIA, D., COLLIER, S. A., BYRNE, M. E., AND MARTIENSSEN, R. A. Specification of leaf polarity in *Arabidopsis* via the trans-acting siRNA pathway. *Current Biology 16*, 9 (2006), 933 – 938.

[109] GIERER, A., AND MEINHARDT, H. A theory of biological pattern formation. *Kybernetik 12*, 1 (1972), 30–39.

[110] GOETHE, J. W. V. *Versuch die Metamorphose der Pflanzen zu erklaren*. Ettinger, Gotha, 1790.

[111] GONÇALVES, B., NOUGUÉ, O., JABBOUR, F., RIDEL, C., MORIN, H., LAUFS, P., MANICACCI, D., AND DAMERVAL, C. An *APETALA3* homolog controls both petal identity and floral meristem patterning in *Nigella damascena* L. (Ranunculaceae). *The Plant Journal 76*, 2 (2013), 223–235.

[112] GREEN, P. B., STEELE, C., AND RENNICH, S. Phyllotactic patterns: a biophysical mechanism for their origin. *Annals of Botany 77*, 5 (1996), 515–528.

[113] GUÉDON, Y., REFAHI, Y., BESNARD, F., FARCOT, E., GODIN, C., AND VERNOUX, T. Pattern identification and characterization reveal permutations of organs as a key genetically controlled property of post-meristematic phyllotaxis. *Journal of theoretical biology 338* (2013), 94–110.

[114] GUERREIRO, J. Phyllotaxis: An interdisciplinary phenomenon. *Physica D: Nonlinear Phenomena 80*, 4 (1995), 356–384.

[115] H, N. Variation and correlation in rays and disk florets of *Aster fastigiatus*. *Botanical Gazette 49* (1910), 371–378.

[116] HAMANT, O., HEISLER, M. G., JÖNSSON, H., KRUPINSKI, P., UYTTEWAAL, M., BOKOV, P., CORSON, F., SAHLIN, P., BOUDAOUD, A., MEYEROWITZ, E. M., ET AL. Developmental patterning by mechanical signals in *Arabidopsis*. *Science 322*, 5908 (2008), 1650–1655.

[117] HAREVEN, D., GUTFINGER, T., PARNIS, A., ESHED, Y., AND LIFSCHITZ, E. The making of a compound leaf: Genetic manipulation of leaf architecture in tomato. *Cell 84*, 5 (1996), 735 – 744.

[118] HARRIS, J. A. A quantitative study of the morphology of the fruit of the bloodroot, *Sanguinaria canadensis*. *Biometrika 7*, 3 (1910), pp. 305–351.

[119] HARRIS, J. A. On the correlation between somatic characters and fertility: Illustrations from the involucral whorl of *Hibiscus*. *Biometrika 8*, 1/2 (1911), 52–65.

[120] HAUSER, M., MORIKAMI, A., AND BENFEY, P. Conditional root expansion mutants of *Arabidopsis*. *Development 121*, 4 (1995), 1237–1252.

[121] HAY, A., BARKOULAS, M., AND TSIANTIS, M. Asymmetric leaves1 and auxin activities converge to repress *BREVIPEDICELLUS* expression and promote leaf development in *Arabidopsis*. *Development 133*, 20 (2006), 3955–3961.

[122] HEISLER, M. G., HAMANT, O., KRUPINSKI, P., UYTTEWAAL, M., OHNO, C., JÖNSSON, H., TRAAS, J., AND MEYEROWITZ, E. M. Alignment between pin1 polarity and microtubule orientation in the shoot apical meristem reveals a tight coupling between morphogenesis and auxin transport. *PLoS Biology 8*, 10 (10 2010), e1000516.

[123] HEISLER, M. G., OHNO, C., DAS, P., SIEBER, P., REDDY, G. V., LONG, J. A., AND MEYEROWITZ, E. M. Patterns of auxin transport and gene expression during primordium development revealed by live imaging of the *Arabidopsis* inflorescence meristem. *Current Biology 15*, 21 (2005), 1899–1911.

[124] HELGUERO, F. D. Variazione ed omotiposi nelle inflorescenze di *Cichorium Intybus* l. *Biometrika 5*, 1/2 (1906), pp. 184–189.

[125] HELLWIG, H., ENGELMANN, R., AND DEUSSEN, O. Contact pressure models for spiral phyllotaxis and their computer simulation. *Journal of Theoretical Biology 240*, 3 (2006), 489–500.

[126] HENDELMAN, A., STAV, R., ZEMACH, H., AND ARAZI, T. The tomato NAC transcription factor *SlNAM2* is involved in flower-boundary morphogenesis. *Journal of Experimental Botany 64*, 18 (2013), 5497–5507.

[127] HENTSCHEL, H., GLIMM, T., GLAZIER, J. A., AND NEWMAN, S. A. Dynamical mechanisms for skeletal pattern formation in the vertebrate limb. *Proceedings of the Royal Society of London. Series B: Biological Sciences 271*, 1549 (2004), 1713–1722.

[128] Hepworth, S. R., Zhang, Y., McKim, S., Li, X., and Haughn, G. W. BLADE-ON-PETIOLE–dependent signaling controls leaf and floral patterning in Arabidopsis. *The Plant Cell Online 17*, 5 (2005), 1434–1448.

[129] Herrera, C. M. *Multiplicity in unity: plant subindividual variation and interactions with animals.* University of Chicago Press, Chicago, 2009.

[130] Hill, J. P., and Malmberg, R. L. Timing of morphological and histological development in premeiotic anthers of *Nicotiana tabacum* cv. Xanthi (Solanaceae). *American Journal of Botany 83*, 3 (1996), 285–295.

[131] Höfmeister, W. F. B. *Allgemeine Morphologie der Gewächse.* W. Engelmann, Leipzig, 1868.

[132] Honma, T., and Goto, K. Complexes of MADS-box proteins are sufficient to convert leaves into floral organs. *Nature 409*, 6819 (2001), 525–529.

[133] Hörandl, E., Paun, O., Johansson, J. T., Lehnebach, C., Armstrong, T., Chen, L., and Lockhart, P. Phylogenetic relationships and evolutionary traits in *Ranunculus* s.l. (Ranunculaceae) inferred from its sequence analysis. *Molecular phylogenetics and evolution 36*, 2 (2005), 305–327.

[134] Houchmandzadeh, B., Wieschaus, E., and Leibler, S. Establishment of developmental precision and proportions in the early *Drosophila* embryo. *Nature 415*, 6873 (2002), 798–802.

[135] Huether Jr, C. A. Constancy of the pentamerous corolla phenotype in natural populations of *Linanthus*. *Evolution 23* (1969), 572–588.

[136] Imhoff, V., Muller, P., Guern, J., and Delbarre, A. Inhibitors of the carrier-mediated influx of auxin in suspension-cultured tobacco cells. *Planta 210*, 4 (2000), 580–588.

[137] Jean, R. *Phyllotaxis: A Systemic Study in Plant Morphogenesis.* Cambridge University Press, 2009.

[138] Joanes, D. N., and Gill, C. A. Comparing measures of sample skewness and kurtosis. *Journal of the Royal Statistical Society: Series D (The Statistician) 47*, 1 (1998), 183–189.

[139] Johansson, J., and Jansen, R. Chloroplast DNA variation and phylogeny of the Ranunculaceae. *Plant Systematics and Evolution 187*, 1-4 (1993), 29–49.

[140] Jönsson, H., Heisler, M., Shapiro, B., Meyerowitz, E. M., and Mjolsness, E. An auxin-driven polarized transport model for phyllotaxis. *Proceedings of the National Academy of the Sciences 103* (2006), 1633–1638.

[141] Kærn, M., Elston, T. C., Blake, W. J., and Collins, J. J. Stochasticity in gene expression: from theories to phenotypes. *Nature Reviews Genetics 6*, 6 (2005), 451–464.

[142] Kanno, A., Saeki, H., Kameya, T., Seadler, H., and Theissen, G. Heterotopic expression of class B floral homeotic genes supports a modified ABC model for tulip (*Tulipa gesnerriana*). *Plant Molecular Biology 52* (2003), 831–841.

[143] Kelley, D. R., Arreola, A., Gallagher, T. L., and Gasser, C. S. ETTIN (ARF3) physically interacts with KANADI proteins to form a functional complex essential for integument development and polarity determination in *Arabidopsis*. *Development 139*, 6 (2012), 1105–1109.

[144] Kerstetter, R., Vollbrecht, E., Lowe, B., Veit, B., Yamaguchi, J., and Hake, S. Sequence analysis and expression patterns divide the maize knotted1-like homeobox genes into two classes. *The Plant Cell Online 6*, 12 (1994), 1877–1887.

[145] Kettle, C., Johnstone, J., Jowett, T., Arthur, H., and Arthur, W. The pattern of segment formation, as revealed by *engrailed* expression, in a centipede with a variable number of segments. *Evolution & Development 5*, 2 (2003), 198–207.

[146] Kierzkowski, D., Nakayama, N., Routier-Kierzkowska, A.-L., Weber, A., Bayer, E., Schorderet, M., Reinhardt, D., Kuhlemeier, C., and Smith, R. S. Elastic domains regulate growth and organogenesis in the plant shoot apical meristem. *Science 335*, 6072 (2012), 1096–1099.

[147] Kim, M., Cui, M.-L., Cubas, P., Gillies, A., Lee, K., Chapman, M. A., Abbott, R. J., and Coen, E. Regulatory genes control a key morphological and ecological trait transferred between species. *Science 322*, 5904 (2008), 1116–1119.

[148] Kim, S., Koh, J., Yoo, M.-J., Kong, H., Hu, Y., Ma, H., Soltis, P. S., and Soltis, D. E. Expression of floral MADS-box genes in basal angiosperms: implications for the evolution of floral regulators. *The Plant Journal 43*, 5 (2005), 724–744.

[149] Kim, S., Soltis, P. S., Wall, K., and Soltis, D. E. Phylogeny and domain evolution in the apetala2-like gene family. *Molecular Biology and Evolution 23*, 1 (2006), 107–120.

[150] Klucher, K. M., Chow, H., Reiser, L., and Fischer, R. L. The *AINTEGUMENTA* gene of *Arabidopsis* required for ovule and female gametophyte development is related to the floral homeotic gene *APETALA2*. *The Plant Cell 8*, 2 (1996), 137–153.

[151] Koga, J. Structure and function of indolepyruvate decarboxylase, a key enzyme in indole-3-acetic acid biosynthesis. *Biochimica et Biophysica Acta (BBA)-Protein Structure and Molecular Enzymology 1249*, 1 (1995), 1–13.

[152] Kosuge, T., Heskett, M. G., and Wilson, E. E. Microbial synthesis and degradation of indole-3-acetic acid: I. the conversion of l-tryptophan to indole-3-acetamide by an enzyme system from *Pseudomonas savastanoi*. *Journal of Biological Chemistry 241*, 16 (1966), 3738–3744.

[153] Kramer, E. M., and Irish, V. F. Evolution of genetic mechanisms controlling petal development. *Nature 399* (1999), 144–148.

[154] Krizek, B. *AINTEGUMENTA* and *AINTEGUMENTA-LIKE6* act redundantly to regulate *Arabidopsis* floral growth and patterning. *Plant Physiology 150*, 4 (2009), 1916–1929.

[155] Krizek, B. A. Ectopic expression of *AINTEGUMENTA* in *Arabidopsis* plants results in increased growth of floral organs. *Developmental genetics 25*, 3 (1999), 224–236.

[156] Kuhlemeier, C. Phyllotaxis. *Trends in Plant Science 12*, 4 (2007), 143–150.

[157] Kunst, L., Klenz, J. E., Martinez-Zapater, J., and Haughn, G. W. Ap2 gene determines the identity of perianth organs in flowers of *Arabidopsis thaliana*. *The Plant Cell 1*, 12 (1989), 1195–1208.

[158] Kwiatkowska, D. Formation of pseudowhorls inpeperomia verticillata (l.) a. dietr. shoots exhibiting various phyllotactic patterns. *Annals of botany 83*, 6 (1999), 675–685.

92

[159] LAITINEN, R., BROHOLM, S., ALBERT, V., TEERI, T., AND ELOMAA, P. Patterns of MADS-box gene expression mark flower-type development in *Gerbera hybrida* (Asteraceae). *BMC Plant Biology 6*, 1 (2006), 11.

[160] LANDAU, R. H., AND PÁEZ, M. J. *Computational physics: Problem solving with computers.* John Wiley & Sons, Inc., 2007.

[161] LAST, R. L., BISSINGER, P. H., MAHONEY, D. J., RADWANSKI, E. R., AND FINK, G. R. Tryptophan mutants in *Arabidopsis*: the consequences of duplicated tryptophan synthase beta genes. *The Plant Cell Online 3*, 4 (1991), 345–358.

[162] LEE, C. S., YEAU, S. H., AND LEE, N. S. Taxonomic status and genetic variation of korean endemic plants, *Eranthis byunsanensis* and *Eranthis pungdoensis* (Ranunculaceae) based on nrDNA ITS and cpDNA sequences. *Journal of Plant Biology 55*, 2 (2012), 165–177.

[163] LEHMANN, N. L., AND SATTLER, R. Homeosis in floral development of *Sanguinaria canadensis* and *S. canadensis* 'multiplex' (Papaveraceae). *American Journal of Botany 80*, 11 (1993), 1323–1335.

[164] LENHARD, M., BOHNERT, A., JRGENS, G., AND LAUX, T. Termination of stem cell maintenance in *Arabidopsis* floral meristems by interactions between *WUSCHEL* and *AGAMOUS*. *Cell 105*, 6 (2001), 805–814.

[165] LENHARD, M., J?RGENS, G., AND LAUX, T. The *WUSCHEL* and *SHOOTMERISTEMLESS* genes fulfil complementary roles in *Arabidopsis* shoot meristem regulation. *Development 129*, 13 (2002), 3195–3206.

[166] LINNÉ, C. V. *Philosophia botanica.* Stockholmiae: Apud Godofr. Kiesewetter, 1751. http://www.biodiversitylibrary.org/bibliography/72943.

[167] LITT, A., AND KRAMER, E. M. The {ABC} model and the diversification of floral organ identity. *Seminars in Cell & Developmental Biology 21*, 1 (2010), 129–137. Tumor-Stroma Interactions Flower Development.

[168] LONG, J. A., MOAN, E. I., MEDFORD, J. I., AND BARTON, M. K. A member of the *KNOTTED* class of homeodomain proteins encoded by the *STM* gene of *Arabidopsis*. *Nature 379*, 6560 (1996), 66–69.

[169] LOZANO, R., ANGOSTO, T., GÓMEZ, P., PAYÁN, C., CAPEL, J., HUIJSER, P., SALINAS, J., AND MARTI?NEZ-ZAPATER, J. M. Tomato flower abnormalities induced by low temperatures are associated with changes of expression of MADS-box genes. *Plant Physiology 117*, 1 (1998), 91–100.

[170] LUDWIG, F. Ueber Variationskurven und Variationsflächen der Pflanzen. *Botanisches Centralblatt LXIV* (1895), 1–8.

[171] LUDWIG, F. Variationsstatistische Probleme und Materialien. *Biometrika 1*, 1 (1901), 11–29.

[172] LUO, D., CARPENTER, R., VINCENT, C., COPSEY, L., AND COEN, E. Origin of floral asymmetry in *Antirrhinum*. *Nature 383*, 6603 (1996), 794–799.

[173] LUO, Y., GUO, Z., AND LI, L. Evolutionary conservation of microRNA regulatory programs in plant flower development. *Developmental Biology 380*, 2 (2013), 133–144.

[174] LYNDON, R. Phyllotaxis and the initiation of primordia during flower development in *Silene*. *Annals of Botany 42* (1978), 1349–1360.

[175] LYNN, K., FERNANDEZ, A., AIDA, M., SEDBROOK, J., TASAKA, M., MASSON, P., AND BARTON, M. K. The *PINHEAD/ZWILLE* gene acts pleiotropically in *Arabidopsis* development and has overlapping functions with the *ARGONAUTE1* gene. *Development 126*, 3 (1999), 469–481.

[176] MACDONELL, W. Cooperative investigations on plants II. variation and correlation in lesser celandine from divers localities. *Biometrika 2*, 2 (1903), 145–164.

[177] MALLORY, A. C., DUGAS, D. V., BARTEL, D. P., AND BARTEL, B. MicroRNA regulation of NAC-Domain targets is required for proper formation and separation of adjacent embryonic, vegetative, and floral organs. *Current Biology 14*, 12 (2004), 1035–1046.

[178] MANU, SURKOVA, S., SPIROV, A. V., GURSKY, V. V., JANSSENS, H., KIM, A.-R., RADULESCU, O., VANARIO-ALONSO, C. E., SHARP, D. H., SAMSONOVA, M., AND REINITZ, J. Canalization of gene expression in the *Drosophila* blastoderm by gap gene cross regulation. *PLoS Biology 7*, 3 (03 2009), e1000049.

[179] MARCHANT, A., KARGUL, J., MAY, S. T., MULLER, P., DELBARRE, A., PERROT-RECHENMANN, C., AND BENNETT, M. J. AUX1 regulates root gravitropism in *Arabidopsis* by facilitating auxin uptake within root apical tissues. *The EMBO Journal 18*, 8 (1999), 2066–2073.

[180] MASHIGUCHI, K., TANAKA, K., SAKAI, T., SUGAWARA, S., KAWAIDE, H., NATSUME, M., HANADA, A., YAENO, T., SHIRASU, K., YAO, H., MCSTEEN, P., ZHAO, Y., HAYASHI, K.-I., KAMIYA, Y., AND KASAHARA, H. The main auxin biosynthesis pathway in *Arabidopsis*. *Proceedings of the National Academy of Sciences 108*, 45 (2011), 18512–18517.

[181] MATSUMOTO, M., AND NISHIMURA, T. Mersenne twister: A 623-dimensionally equidistributed uniform pseudo-random number generator. *ACM Transactions on Modeling and Computer Simulation 8*, 1 (Jan. 1998), 3–30.

[182] MATTHEWS, J., AND ROGER, J. Variation in *Trientalis europaea* Linn. *Journal of Botany 79* (1941), 80–83.

[183] MAYER, K. F., SCHOOF, H., HAECKER, A., LENHARD, M., JRGENS, G., AND LAUX, T. Role of *WUSCHEL* in regulating stem cell fate in the *Arabidopsis* shoot meristem. *Cell 95*, 6 (1998), 805–815.

[184] MCADAMS, H. H., AND ARKIN, A. Stochastic mechanisms in gene expression. *Proceedings of the National Academy of Sciences 94*, 3 (1997), 814–819.

[185] MCCONNELL, J., AND BARTON, M. Leaf polarity and meristem formation in *Arabidopsis*. *Development 125*, 15 (1998), 2935–2942.

[186] MCCONNELL, J. R., EMERY, J., ESHED, Y., BAO, N., BOWMAN, J., AND BARTON, M. K. Role of phabulosa and phavoluta in determining radial patterning in shoots. *Nature 411*, 6838 (2001), 709–713.

[187] MCSTEEN, P., AND LEYSER, O. Shoot branching. *Annual Review of Plant Biology 56*, 1 (2005), 353–374. PMID: 15862100.

[188] MEICENHEIMER, R. D. Relationships between shoot growth and changing phyllotaxy of *Ranunculus*. *American Journal of Botany 66*, 5 (1979), 557–569.

[189] MIRABET, V., BESNARD, F., VERNOUX, T., AND BOUDAOUD, A. Noise and robustness in phyllotaxis. *PLoS Computational Biology 8*, 2 (02 2012), e1002389.

[190] MIURA, T. Turing and Wolpert work together during limb development. *Science Signaling 6*, 270 (2013), pe14.

[191] MIZUKAMI, Y., AND FISCHER, R. L. Plant organ size control: Aintegumenta regulates growth and cell numbers during organogenesis. *Proceedings of the National Academy of Sciences 97*, 2 (2000), 942–947.

[192] MOLNAR, A., MELNYK, C. W., BASSETT, A., HARDCASTLE, T. J., DUNN, R., AND BAULCOMBE, D. C. Small silencing rnas in plants are mobile and direct epigenetic modification in recipient cells. *Science 328*, 5980 (2010), 872–875.

[193] MORÉ, J. J. The Levenberg-Marquardt algorithm: implementation and theory. In *Numerical analysis*, vol. 630. Springer, 1978, pp. 105–116.

[194] MOUSSIAN, B., SCHOOF, H., HAECKER, A., JÜRGENS, G., AND LAUX, T. Role of the *ZWILLE* gene in the regulation of central shoot meristem cell fate during *Arabidopsis* embryogenesis. *The EMBO journal 17*, 6 (1998), 1799–1809.

[195] MUDUNKOTHGE, J. S., AND KRIZEK, B. A. Three *Arabidopsis AIL/PLT* genes act in combination to regulate shoot apical meristem function. *The Plant Journal 71*, 1 (2012), 108–121.

[196] NAKAMURA, T., FUKUDA, T., NAKANO, M., HASEBE, M., KAMEYA, T., AND KANNO, A. The modified ABC model explains the development of the petaloid perianth of agapanthus praecox ssp. orientalis (agapanthaceae) flowers. *Plant Molecular Biology 58*, 3 (2005), 435–445.

[197] NEWELL, A. C., SHIPMAN, P. D., AND SUN, Z. Phyllotaxis: cooperation and competition between mechanical and biochemical processes. *Journal of Theoretical Biology 251*, 3 (2008), 421–439.

[198] NEWMAN, S., AND FRISCH, H. Dynamics of skeletal pattern formation in developing chick limb. *Science 205*, 4407 (1979), 662–668.

[199] NORMANLY, J., COHEN, J. D., AND FINK, G. R. *Arabidopsis thaliana* auxotrophs reveal a tryptophan-independent biosynthetic pathway for indole-3-acetic acid. *Proceedings of the National Academy of Sciences 90*, 21 (1993), 10355–10359.

[200] NÜSSLEIN-VOLHARD, C., AND WIESCHAUS, E. Mutations affecting segment number and polarity in *Drosophila*. *Nature 287*, 5785 (1980), 795–801.

[201] OHNO, M. *Anemone flaccida* Fr. Schm. In *Field Watching 3: Walking throughout the spring field*, S. Kawano and H. Tanaka, Eds. Hokuryukan, Tokyo, 1991, pp. 60–63.

[202] OHTA, T., KIYOSE, J., AND MIMURA, M. Collision of propagating pulses in a reaction-diffusion system. *Journal of the Physical Society of Japan 66*, 5 (1997), 1551–1558.

[203] OKADA, K., UEDA, J., KOMAKI, M. K., BELL, C. J., AND SHIMURA, Y. Requirement of the auxin polar transport system in early stages of *Arabidopsis* floral bud formation. *The Plant Cell Online 3*, 7 (1991), 677–684.

[204] OTSUGA, D., DEGUZMAN, B., PRIGGE, M. J., DREWS, G. N., AND CLARK, S. E. Revoluta regulates meristem initiation at lateral positions. *The Plant Journal 25*, 2 (2001), 223–236.

[205] OUYANG, J., SHAO, X., AND LI, J. Indole-3-glycerol phosphate, a branchpoint of indole-3-acetic acid biosynthesis from the tryptophan biosynthetic pathway in *Arabidopsis thaliana*. *The Plant Journal 24*, 3 (2000), 327–334.

[206] OZBUDAK, E. M., THATTAI, M., KURTSER, I., GROSSMAN, A. D., AND VAN OUDENAARDEN, A. Regulation of noise in the expression of a single gene. *Nature genetics 31*, 1 (2002), 69–73.

[207] PA, S., REINHARDT, D., AND KUHLEMEIER, C. The auxin influx carrier is essential for correct leaf positioning. *The Plant Journal 32* (2002), 509–517.

[208] PAULSSON, J. Summing up the noise in gene networks. *Nature 427* (2004), 415–418.

[209] PAYER, J.-B., AND FILIPOWICZ, K. *Traité d'organogénie comparée de la fleur*. Librairie de Victor Masson, Paris, 1857.

[210] PEARSON, K. Contributions to the mathematical theory of evolution. II. Skew variation in homogeneous material. *Philosophical Transactions of the Royal Society of London. A* (1895), 343–414.

[211] PEARSON, K., AND YULE, G. Variation in ray-flowers of *Chrysanthemum leucanthemum*, 1133 heads gathered at Keswick, during July, 1895, by K. Pearson and GU Yule. *Biometrika 1*, 3 (1902), 319–319.

[212] PEAUCELLE, A., LOUVET, R., JOHANSEN, J. N., HÖFTE, H., LAUFS, P., PELLOUX, J., AND MOUILLE, G. *Arabidopsis* phyllotaxis is controlled by the metyl-esterification status of cell-wall pectins. *Current Biology 18* (2008), 1943–1948.

[213] PEAUCELLE, A., LOUVET, R., JOHANSEN, J. N., SALSAC, F., MORIN, H., FOURNET, F., BELCRAM, K., GILLET, F., H?FTE, H., LAUFS, P., MOUILLE, G., AND PELLOUX, J. The transcription factor BELLRINGER modulates phyllotaxis by regulating the expression of a pectin methylesterase in *Arabidopsis*. *Development 138*, 21 (2011), 4733–4741.

[214] PEAUCELLE, A., MORIN, H., TRAAS, J., AND LAUFS, P. Plants expressing a miR164-resistant *CUC2* gene reveal the importance of post-meristematic maintenance of phyllotaxy in *Arabidopsis*. *Development 134* (2007), 1045–1050.

[215] PEDRAZA, J. M., AND VAN OUDENAARDEN, A. Noise propagation in gene networks. *Science 307*, 5717 (2005), 1965–1969.

[216] PELAZ, S., DITTA, G. S., BAUMANN, E., WISMAN, E., AND YANOFSKY, M. F. B and C floral organ identity functions require *SEPALLATA* MADS-box genes. *Nature 405*, 6783 (2000), 200–203.

[217] PINON, V., PRASAD, K., GRIGG, S. P., SANCHEZ-PEREZ, G. F., AND SCHERES, B. Local auxin biosynthesis regulation by PLETHORA transcription factors controls phyllotaxis in *Arabidopsis*. *Proceedings of the National Academy of Sciences 110*, 3 (2013), 1107–1112.

[218] PLEDGE, J. H. Second contribution on numerical variation of parts in *Ranunculus repens* (L.). *Natural Science 12*, 73 (1898), 179–189.

[219] POLLMANN, S., MLLER, A., PIOTROWSKI, M., AND WEILER, E. Occurrence and formation of indole-3-acetamide in *Arabidopsis thaliana*. *Planta 216*, 1 (2002), 155–161.

[220] POLLMANN, S., NEU, D., AND WEILER, E. W. Molecular cloning and characterization of an amidase from *Arabidopsis thaliana* capable of converting indole-3-acetamide into the plant growth hormone, indole-3-acetic acid. *Phytochemistry 62*, 3 (2003), 293–300.

[221] POTTEN, C., AND LOEFFLER, M. Stem cells: attributes, cycles, spirals, pitfalls and uncertainties. lessons for and from the crypt. *Development 110*, 4 (1990), 1001–1020.

[222] PRASAD, K., GRIGG, S. P., BARKOULAS, M., YADAV, R. K., SANCHEZ-PEREZ, G. F., PINON, V., BLILOU, I., HOFHUIS, H., DHONUKSHE, P., GALINHA, C., MÄHÖNEN, A. P., MULLER, W. H., RAMAN, S., VERKLEIJ, A. J., SNEL, B., REDDY, G. V., TSIANTIS, M., AND SCHERES, B. *Arabidopsis* PLETHORA transcription factors control phyllotaxis. *Current Biology 21*, 13 (2011), 1123–1128.

[223] Prigge, M. J., Otsuga, D., Alonso, J. M., Ecker, J. R., Drews, G. N., and Clark, S. E. Class III homeodomain-leucine zipper gene family members have overlapping, antagonistic, and distinct roles in *Arabidopsis* development. *The Plant Cell Online 17*, 1 (2005), 61–76.

[224] Radwanski, E. R., Barczak, A. J., and Last, R. L. Characterization of tryptophan synthase alpha subunit mutants of *Arabidopsis thaliana*. *Molecular and General Genetics MGG 253*, 3 (1996), 353–361.

[225] Ramírez-Domenech, J. I., and Tucker, S. Comparative ontogeny of the perianth in mimosoid legumes. *American Journal of Botany* (1990), 624–635.

[226] Reinhardt, D., Frenz, M., Mandel, T., and Kuhlemeier, C. Microsurgical and laser ablation analysis of leaf positioning and dorsoventral patterning in tomato. *Development 132*, 1 (2005), 15–26.

[227] Reinhardt, D., Mandel, T., and Kuhlemeier, C. Auxin regulates the initiation and radial position of plant lateral organs. *The Plant Cell 12* (2000), 507–518.

[228] Reinhardt, D., Pesce, E., Stieger, P., Mandel, T., Baltensperger, K., Bennett, M., Traas, J., Friml, J., and Kuhlemeier, C. Regulation of phyllotaxis by polar auxin transport. *Nature 426*, 6964 (2003), 255–260.

[229] Ren, Y., Chang, H., and Endress, P. Floral development in Anemoneae (Ranunculaceae). *Botanical Journal of the Linnean Society 162* (2010), 77–100.

[230] Richards, F. Phyllotaxis: Its quantitative expression and relation to growth in the apex. *Philosophical Transactions of the Royal Society of London B 235* (1951), 509–564.

[231] Richardson, M., Allen, S., Wright, G., Raynaud, A., and Hanken, J. Somite number and vertebrate evolution. *Development 125*, 2 (1998), 151–160.

[232] Ridley, J. Packing efficiency in sunflower heads. *Mathematical Biosciences 58*, 1 (1982), 129 – 139.

[233] Riechmann, J. L., Krizek, B. A., and Meyerowitz, E. M. Dimerization specificity of *Arabidopsis* MADS domain homeotic proteins APETALA1, APETALA3, PISTILLATA, and AGAMOUS. *Proceedings of the National Academy of Sciences 93*, 10 (1996), 4793–4798.

[234] Rldley, J. Computer simulation of contact pressure in capitula. *Journal of Theoretical Biology 95*, 1 (1982), 1–11.

[235] Ro, K.-E., Keener, C. S., and McPheron, B. A. Molecular phylogenetic study of the Ranunculaceae: utility of the nuclear 26S ribosomal DNA in inferring intrafamilial relationships. *Molecular Phylogenetics and Evolution 8*, 2 (1997), 117–127.

[236] Ronse De Craene, L. P. *Floral Diagrams: An aid to understanding flower morphology and evolution*. Cambridge University Press, Cambridge, 2010.

[237] Ronse De Craene, L. P., and Brockington, S. F. Origin and evolution of petals in angiosperms. *Plant Ecology and Evolution 146*, 1 (2013), 5–25.

[238] Ronse De Craene, L. P., and Smets, E. F. Morphological studies in Zygophyllaceae. I. The floral development and vascular anatomy of *Nitraria retusa*. *American Journal of Botany 78*, 10 (1991), 1438–1448.

[239] Ronse Decraene, L., and Smets, E. Merosity in flowers: Definition, origin, and taxonomic significance. *Plant Systematics and Evolution 191*, 1-2 (1994), 83–104.

[240] Rosenberg, M. I., Lynch, J. A., and Desplan, C. Heads and tails: Evolution of antero-posterior patterning in insects. *Biochimica et Biophysica Acta (BBA) - Gene Regulatory Mechanisms 1789*, 4 (2009), 333–342.

[241] Roy, S. K. The variation of organs of individual plants. *Journal of Genetics 58*, 2 (1963), 147–176.

[242] Rudall, P. J. All in a spin: centrifugal organ formation and floral patterning. *Current Opinion in Plant Biology 13*, 1 (2010), 108 – 114.

[243] Rudall, P. J., Sokoloff, D. D., Remizowa, M. V., Conran, J. G., Davis, J. I., Macfarlane, T. D., and Stevenson, D. W. Morphology of Hydatellaceae, an anomalous aquatic family recently recognized as an early-divergent angiosperm lineage. *American Journal of Botany 94*, 7 (2007), 1073–1092.

[244] Running, M. P., and Meyerowitz, E. M. Mutations in the *PERIANTHIA* gene of *Arabidopsis* specifically alter floral organ number and initiation pattern. *Development 122* (1996), 1261–1269.

[245] S, D., and Y, C. Phyllotaxis as a physical self-organized growth process. *Phys. Rev. Lett. 68* (Mar 1992), 2098–2101.

[246] Sachs, T. Polarity and the induction of organized vascular tissues. *Annals of Botany 33*, 2 (1969), 263–275.

[247] Sahlin, P., Söderberg, B., and Jönsson, H. Regulated transport as a mechanism for pattern generation: capabilities for phyllotaxis and beyond. *Journal of Theoretical Biology 258* (2009), 60–70.

[248] Sakamoto, Y., Ishiguro, M., and Kitagawa, G. Akaike information criterion statistics. *Dordrecht, The Netherlands: D. Reidel* (1986).

[249] Salazar-Ciudad, I., Solé, R. V., and Newman, S. A. Phenotypic and dynamical transitions in model genetic networks II. application to the evolution of segmentation mechanisms. *Evolution & Development 3*, 2 (2001), 95–103.

[250] Salisbury, E. The organization of the Ranunculaceous flower with especial regard to the correlated variations of its constituent members. *Proceedings of the Royal Society of London. Series B. Biological Sciences 183*, 1072 (1973), 205–225.

[251] Salisbury, E. J. Variation in *Eranthis hyemalis*, *Ficaria verna*, and other members of Ranunculaceae, with special reference to trimery and the origin of the perianth. *Annals of Botany os-33*, 1 (1919), 47–79.

[252] Salisbury, E. J. Variation in *Anemone apennina*, L., and *Clematis vitalba*, L., with special reference to trimery and abortion. *Annals of Botany os-34*, 1 (1920), 107–116.

[253] Salisbury, E. J. On the morphology and ecology of *Ranunculus parviflorus*, L. *Annals of Botany os-45*, 4 (1931), 539–578.

[254] Salisbury, E. J. On the morphology, ecology, and distribution of *Ranunculus lenormandi* F. Schultz and *R. hederaceus* L.

[255] Salisbury, E. J. Variation in the flowers of *Ranunculus circinatus* Sibth. *Kew Bulletin 14*, 1 (1960), 34–36.

[256] Sanchez, A., and Golding, I. Genetic determinants and cellular constraints in noisy gene expression. *Science 342*, 6163 (2013), 1188–1193.

[257] Satina, S., Blakeslee, A., and Avery, A. G. Demonstration of the three germ layers in the shoot apex of datura by means of induced polyploidy in periclinal chimeras. *American Journal of Botany* (1940), 895–905.

95

[258] Saunders, P., Ed. *Morphogenesis: Collected works of A. M. Turing.* North-Holland, 1992.

[259] Sauvages de la Croix, F. B. d. *Methodus foliorum.* A La Haye : [s.n.], 1751. http://www.biodiversitylibrary.org/bibliography/74323.

[260] Sawa, S., Watanabe, K., Goto, K., Kanaya, E., Morita, E. H., and Okada, K. *FILAMENTOUS FLOWER,* a meristem and organ identity gene of *Arabidopsis,* encodes a protein with a zinc finger and HMG-related domains. *Genes & Development 13,* 9 (1999), 1079–1088.

[261] Schöffel, K. Untersuchungen über den blütenbau der Ranunculaceen. *Planta 17* (1932), 315–371.

[262] Schoof, H., Lenhard, M., Haecker, A., Mayer, K. F., Jürgens, G., and Laux, T. The stem cell population of *Arabidopsis* shoot meristems is maintained by a regulatory loop between the *CLAVATA* and *WUSCHEL* genes. *Cell 100,* 6 (2000), 635–644.

[263] Schoute, J. C. Beitrage zur Blattstellungslehre. I. Die Theorie. *Recueil Des Travaux Botaniques Neerlandais 10* (1913), 153–325.

[264] Schruff, M. C., Spielman, M., Tiwari, S., Adams, S., Fenby, N., and Scott, R. J. The auxin response factor 2 gene of arabidopsis links auxin signalling, cell division, and the size of seeds and other organs. *Development 133,* 2 (2006), 251–261.

[265] Schwendener, S. *Mechanische Theorie der Blattstellungen.* W. Engelmann, Leipzig, 1878.

[266] Sehr, E. M., and Weber, A. Floral ontogeny of Oleaceae and its systematic implications. *International journal of plant sciences 170,* 7 (2009), 845–859.

[267] Seo, M., Akaba, S., Oritani, T., Delarue, M., Bellini, C., Caboche, M., and Koshiba, T. Higher activity of an aldehyde oxidase in the auxin-overproducing *superroot1* mutant of *Arabidopsis thaliana. Plant Physiology 116,* 2 (1998), 687–693.

[268] Sharma, B., Guo, C., Kong, H., and Kramer, E. M. Petal-specific subfunctionalization of an apetala3 paralog in the ranunculales and its implications for petal evolution. *New Phytologist 191,* 3 (2011), 870–883.

[269] Sheth, R., Marcon, L., Bastida, M. F., Junco, M., Quintana, L., Dahn, R., Kmita, M., Sharpe, J., and Ros, M. A. Hox genes regulate digit patterning by controlling the wavelength of a Turing-type mechanism. *Science 338,* 6113 (2012), 1476–1480.

[270] Shibata, T., and Fujimoto, K. Noisy signal amplification in ultrasensitive signal transduction. *Proceedings of the National Academy of Sciences of the United States of America 102,* 2 (2005), 331–336.

[271] Shubin, N., Tabin, C., and Carroll, S. Fossils, genes and the evolution of animal limbs. *Nature 388,* 6643 (1997), 639–648.

[272] Shull, G. A quantitative study of variation in the bracts, rays, and disk florets of *Aster Shortii, A. novae-angliae, A. puniceus,* and *A. prenanthoides. The American Naturalist 36* (1902), 111–153.

[273] Sieber, P., Wellmer, F., Gheyselinck, J., Riechmann, J. L., and Meyerowitz, E. M. Redundancy and specialization among plant micrornas: role of the mir164 family in developmental robustness. *Development 134,* 6 (2007), 1051–1060.

[274] Siegfried, K., Eshed, Y., Baum, S., Otsuga, D., Drews, G., and Bowman, J. Members of the *YABBY* gene family specify abaxial cell fate in *Arabidopsis. Development 126,* 18 (1999), 4117–4128.

[275] Sinha, N., Williams, R., and Hake, S. Overexpression of the maize homeo box gene, knotted-1, causes a switch from determinate to indeterminate cell fates. *Genes & Development 7,* 5 (1993), 787–795.

[276] Smith, L., Greene, B., Veit, B., and Hake, S. A dominant mutation in the maize homeobox gene, knotted-1, causes its ectopic expression in leaf cells with altered fates. *Development 116,* 1 (1992), 21–30.

[277] Smith, R., Kuhlemeier, C., and Prusinkiewicz, P. Inhibition fields for phyllotactic pattern formation: a simulation study. *Canadian Journal of Botany 84* (2006), 1635–1649.

[278] Smith, R. S., Guyomarc'h, S., Mandel, T., Reinhardt, D., Kuhlemeier, C., and Prusinkiewicz, P. A plausible model of phyllotaxis. *Proceedings of the National Academy of Sciences of the United States of America 103,* 5 (2006), 1301–1306.

[279] Smyth, D. R., Bowman, J. L., and Meyerowitz, E. M. Early flower development in *Arabidopsis. The Plant Cell 2* (1990), 755–767.

[280] Sokal, R., and Rohlf, F. Biometry (fourth edition). *WH Freman and company: New York* (2012).

[281] Soltis, D. E., Chanderbali, A. S., Kim, S., Buzgo, M., and Soltis, P. S. The ABC model and its applicability to basal angiosperms. *Annals of Botany 100* (2007), 155–163.

[282] Souer, E., van Houwelingen, A., Kloos, D., Mol, J., and Koes, R. *The No Apical Meristem* gene of petunia is required for pattern formation in embryos and flowers and is expressed at meristem and primordia boundaries. *Cell 85,* 2 (1996), 159 – 170.

[283] Spencer, W. P. Variation in petal number in the bloodroot, *Sanguinaria canadensis. American Naturalist 78,* 774 (1944), 85–89.

[284] Srinivasan, C., and Mullins, M. Flowering in *Vitis*: Conversion of tendrils into inflorescences and bunches of grapes. *Planta 145,* 2 (1979), 187–192.

[285] Steeves, T., and Sussex, I. *Patterns in Plant Development.* Cambridge University Press, 1989.

[286] Stellari, G. M., Jaramillo, M. A., and Kramer, E. M. Evolution of the *APETALA3* and *PISTILLATA* lineages of MADS-box?containing genes in the basal angiosperms. *Molecular Biology and Evolution 21,* 3 (2004), 506–519.

[287] Stepanova, A. N., Robertson-Hoyt, J., Yun, J., Benavente, L. M., Xie, D.-Y., Doleal, K., Schlereth, A., Jrgens, G., and Alonso, J. M. *TAA1*-mediated auxin biosynthesis is essential for hormone crosstalk and plant development. *Cell 133,* 1 (2008), 177 – 191.

[288] Stepanova, A. N., Yun, J., Robles, L. M., Novak, O., He, W., Guo, H., Ljung, K., and Alonso, J. M. The *Arabidopsis* YUCCA1 flavin monooxygenase functions in the indole-3-pyruvic acid branch of auxin biosynthesis. *The Plant Cell Online 23,* 11 (2011), 3961–3973.

[289] Stevens, P. F. Angiosperm phyllogeny website. version 13, september 2013 [and more or less continuously updated since]. http://www.mobot.org/MOBOT/research/APweb/, 2001 onwards.

[290] STOMA, S., LUCAS, M., CHOPARD, J., SCHAEDEL, M., TRAAS, J., AND GODIN, C. Flux-based transport enhancement as a plausible unifying mechanism for auxin transport in meristem development. *PLoS computational biology 4*, 10 (2008), e1000207.

[291] SUGIURA, N. Further analysis of the data by Akaike's information criterion and the finite corrections. *Communications in Statistics-Theory and Methods 7*, 1 (1978), 13–26.

[292] SWAIN, P. S., ELOWITZ, M. B., AND SIGGIA, E. D. Intrinsic and extrinsic contributions to stochasticity in gene expression. *Proceedings of the National Academy of Sciences 99*, 20 (2002), 12795–12800.

[293] SWARUP, K., BENKOVÁ, E., SWARUP, R., CASIMIRO, I., PÉRET, B., YANG, Y., PARRY, G., NIELSEN, E., DE SMET, I., VANNESTE, S., ET AL. The auxin influx carrier lax3 promotes lateral root emergence. *Nature Cell Biology 10*, 8 (2008), 946–954.

[294] TALBERT, P., ADLER, H., PARKS, D., AND COMAI, L. The *REVOLUTA* gene is necessary for apical meristem development and for limiting cell divisions in the leaves and stems of *Arabidopsis thaliana*. *Development 121*, 9 (1995), 2723–2735.

[295] TAMURA, M. Taxonomical and phylogenetical consideration of the ranunculaceae. *Acta Phytotax. Geobot 20* (1962), 71–81. http://ci.nii.ac.jp/els/110003762869.pdf?id=ART0004974639.

[296] TEN TUSSCHER, K. H., AND HOGEWEG, P. Evolution of networks for body plan patterning; interplay of modularity, robustness and evolvability. *PLoS Computational Biology 7*, 10 (10 2011), e1002208.

[297] THATTAI, M., AND VAN OUDENAARDEN, A. Intrinsic noise in gene regulatory networks. *Proceedings of the National Academy of Sciences 98*, 15 (2001), 8614–8619.

[298] THEISSEN, G., BECKER, A., DI ROSA, A., KANNO, A., KIM, J. T., MÜNSTER, T., WINTER, K.-U., AND SAEDLER, H. A short history of MADS-box genes in plants. *Plant Molecular Biology 42* (2000), 115–149.

[299] THEISSEN, G., AND MELZER, R. Molecular mechanisms underlying origin and diversification of the angiosperm flower. *Annals of Botany 100*, 3 (2007), 603–619.

[300] THEISSN, G. Development of floral organ identity: stories from the MADS house. *Current Opinion in Plant Biology 4*, 1 (2001), 75–85.

[301] THORNLEY, J. Phyllotaxis. I. A mechanistic model. *Annals of botany 39*, 3 (1975), 491–507.

[302] TIKHODEEV, O., AND TIKHODEEVA, M. Variablity of the flower structure in european starflower (*Trientalis europaea* L.) in natural populations. *Russian Journal of Ecology 32* (2001), 206–210.

[303] TOBEÑA-SANTAMARIA, R., BLIEK, M., LJUNG, K., SANDBERG, G., MOL, J. N., SOUER, E., AND KOES, R. FLOOZY of petunia is a flavin mono-oxygenase-like protein required for the specification of leaf and flower architecture. *Genes & development 16*, 6 (2002), 753–763.

[304] TOWER, W. Variation in the ray-flowers of *Chrysanthemum leucanthemum* L. at Yellow Springs, Greene Co., O., with remarks upon the determination of modes. *Biometrika 1*, 3 (1902), 309–309.

[305] TRAAS, J. Phyllotaxis. *Development 140*, 2 (2013), 249–253.

[306] TROLL, W. Morphologie der schildförmigen blätter. *Planta 17*, 1 (1932), 153–230.

[307] TSIANTIS, M., SCHNEEBERGER, R., GOLZ, J. F., FREELING, M., AND LANGDALE, J. A. The maize rough sheath2 gene and leaf development programs in monocot and dicot plants. *Science 284*, 5411 (1999), 154–156.

[308] TUCKER, M., ROODBARKELARI, F., TRUERNIT, E., ADAMSKI, N., HINZE, A., LOHMULLER, B., WURSCHUM, T., AND LAUX, T. Accession-specific modifiers act with ZWILLE/ARGONAUTE10 to maintain shoot meristem stem cells during embryogenesis in *Arabidopsis*. *BMC Genomics 14*, 1 (2013), 809.

[309] TUCKER, M. R., HINZE, A., TUCKER, E. J., TAKADA, S., J?RGENS, G., AND LAUX, T. Vascular signalling mediated by ZWILLE potentiates WUSCHEL function during shoot meristem stem cell development in the *Arabidopsis* embryo. *Development 135*, 17 (2008), 2839–2843.

[310] TUCKER, S. C. Floral ontogeny in Sophoreae (Leguminosae: Papilionoideae). I. *Myroxylon* (Myroxylon group) and *Castanospermum* (Angylocalyx group). *American Journal of Botany* (1993), 65–75.

[311] TURING, A. M. The chemical basis of morphogenesis. *Philosophical Transactions of the Royal Society of London B 237*, 641 (1952), 37–72.

[312] VAN BERKEL, K., DE BOER, R. J., SCHERES, B., AND TEN TUSSCHER, K. Polar auxin transport: models and mechanisms. *Development 140*, 11 (2013), 2253–2268.

[313] VAN ITERSON, G. *Mathematische und microscopisch-anatamische Studien über Blattstellungen, nebst Betraschungen über der Schalenbau der Miliolinen Gustav-Fischer-Verlag*. G. Fischer, Jena, 1907.

[314] VAN MOURIK, S., KAUFMANN, K., VAN DIJK, A. D., ANGENENT, G. C., MERKS, R. M., AND MOLENAAR, J. Simulation of organ patterning on the floral meristem using a polar auxin transport model. *PLoS ONE 7*, 1 (01 2012), e28762.

[315] VAUCHERET, H. Plant ARGONAUTES. *Trends in Plant Science 13*, 7 (2008), 350 – 358.

[316] VEDEL, V., APOSTOLOU, Z., ARTHUR, W., AKAM, M., AND BRENA, C. An early temperature-sensitive period for the plasticity of segment number in the centipede *Strigamia maritima*. *Evolution & Development 12*, 4 (2010), 347–352.

[317] VILLANUEVA, J. M., BROADHVEST, J., HAUSER, B. A., MEISTER, R. J., SCHNEITZ, K., AND GASSER, C. S. *INNER NO OUTER* regulates abaxial? adaxial patterning in *Arabidopsis* ovules. *Genes & Development 13*, 23 (1999), 3160–3169.

[318] VOGEL, H. A better way to construct the sunflower head. *Mathematical Biosciences 44*, 3–4 (1979), 179–189.

[319] VOLLBRECHT, E., REISER, L., AND HAKE, S. Shoot meristem size is dependent on inbred background and presence of the maize homeobox gene, knotted1. *Development 127*, 14 (2000), 3161–3172.

[320] VOLLBRECHT, E., VEIT, B., SINHA, N., AND HAKE, S. The developmental gene *Knotted-1* is a member of a maize homeobox gene family.

[321] WAITES, R., AND HUDSON, A. phantastica: a gene required for dorsoventrality of leaves in antirrhinum majus. *Development 121*, 7 (1995), 2143–2154.

[322] WARDLAW, C. W. Phyllotaxis and organogenesis in ferns. *Nature 164* (1949), 167–169.

[323] WEBERLING, F., AND PANKHURST, R. *Morphology of Flowers and Inflorescences*. Cambridge University Press, 1992.

97

[324] Weigel, D., Alvarez, J., Smyth, D. R., Yanofsky, M. F., and Meyerowitz, E. M. *LEAFY* controls floral meristem identity in *Arabidopsis*. *Cell 69*, 5 (1992), 843–859.

[325] Weiler, E. W., and Schrder, J. Hormone genes and crown gall disease. *Trends in Biochemical Sciences 12*, 0 (1987), 271 – 275.

[326] Weir, I., Lu, J., Cook, H., Causier, B., Schwarz-Sommer, Z., and Davies, B. Cupuliformis establishes lateral organ boundaries in antirrhinum. *Development 131*, 4 (2004), 915–922.

[327] Weldon, W. Change in organic correlation of *Ficaria ranunculoides* during the flowering season. *Biometrika 1* (1901), 125–128.

[328] Whitehead, H. Variation in the moscatel. *Biometrika* (1902), 108–113.

[329] Wiesner, J. Bemerkungen ?ber rationale und irrationale divergenzen. *Flora, oder allgemeine botanische zeitung 58*, 8 (1875), 113–115.

[330] Wiesner, J. Bemerkungen ?ber rationale und irrationale divergenzen. *Flora, oder allgemeine botanische zeitung 58*, 9 (1875), 139–143.

[331] Woodward, A. W., and Bartel, B. Auxin: Regulation, action, and interaction. *Annals of Botany 95*, 5 (2005), 707–735.

[332] Yamaguchi, N., Wu, M.-F., Winter, C. M., and Wagner, D. *LEAFY* and polar auxin transport coordinately regulate *Arabidopsis* flower development. *Plants 3*, 2 (2014), 251–265.

[333] Yang, Y., Hammes, U. Z., Taylor, C. G., Schachtman, D. P., and Nielsen, E. High-affinity auxin transport by the {AUX1} influx carrier protein. *Current Biology 16*, 11 (2006), 1123 – 1127.

[334] Yule, G. U. Variation of the number of sepals in *Anemone nemorosa*. *Biometrika 1*, 3 (1902), 307–309.

[335] Zhang, R., Guo, C., Zhang, W., Wang, P., Li, L., Duan, X., Du, Q., Zhao, L., Shan, H., Hodges, S. A., Kramer, E. M., Ren, Y., and Kong, H. Disruption of the petal identity gene *APETALA3-3* is highly correlated with loss of petals within the buttercup family (ranunculaceae). *Proceedings of the National Academy of Sciences 110*, 13 (2013), 5074–5079.

[336] Zhao, Y., Christensen, S. K., Fankhauser, C., Cashman, J. R., Cohen, J. D., Weigel, D., and Chory, J. A role for flavin monooxygenase-like enzymes in auxin biosynthesis. *Science 291*, 5502 (2001), 306–309.

[337] Zimmermann, R., and Werr, W. Pattern formation in the monocot embryo as revealed by namand cuc3 orthologues from zea mays l. *Plant Molecular Biology 58*, 5 (2005), 669–685.

General Index

Gene Name Index

Taxonomic Index